Combustion zone investigation in fuel flexible suspension fired boilers, Experimental

Clausen, Sønnik; Fateev, Alexander; Hvid, Søren Lovmand; Beutler, Jacob Benjamin; Evseev, Vadim

Publication date:
2011

Document Version
Publisher's PDF, also known as Version of record

Combustion zone investigation in fuel flexible suspension fired boilers, Experimental

Risø-R-Report

Sønnik Clausen, Alexander Fateev, Søren Lovmand Hvid, Jacob Beutler, Vadim Evseev

Risø-R-1751(EN)
August 2011

Risø DTU
National Laboratory for Sustainable Energy

Author: Sønnik Clausen, Alexander Fateev, Søren Lovmand Hvid, Jacob Beutler, Vadim Evseev
Title: Combustion zone investigation in fuel flexible suspension fired boilers, Experimental
Division: Risø DTU

Risø-R-1751(EN)
August 2011

ISSN 0106-2840
ISBN 978-87-550-3850-9

Contract no.: PSO 2007-7333

Group's own reg. no.: 1750182

Sponsorship: energinet.dk, Dong Energy

Cover :
Infrared picture of straw particles in flue gas in tail of coal straw flame being collected at port D (middle boiler). Particle sampling probe was inserted 1.5 m from boiler side wall and 6.72 from burner wall for sampling of particles. IR pictures are recorded at 100 Hz using IR camera mounted with water-cooled endoscope optics, 3.9 µm optical filter to eliminate thermal gas radiation and 333 µs exposure time to "freeze" movement of particles.

Pages: 127
Tables: 7
References: 18

Information Service Department
Risø National Laboratory for Sustainable Energy
Technical University of Denmark
P.O.Box 49
DK-4000 Roskilde
Denmark
Telephone +45 46774005
bibl@risoe.dtu.dk
Fax +45 46774013
www.risoe.dtu.dk

Abstract:

The purpose of the project is to obtain data for full-scale validation of predictive models for combustion and co-combustion of biomass in utility boilers. In addition, focus was on development of innovative optical measuring techniques as a means to increase data quality by fast measurements and to cut measurement costs.

All measurements were carried out on a Mitsui-Babcock Low-NO_x wall burner at Studstrup power plant, unit 4, Denmark in October and November 2009. Measurements on a pure coal (reference), coal-straw and coal-wood flame have been obtained. Special attention was paid to the coal-straw flame at conditions close to daily co-firing operation. 4 measurement ports was used for mapping of flames with a distance up to 6.72 m from burner wall using 5 m and 7 m long water-cooled probes.

Gas temperatures and gas composition were measured by FTIR fibre-optic probe and extractive gas sampling for all type of flames. Additional, fast O_2, NO and SO_2 measurements using UV fibre-optic probe was performed in coal-straw flame. Particles were sampled for further analysis at selected positions with a special designed particle extraction probe to handle large straw particles. Axial and tangential velocities for coal-straw flame were mapped by Laser Doppler velocimetry (LDA) in 235 points. High speed IR-camera with water-cooled endoscope optics has been used to grab images of particle flow patterns and dispersion in flames. The IR-camera was also used with a grating spectrometer to measure gas and particle temperature with 1000 Hz.

Al flames were highly turbulent and very large variations in temperature and gas concentrations are observed. Gas temperature profiles for all three flames become fairly similar 4 m away from burner wall, whereas large variations in gas composition profiles are found. LDA velocity measurements for the coal-straw flame show that the simple gas flow field expected for a single burner is smeared out shortly after start of flame due to interaction with other burners.

Contents

Preface

Measurements were performed on a full scale power plant operating at loads determined by the marked (windmills, weather, consumption, etc.). Stable operation of the boiler during measurements is a wish from an experimental point of view, but very costly over many days and it is important to keep tight time schedule. Several measurement methods were used for large scale flame measurements for the first time, i.e. LDA, UV-probe and particle sampling probe designed for sampling of large straw and wood particles, and was tested on flame with boiler load variations before final campaign. The final campaign was split into two periods with approx.. 3 weeks space between them. All measurements were carried out as scheduled once leaving very little time to look at data and no time to repeat a measurement. Measurements were skipped in situations with problems, e.g. blocking of gas sampling line in regions of flame with very high particle load. This gives some empty points in data set, but lack of data for those point should not lead to a surprise (regions known to be fuel rich, high CO, low O_2, etc).

The team involved in the project and their role briefly:

Søren Lovmand Hvid, DONG Energy: Project leader, planning

Rasmus Glar Nielsen, DONG Energy: Measurement ports

Klaus Ulrik Grouleff, DONG Energy: Planning, participation in measurement campaign

Jacob Benjamin Beutler, Brigham Young University (BYU): LDA, particles, measurement campaign

Alexander Fateev, Risø DTU: UV-measurements, extractive gas sampling, measurement campaign

Karsten Lindorff Nielsen, Risø DTU: Design experimental equipment, measurement campaign

Sønnik Clausen, Risø DTU: Planning, FTIR, LDA, measurement campaign

Vadim Evseev, Risø DTU: Fast IR spectroscopy measurements

Contact persons at Studstrup power plant: Kim Thielsen and Bent Juul Larsen.

File:*Report_Combustion zone investigation in fuel flexible suspension fired boilers_v42.doc*

1 Introduction

Previous investigations, laboratory experiments as well as detailed measurements on a smaller pilot scale swirl stabilized combustor have provided the basis for the formulation and development of a CFD model for biomass particle conversion as well as pilot scale validation. Validation on a full-scale foundation is necessary before the developed model can be effectively used as a tool to perform predictive analysis of boiler retrofit (or design) for biomass suspension firing or co-firing. The project will round off the research effort in the development of the co-firing technology through full-scale validation data obtained at the Studstrup power plant, unit 4.

The validation will be performed by:

- Measurements in the combustion zone on a full-scale co-fired swirl-stabilized burner including particle conversion, gas species and temperature

- Detailed combustion zone simulation using the CFD model developed

- Necessary adjustment of the model to provide sufficient accuracy in the prediction of the combustion process, and to do so within an affordable computational effort

- Model validation for pure biomass combustion and co-firing conditions

The purpose of the project is to obtain data for full-scale validation of predictive models for combustion and co-combustion of biomass in utility boilers, to perform the model validation and to apply the models for two existing boilers (SSV4 and AVV2). The main project purpose is, through application of a validated model, to improve the combustion process in terms of emissions from biomass fired or co-fired plants and to facilitate the introduction of a wider band of biomass fuels in existing power plants. The project is divided into two main work packages, i.e. full-scale combustion zone measurements and CFD modelling, validation and analysis. Only the experimental work package is described in this report. The full-scale measurements and modelling efforts are crucial to the future use of the developed models as tools to guide the design and optimisation of biomass fired plants and in the introduction of new biomass fuels.

In addition, focus will be on development of innovative optical measuring techniques as a means to increase data quality by fast measurements and to cut measurement costs. The FTIR spectroscopy is in the project supplemented by UV-spectroscopy measurement of oxygen, SO_2 and NO. Thermal imaging is used for visualisation of bio mass particle flow.

1.1 Background and other work

Several investigations have been carried out with measurements in the near-burner region of pf flames. These investigations include some or all of the following information: velocity fields, gas temperatures, particle temperatures, gas composition data, and carbon burnout. Most of these investigations have been on coal flames, ref. 3 and 7-12, and most of these have been in pilot-scale systems. There are relatively few biomass or biomass-coal blend flame investigations and these are almost entirely in pilot-scale systems. Some important flame characteristics, such as the stoichiometry and intermittency of oxygen

near the flame center, quite likely change with increasing scale. Measurements from within a biomass or co-fired flame are rarer. Several parametric investigations have been performed with emissions analyzed.

While some of these investigations were performed on close to commercial-scale burners, none were from a burner in a multi-burner combustor. Because factors affecting operation of a swirl-stabilized burner scale in different ways, there is uncertainty as to whether results from bench-scale measurements accurately represent commercial scale burners. For example, it is necessary to burn smaller biomass particles in the bench-scale burners than in commercial scale to achieve stable flames. Also heat transport by radiation cannot be accurately scaled from commercial boilers to a single burner facility.

1.2 Applied measurement techniques and overview

Flame measurements are difficult in general, e.g. we have observed deviations of 50-200°C in gas temperature performed by different methods in large flames and large deviations in measured CO concentration using extractive probe with particle filter at inlet and FTIR fibre-optic probe in dense flames. Penetration of light is limited to 10-30 cm in the densest zone of pulverized large scale flames, i.e. it is not possible to use optical diagnostic methods from openings in boiler walls. Water-cooled fibre-optic probes that can be inserted in flame are used in this project to overcome those problems.

Fast in situ measurements of gas temperature and gas composition can directly relate to transient phenomena appearing in a flame or hot flue gases caused by e.g. instabilities, poor gas mixing and formation of quasi-stable moving structures. A typical time scale for these fast events is in the range from a few microseconds, making measurements very difficult. However in practice measurements on a millisecond time scale can be sufficient in order to follow the dynamics of the combustion process in particular in larger combustion systems.

Following optical methods are used in this project:

a) FTIR fibre-optic probe: measurement of gas temperature, gas components (CO, CO_2, C_xH_y, H_2O),
b) UV fibre-optic probe: measurement of gas temperature, NO, SO_2, O_2 and other gas components,
c) LDA: velocity (2 components/2D),
d) IR-camera with water-cooled endoscope optics: surface temperature of fuel particles and visualization of particle flow and mixing in flames.
e) IR-camera with grating spectrometer: fast temperature measurements of gas and particles

Following extractive methods are used:

f) Particle sampling probe: ø17 mm sampling diameter and water-cooled bended tip with quench gas for sampling of very large straw particles (burn out, etc.),
g) Extractive gas sampling: External gas analysis based on FTIR and UV spectroscopy (wet gas) and paramagnetic O_2-analyzer (dry gas).

Extractive gas sampling and FTIR fibre-optic measurements was performed at the same time using the same water-cooled probe, i.e. non-intrusive and extractive gas concentration results can be compared.

A 5 m long multi-purpose water-cooled probe was developed in the project based on experience from a 9 m long water-cooled probe developed in PSO 2003-4805 “Channel formation in Boilers”.

Two 5 m long and 60.3 mm diameter water-cooled probes were manufactured specially for the measurement campaign to be inserted up to 4 m into boiler. Water-cooling principles and dimensions of probe has been standardised that allow use of the same probe for all type of measurements, which in principle also could include other type of measurements as suction pyrometer and optical particle sizing by image processing.

Overview of all measurements performed can be found Table 1 and details in the spreadsheet file "NearBurner_time.xls". Test measurements performed before final campaign is not included in table.

Table 1 Overview flame measurements

Date	Start time	End time	Text	FTIR-probe	Extractive gas	LDA	Particle sampling	UV-probe	IR-camera
25 Oct.	17:00	24:00	Installation						
26 Oct.	07:30	23:30	Experiments, coal + straw			**X**			
27 Oct.	07:30	21:30	Experiments, coal + straw	**X**	**X**				
28 Oct.	07:30	22:00	Experiments, coal + straw	**X**	**X**				
29 Oct.	08:00	21:00	Experiments, coal + straw				**X**		**X**
30 Oct.	08:00	22:00	Experiments, coal + straw					**X**	
18 Nov.	08:00	23:59	Experiments, coal + wood	**X**	**X**		**X**		**X**
19 Nov.	08:00	12:30	Experiments coal + long straw				**X**		**X**
19 Nov.	13:00	17:30	Experiments coal	**X**	**X**				
19 Nov.		23:00	Experiments coal + long straw				**X**		

The main focus was on the coal-straw flame at full load as seen in Table. Experimental time for campaign was limited by need of stable operation conditions of boiler and amount of wood available for the coal-wood flame experiments.

Experimental equipment was mainly developed at Risø DTU. Particle extraction probe head was designed to collect particles through the 5-m probes and built at BYU's Precision Machining Laboratory.

2 Plant description and unit operational data

2.1 Boiler and burner

The Studstrup Boilers (two sister units: 3 & 4) were commissioned in 1984. The boiler is a Babcock two-pass once-through benson-type boxer-fired boiler, Figure 1, equipped with 24 Mitsui-Babcock Low-Nox burners. Four of these burners located on the upper burner level (the four central burners) have been retrofitted to allow for simultaneous feeding of two separate pulverized fuels (coal and straw). This has been facilitated by relocating the core oil-lance and ignition lance to penetrate the tertiary air register and introducing the cofire fuel (in this case straw) through a central straw feeding pipe, see Figure 2 and Figure 3.

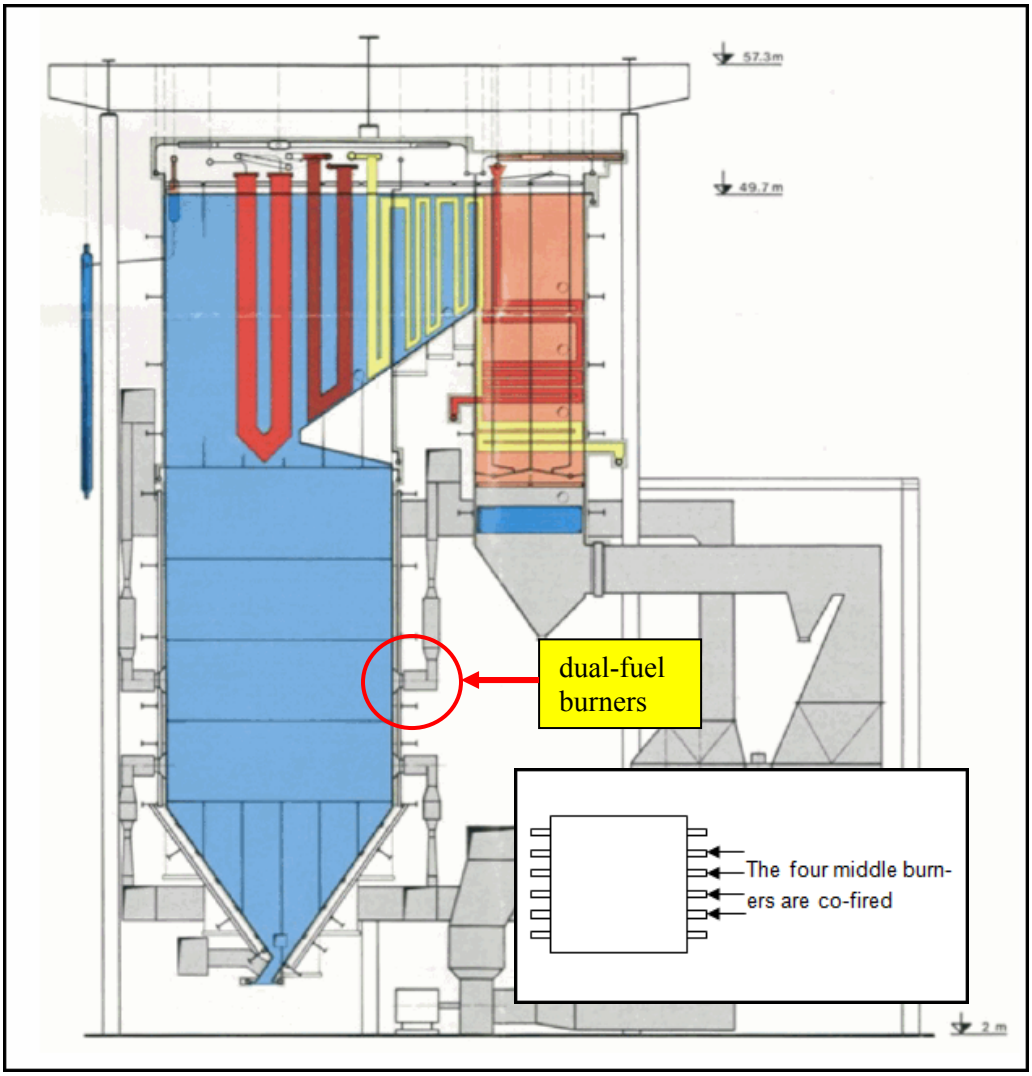

Figure 1 The Studstrup Unit 4 Boiler, insets showing arrangement of dual-fuel burners.

Figure 2 . The Mitsui-Babcock Low-NOx burner in standard configuration.

Figure 3 The Mitsui-Babcock Low-NOx burner in dual-fuel configuration.

For the purpose of obtaining access to a dual-fuel burner, burner #46 located next to the sidewall was rebuilt into a dual-fuel burner and a straw feeding pipe was subsequently relocated from burner #45 to burner #46, see Figure 4. This made it possible to reach into and across the entire flame structure of a co-fired burner with water-cooled probes as it is sketched in Figure 5 although not achieving such a fine resolution as indicated in this figure.

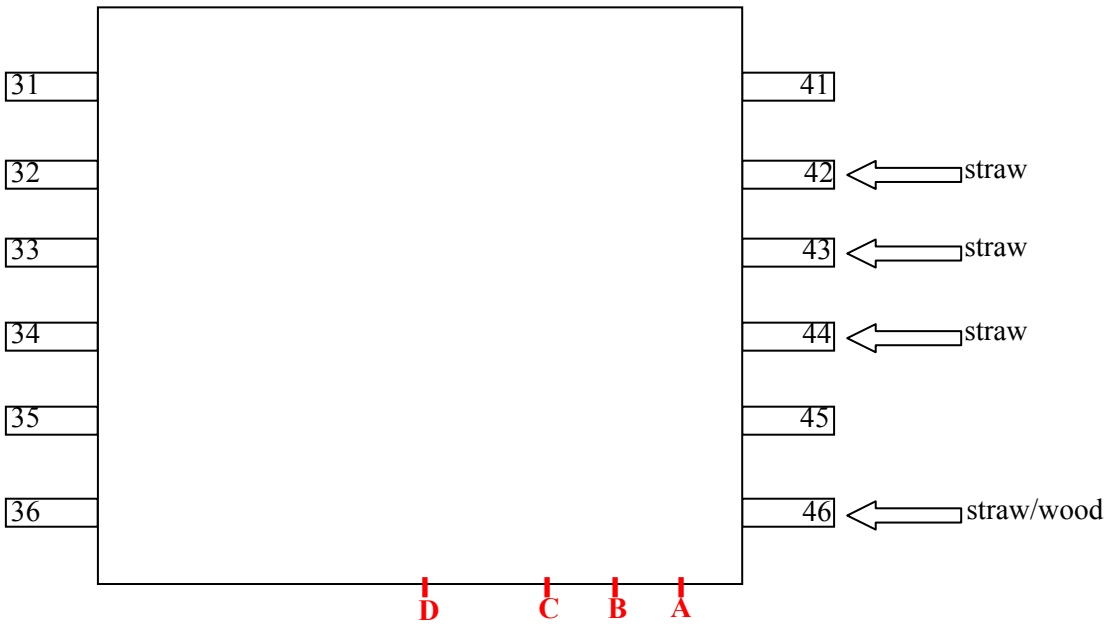

Figure 4 Sketch of plan arrangement at elevation 23500 displaying burner notation, arrangement of biomass fed burners and measurement port positions for the test campaigns.

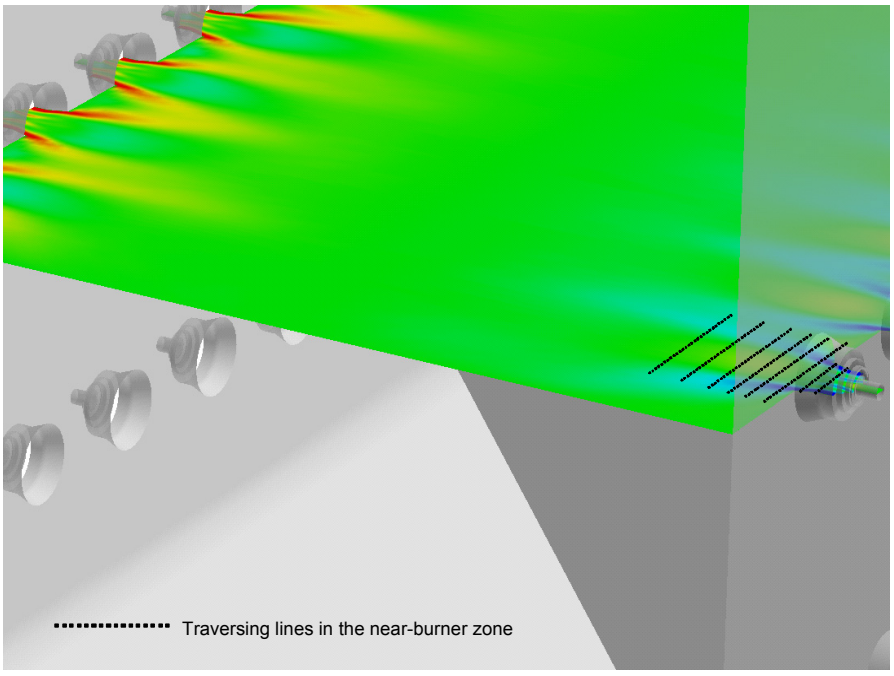

Figure 5 Artistic impression of measurement lines across the burner flame structure.

2.2 Measurement ports

Four measurement ports were established on the top burner gallery. The original intention to position 6 ports had to be aborted due to spatial constraints of other equipment (wall soot blowers) and the necessary physical extent of the measurement ports. A measurement port is shown in Figure 6 and Figure 7 as it is being prepared at the power plant.

Figure 6 Measurement port welded into the side wall before packing and isolating.

Figure 7 Measurement port before outer isolation.

Measurement port positions

Port A) Port centreline (CL) is 1220 mm from the back wall (approx. 1700 mm in front of burner mouth). Port CL elevation is 23554 mm opposed to the burner CL elevation of 23222 mm.

Port B) Port centreline (CL) is 2620 mm from the back wall (approx. 3100 mm in front of burner mouth). Port CL elevation is 23554 mm opposed to the burner CL elevation of 23222 mm.

Port C) Port centreline (CL) is 4020 mm from the back wall (approx. 4500 mm in front of burner mouth). Port CL elevation is 23554 mm opposed to the burner CL elevation of 23222 mm.

Port D) Port centreline (CL) is 6720 mm from the back wall (approx. 7200 mm in front of burner mouth). Port CL elevation is 23554 mm opposed to the burner CL elevation of 23222 mm. This port is positioned at boiler CL midway between the front and back walls.

The measurement port positions are shown in Figure 8.

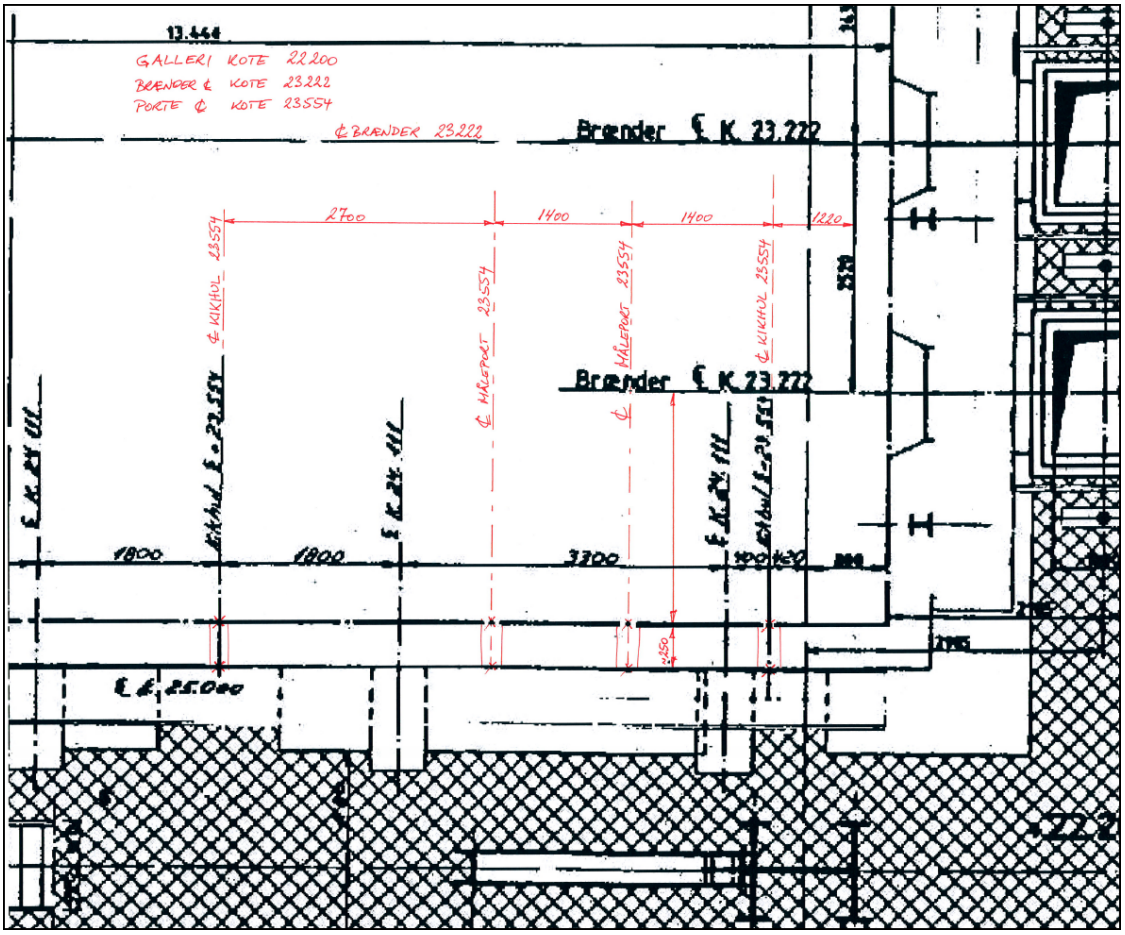

Figure 8 Measurement port positions.

For the alternative biomass (wood dust) test campaign, several options for introducing wood into the biomass feeding pipe was considered as illustrated in Figure 9. In the end, it was decided to feed in wood dust (or wood particles) just before the rotary valve (red arrow) which dumps the biomass into the high(er) pressure dust conveying pipe. In this way, the uncertainty about how much biomass might be lost (in stone traps and other places) was removed, and doubts about the suitability of the straw transporting equipment to transport wood instead of straw was also avoided.

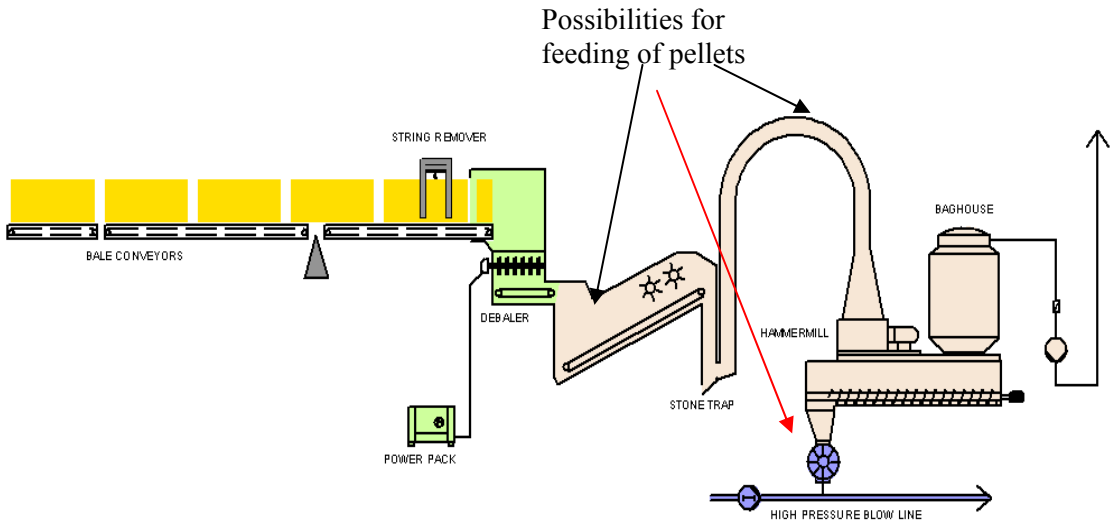

Figure 9 Options for introduction of wood dust into the straw feeding system. Wood dust came from crushed wood pellets with a content of some larger fractions from pellets.

2.3 Operating conditions during campaigns

For the measurement campaigns, prime importance was on maintaining stable conditions for burner #46 and to some extent also the neighbouring burner #45 as this was assumed to be able to impact burner #46 operation – at least in the outer flame area. Boiler load conditions were therefore not required to be stable and the plant was allowed to adjust load according to prevailing conditions (electricity and heat demand).

An overview of plant conditions for the two measurement campaigns, 26-30 October 2009 (coal & straw) and 18-19 November 2009 (coal & wood; coal alone) is provided in Appendix A, where time series plots of relevant parameters for the test days are shown and a short description of the content of each signal is provided.

3 Laser Doppler velocity measurements

Risø DTU has earlier used LDA for velocity measurements in 1.3 MW coal flames, ref. 3. It was found that measurements in such a flame is difficult for a distance larger than approx. 1.2 m between lens and focal point due to beam steering, absorption of light in dense flames and the fact that LDA signal decrease with a factor of $1/f^4$, where f is the focal length. Therefore, a LDA head build into a water-cooled probe must be used to map full scale flames and boilers. Experimental setup and results are shortly described in the following. Details about experimental setup and results can furthermore be found in ref. 4.

3.1 Experimental setup LDA

Risø DTU's existing fibre optic laser Doppler anemometer (LDA) system was up-dated to perform 2D velocity measurements in large flames. A ø27 mm LDA fibre-optic head with 10 m fibre-optic cable and mounted with a 160 mm focal length lens was mounted in the water-cooled probe. Measurement volume dimensions are calculated to 0.074 mm in diameter and 1.57 mm long at 488 nm, and with a fringe spacing of 5.2 µm. The LDA head is protected from thermal radiation from flame via an insert with a quartz window. The insert reduces thermal radiation significantly by reduction of the throughput (area x solid angle) and by absorption of infrared light by the quarts window. A minor purge flow is used to avoid penetration of small particle into the probe. Concept was tested with a dummy LDA head in coal-straw flame on 7 October 2008 and temperature of LDA head raised from 23.3°C (temperature of cooling water) to 30.0°C when probe with LDA head was inserted fully in flame. Dantec Dynamics specifies an upper temperature limit of 45°C for the fibre-optic head. BSA processors were rented from DTU MEK for the measurement campaigns to avoid using Risø DTU's older FVA processor. The two signal processors used are BSA series 57N running the BSA version 2.1 software, also available from Dantec Dynamics.

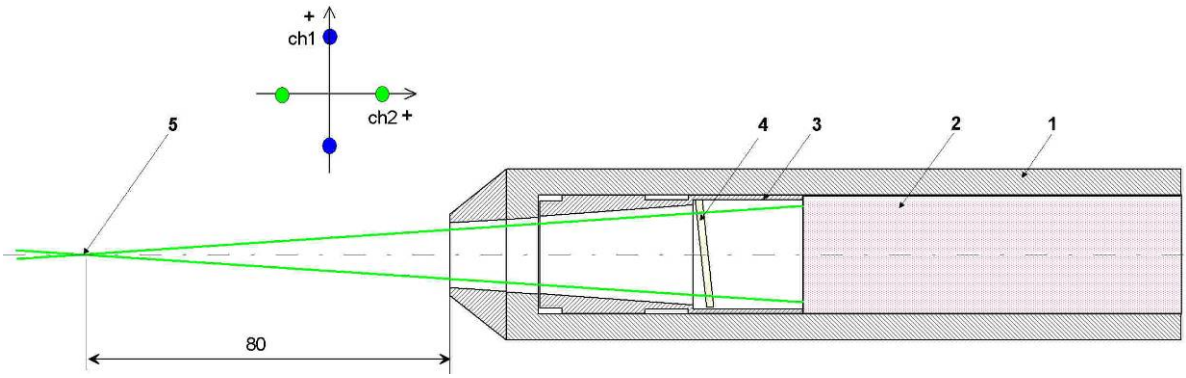

Figure 10 Fibre-optic LDA head (2) ø27 x 205 mm with 160 mm lens mounted in water-cooled probe (1) for velocity measurements in large scale flames. 2 x 2 laser beams define the measurement volume (5) that is placed 80 mm in front of probe and positive directions of raw data velocities. LDA fibre-optic head is protected by thermal radiation and particles by insert (3) and tilted quartz window (4). Positive direction of raw data for channel 1 (blue, 488 nm) and channel 2 (green, 514.5 nm) is illustrated.

Parametric tests were done on the settings for the LDA system prior to the actual measurement campaign. These tests were run to maximize the sampling rate. This would ensure that the velocity of the large

particles that do not follow gas flow is diluted out by the velocities of the much more abundant small particles. Thus the gas velocity can be approximated by the LDA particle velocities measured. High sampling rates were obtained in all positions, indicating that LDA signals mainly come from fine fuel or ash particles. Sampling rates exceeding 5000 Hz can be obtained.

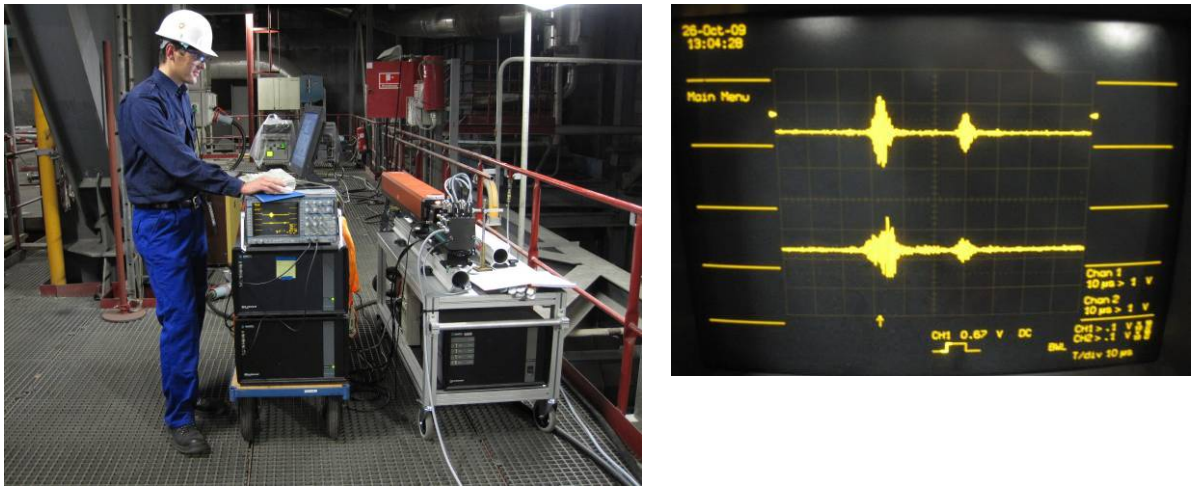

Figure 11 Jacob Beutler with LDA system, left picture. Quality of Doppler Burst was in general of good quality for both channels and was monitored on oscilloscope (10μs/div), right picture.

Fibre-optic LDA head is connected to transmitter unit model 60X41 placed on a trolley together with a 6 W Coherent 306 water-cooled argon-ion laser. Only 160 mW laser power was needed to obtain good LDA signals and sufficient high data rate of approx. 1 kHz. It is attempted to collect raw data over 1 minute to smooth out fluctuations in flow and obtain stable statistical mean values of velocities.

Figure 12 Mapping of velocities with LDA at port D with LDA head inserted in 5 m long water-cooled probe. Different vertical positions in flame were mapped by tilting probe. Port A was difficult to map due to large building frame structure behind port A.

The flame velocity field is highly turbulent as seen in Figure 13 and RMS (1 standard deviation) values are often close to average values.

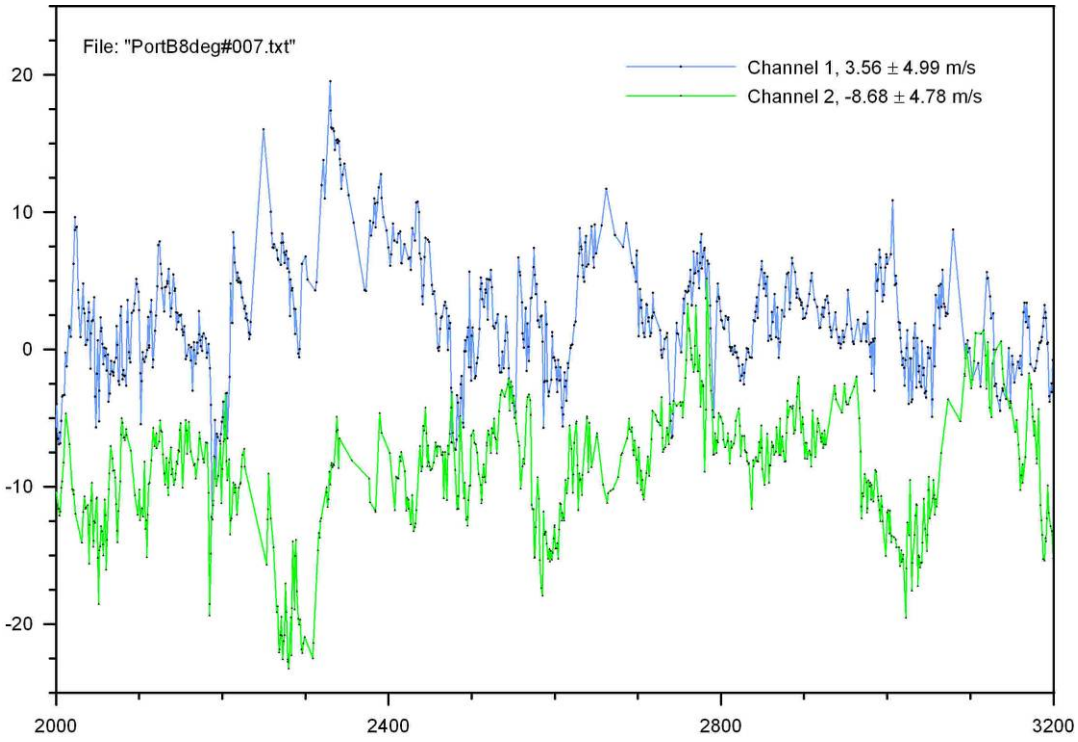

Figure 13 Example of measured raw data/velocities time series in coal-straw flame with LDA at port B, tilt 8 degree and 275 cm from boiler wall (outside the recirculation zone). Raw data for a period of 1.2 s is shown for a time series of 60 s (approx. 23000 data point per channel). Green curve shows the axial gas velocity component (flow away from burner) and blue is vertical velocity component (flow moving upwards).

3.2 LDA results

Overview of all LDA measurements and statistics can be found in Excel file “LDAvelocities.xls”.

The results of the measurements are difficult to display and even more difficult to understand in static figures, as appear here. Figure 14 illustrates the sampling grid for the velocity measurements. The points represent locations away from the burner wall (nearly horizontal axis), across the burner face (nearly vertical axis), and in the direction of flow from the burner (axis nearly into the page) where velocities were measured, displayed in the burner flow direction. The burner exit center line is located approximately in the center of this grid and start of grid is approx. 1 m behind burner wall/measurement grid. Probe access was from the left (as seen here) side of the flow through a narrow slit installed between steam tubes. The points nearest the burner are about 1.7 m from the burner outlet, or about 1.2 m from the boiler front wall, with the burner quarl recessed about 0.5 m into the wall. The points furthest in the flow direction are approximately at the center of the boiler (about 7.0 m from the front wall). The generally fan-shaped pattern of points results from the physically limited range of angles at which the probe could be placed because of structural components outside the sampling window. The measurements along the side of the figure are in cm.

A total of 235 measurement locations are included in the grid, with replicate or near-replicate measurements at 22 of these points. Most commonly, only two replicates are included, though there are some points with three and four replicates each. The measurements at replicated points occurred at significantly different times and provide some measure of data precision. Table 2 summarizes this analysis for the case of replicated results, which is located at position (272.32, 38.27, 262.00) in the plots, or at the approximate middle of the diagnostic area. As seen in the table 2, the standard deviation of the mean velocities based on 4 replicas (row 2, two first values) is much smaller than rms of the measured velocity (row 2, two last values) of flow, i.e. the standard deviation is approx. 0.7 m/s on mean velocity on four repeated measurements compared with rms values of approx. 5.1 m/s.

Table 2. Statistical analysis of measurements based on four replicated results

	Axial Vel	Vert Vel	Axial rms Vel	Vert rms Vel
mean	8.77	3.67	5.05	5.30
Std. Dev.	0.60	0.78	0.21	0.35
Coef. Variation	0.07	0.21	0.04	0.07

The axial and vertical mean velocities (axial rms and vertical rms velocities appear in ref. 16) are plotted in Figures 15-18 and Figure 19-22, respectively.

As seen, the primary features of the burner velocity profiles appear in the figure 15 (axial flow) and figure 19 (tangential flow). The axial flow reverses along the center line, forming an internal recirculation zone, around which the velocities are quite high in the axial direction. The region of high axial velocity forms a toroidal structure around the recirculation or reverse flow region as expected and as seen by the tubular structure of the velocity contours. The lift velocity reflects the same toroidal structure, except that the magnitude is negative on the left and positive on the right side of this zone. The axial and especially the vertical/lift velocities decay with increasing distance from the burner, except that the vertical velocity decays to a finite value, representative of the overall upward flow through the boiler. The influences of both vertical and downward neighbour burners also appear in these diagrams.

The rms velocity diagrams in ref. 16 show that velocity fluctuations do not scale with velocity magnitude, as is commonly assumed in models. Specifically, the axial velocity rms values are low at the center of their toroidal structure and high near the edges whereas the average values show the opposite trend. The measured trend makes more sense if one considers that the outside regions of the toroid will most strongly interact with the other velocities in the boiler and hence show more variation.

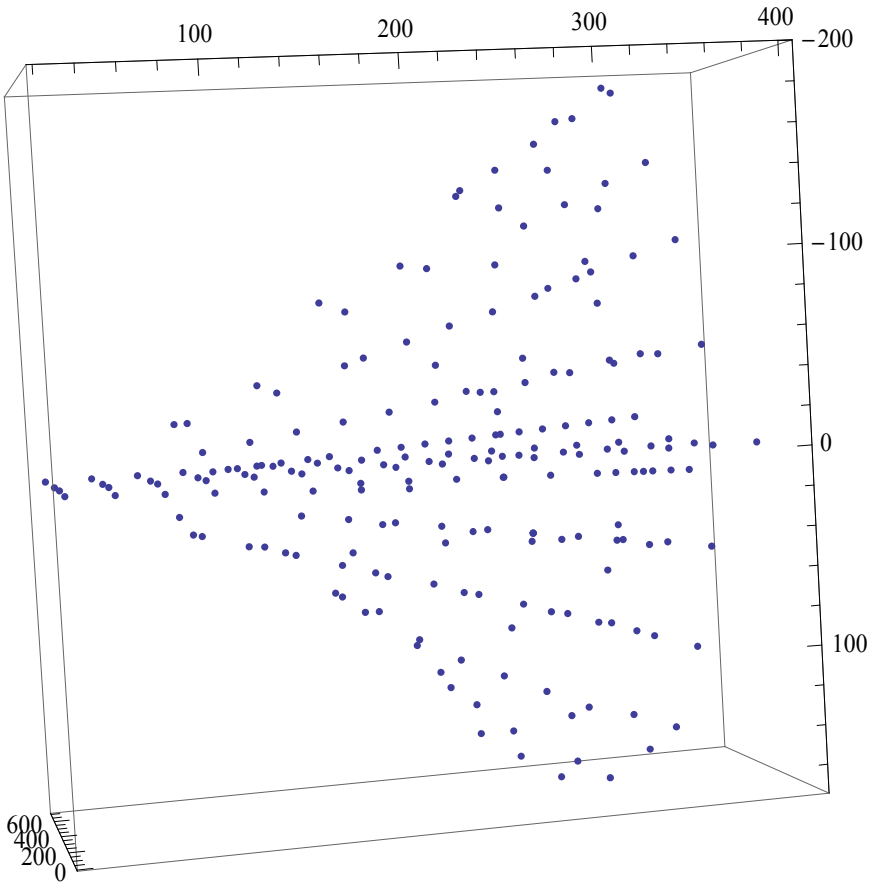

Figure 14 3-D pattern of sampling points from the wall (left) into the boiler. The measurements represent distances away from the wall (nearly horizontal axis), across the burner face (nearly vertical axis), and in the direction of flow from the burner (axis nearly into the page). The measurements along the side of the figure are in cm. The grid has 235 measurement points totally.

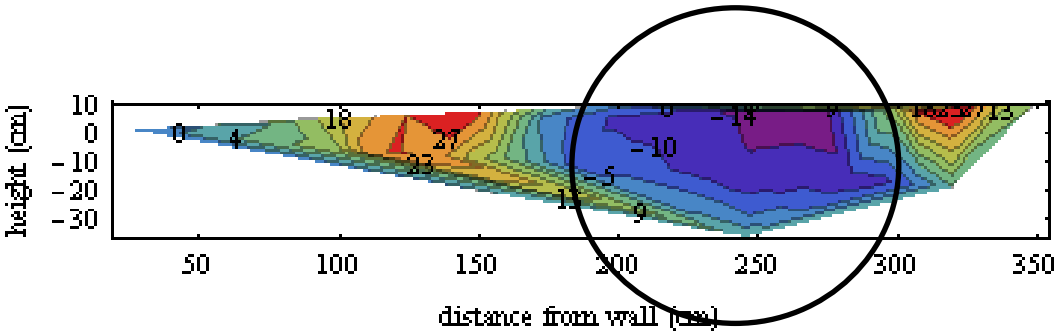

Figure 15 Axial velocities at 1.22 meters from quarl exit, port A. Notice high reverse velocities of -14 m/s in the internal recirculation zone (IRZ). Also high velocities seen from secondary/tertiary air around IRZ. Building structure behind port A limits mapping area of flame. Black circle illustrate the burner quarl. Distance is from side wall.

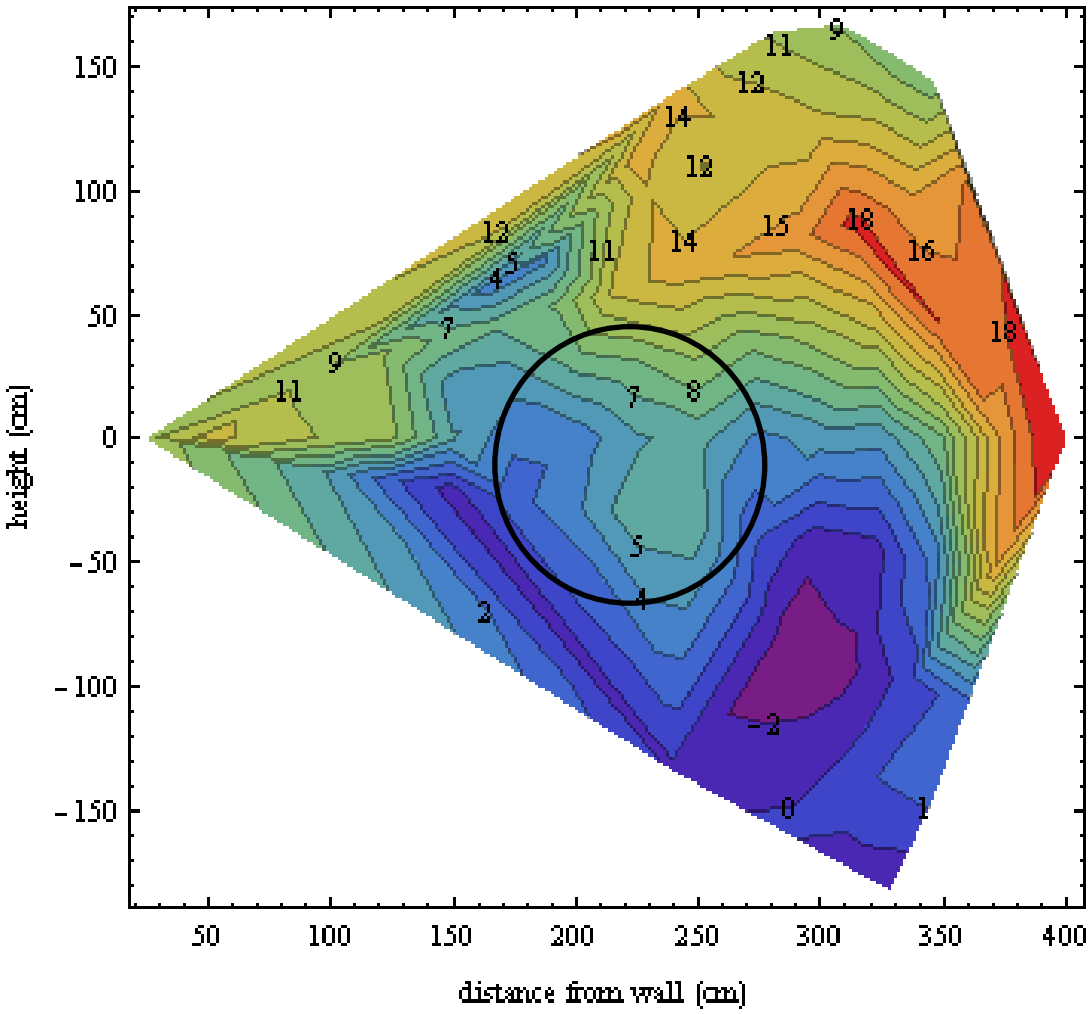

Figure 16 Axial velocities at 2.62 meters from quarl exit, port B. Higher velocities are still evident in secondary/tertiary air region with lower velocities around the centre. The recirculation zone is shifted downwards (black circle: burner quarl).

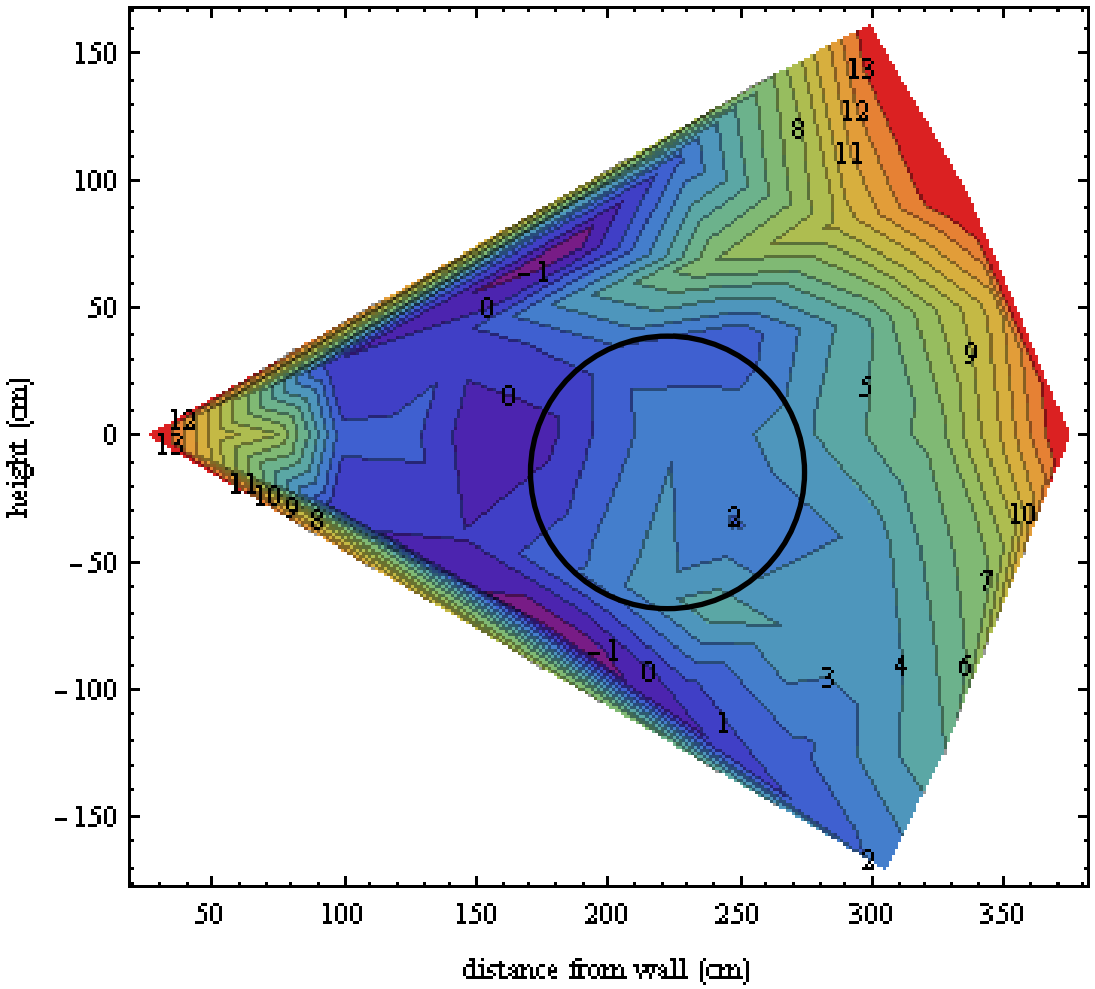

Figure 17 Axial velocities 4.02 meters from quarl exit, port C. This appears to be the end of the IRZ.

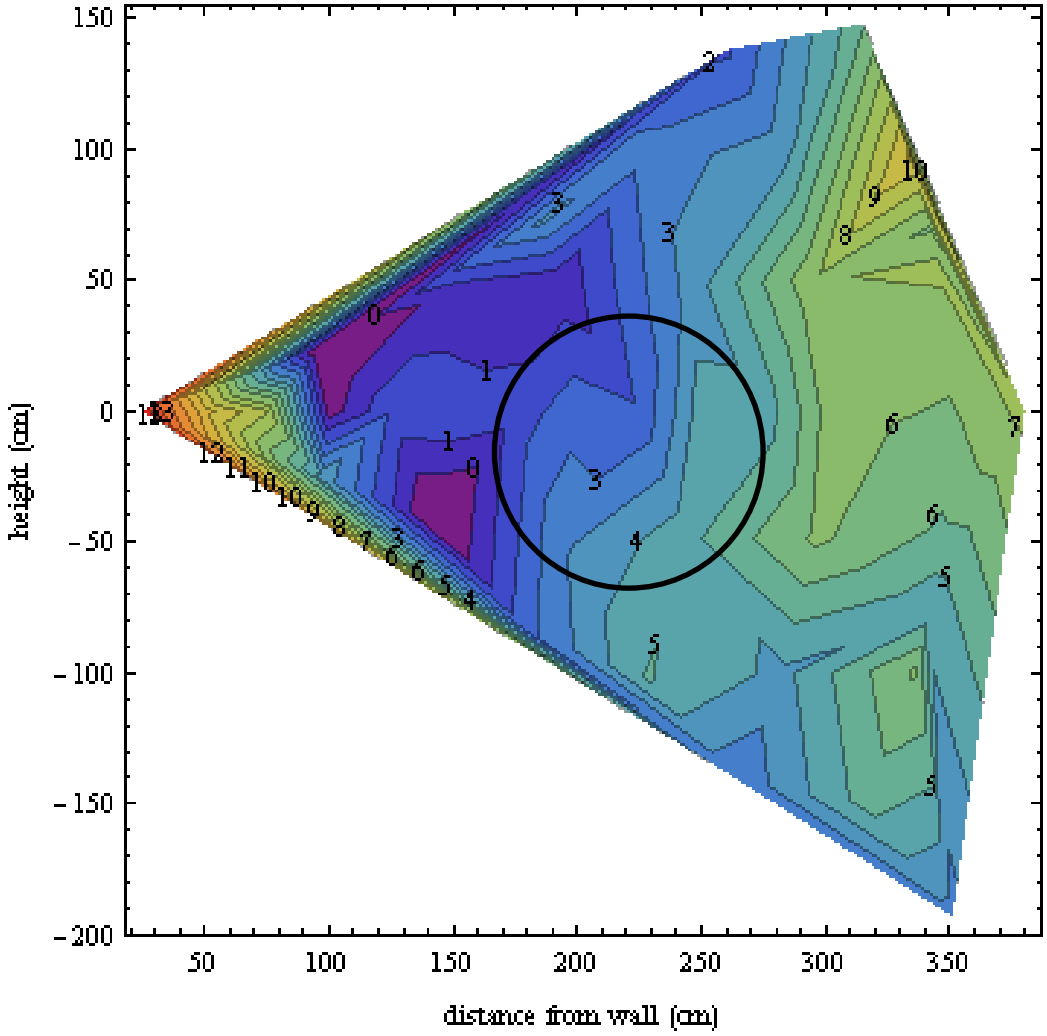

Figure 18 Axial velocities at 6.72 meters from quarl exit (center of the boiler), port D. Low velocities expected since opposing flame regions meet at center of boiler.

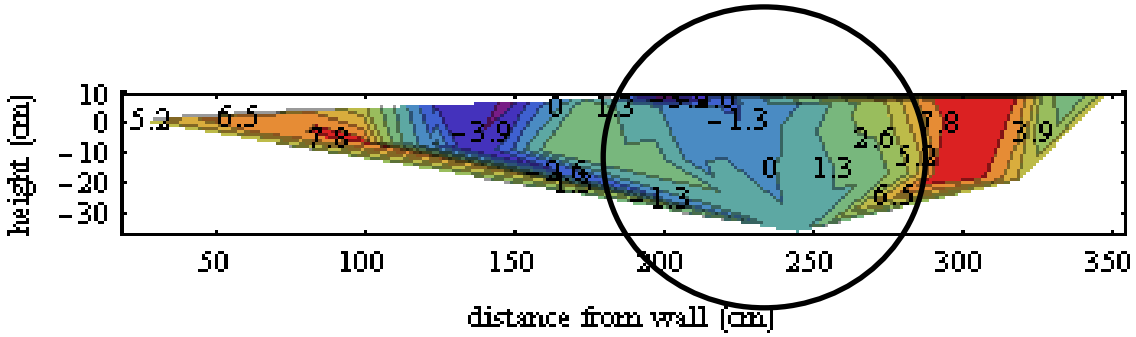

Figure 19 Vertical velocities 1.22 meters from quarl exit, port A. Secondary/tertiary air swirl is counter-clockwise for burner no. 46 and clearly seen from data. View direction in direction of main flow or seen from the burner.

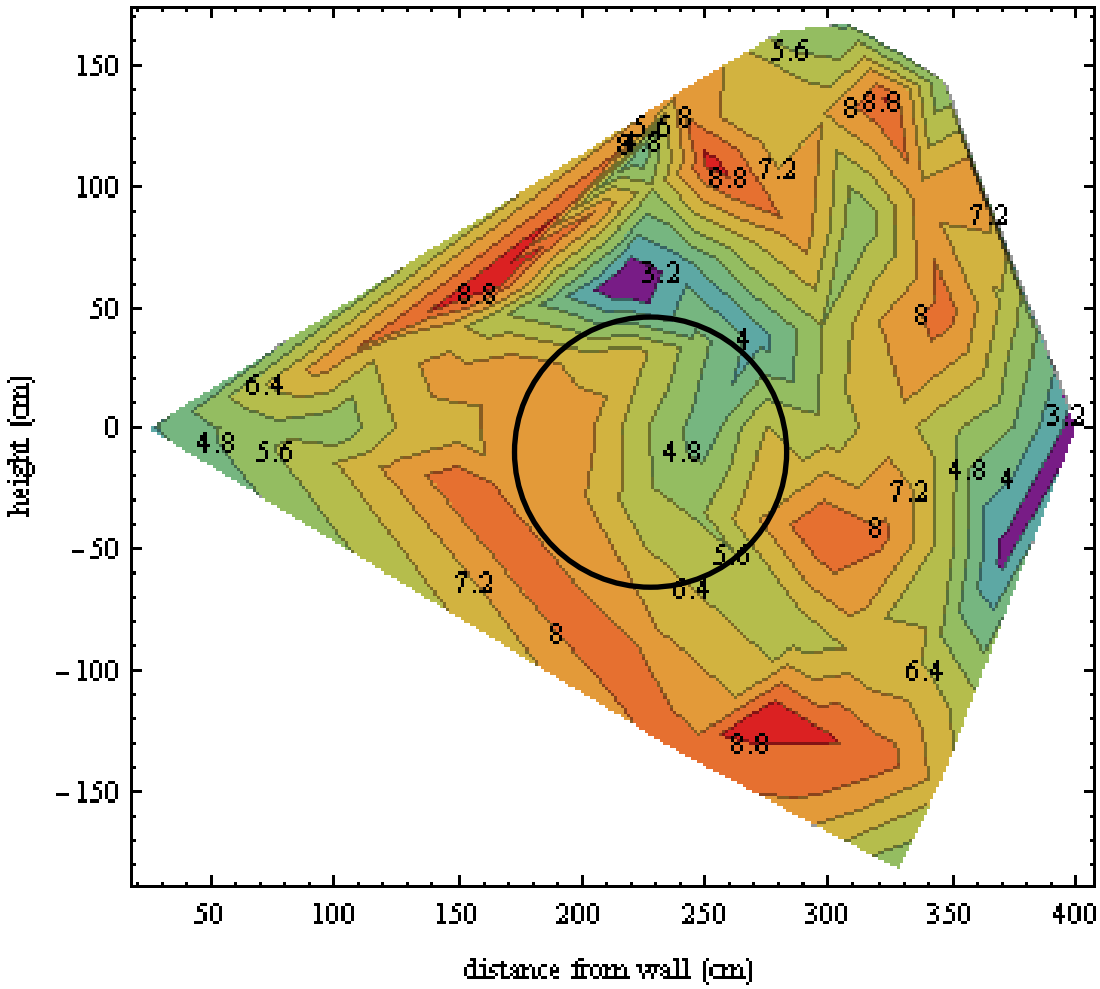

Figure 20 Vertical velocities 2.62 meters from quarl exit, port B. Simple swirl pattern of flow in burner is not seen as at port A.

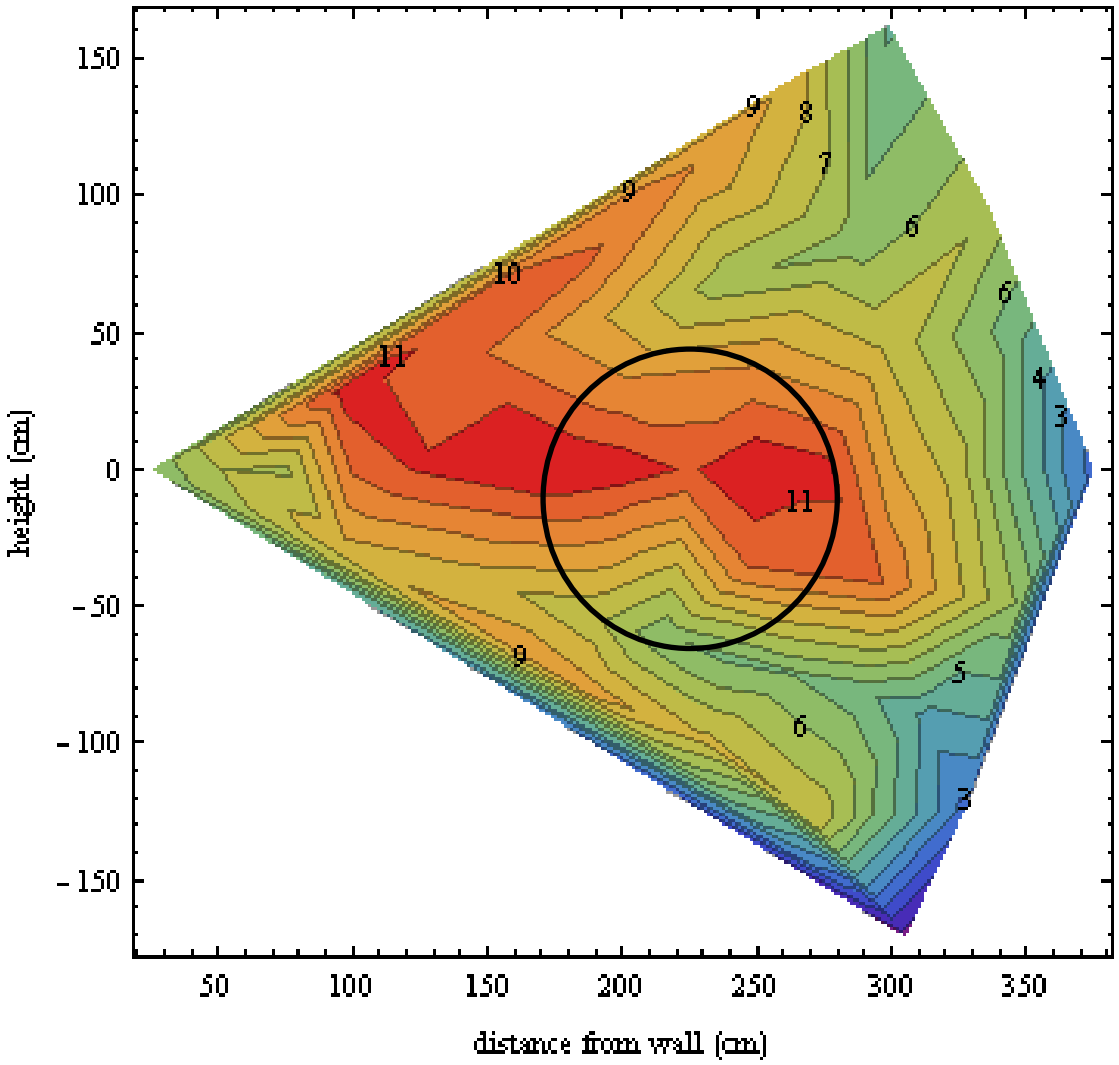

Figure 21 Vertical velocities 4.02 meters from quarl exit. Average vertical velocity continues to increase as flame lifts.

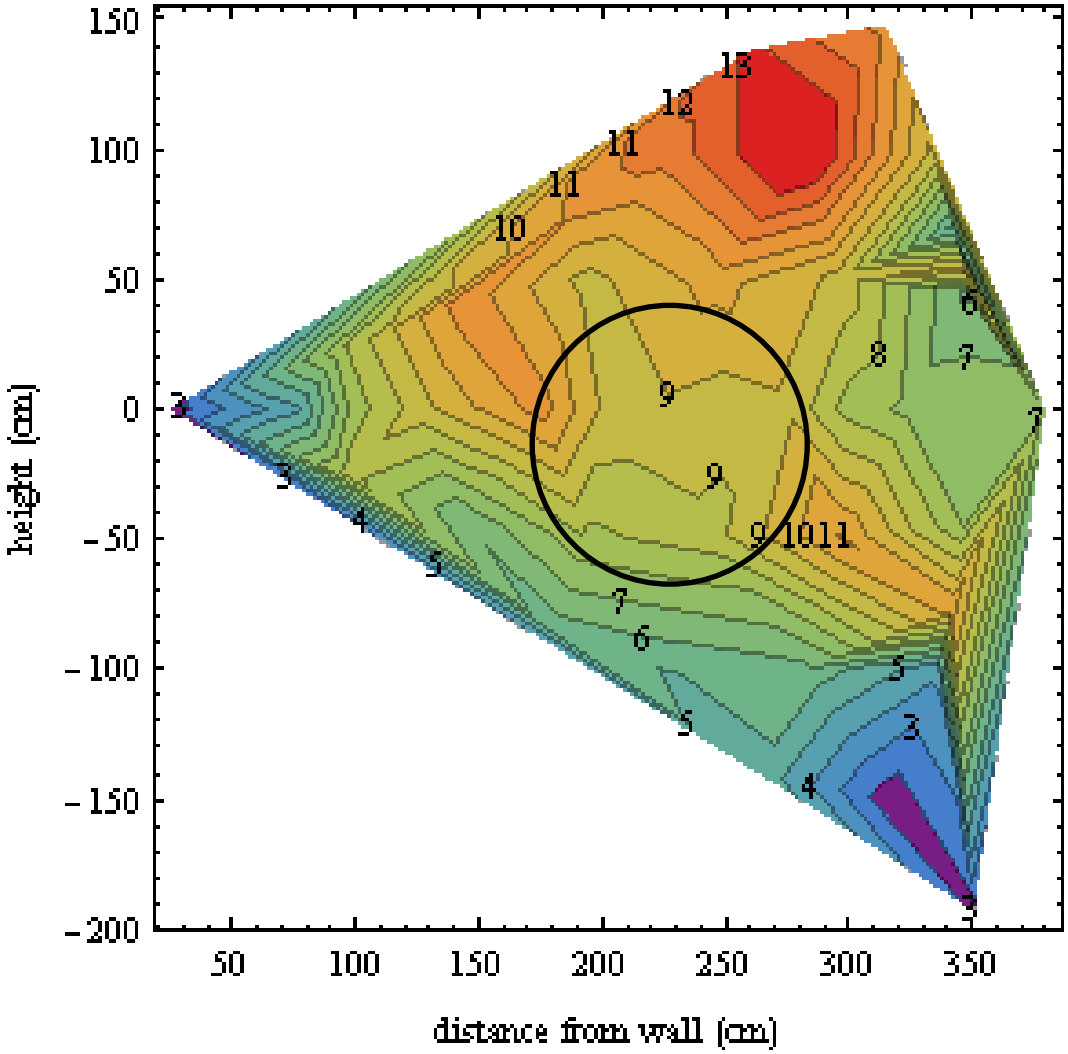

Figure 22 Vertical velocities 6.72 meters from quarl exit, port D, middle boiler.

3.2.1 Conclusion LDA

Experimental, laser-based velocity and velocity fluctuation measurements in the near-burner region of an operating, utility-scale boiler firing a blend of coal and straw show clear indications of internal recirculation zones, toroidal axial and tangential velocities around this recirculation zone, relatively rapid decay, and significant burner-burner interaction. All of these features agree with theoretical and design features of these flows. These measurements are part of a larger campaign to characterize the near-burner flame structure with experimental and theoretical velocity, temperature, gas composition, and particle measurements at utility scale. These may be the first data of this type describing co-fired flames and possibly any near-burner flame from a utility-scale boiler. As with any commercial-scale measurement, flow access and maintaining steady operation represent major challenges in this work, though this investigation went to great lengths to address both. Up to four replicate measurements were made at some location at different times during the campaign. Variation among these replicates is small compared to the trends in the data and the measured velocity fluctuation at that point, indicating that the data are at least semi-quantitative.

It was a surprise for the team that LDA was easy to apply in full scale flames and very nice signals and high date rate can be obtained at any position in the flame. LDA fibre-optical head was mounted in a 5 m long water-cooled probe sufficient for mapping of the flow field of a wall burner, but length of probe can in principle be extended to 9 m using same probe design and cooling principles for mapping of flow fields in other regions of large boilers.

4 Thermal imaging of flame

A water-cooled endoscope was developed in the project for fast thermal imaging of flames, see Figure 23. IR-camera is less sensitive (approx. a factor 10) to thermal radiation from soot compared with a video camera, i.e. pictures or movies of fuel particle flow in large flames can be recorded with better quality in mid infra red spectral region than in the visible. Thermal radiation by soot dominates in the visible region. Therefore, video pictures of flames show mainly part of flame with high temperature and soot concentration (high CO, C_xH_y) and colder regions of flame (large fuel particles) become more difficult to see in pictures than using an IR-camera sensitive at 3.9 µm.

Figure 23 Inspection of flame using IR-camera with water-cooled endoscope optics.

4.1 Coal-straw flame

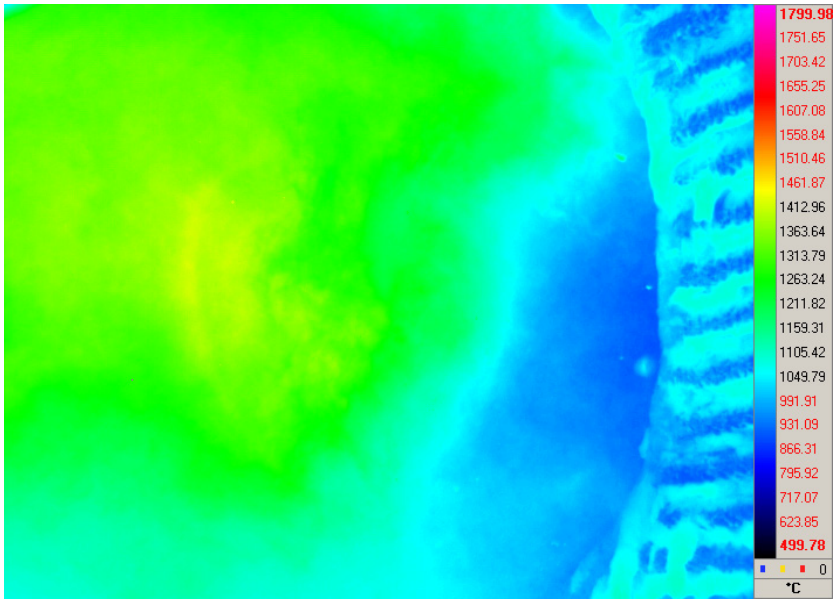

Figure 24 Thermal image of near burner field. Burner seen from port A ”testfile09.ptw” frame 518. Fuel: coal + straw. Date: 19 Oct. 2009. IR-camera with 3.9 µm optical filter and 24 µs exposure time. Direct view with IR-camera without endoscope optics. Colour scale is in °C.

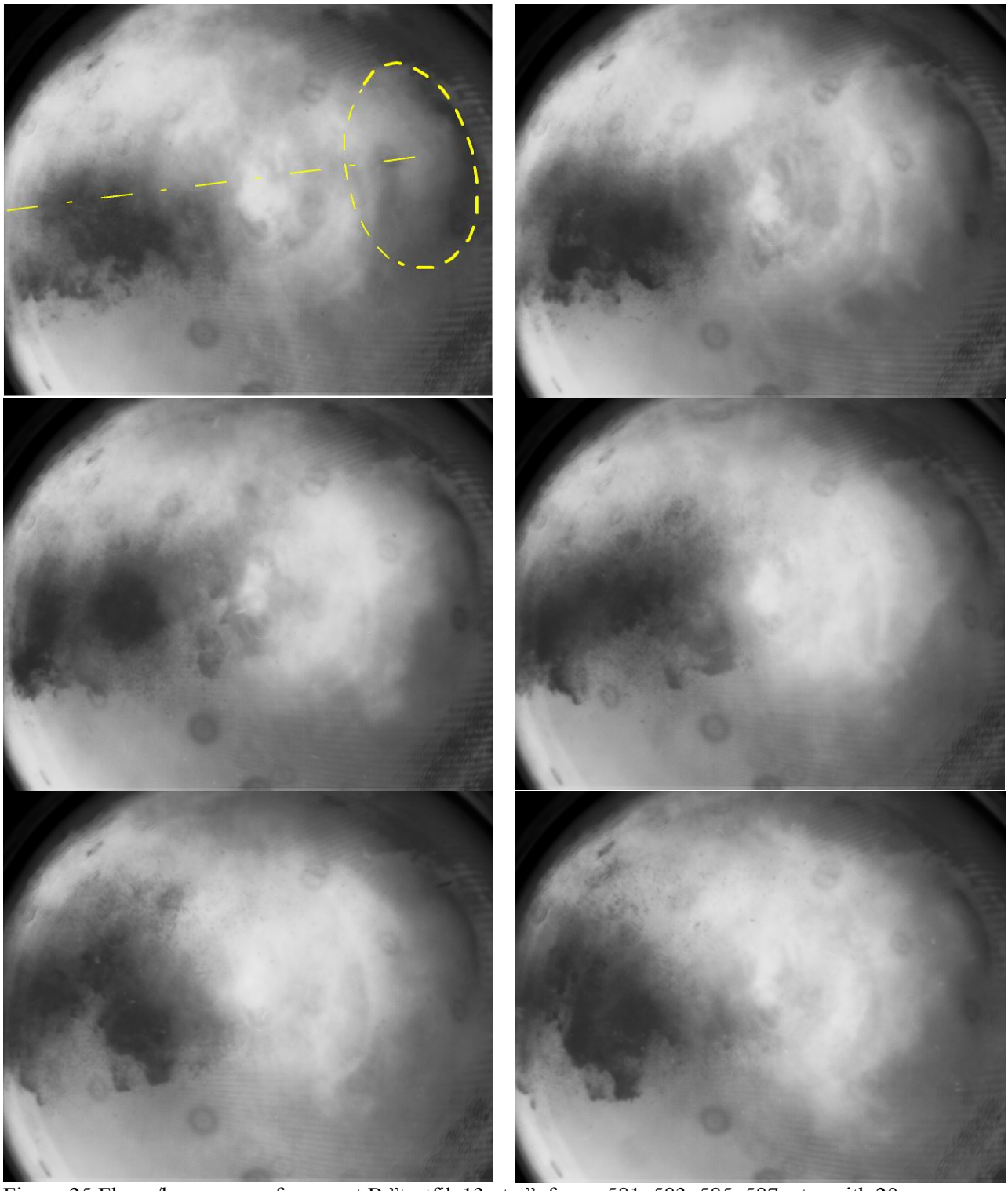

Figure 25 Flame/burner seen from port B ”testfile13.ptw” frame 581, 583, 585, 587, etc. with 20 ms between frames. Circle with yellow dashed line illustrate the quarl of burner exit and the dashed line geometrical centre line of burner in first picture. Movement of straw particle structures in direction away from burner (from right to left in pictures) can be tracked by eye in images. Large variations in straw particle density locally is observed between burner and port B. Endoscope optic mounted on IR camera, 3.9 µm optical filter and 333 µs exposure time.

Brightness temperature image (emissivity set to 1.00) of coal-straw flame with 3.9 µm optical filter in shown in figure 24. Surface/particle temperatures of approx. 850°C (blue region) is observed inside the quarl region, but surface temperatures of particles increase to approx. 1250°C (green region, figure 24) shortly after leaving the burner. Particle temperatures are probably significantly lower in the core of the flame which cannot be seen due to the high density of particles.

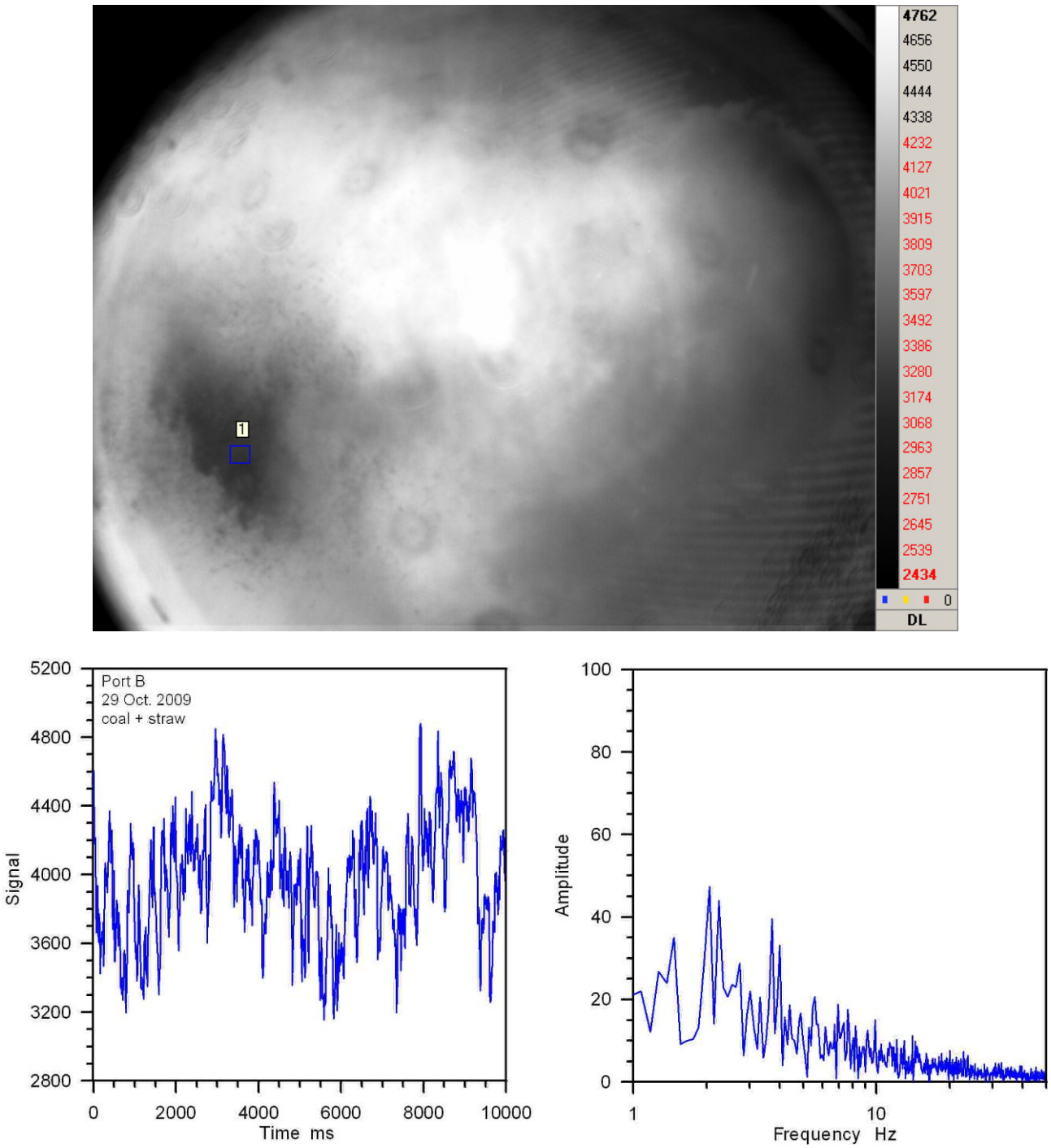

Figure 26 Example of intensity fluctuations found from thermal images of flame from port B, based on 1000 frames in file ”testfile13.ptw”. “1” is area of interest analysed shown in image. Fluctuations have an approximately 1/f noise power spectrum, plot at right.

Intensity fluctuations in the IR pictures, figure 26, reflect fluctuations of fuel particle concentration and temperature. Fluctuations have an approximately 1/f noise power spectrum, i.e. frequency spectrum is inversely proportional to the frequency. "1/f-like" noises occur widely in nature. In this system it can be seen as a *long-term effect*, where something suddenly happens like straw moves from one side of burner to another, suddenly no straw flow, etc.

Surface temperature of flame (fuel particles) is lower in burner region for the coal-straw flame than the pure coal flame. Similar, upper part of coal-straw flame is hotter than the lower part. Temperature field of coal-straw flame is less stable with large structures in temperature field and ignition happens sometimes outside burner.

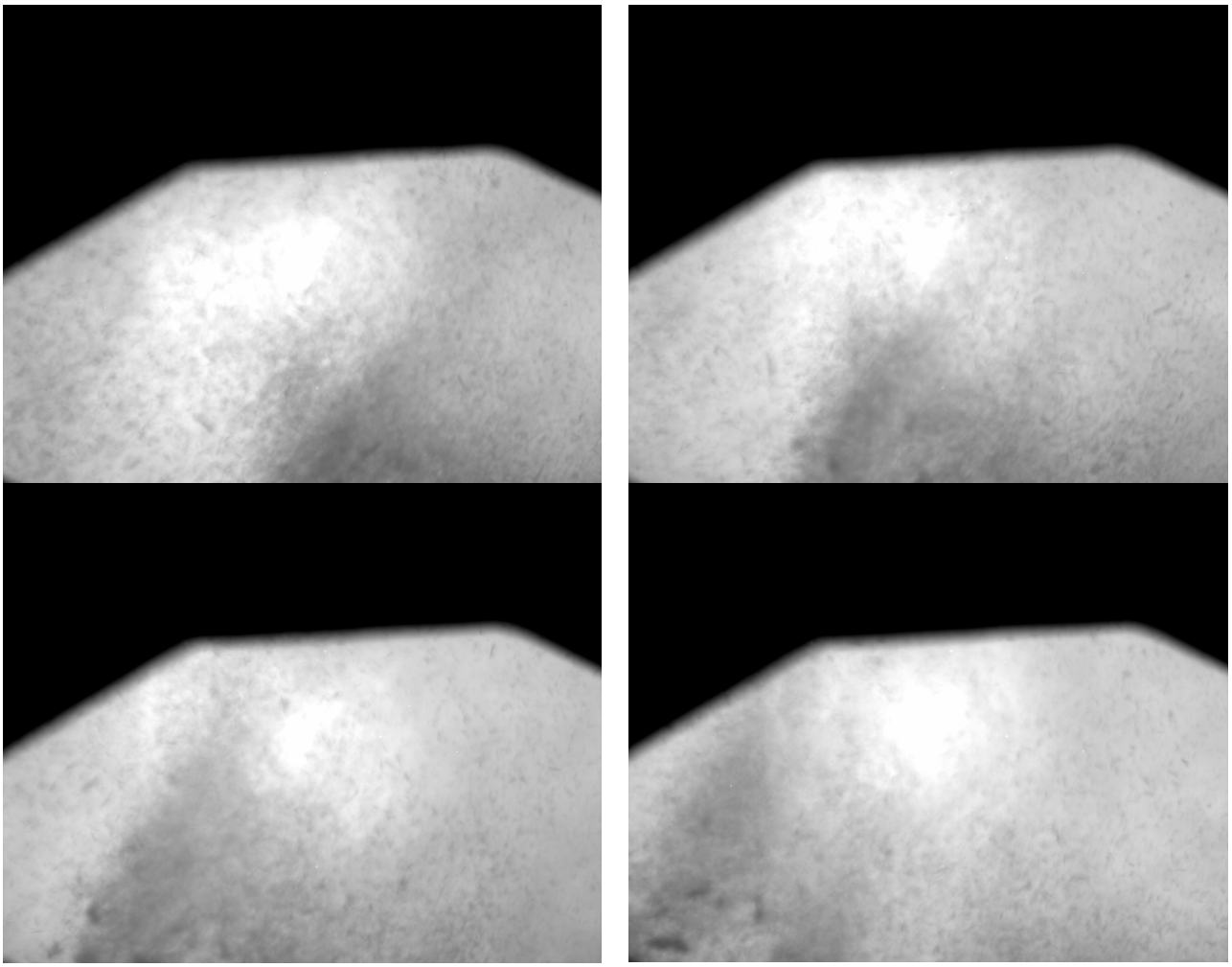

Figure 27 Straw particles seen from port B ”testfile07.ptw” frame 929, 931, 933 and 935 with 20 ms between frames. Movement of straw particles in structures (from right to left in pictures) can be tracked by eye in images. Straw particle densities vary locally at port B. IR-camera with 3.9 µm optical filter and 24 µs exposure time.

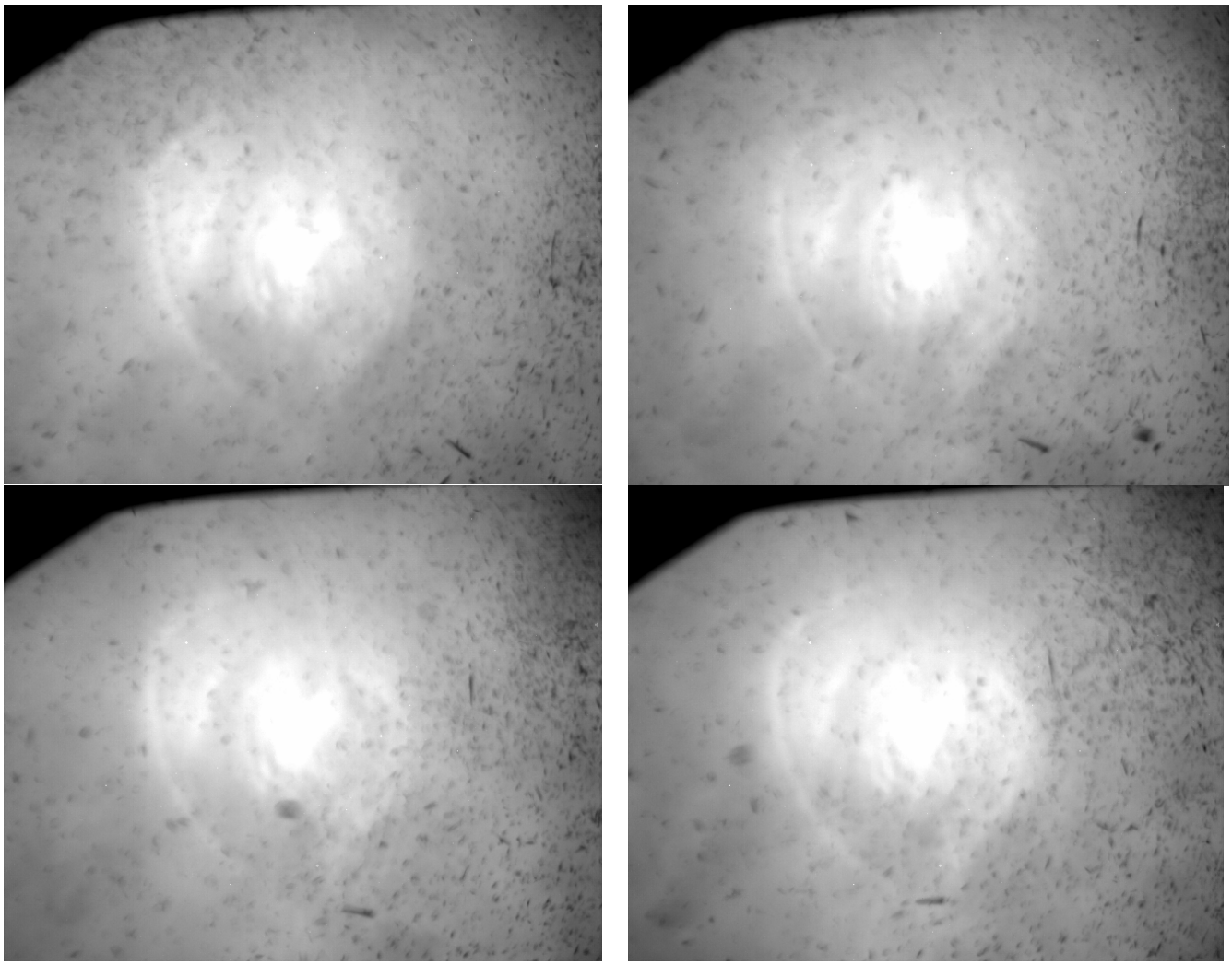

Figure 28 Straw particles seen from port C ”testfile05.ptw” frame 230, 231, 232 and 233 with 10 ms between frames. Movement of large straw particles can be tracked by eye in images. Straw particle appears to be spread fairly uniform at port C most of the time. IR-camera with 3.9 µm optical filter and 24 µs exposure time.

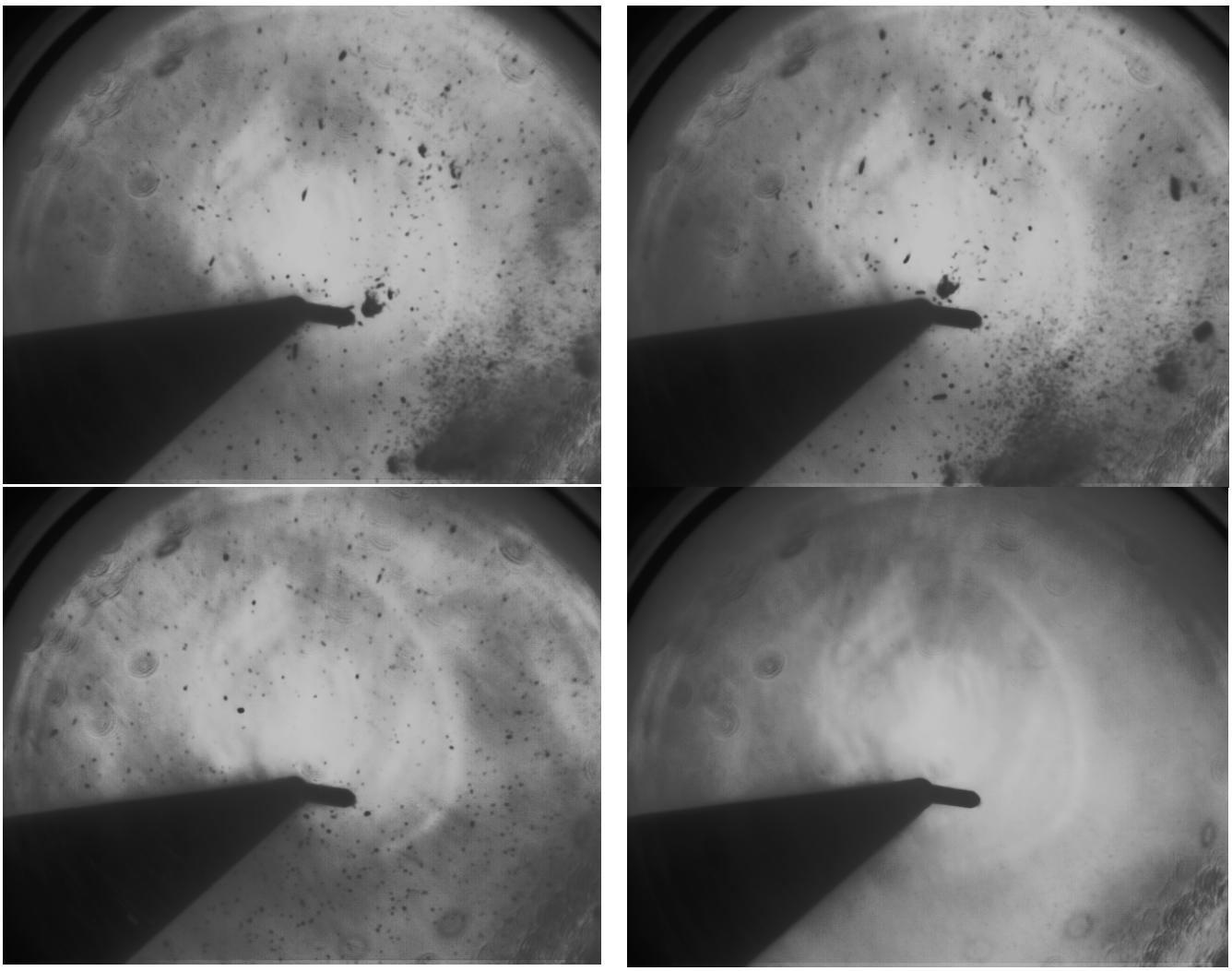

Figure 29 Straw particles seen from port D ”testfile18.ptw” frame 944, 946, 986 and 786 (no straw particles seen). Probe for sampling of particles, seen in pictures, was inserted 1.5 m. Endoscope optic mounted on IR camera, 3.9 µm optical filter, 100 Hz recording rate of pictures and 333 µs exposure time.

The distribution of straw particles is still not uniform in tale of flame as seen from images recorder at port D (6.72 m from burner wall). Large moving structures with high concentration of straw particles are still seen. This behaviour can cause problems with poor conversion of straw particles as particles transported in structures with low temperature and thermal heat transfer by radiation to particles is strongly reduced.

Velocity of moving structures can be found if distance to structure is known, e.g. a lump of straw particles close to particle sampling probe tip is seen in first 2 images shown in Figure above. Δx = 0.18 m (structure close to 18 cm wide tip of probe and moves horizontal) and Δ= 20 ms (two frames between images) giving a velocity of 9 m/s.

4.2 Coal-wood flame

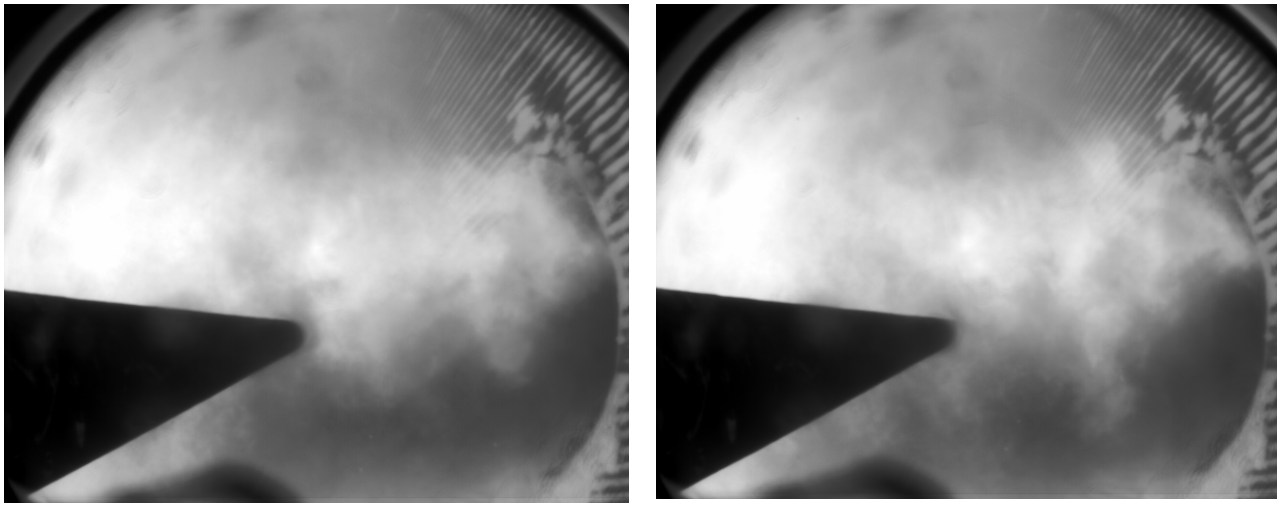

Figure 30 Coal-wood flame seen from port A ”wood50.ptw” frame 257 and 258. Probe for sampling of particles is seen in pictures, was inserted 2.4 m and tilted 12.1°. Endoscope optic mounted on IR camera, 3.9 μm optical filter and 333 μs exposure time, 100 Hz frame rate.

Hot particles in upper boundary of flame are moving to the left and downwards in pictures in Figure 30 as expected from swirl orientation. The burner is a wall burner and ignition is likely to be affected by incoming radiation heat flux from boiler wall (900°C, 107 kW/m^2) is around a factor 4 less than from surrounding flames/hot flue gas (1400°C, 444 kW/m^2). The swirl rotates hot regions into cold regions in flame. The tip of particle sampling probe is invisible due to the large particle concentration that might limit penetration of light to 10-20 cm in pulverised flames close to burner exit (ref. 13).

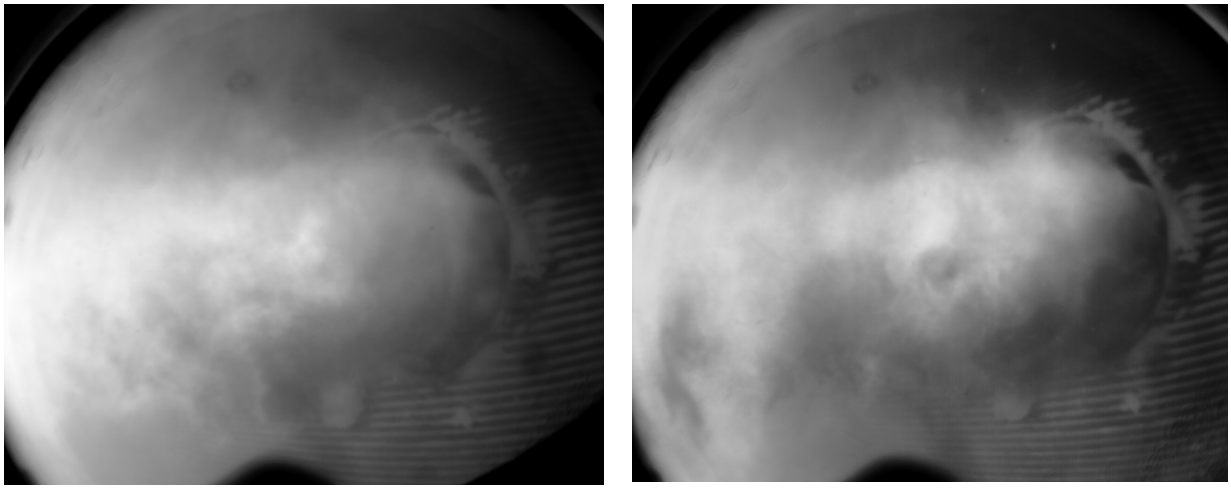

Figure 31 Situation where straw line is out (left, “wood52.ptw”, frame 92) and when straw line is up again (right, “wood54.ptw”, frame 358). Burner seen from port B with same intensity scale in both cases.

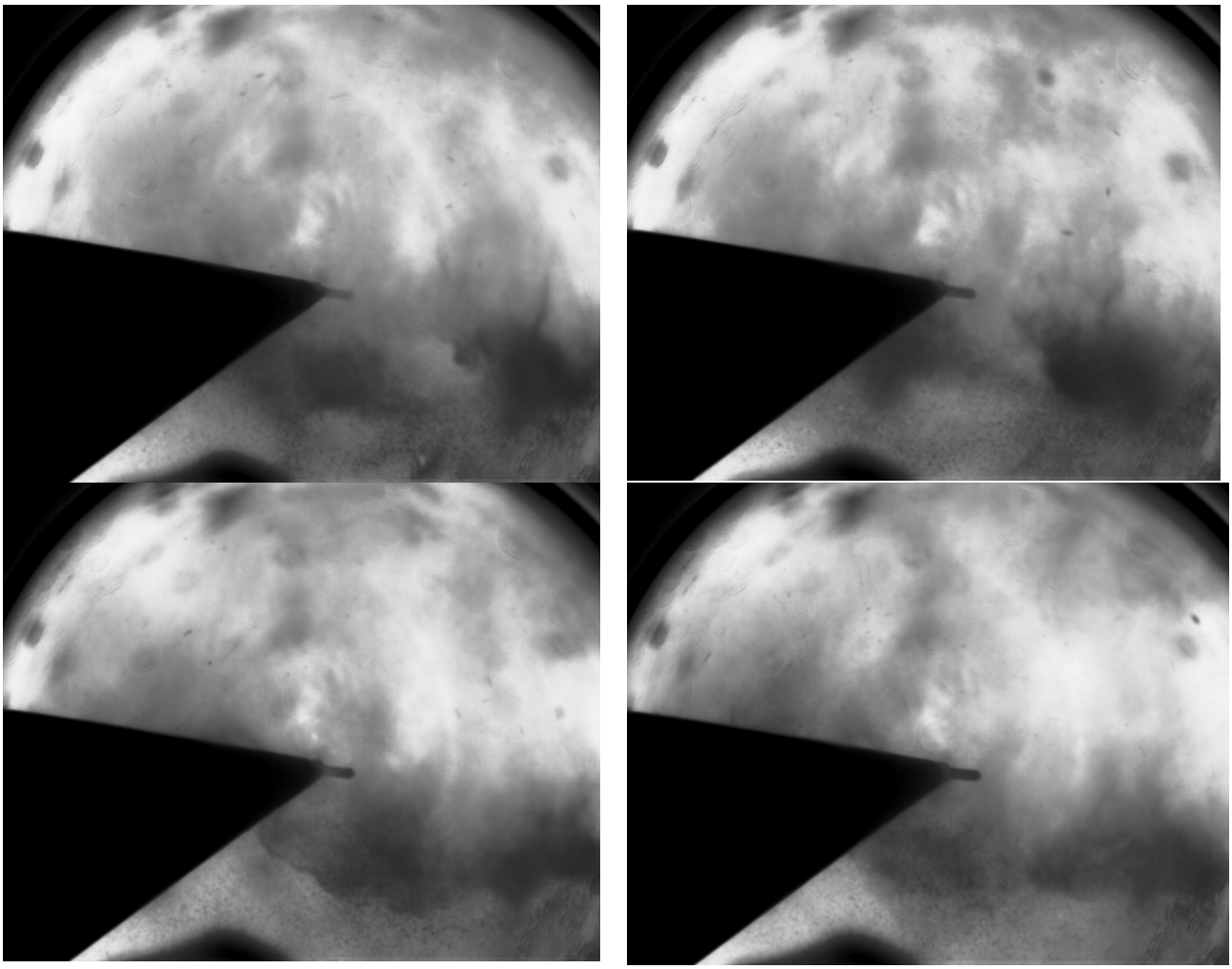

Figure 32 Coal-wood flame seen from port B ”wood51.ptw” frame 398, 400, 404 and 406. Probe was inserted 2.5 m and tilted 0°. Endoscope optic mounted on IR camera, 3.9 µm optical filter and 333 µs exposure time, 100 Hz frame rate. Wood particles are seen in lower part of flame as for the straw in coal-straw flames.

It is clear from images recorded at port B and C that the distribution of wood particles is not uniform at all in the flame. It looks more like a jet of wood particles penetrating a recirculation zone that breaks up into large structures with high concentration of wood particles.

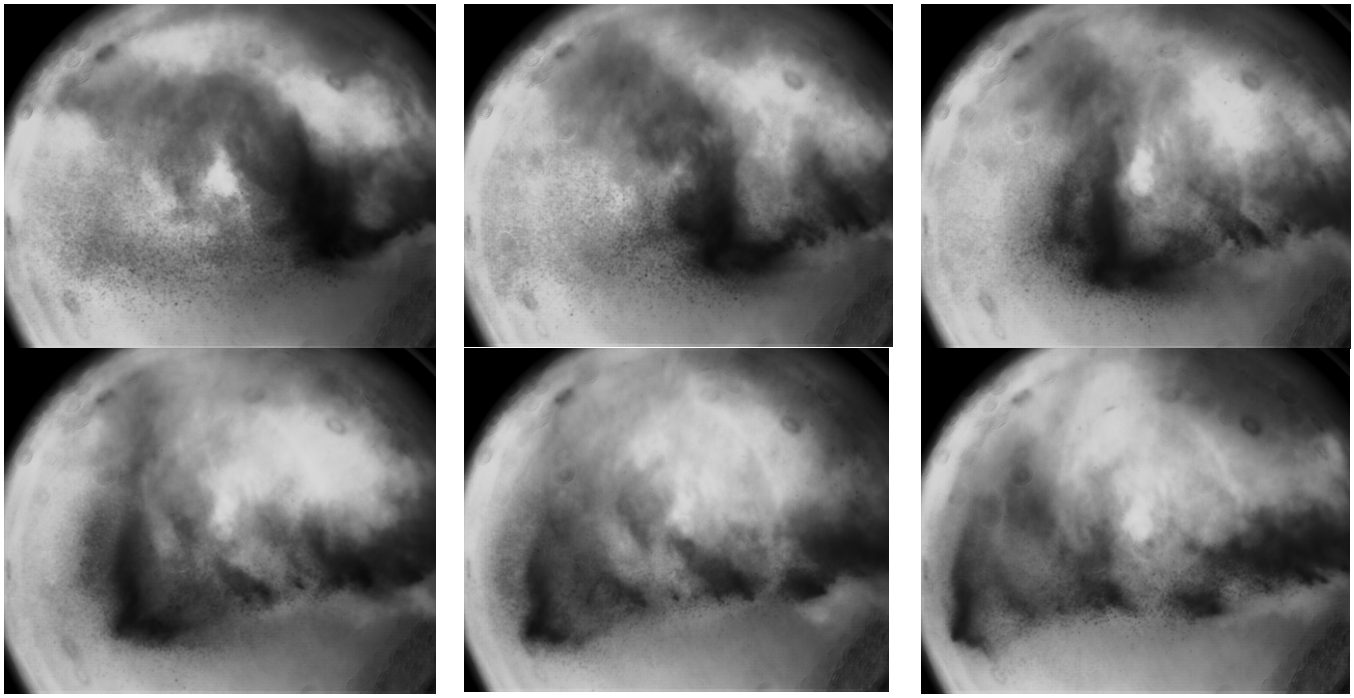

Figure 33 Coal-wood flame seen from port B ”wood41.ptw” frame 437, 440, 443, 446, 449 and 452. Movement of straw particle structures (dark zones/structures) can be tracked by eye in images. Large variations in wood particle density locally is observed between burner and port B. Endoscope optic mounted on IR camera, 3.9 µm optical filter and 333 µs exposure time, frame rate IR-camera was 100 Hz or 10 ms between images.

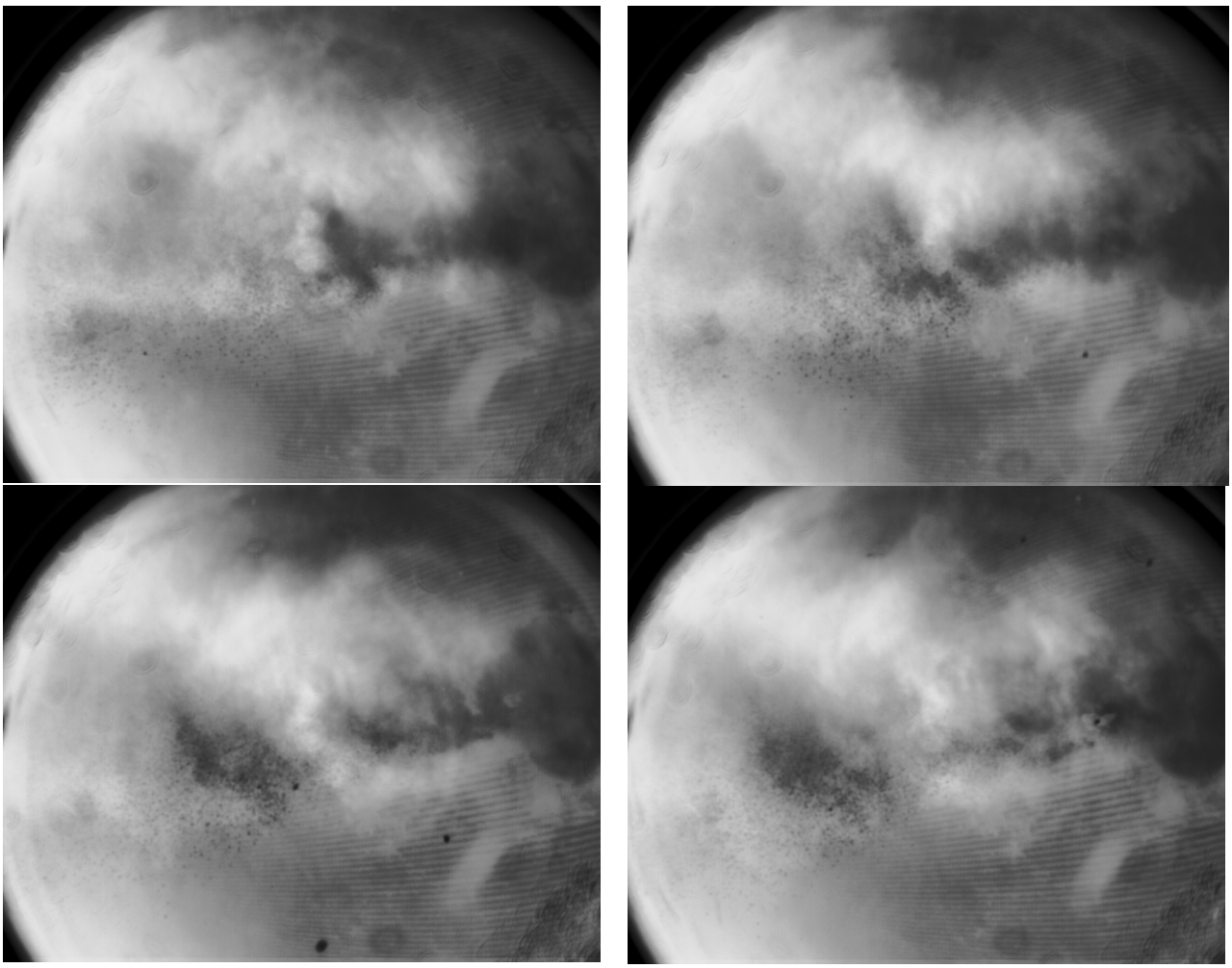

Figure 34 Coal-wood flame seen from port C ”wood43.ptw” frame 170, 172, 174 and176. Endoscope optic mounted on IR camera, 3.9 µm optical filter and 333 µs exposure time, frame rate IR-camera was 100 Hz.

Table 3 Overview thermal images of coal-straw flame

Date, time	File name	Port	Text
29/10-09, 13:39	Testfile05.ptw	C	No endoscope, 3.9 µm filter, dt=24µs
29/10-09, -	Testfile06.ptw	C	No endoscope, 3.9 µm filter, dt=24µs
29/10-09, -	Testfile07.ptw	B	No endoscope, 3.9 µm filter, dt=24µs
29/10-09, -	Testfile07-11.ptw	A	No endoscope, 3.9 µm filter, dt=24µs
29/10-09, 15:08	Testfile12-14.ptw	B	Endoscope, 3.9 µm filter, dt=333µs
29/10-09, 15:19	Testfile15.ptw	B	Endoscope, 3.9 µm filter, dt=333µs, probe 2.5 m, tilt=-11.7° (up)
29/10-09, 15:xx	Testfile17.ptw	B	Endoscope, 3.9 µm filter, dt=333µs, probe 2.5 m, tilt=13.1°
29/10-09, 16:25	Testfile18.ptw	D	Endoscope, 3.9 µm filter, dt=333µs, probe 1.5 m, tilt=-0.4°
29/10-09, 16:xx	Testfile19.ptw	D	Endoscope, 3.9 µm filter, dt=333µs, probe 2.5 m, tilt=-0.4°

Table 4 Overview thermal images of coal-wood flame

Date, time	File name	Port	Text
18/11-09, 8:43	Wood38-39.ptw	B	Endoscope, 3.9 µm filter, dt=333µs, sub1:5
18/11-09, 9:00	Wood40.ptw	B	Endoscope, 3.9 µm filter, dt=333µs, view burner
18/11-09, 9:01	Wood41.ptw	B	Endoscope, 3.9 µm filter, dt=333µs, view straight into flame
18/11-09, 9:03	Wood42.ptw	C	Endoscope, 3.9 µm filter, dt=333µs
18/11-09, 9:08	Wood43.ptw	C	Endoscope, 3.9 µm filter, dt=333µs, view burner
18/11-09, 9:12	Wood44.ptw	C	Endoscope, 3.9 µm filter, dt=333µs, view straight into flame
18/11-09, 9:27	Wood45.ptw	D	Endoscope, 3.9 µm filter, dt=333µs, view straight into flame
18/11-09, 9:44	Wood46.ptw	B	Endoscope, 3.9 µm filter, dt=333µs, 2.5 m, 0°
18/11-09, 9:50	Wood47.ptw	B	Endoscope, 3.9 µm filter, dt=333µs, 2.5 m, 5.8° (down)
18/11-09, 10:40	Wood48.ptw	C	Endoscope, 3.9 µm filter, dt=333µs, 2.5 m, 0°
18/11-09, 12:08	Wood49.ptw	D	Endoscope, 3.9 µm filter, dt=333µs, 2.5 m, 0°
18/11-09, 12:50	Wood50.ptw	A	Endoscope, 3.9 µm filter, dt=333µs, 2.4 m, 12.1°
18/11-09, 13:10	Wood51.ptw	B	Endoscope, 3.9 µm filter, dt=333µs, 2.5 m, 0°
19/11-09, 10:33	Wood52.ptw	B	Endoscope, 3.9 µm filter, dt=333µs, look at burner 49, straw out
19/11-09, 10:34	Wood53.ptw	B	Endoscope, 3.9 µm filter, dt=333µs, view into flame, straw out
19/11-09, 10:49	Wood54.ptw	B	Endoscope, 3.9 µm filter, dt=333µs, look at burner 49
19/11-09, 10:50	Wood55.ptw	B	Endoscope, 3.9 µm filter, dt=333µs, view straight into flame
19/11-09, 11:55	Wood56.ptw	C	Endoscope, 3.9 µm filter, dt=333µs, look at burner 49
19/11-09, 11:56	Wood57.ptw	C	Endoscope, 3.9 µm filter, dt=333µs, view straight into flame
19/11-09, 12:01	Wood58.ptw	D	Endoscope, 3.9 µm filter, dt=333µs, view straight into flame 18°
19/11-09, 12:02	Wood59.ptw	D	Endoscope, 3.9 µm filter, dt=333µs, view straight into flame 21°
19/11-09, 12:21	Wood60.ptw	D	Endoscope, 3.9 µm filter, dt=333µs, view 45° backwards 26° down

Table 5 Overview thermal images intensity versus temperature of blackbody

Date, time	**File name**	**Port**	**Text**
19/11-09, 13:53	Wood62.ptw	-	Endoscope, 3.9 µm filter, 333µs, T_{BB} = 500°C -> I = 1030±8
19/11-09, -	Wood63.ptw	-	Endoscope, 3.9 µm filter, 333µs, T_{BB} = 25°C -> I = 676±8
19/11-09, -	Wood64.ptw	-	Endoscope, 3.9 µm filter, 333µs, T_{BB} = 700°C -> I = 1605±21
19/11-09, -	Wood65.ptw	-	Endoscope, 3.9 µm filter, 333µs, T_{BB} = 800°C -> I = 2002±29
19/11-09, 14:32	Wood66.ptw	-	Endoscope, 3.9 µm filter, 333µs, T_{BB} = 900°C -> I = 2397±14

5 Extractive gas sampling

Extractive gas sampling is usually the preferred method in flame measurement. The combination of extractive and optical method in the project is used for comparison of results in complex flame measurements.

5.1 Gas sampling line and movable gas measurement bench

Two 50 cm long gas cells for simultaneous UV/IR-absorption measurements, a sophisticated paramagnetic oxygen analyzer, calibrated mass-flow controllers, a pressure gauge and a pump are used in order to make gas measurements and control pressure and gas flow during measurements. The data acquisition system continuously records the main sampling parameters such as sampling gas flow, gas temperature, pressure in the UV/IR gas cells and oxygen concentration. The temperature in the gas sampling line (from the probe to the tow gas cells) is kept constant at 150ºC by electronically controlled heaters. A Bomem MB100 FTIR spectrometer with the built-in IR light source and external DTGS detector is used for IR-absorption measurements. For UV-absorption measurements a highly-stable D2-lamp is utilized as a light source. UV-absorption spectra record with Acton 0.5 m spectrometer equipped with a UV enhanced CCD camera.

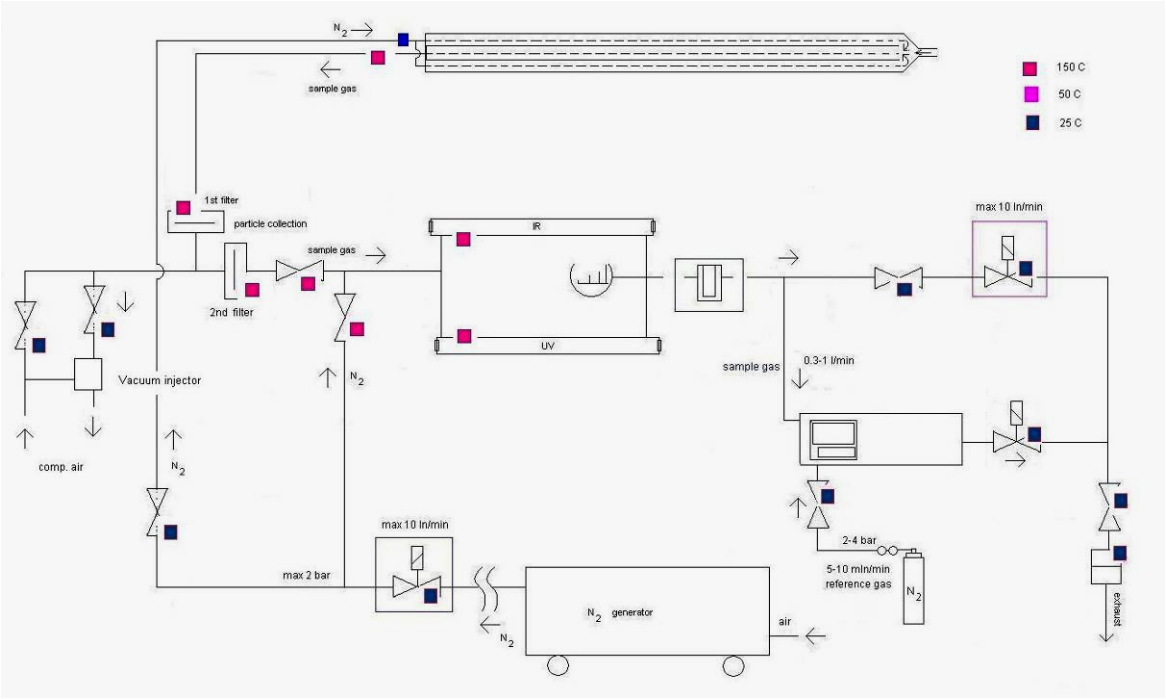

Figure 35 Diagram of gas sampling system.

In the measurement campaigns UV absorption spectroscopy has been used for measurements of SO_2 and NO concentrations, whereas IR absorption spectroscopy is used for measurements of H_2O, CO_2, CO and SO_2 concentrations. UV and IR SO_2 absorption measurements have always shown an excellent agreement, see Ch. 5.1.1. A general view of the movable gas measurement bench is shown in Figure 36.

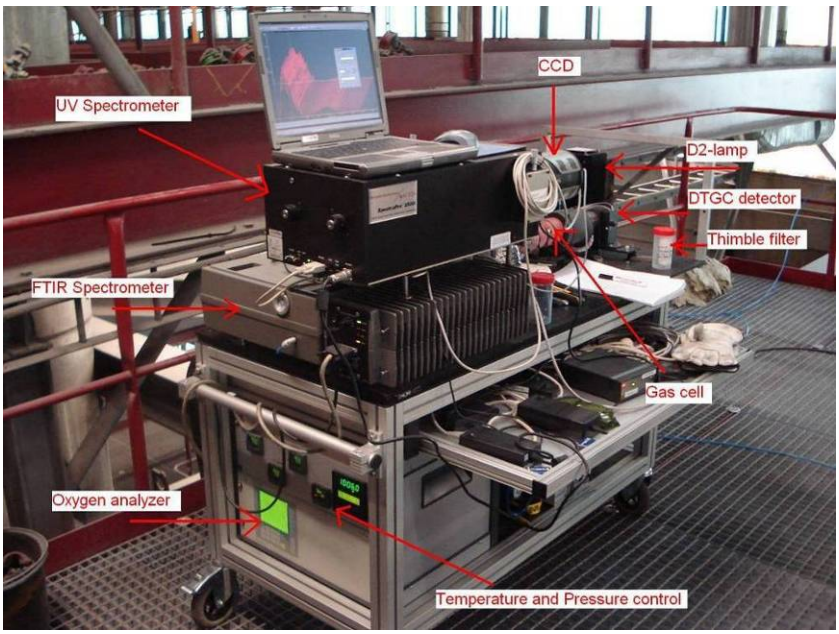

Figure 36 A general view of the movable gas measurement bench used during measurements at SSV4 unit.

5.1.1 Set-up calibration for oxygen and IR/UV absorption measurements

Performances of the movable gas measurement bench and data analysis approach in UV/IR absorption measurements have been proven on various reference gas mixtures: N_2+NO, N_2+SO_2, N_2+CO_2 and N_2+H_2O at concentrations of the species under interest typical in combustion.

In Figure 37a part of SO_2 UV absorption cross section spectrum measured in the UV gas cell (upper panel, blue) at 150^{o}C together with data available from the work Manatt *et al* (1993) (lower panel, red, 20^{o}C) is shown. This absorption band has been used in SO_2 concentration calculations because validity of the Lambert-Beer absorption law at SO_2 concentrations up to 1300 ppm. Although spectra in the Fig. 5 were measured at different spectral resolutions and temperatures (the later causes broadening of the band fine structure) the integral over the SO_2 absorption band in 240-335 nm remains the same: 3.406×10^{-17} and 3.419×10^{-17} for experimental spectrum and spectrum from the work Manatt *et al* (1993), respectively.

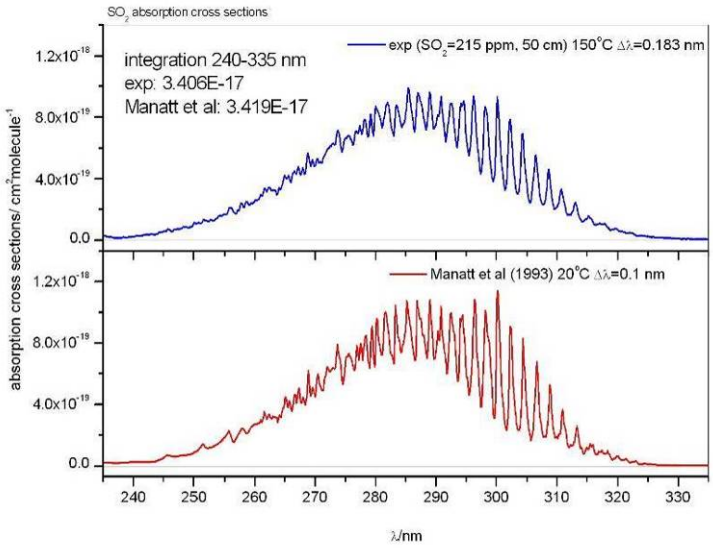

Figure 37 Apparent SO_2 absorption cross sections measured in the UV gas cell at 150°C, SO_2=215 ppm, L=50 cm, p=1.050 bar and $\Delta\lambda$=0.183 nm (upper panel, blue) and SO_2 absorption cross sections from the work Manatt *et al* (1993) at 20°C and $\Delta\lambda$=0.1 nm (lower panel, red).

Non-linear effects in NO(A_0-X_0) absorption band, λ=226 nm, which has been chosen for NO concentration calculations appear at NO>700 ppm. However with a proper correction in the Lambert-Beer law absorption measurements can even be done at higher NO concentrations. In Figure 38 CO_2 (10%) IR reference transmission spectrum measured in the IR gas cell is shown (upper panel, blue). In the lower panel calculated CO_2 transmission spectrum at the same conditions based on HITEMP-1000 database is also shown (red). One can see very well agreement between measurements and calculations.

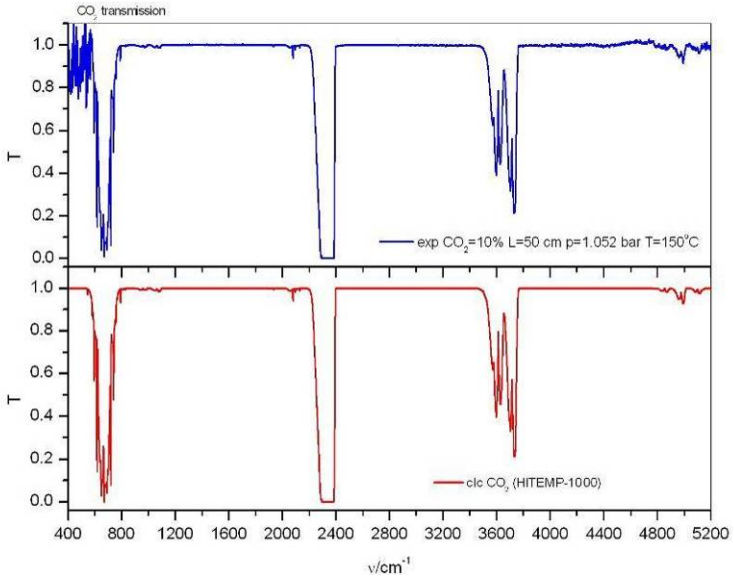

Figure 38 Reference CO_2 transmission spectrum measured in the movable gas measurement bench at 150°C, CO_2=10%, L=50 cm, p=1.052 bar and $\Delta\nu$=2.5 cm^{-1} (upper panel, blue) and calculated one based on HITEMP-1000 database at the same conditions (lower panel, red).

A deviation between integrals calculated over the third CO_2 absorption band (3492.80-3776.30 cm^{-1}) from experimental and calculated (HITEMP-1000) spectra is 1.4% that is a quality of the database. The third CO_2 absorption band calculated based on HITEMP-1000 database has been used in CO_2 concentration calculations with a correction to non-linear absorption in Lambert-Beer law that starts to be observed at CO_2 > 2%.

Water absorption can also be calculated with use of HITEMP-1000 database. However in the range used for calculations of water concentration from the experimental spectra, 2865-4231 cm^{-1}, a deviation between calculations and a reference N_2+H_2O(10%) absorption spectrum is about 18%, Figure 39 (upper panel). Reference spectra at H_2O(10%) and H_2O(15%) are matching within around 8%, Figure 39 (lower panel). Therefore measured reference water band (2865-4231 cm^{-1}) at H_2O(10%) has been used in the data analysis.

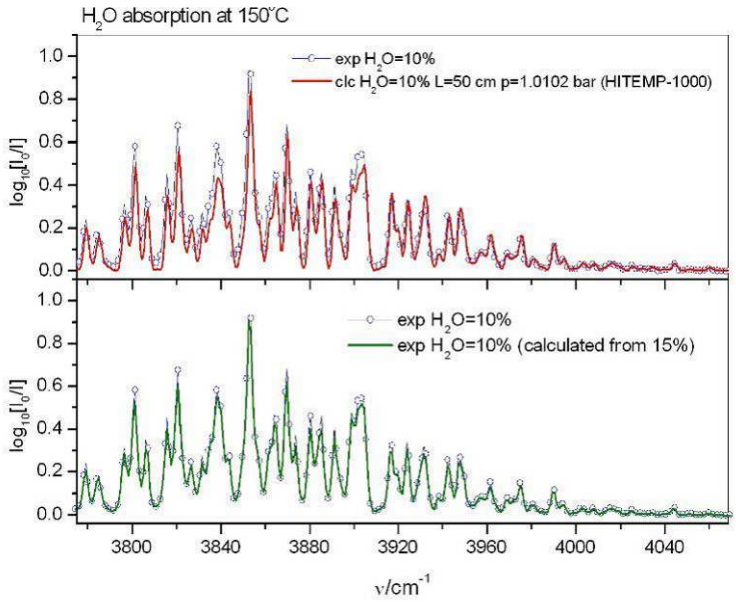

Figure 39 Upper panel: a reference H_2O (10%) absorption spectrum in 2865-4231 cm^{-1} (blue opened circles) and it calculation based on HITEMP-1000 database (red line). Lower panel: reference H_2O (10%) absorption spectrum (blue opened circles) and calculated H_2O(10%) spectrum (olive) from the reference H_2O=15% one. L=50 cm, p=1.0102 bar. Resolution $\Delta\nu$=2.5 cm^{-1}.

A reference and calculated SO_2 (489 ppm) absorption spectra (based on HITRAN-2004) are shown in Figure 40 (upper panel). As one can see the database gives underestimated integral absorption (13.2%) in 1300-1405 cm^{-1} used for SO_2 calculations. Reference spectra measured at two different SO_2 concentrations (489 and 1037 ppm) can be matched (0.03%), Figure 40 (lower panel). Therefore the reference SO_2(489 ppm) absorption spectrum has been used in SO_2 calculations.

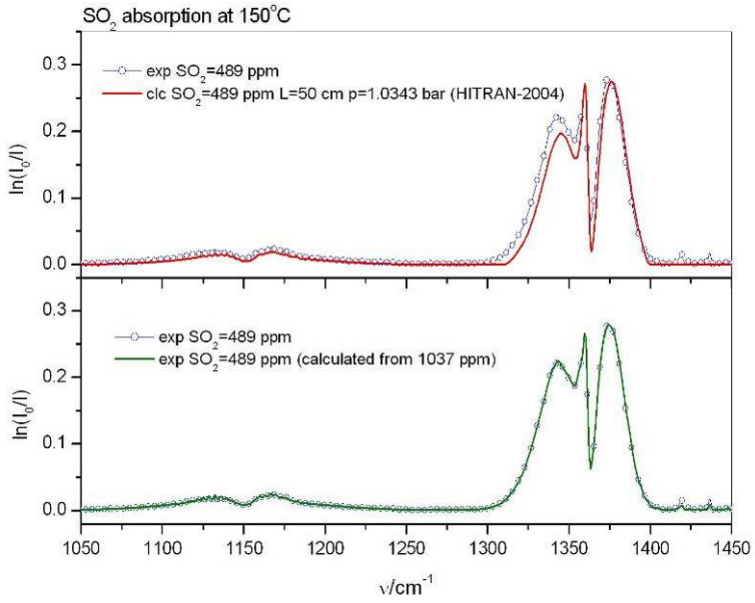

Figure 40 Upper panel: a reference SO_2(489 ppm) absorption spectrum (blue opened circles) and it calculation based on HITRAN-2004 database (red line). Lower panel: reference SO_2(489 ppm) absorption spectrum (blue opened circles) and calculated SO_2(489 ppm) spectrum (olive) from the reference SO_2(1037 ppm) one. L=50 cm, p=1.0343 bar. Resolution $\Delta\nu$=2.5 cm^{-1}.

Oxygen paramagnetic analyzer calibration has been checked at N_2(100%), ambient air and O_2(100%) as the "sampling" gas flows. It was found excellent agreement between all measurements.

5.2 Results extractive gas sampling

Extractive gas concentrations for O_2, CO_2, H_2O, CO, SO_2, NO, HCN, CH_4, C_2H_2 and C_2H_4 are given for each measurement point with reference to measurement port and distance from inner boiler wall. Extrative gas concentration measurements and details about positions can be found in Excel files "18112009.xls" for coal-wood flame, "19112009.xls" for coal flame, and "27102009.xls" and "28102009.xls" for coal-straw flame. Selected results are plotted in the following.

5.2.1 Coal-Straw flame

The coal-straw flame in regions with high content of large straw particles, yellow zones in plots in figures below, was the most difficult flame to map as the sampling line is blocked shortly after gas is extracted from probe. Late combustion arises in coal-straw flame seen from CO_2 level at port B and C compared pure coal and coal-wood flame. Raise in CO level at distance over 4 m from boiler wall is likely to be caused by neighbour flame 2.52 m beside burner.

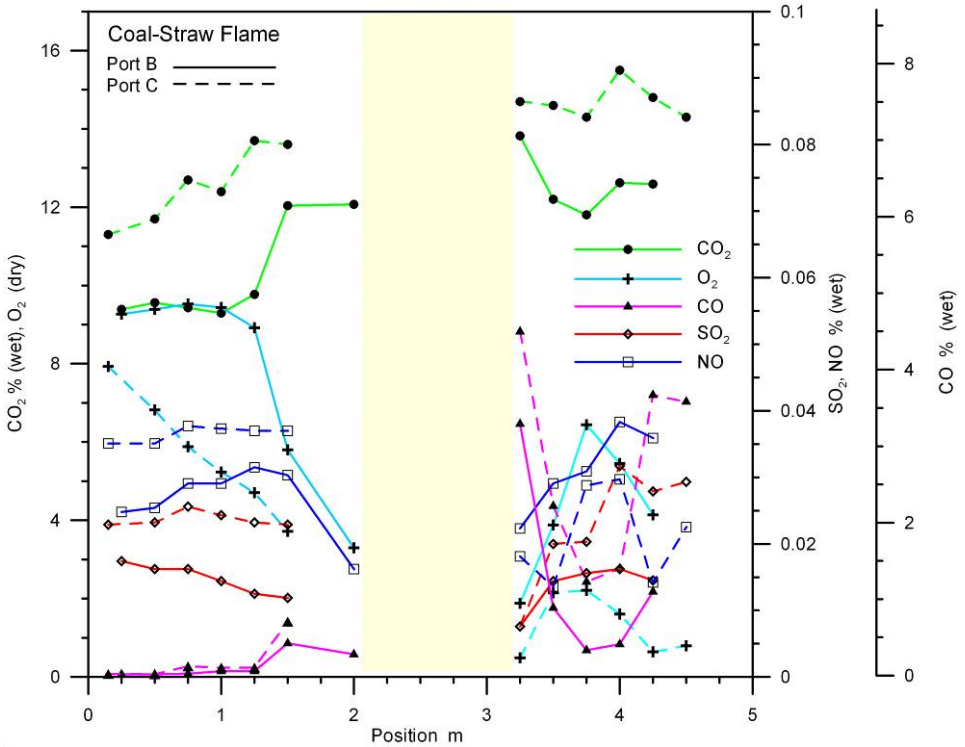

Figure 41 Selected gas concentrations measured in coal-straw flame by extractive sampling at port B and C, 2.62 m and 4.02 m from burner wall. Measurement points at 1.75/2.25 – 3.0 m (yellow region in plot) were not collected due problems with blocking of extractive probe due to high particle load.

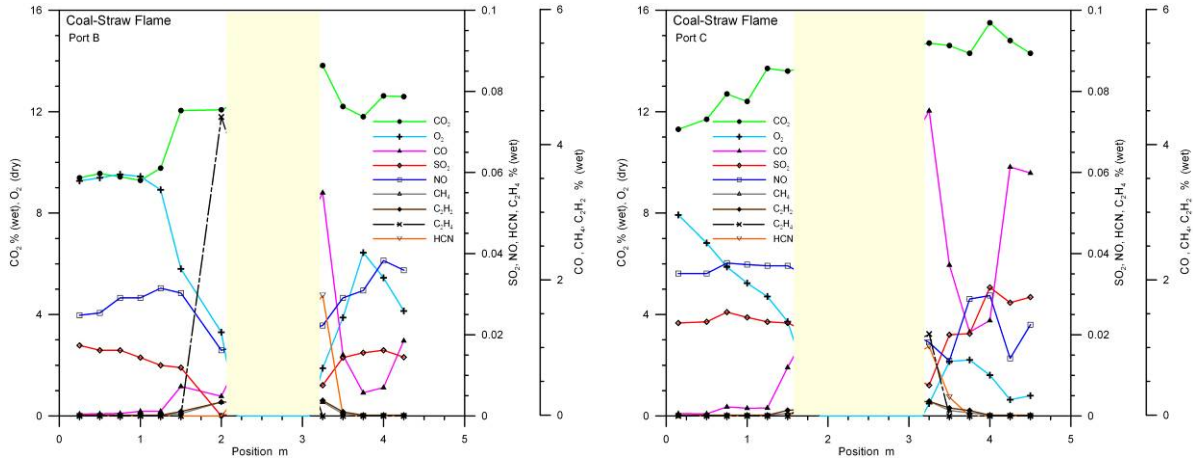

Figure 42 All gas concentrations measured in coal-straw flame by extractive sampling at port B and C.

5.2.2 Coal-Wood flame

CO_2 and O_2 profiles at port B and C differ from coal-straw flame in many ways, e.g. O_2 level is higher at port C than B for coal-straw flame and flame is wider (seen from CO profile). Very high levels of hydrocarbons are seen compared to two other flames, i.e. large amounts of volatiles is released from wood particles at port B and C.

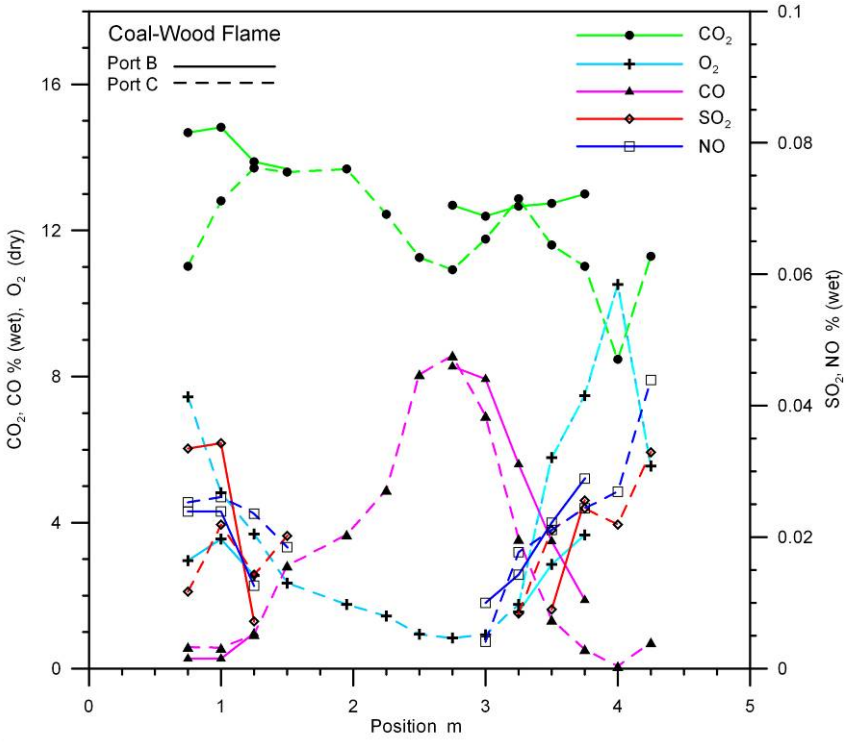

Figure 43 Gas concentrations measured in coal-wood flame by extractive sampling at port B and C, 2.62 m and 4.02 m from burner wall. Measurement points at 1.75 – 2.75 m were not collected at port B due problems with blocking of extractive probe.

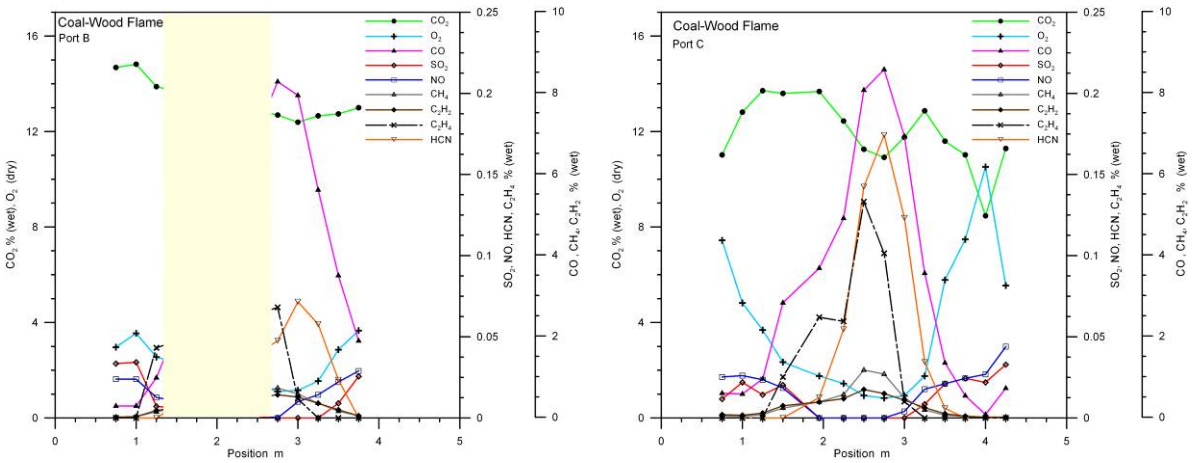

Figure 44 All gas concentrations measured in coal-wood flame by extractive sampling at port B and C.

5.2.3 Coal flame

The pure coal flame was mapped as reference for comparison with coal-straw and coal-wood flame. Centre of flame moves away from boiler wall towards neighbour flame which is not seen for the two other flames.

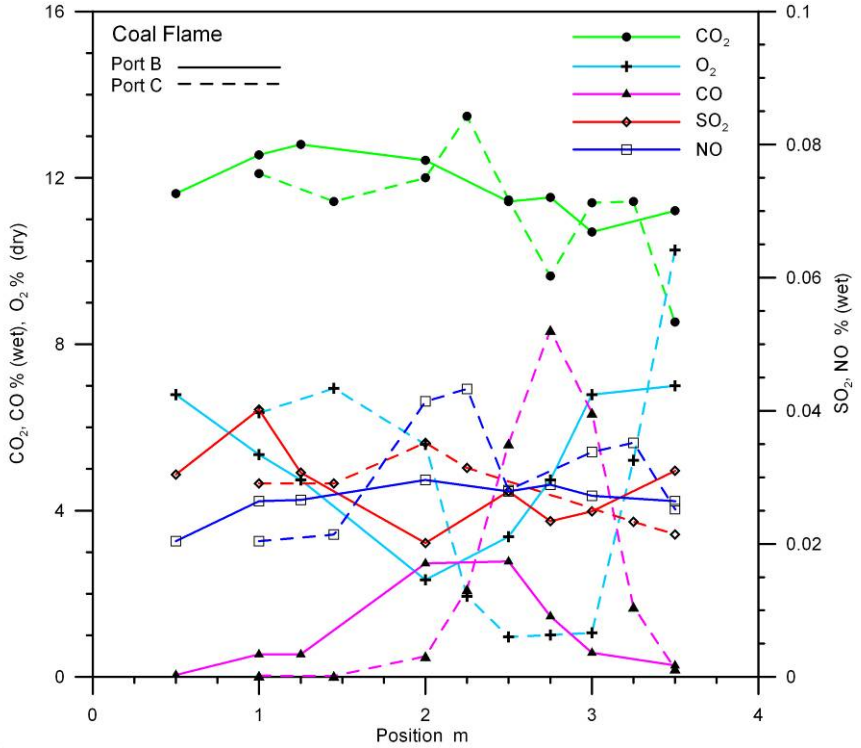

Figure 45 Gas concentrations measured in coal flame by extractive sampling at port B and C, 2.62 m and 4.02 m from burner wall.

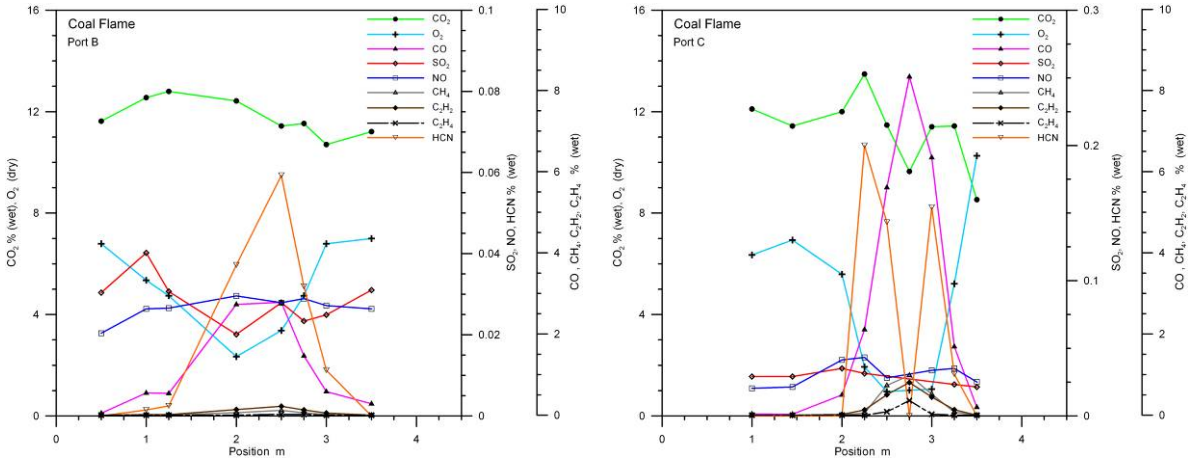

Figure 46 All gas concentrations measured in coal flame by extractive sampling at port B and C.

6 Particle sampling and results

It is important that inlet of particle collecting tip is cold. Any hot spot will start-up deposit of slag and particles and will over time affect the particle sampling as hole is partially blocked. Sharp edge of particle collecting tip was therefore rounded.

Particles were sampled in several locations throughout the 3 co-fired flames. The three flames included: a coal-short straw (straw passes through 16mm mesh), coal-long straw (straw passes through 32mm mesh), and coal-wood flames, hereafter referred to as the SS, LS, and Wood flame. An attempt was made to sample particles isokinetically so samples collected could give an indication of particle loading throughout the flames. Visual inspection of the particle samples provide general information about mixing of the two fuels and combustion stage of the particles. Proximate and ultimate analysis including ash composition was performed by Dong Energy's Chemical Laboratory located at the Ensted plant. This data provides a more quantitative coal-biomass split along with quantitative burnout data.

6.1 Particle Sampling Setup

Particle extraction measurements rely on LDA data to attempt isokinetic (constant velocity) sampling. However, it is difficult to define isokinetic sampling from within a highly turbulent, swirl-stabilized flame. Because the flame consists of fluctuating flamelets and turbulent flow that fluctuates faster than the response time of a sampling system, isokinetic sampling can be defined as measuring at a rate that ensures the sampling velocity is equal to a mass-weighted average of the flow velocity.

The majority of the large particles do not follow the gas flow within the flame. This is most easy to understand in the internal recirculation zone (IRZ), through which the large particles penetrate due to momentum. With decreasing particle sizes, the particles will decelerate to a greater degree. With very small particle sizes, the drag forces on the particles cause the particles to turn and essentially follow the gas flow. For coal, the majority of particles by particle count do follow the gas flow and this may be true for biomass also depending on particle size distribution, but the majority of the particle flow by mass is expected to penetrate through the IRZ. The conversion history of all particles is interesting, but that of the larger particles has a higher priority in this work, so the probe head will be turned towards the burner for all measurement positions. Gas velocities outside the IRZ zone still fluctuate but to a lesser extent.

The general particle extraction setup schematic appears in Figure 47. Dry N_2 is used for quench and ideally a quench rate of 7-10 times the sampling rate is desired to quench homogeneous and heterogeneous reactions. The rest of the equipment design is selected/designed based on knowledge from particle extraction at BYU (Damstedt, 2007, Wu et al., 2007).

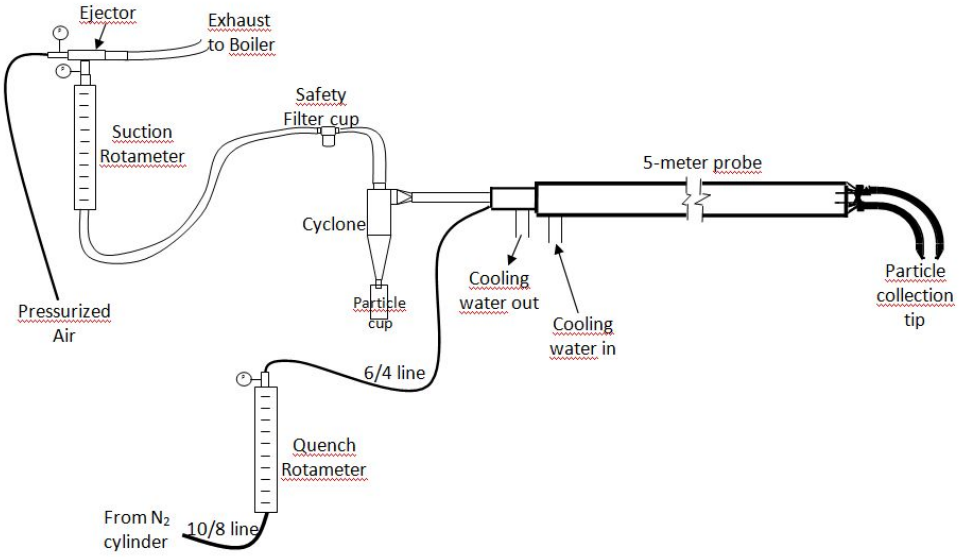

Figure 47 Schematic diagram of particle extraction equipment.

The particle extraction probe head was designed to collect particles through the 5-m probes (Figure 48). This view clearly shows the outer 2 annulus for water supply and return to the tip and the inner annulus for carrying quench gas to be injected into incoming sample flow approximately 1 cm from the tip. The inner diameter (ID) of the sampling tube (inner tube) is 16.6 mm. This was limited by the bottleneck in the quench gas annulus created by connecting the probe head to the probe with a straight nipple. All the other tubes were also reduced to minimize flow disturbance, but still allowing for adequate cooling of the probe tip. The outer diameter (OD) of the tip is 38.1 mm compared to 60.3mm diameter probe. Figure 50 is a representation of the probe head built at BYU's Precision Machining Laboratory.

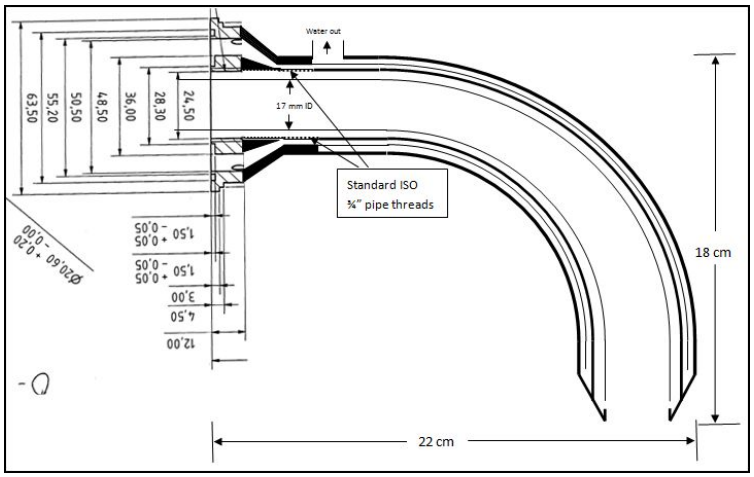

Figure 48 Cross-section view of particle sampling probe head with dimensions.

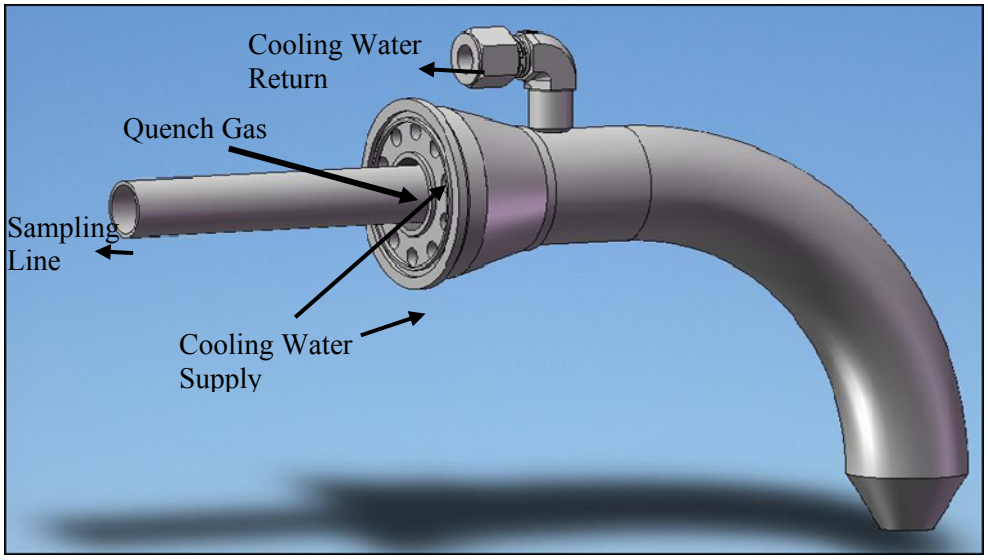

Figure 49 Particle sampling probe head.

Several different cyclone designs were considered. One was designed according to guidelines given in Perry's Handbook and compared to several designs derived from correlations in Aspen. The chosen design was a scale up of the SPS High Efficiency cyclone in Aspen. This design had a 50% cut-off particle diameter of 1.6 µm, but simulations failed in Aspen due to plugging concerns. The final design was scaled up to minimize plugging, but with a decrease in efficiency. It has a 50% cut-off diameter of 4.3 µm for coal and 7 µm for straw. There were still some plugging problems at the point where the inlet changes from around to rectangular inlet. However, these occurrences were rare enough to allow particle collection at all desired positions.

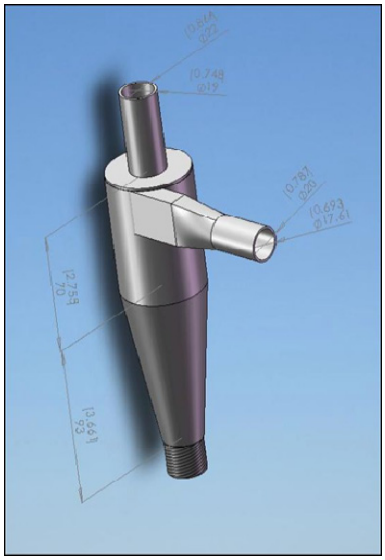

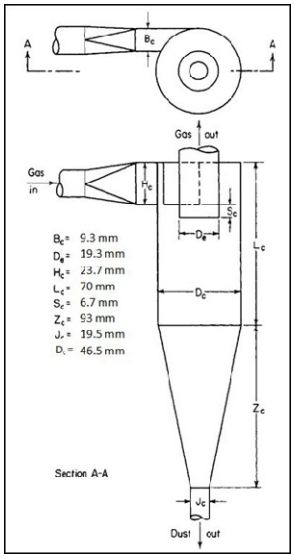

Figure 50 Solid-Gas separating cyclone with 50% cut-off diameter of 4 microns. Image on right with dimensions is modified from Perrys p. 17-27

A few problems were encountered during particle collection tests. Larger particles sometimes passed through the cyclone and got stuck in the rotameters, making them unreliable. Through observation, it was found that a clump of particles would randomly enter the cyclone at once. This was either due to the fuel agglomerating in the feeding system or a partial plug in the probe tip or cyclone entrance. In case of a plug, a vacuum of up to (down to) -0.2 barg would build up downstream and the pressure drop could cause the plug to break free. This brief moment of high particle loading in the cyclone would break the cyclone flow pattern and some large particles could get sucked into the exhaust. This problem was mitigated by placing a safety filter with 1 mm filter holes downstream of the cyclone.

Another problem was the very fine particles that passed through the cyclone and safety filter. Some of the particles would deposit on the rotameter (variable area flow meter) walls and float. This would again make the flow measurement unreliable. The air supply to the ejector was stable due to being passed through a pressure regulator, so if there was no plugging and the deposition amount was low, the flow through the rotameter was assumed constant. However, as the safety filter started to collect more particles, the pressure drop in the system increased and thus the ejector flow needed to be increased. This problem was mitigated by controlling the sample flow rate by the pressure readings. An assumption was made that the pressure inside the boiler remained constant so the pressure drop across the system was linearly proportional to the vacuum pressure at the rotameter. The probe was taken out of the boiler and the system cleaned so the flow reading on the rotameter was reliable. Then the ejector supply pressure needed to keep an accurate flow was tabulated based on different pressure drops across the system. The pressure drops were created by blocking the probe tip by varying degrees. When the rotameter got dirty, the flow could still be kept constant by adjusting the ejector air supply pressure.

A third problem is that the particle size distribution will be biased towards the large particles because the small particles that pass through the cyclone were not collected. Ideally a collection filter with a very small retention grade (≤ 1 μm) would have been installed immediately after the cyclone. The filter would need to be changed with each change of position and included with the particles collected in the cyclone. Because the cyclone was less efficient than optimal due to upscaling to minimize plugging, this fine filter would have plugged much more than once per position. The filter would have had to be replaced several times at each point and the constant increase and decrease in system pressure drop would have made isokinetic sampling practically impossible. It would also be difficult to accurately use the sampling time data. This would have also greatly increased sampling time per point and thus decreased the number of sampling points and spatial resolution. Finally, the conversion history of the larger particles was most interesting in this project.

A fourth issue was accurately determining the sampling time which is used to estimate the particle loading at each flame position measured. During testing, partial plugging of the probe/cyclone was often a problem and it was not always evident that the sampling cup only contained sample from the current position. The majority of the plugging issues were resolved by changing the sampling standard operating procedures (SOP). Instead of turning off the sampling flow while moving the probe, this was left on and a temporary sampling cup connected to the cyclone dust outlet. Thus the probe tip would not fill particles whose momentum carried them into the probe. Once the probe was in position, the sample cup was exchanged with a new cup and sampling time was started. There still were some positions where a partial plug occurred during sampling and these positions were noted so the sampling rate will not be used in the determination of particle loading throughout the flame region.

6.2 Particle analysis

Particles samples were obtained throughout the LS, SS, and wood flames. Samples were collected along the biomass fuel centerline approximately every 50 cm. Particles were also sampled at radial positions at axial distances equal to the port locations. The number of particle samples collected in each flame is shown in Table6. High resolution CMOS images have been taken of each sample and will be used a visual means to compare relative particle conversion histories.

Table 6. Number and type of particle samples collected in each cofired flame

type of sample	SS	Wood	LS
Coal Fuel samples	6	2	1
Biomass fuel samples	4	2	1
Char samples	28	30	11

The larger portions of the biomass have been separated from the coal & small biomass particles by passing each sample through a 250 µm sieve. This size was chosen after sieving a sample on a stack of 3 sieves: 300, 250, and 180 µm. By visual inspection, no coal remained on either the 300 or 250 sieve, but a noticeable amount was retained on the 180 µm sieve. The smaller particle portions is a mixture of both biomass and coal, but will be referred to hereafter as coal and the larger fraction will be referred to hereafter as biomass. These samples are being analyzed separately.

Particles were then sent to Dong Energy's certified analysis laboratory at Enstedværket for proximate, ultimate, and ash elemental analyses. Due to small sample sizes and cost, standard analysis procedures will not always be followed. The standard methods were used for analysis of all the fuel samples including replicate measurements made for each sample because this data can directly be used as input data in modelling.

Standard methods require at least 1 gram of material for each moisture, volatiles, ash, and ash elemental composition determinations. With the exception of the biomass fraction of the wood flame samples, there is generally not sufficient sample for these determinations. Only a single determination will be made on each char sample.

A few experiments were performed at the Ensted laboratory to estimate the error or bias added by deviating from the standard methods. The volatile determination will be made on the fuel samples according to the standard method. A volatile determination will also be made on a fuel sample where only 500 mg of sample is used and again with only 250 mg. Replicate measurements will be performed with each mass to characterize the precision and accuracy dependence on sample size.

Table 7 lists the analysis to be performed on the char particle samples. The ash determination will be done by summing up the weights of the oxides of the inorganic material when in their highest oxidation state. Only a single determination will be made. Analysis of fuel samples will also include the ash and calorific value determination per standard methods. Also a double determination will be done for analysis of fuel samples. For the ash elemental analysis, the raw fuel will be digested rather than the ash from the ashing test because of concern of mineral volatilizing during the ashing test. This is consistent with what is normally done for biomass fuels (Livingston, 2007).

Table 7 Analysis to be performed on "char" samples.

Priority	Analysis	Required sample (mg)
1	Moisture analysis	1000*
2	C, H, N analysis	5
3	Ash Elemental Analysis including Cl	20-50
4	Volatile	1000*

*Less material will be used for these analysis when too little sample exists.

Images taken of the extracted particles give an indication of the combustion rates of different types of particles. The appendix contains a series of images of particles sampled mainly in the highly concentrated straw portion of the flame as you move axially into the boiler. Figure 51 displays 4 of these pictures. The very thin leaf portions and thin needle like portions of the straw burn out earliest and are almost completely burned out in the first 260 cm. However a large portion of the smashed stalk and straw knees are still very yellow as far as 350 cm into the boiler indicating these portions are still in the devolatilization stage of combustion. 450 cm into the boiler these have begun to darken indicating char oxidation is beginning. The majority of the stalk appears to be completely oxidized by the center of the boiler leaving only straw knees and ash. The straw knees are still intact at this point and some still may be devolatilizing. The continued devolatilization of straw knees after all other particles appear to be burned out could cause secondary flame structures completely detached from the primary flame structure. Further investigation of gas compositions is needed to see if a large secondary flame structure exists.

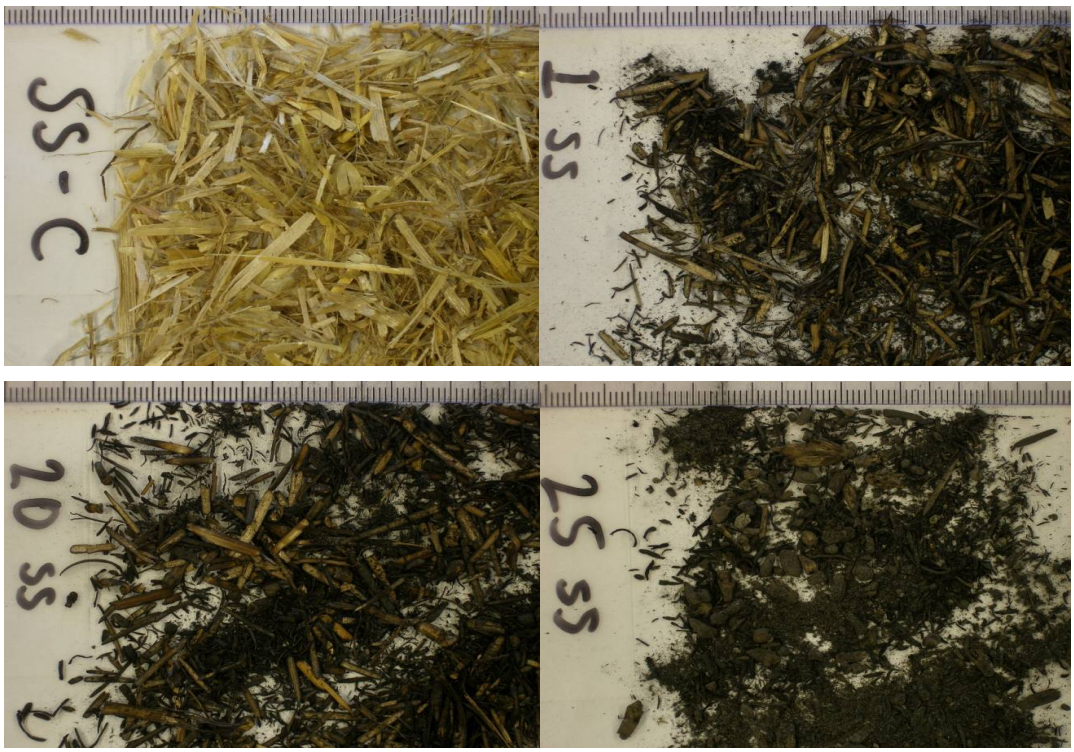

Figure 51 Series of particle samples along axial line from the center of burner. SS-C is unburnt straw from straw feeding line, 1 SS was sampled 262 cm from front wall (port B), 20 SS is 450 cm from front wall, and sample 25 SS is 672 cm from the front wall (port D, center of boiler). Scale above pictures with 1 mm graduation.

6.3 Particle Burnout Results

Jacob will consider to workout on getting the coal-biomass split and burnout of each type of particle correct. Excel file with results exist, but plots were not ready to be put in the report at the deadline.

7 Measurements of temperature and gas composition by IR probe

Two different IR techniques have been applied. A new fast method for measurement of gas temperature with 1 ms time resolution was tested and details described in the following. This method is based on fast IR-camera and setup was developed in ForskEL project no. 0079.

7.1 Fast temperature measurements in coal-straw flame

Fourier Transform Infra Red (FTIR) spectroscopy is known to be a reliable method for gas temperature measurements and can be comparatively easily used on an industrial scale such as a boiler of a power plant. However data rate is not sufficient to monitor and follow fast temperature fluctuations. In an effort to eliminate this drawback, a new IR spectroscopic-imaging system has been developed at *Risø DTU* as part of energinet.dk project no. 2008-1-0079.

The fibre and probe used for the presented system are the same as for the FTIR system. However, the grating spectrometer, Acton spectrometer with gold optics, and the IR camera, Cedip model Titanium, are used here as the spectroscopic system instead of the FTIR spectrometer.

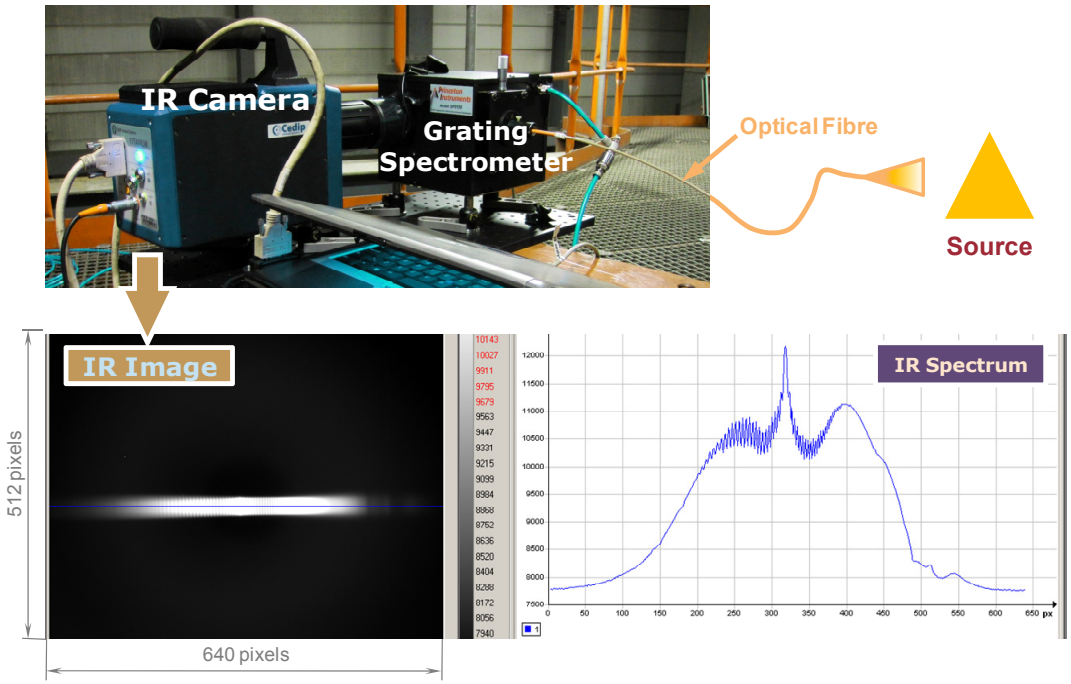

Figure 52 Grating spectrometer for fast measurement of IR spectra. Upper picture: IR-camera and grating spectrometer coupled to optical fibre. Below, left: image of light from IR fibre, and right: resulting IR spectrum. Data rate of 1 – 3 kHz can be obtained by windowing IR camera image to region of interest.

The IR camera is focused on the rear focal plane of the grating spectrometer and thus gives the IR image of an IR spectrum, see figure. The spectrum can be obtained from the image using a simple data processing method. A typical working spectral region is 3.8 to 4.8 μm (2080 to 2630 cm^{-1}), i.e. in a spectral region where gas radiation from CO and CO_2 and thermal radiation from surfaces (3.9 μm) can be detected. The integration time was set to 1 millisecond giving the data rate of 1000 spectra per second. This data rate is much greater than that of a commercial FTIR spectrometer (2-80 Hz). The presented system is flexible and can be easily modified, e.g. exposure time can be reduced down to 7μs or signal from 2-5 optical fibres can be monitored simultaneously.

7.1.1 Results fast grating spectrometer measurements

It is possible to calculate the temperature of CO_2 and solid surfaces from the spectra using corresponding parts of the working spectral region. Gas temperature was found from emission at CO_2 band at 2349.1 cm-1 (4.26 μm), whereas surface brightness temperature is calculated at 2564 cm^{-1} (3.9 μm). The probe was inserted into several positions inside the flame at port B. No beam stop was mounted on probe. For each position, the temperature of gases and particles was measured with the rate of 1 kHz for 10 s at each point.

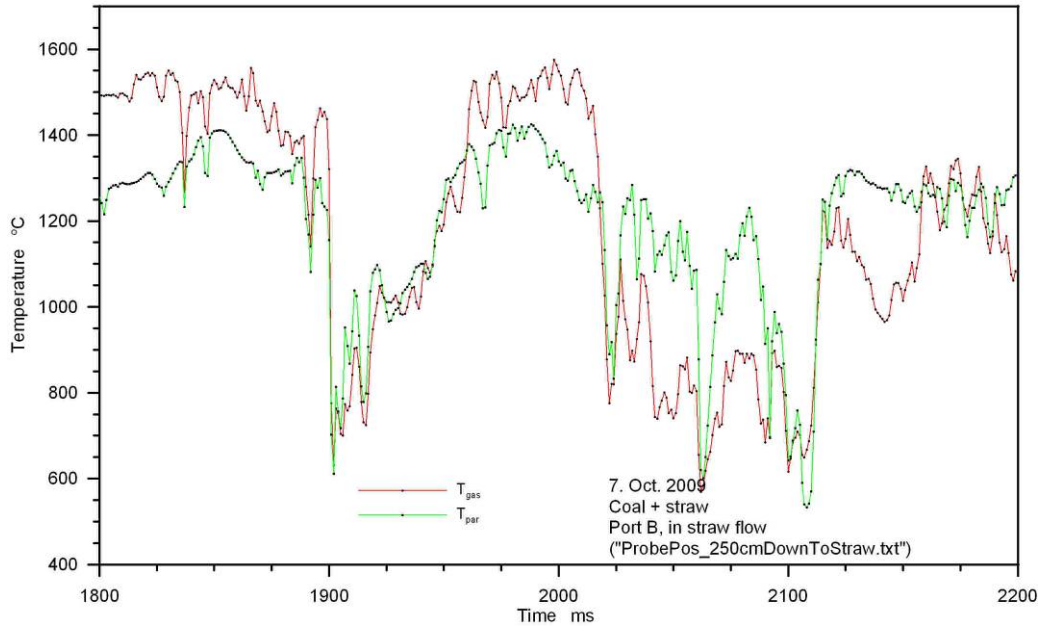

Figure 53 Example of measured local gas temperature (red curve) and brightness temperature of surfaces (green) for probe inserted into straw flow at port B, i.e. inserted 250 cm from boiler wall and probe tilted downwards. Measurement performed on 7th October 2009 at 18:00 during test programme with data rate of 1000 Hz. Only 400 ms period is shown out of 10 s.

1 ms data rate is sufficient to resolve details in temperature fluctuations, see figure. Very large temperature fluctuations are observed for probe inserted into straw flow. Brightness surface temperatures down to 500°C are seen when straw particles block or partial block the field of view of probe. Gas temperature fluctuations follow to some extent particle temperature variations in zone with high density of straw. The gas temperature is sometimes less than the particles temperature, which indicates structures of the primary air are still surrounding straw particles. The fast temperature measurements show that straw feeding is jet like with very large variations in particle density at port B.

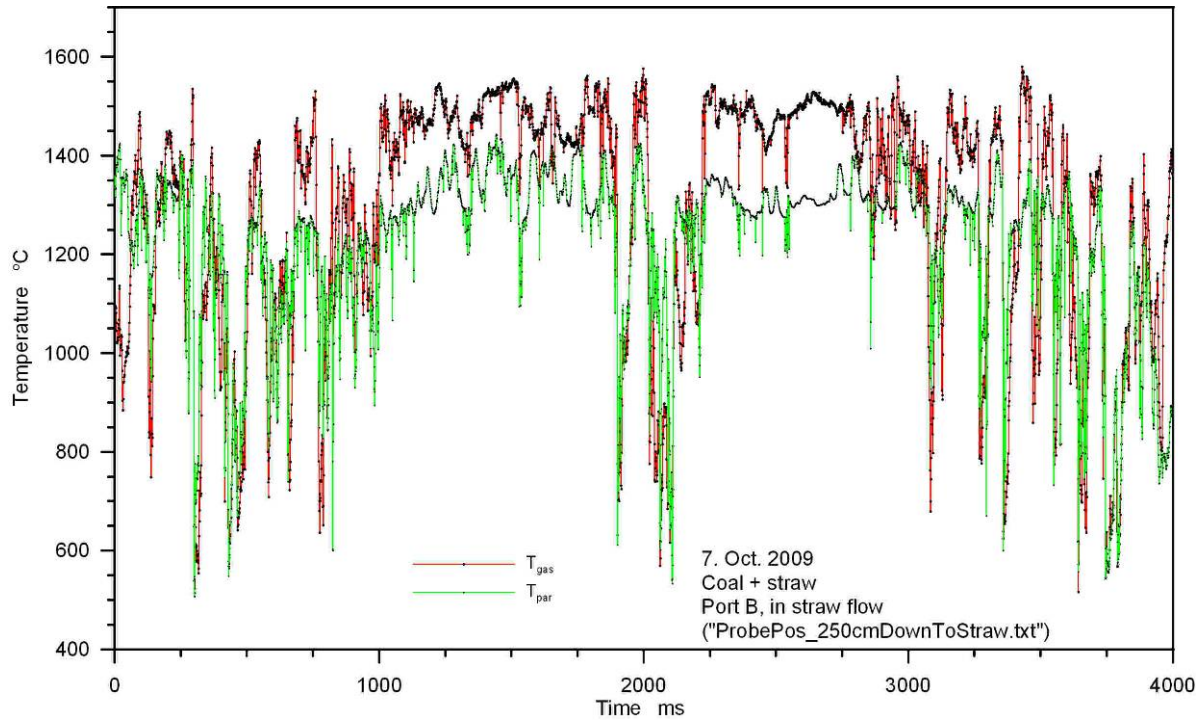

Figure 54 Measurement probe inserted over straw flow at port B, i.e. inserted 250 cm from boiler wall and probe tilted downwards (inside straw flow).

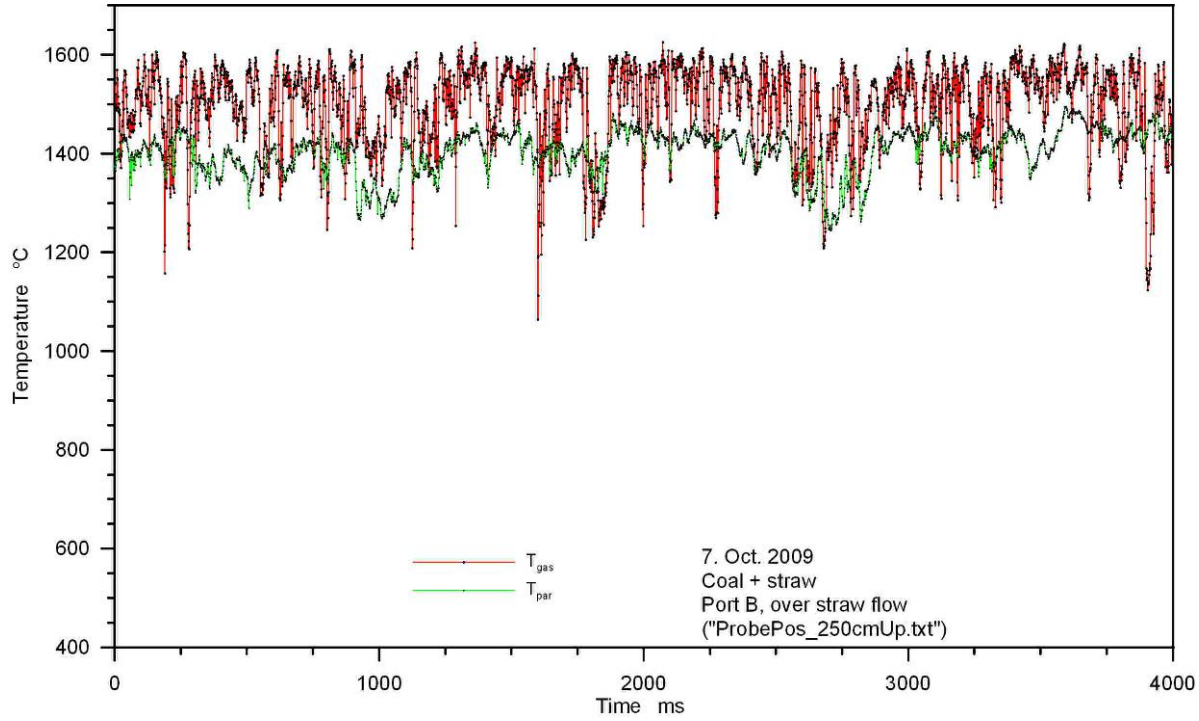

Figure 55 Measurement probe inserted over straw flow at port B, i.e. inserted 250 cm from boiler wall and probe tilted upwards (outside straw flow).

The mixing of fuel and gas in coal-straw flame could be better from a quick look at Figure 54, i.e. periods of 0.9s are observed with few straw particles (few spikes with low temperature). IR pictures of straw flow from burner show similar behaviour.

7.2 FTIR probe measurements

The FTIR technique has been used in many other energy research projects earlier. Nevertheless, problems arise using the method for gas analysis in particle dense regions of flame with high turbulence. FTIR fibre-optic method is in practice easy to apply, accurate and gives valuable details about gas temperature fluctuations for gas temperature measurement in large flames and boilers. A suction pyrometer could also have been used to obtain average gas temperature measurements, but it would require more experimental time (2-3 times) and blocking of suction pyrometer is expected to cause problems (extra time, raised uncertainty for some points).

All gas concentration values on wet basis except extractive O_2 values on dry basis in following.

7.2.1 Experimental setup FTIR probe measurements

A special 7 m long probe was designed for the measurement campaign to measure simultaneously 1) gas temperature and gas composition with fibre-optics using FTIR spectroscopy and 2) extractive gas sampling. The probe is designed with two water inlets to control the temperature inside the probe with fibre-optics (typical 21 – 33 ºC) and the temperature profile along the probe to obtain uniform temperature of approx. 60 ºC around the 6/4 mm stainless steel tube used for extractive sampling of flue gas. Probe diameter is 60.3 mm and weight is approx. 55 kg. 1" hoses were used for inlet and outlet cooling water. Two fire hoses were used for water supply with a pressure of approx. 3.5 bar and 6 bar.

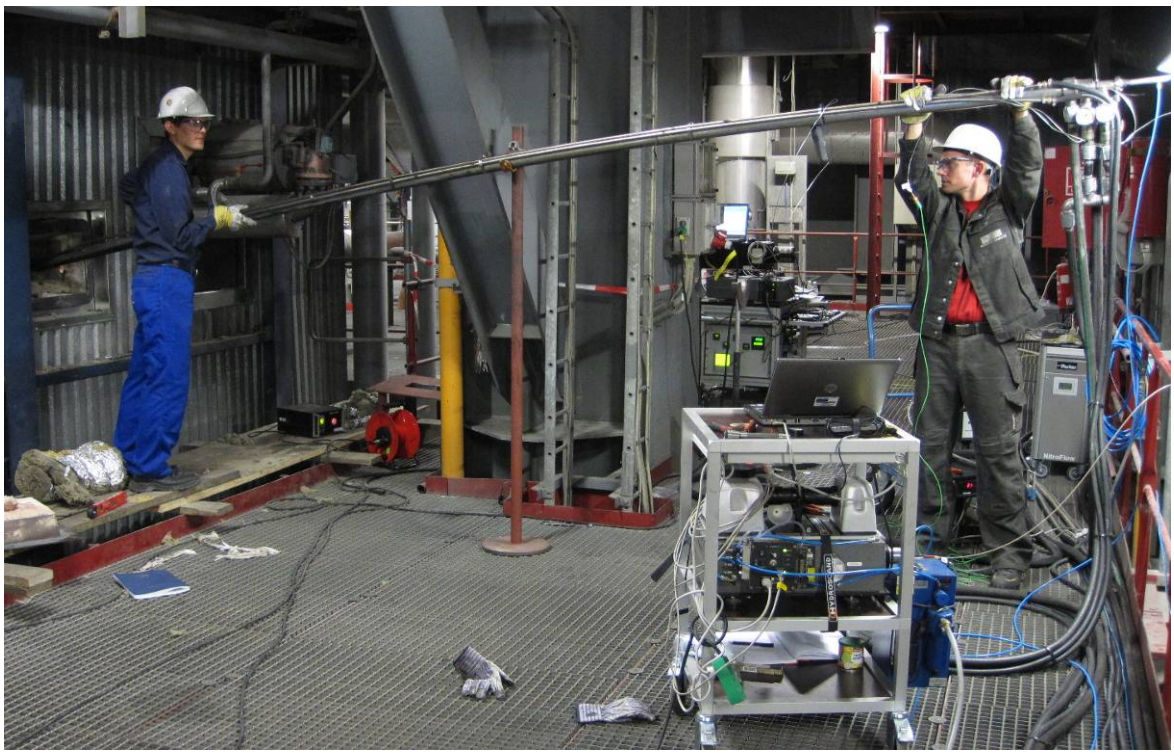

Figure 56 Experimental setup used during temperature and gas concentration measurements. 7 m long water-cooled probe inserted in boiler with IR fibre connected to FTIR spectrometer for collection of thermal emission spectra. A heated gas sampling line from probe is connected to extractive gas analysing system (seen in background).

A transportable blackbody is used to calibrate the FTIR fibre optic system before and after measurement of a profile. The temperature of the blackbody was 897ºC ±3 ºC at 900 ºC setpoint according to certificate IR20075. This procedure is a part of the quality system to define uncertainty on temperature measurements. The calibration result before and after measurements is compared to detect any changes in the system, e.g. attenuation of signal due to slag on ceramic probe tip, rotation of fibre during experiment or any other problems. Deviation in signal is usually below 1-2%. Uncertainty on gas temperature would normally be 10-15 ºC, can be as small as 3-5 ºC at 1200 ºC.

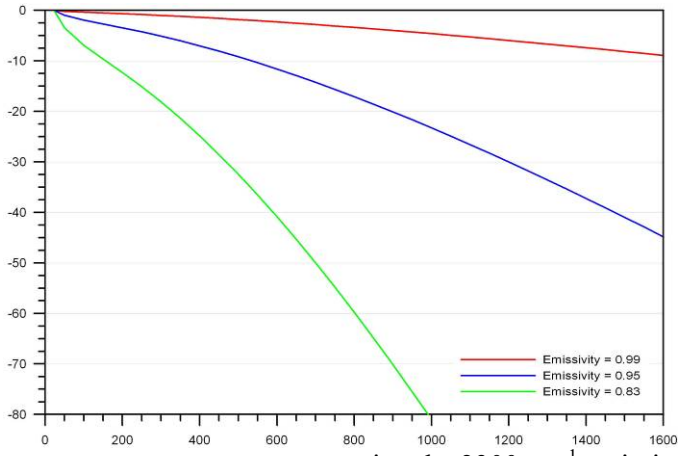

Figure 57 Measurement errors on gas temperature using the 2300 cm^{-1} emission band of CO_2 at three emissivities of gas band, i.e. 0.99 (1%), 0.95 (5%) and 0.83 (17%). X-axis: gas temperature in ºC and Y-axis: deviation in ºC calculated from Plancks law.

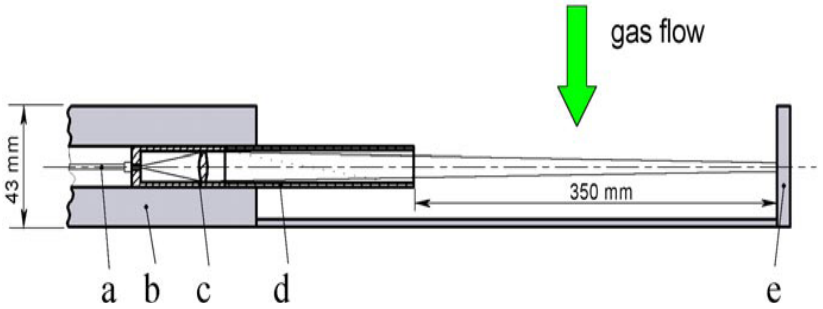

Figure 58 A cross-sectional view of the FTIR probe head to be used in traditional boilers: a, infrared fibre; b, water-cooled stainless steel probe; c, optical mount; d, protection tube; e, water-cooled beam stop. The optical path (dotted line) and optimum flow direction towards the measuring volume is indicated. The arrow illustrates the desired gas direction with minimum disturbance of the measuring volume conditions in front of the probe tip. Path length is typically 200-250 mm.

A water-cooled beam is not required for measurement of gas temperature, i.e. gas temperature can be measured without the risk of cooling the gas from the water-cooled tubes (8x6 mm tubes) used for cooling the beam stop. However, for simultaneous measurement of gas temperature and gas composition a known optical path length must be used and a water-cooled beam-stop was mounted on the probe. The probe was oriented in the flame to minimize cooling of the gas in the optical path between the ceramic tip and the beam stop.

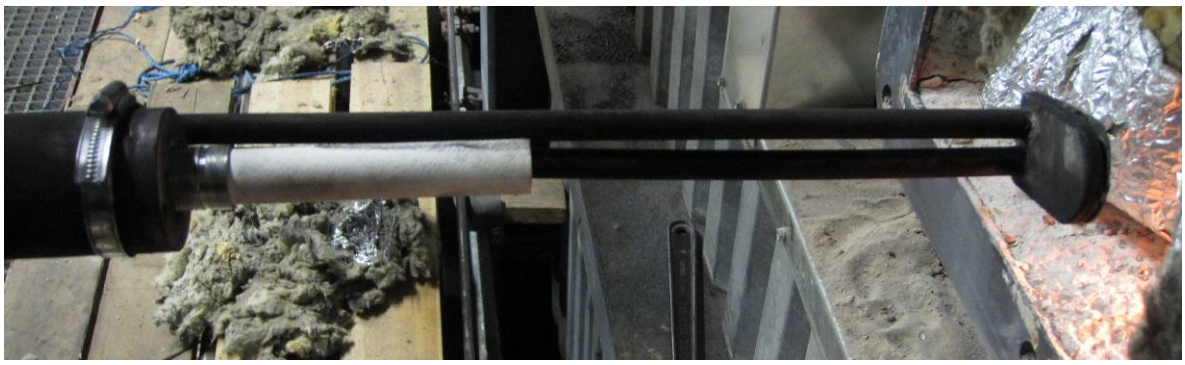

Figure 59 FTIR probe with 250 mm between tip of ceramic tube and water-cooled beam stop (right in picture).

100 snap shot spectra were collected for each measurement point with a rate of approx. 1 scan per second. Spectra are stored in a multi-file named e.g. cac.interferogram.spc (cac: code of port, code serie no. and code point no.). Local gas temperature, best grey body fit of radiation from surfaces (particles), etc. can be calculated for each spectrum, an example is shown in Figure 60. Average gas temperature and RMS value of gas temperature fluctuations can be calculated from the 100 spectra measured over approx. 100 seconds.

7.2.2 Analysis of temperature from FTIR spectra

Gas temperature is found from thermal emission from CO_2 at 2350 cm^{-1} (4.3 µm) by simple best match with Planckian curve, red curve in figure below.

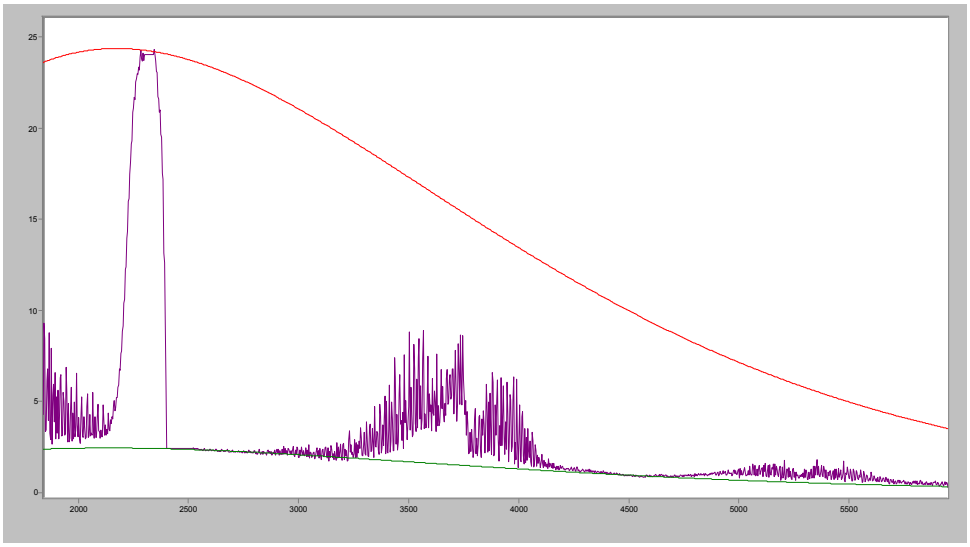

Figure 60 Example of measured emission spectrum (blue curve) in a with FTIR fibre-optic probe at ordinary atmospheric combustion with 25 cm pathlength. Red curve is blackbody curve at 836.0ºC found from radiance at CO_2 peak at 2350 cm^{-1}. Background radiation from particles in gas is fitted with a grey body (green curve) 816.9ºC and emissivity of 0.106. Single scan spectrum with 2 cm^{-1} spectral resolution. X-axis in wavenumbers (cm^{-1}) and Y-axis in radiance (W/m^2 cm^{-1} sr).

	A	B	C	D	E	F	G	H	I	J	K	L	M	N	O
19	No.	Time	T_local	T_std	T_peak	T_3700	T_back	E_back	T_3.9	C_H2O_%	CO2_2350_%	CO2%_3700_%	CO_ppm	CxHy_ppm	HCl_ppm
20	1	61020	1178.5	105.2	1315.9	1026.6	1117.3	0.333	724.4	11.7	15.3	16.2	6300.47	0	13
21	2	61021	1162.8	10.1	1177.8	935.2	997.3	0.323	651.6	10.9	14.3	15.3	962.441	0	49
22	3	61022.1	1203.4	12.9	1214.2	985.2	1042.8	0.343	690.2	12.5	15	18	1018.78	18	-34
23	4	61023.1	1248.6	18.9	1268.7	1011.2	1212.5	0.316	760.3	8.9	12	14.4	6672.54	0	-96
24	5	61024.2	1349.1	18.5	1361.2	980.8	1029.9	0.3	651.4	8.9	10.1	12.7	2184.27	38	26
25	6	61025.2	1384.7	18.1	1403.9	1000.4	1013.3	0.289	635.3	9.9	13.8	13.5	421.362	126	-19
26	7	61026.2	1379.1	16.1	1389.7	1017.3	951.2	0.399	674.2	11.2	12.8	14.7	295.775	0	21
27	8	61027.3	1316.5	4.4	1318.2	992	1013.6	0.351	678.4	10.3	11.3	14.5	2836.85	0	-62
28	9	61028.3	1146.8	19.8	1171.1	934.1	1029.5	0.305	657	10.7	12.6	15	835.681	0	-28
29	10	61029.4	1281.9	22.3	1304.5	1019.9	1169.9	0.346	764.9	9	11	13.8	3295.77	0	40
30	11	61030.4	1124.6	20.2	1157.6	938.5	1039.7	0.282	644.2	12	14.9	17.1	362.676	0	41
31	12	61031.4	1238.4	28.3	1264.3	994.5	1007.5	0.373	691.5	11.6	13.8	17.1	381.455	0	32
32	13	61032.5	1152.4	52.7	1253.4	969.4	1042.9	0.309	666	10.4	14.7	15.6	1223	0	90
33	14	61033.5	1309.9	19.7	1326.2	1003.9	998.9	0.363	679.6	10.8	13.6	15.5	1181.92	0	-44
34	15	61034.5	1197.7	16.7	1222.7	984.8	1050.6	0.351	701.6	11.5	15.7	17	967.136	0	-9
35	16	61035.6	1162.4	15.5	1180	956	1059.4	0.276	649.8	12.2	16.5	17.4	166.667	769	-7
36	17	61036.6	1211	17.4	1226.4	951.3	1028.4	0.302	652.5	10.3	12.1	14.9	500	0	140
37	18	61037.7	1197	17.2	1211.5	926.4	1001.1	0.265	611.1	9.9	11.1	14.2	164.319	0	-26
38	19	61038.7	1290.3	13.9	1298.9	932.7	1020	0.267	622.5	8.1	8.5	11.4	2411.97	0	4
39	20	61039.7	1278	11.7	1283.9	998.7	1172.3	0.251	680.8	10.9	11.9	15.7	3083.33	0	18
40	21	61040.8	1244.6	13.9	1253.2	946	987	0.327	649.5	9.4	10.9	14	4583.33	0	92
41	22	61041.8	1231.9	7.2	1235.3	960.9	1027.8	0.333	675.8	10.2	12.4	14.8	241.784	0	52
42	23	61042.9	1268.4	18.9	1280.4	962.8	1088.4	0.262	650.3	9.6	10.4	13.7	2042.25	0	-7
43	24	61043.9	1158.4	43.4	1234.2	990.7	1114.7	0.301	695.4	11.7	15.7	16.9	4394.37	601	66
44	25	61044.9	1377.9	12.7	1385.7	1039.9	1161.4	0.325	742.3	9.2	11.9	14.1	-56.338	0	161
45	26	61046	1329.4	21.7	1344.9	970.2	998.7	0.297	633.9	9.8	9.3	12.7	280.516	73	12
46	27	61047	1191.3	24.2	1214.1	961.1	1042.2	0.286	647	11.5	13.5	16.3	1379.11	0	2
47	28	61048.1	1215.3	7.4	1222.1	991	1180.7	0.275	707.8	11.1	14.3	16.4	3112.68	0	-113
48	29	61049.1	1281.1	23.9	1299.6	990.1	1008.2	0.332	667.2	10.8	12.2	15.5	316.901	418	49

Figure 61 File structure of FTIR temperature measurements. Example data file cac.dat, position 0.75 m (from wall), coal-wood flame at port B. Temperatures in °C. Header of file is not shown.

Structure of temperature data extracted from FTIR spectra is shown in Figure 61. Note, statistical information in the header is based on 60 scans out of 120 scans. Column B is time in seconds, e.g. 46681 s (row 14) equals time (hh:mm:ss) 12:58:01. Column C T_local is local gas temperature in front of probe tip in ºC. T_std is standard deviation on local gas temperature measurement. Column E, T_peak is max. gas temperature measured along the field of view of probe based on hot band (red wing) of CO_2 band at 2350 cm^{-1}. T_3700 the average gas temperature along line of sight (useful for long path cross stack measurements, not used in this work). T_back (temperature) and E_back (emissivity) is best fit to a grey body in regions without gas bands. T_3.9 is surface brightness temperature. The brightness temperature (emissivity set to 1.00) at 3.9 µm (Column I) is mainly thermal radiation from beam stop and fuel particles (dark curve), and fast fluctuations comes from fuel and ash particles in the optical field of view of probe. Column J: H_2O content in gas, column K and L CO_2 concentration calculated at two different spectral regions, column M CO concentration in ppm and column N C_xH_y (hydrocarbons) value normalised to same area of absorption peak as for CH_4.

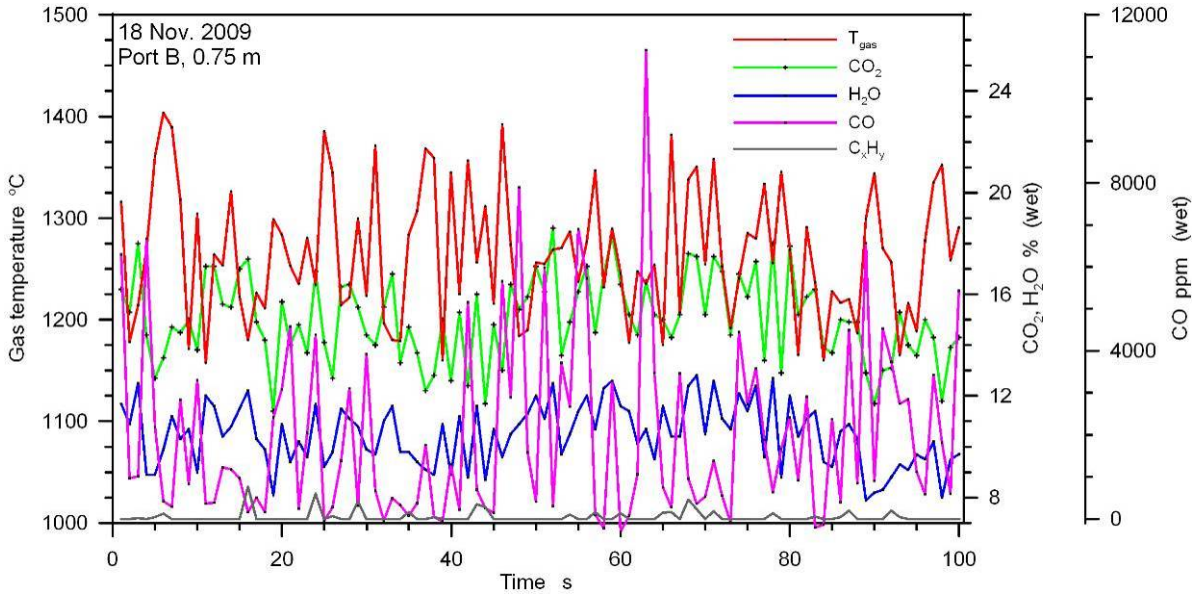

Figure 62 Measured gas temperature (red curve) 0.75 m from wall at port B for coal-wood flame. Gas temperature (Column C) fluctuates between 1158ºC and 1404ºC during period of 100 s. A suction pyrometer measurement should be close to mean value of 1266ºC. RMS value on gas temperature is 64ºC and it indicates a situation with incomplete mixing of gas and fuel, e.g. a RMS value of 15-50ºC is normally seen at super heater level in ordinary coal combustion boilers.

7.2.3 Analysis of gas composition FTIR spectra

CO_2 and H_2O bands are seen clearly in all measured spectra over a path length of nominal 250 mm. Gas temperature is assumed to be uniform over the 250 mm optical path length. This assumption can lead to too low gas concentrations in region with non-uniform temperature distribution over the 250 mm optical path as emitted thermal radiation from gas increase with temperature whereas gas with low temperature in the optical path contribute less to measured emission spectrum. This effect is most pronounced for CO_2.

Very high CO peak concentrations are observed at most measurement points which indicate poor mixing and incomplete combustion. Absorption features from C_xH_y can sometimes be observed in the spectra. Trace gases like NO and SO_2 cannot be seen in infrared spectra as expected due a very short path length of 250 mm (normally 6 m path length is required at a gas temperature of 180°C), nevertheless, both gas components might be measured optically by UV-spectroscopy or by extractive gas sampling.

Detection limits for single scan measurements approximately, i.e. single scan spectrum over ½ s.:
CO: 600 ppm
C_xH_y: 1000 ppm
HCl: 20-100 ppm

Detection limits can in principle be reduced by a factor of 11 by increasing measurement time from 0.5 til 60 s.
Data analysis of measured raw data is fully automated for each profile (batch job). Gas composition was found using program “studs_multi_auto_c.ab” ver. 1.5 2009. Basis principles and reference data for gas components are similar to earlier projects, but program have been improved for faster and more automated analysis of spectra.

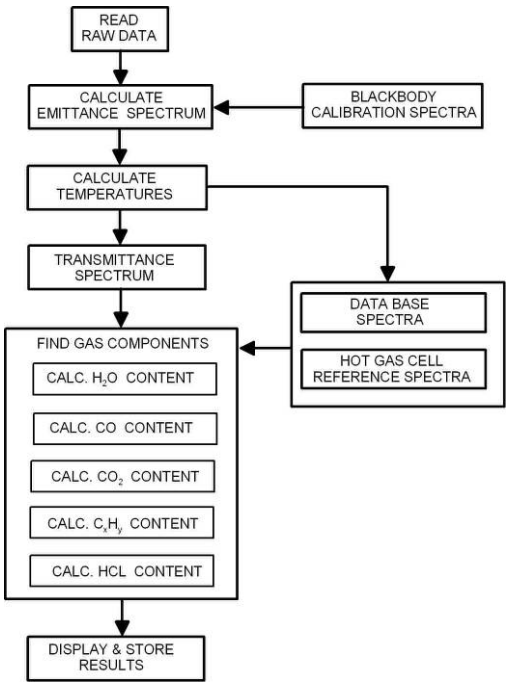

Figure 63 Diagram over data analysis of FTIR data. Software is based on Array basic software GRAMS version 7.0 from Galactic/Thermo.

7.2.4 FTIR results for coal-wood flame

Optical and extractive gas measurements is first compared at port B for two measurement points, 1 point inside and 1 point outside flame, followed by presentation of profiles for coal-wood flame.

Optical and extractive gas measurements were carried out with the same probe in parallel. Acquisition of both systems was attempted to be started at the same time, but they might be separated in time by 30-100 s. Furthermore, extractive sampling point in water-cooled probe is placed 150 mm behind start of optical path used for optical measurements.

CO_2 concentration is found to be 13.9% inside flame and 14.7% outside by extractive method, Figure 64. Slightly higher concentration is measured by FTIR optical probe, i.e. 14.5% and 15.0%. Agreement appears to be acceptable taking into account measured fluctuations in CO_2 concentration over time with 1 standard deviation (RMS) of 1.6%-1.7%.

Measured H_2O concentration by FTIR optical probe is fairly constant approx. 10% inside and outside flame close to expected value, Figure 65. Significantly lower H_2O level, 2.8 – 3.4%, is measured by extractive method, which can be explained by condensation problem at connection of heated sampling line and water-cooled probe. This problem happens sometimes for measurements close to boiler wall, but the problem has been solved after campaign by additional heating of junction.

Fair agreement is observed for measured CO average level by optical and extractive method 2712 ppm extractive versus 2006 ppm optical outside flame and 9699 ppm extractive versus 10442 ppm optical inside flame, Figure 66. Very large variations in CO concentration are measured by FTIR optic probe at both positions in flame, i.e. 0 – 12000 ppm outside flame and 0-32000 ppm in flame. The spiky CO concentration behaviour in time series measurements is typical of what is observed

using optical methods in pf flames. It is our experience that CO appears as spikes, probably with origin from larger structures in near burner field of flames that never mix up in the boiler, at super heater and later on for as well pure coal and biomass fired boilers.

Large gas temperature fluctuations, Figure 57, are observed at both positions, i.e. 1150-1400°C (average 1268°C) at wall and 1225-1575°C (average 1398°C) in flame.

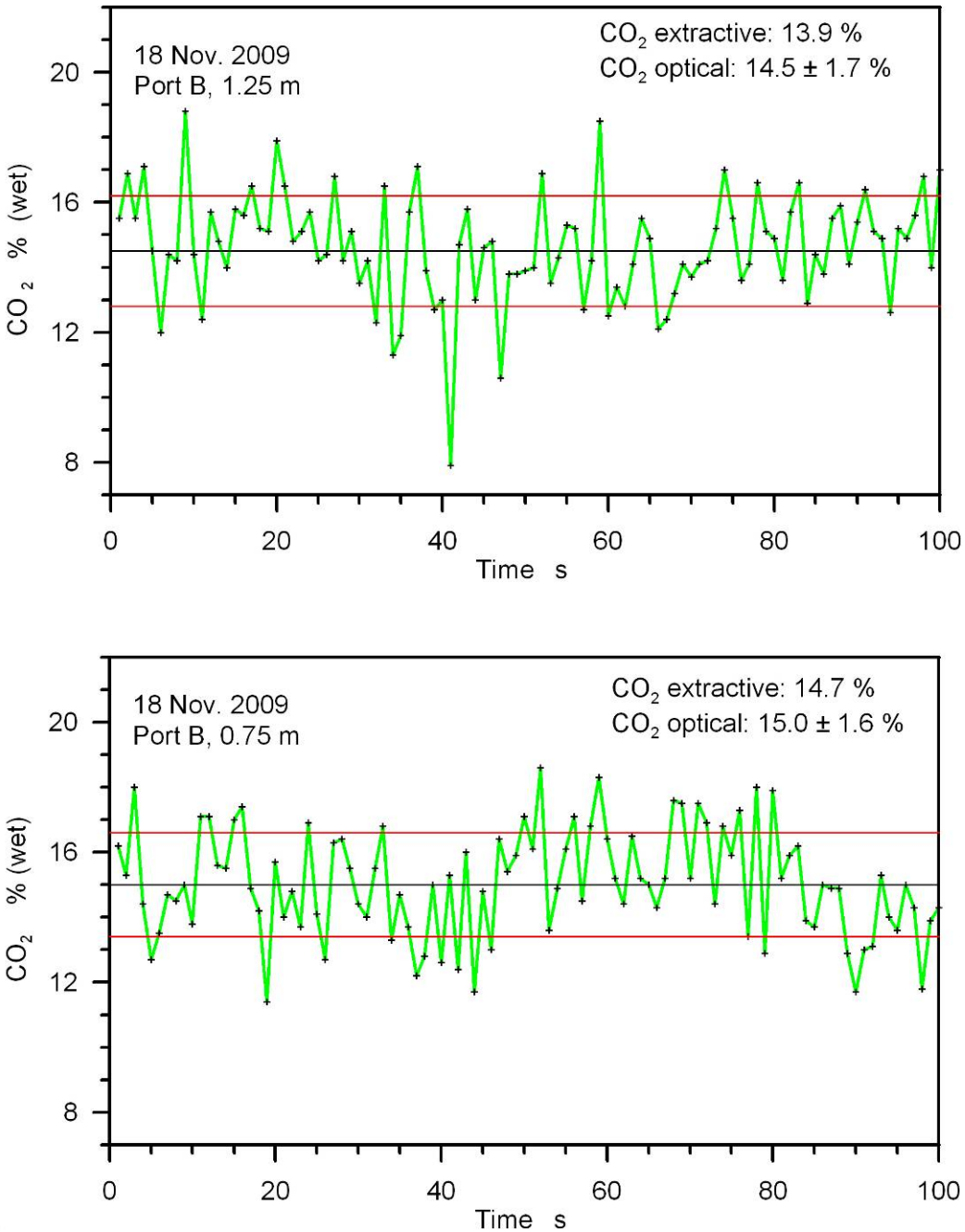

Figure 64 Comparison of measured CO_2 concentration by optical method (FTIR fibre-optic probe) and extractive gas sampling at 2 positions. Black and red lines are average and standard deviation on optical measurements. Coal-wood flame.

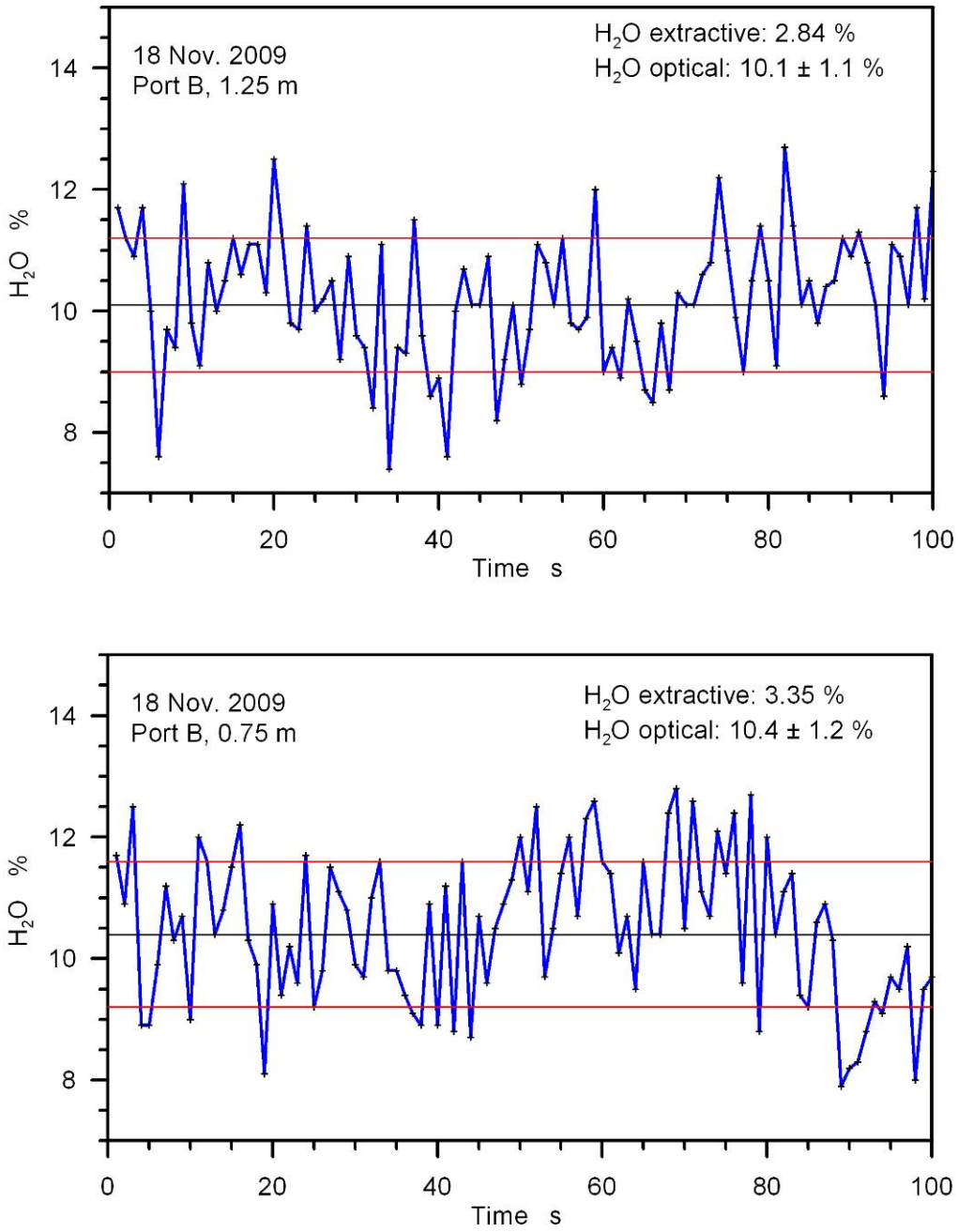

Figure 65 Comparison of measured H_2O concentration by optical method (FTIR fibre-optic probe) and extractive gas sampling at 2 positions. Black and red lines are average and standard deviation on optical measurements. Coal-wood flame Studstrup Unit 4. Problems with condensation of water in sampling line in intrusive measurements.

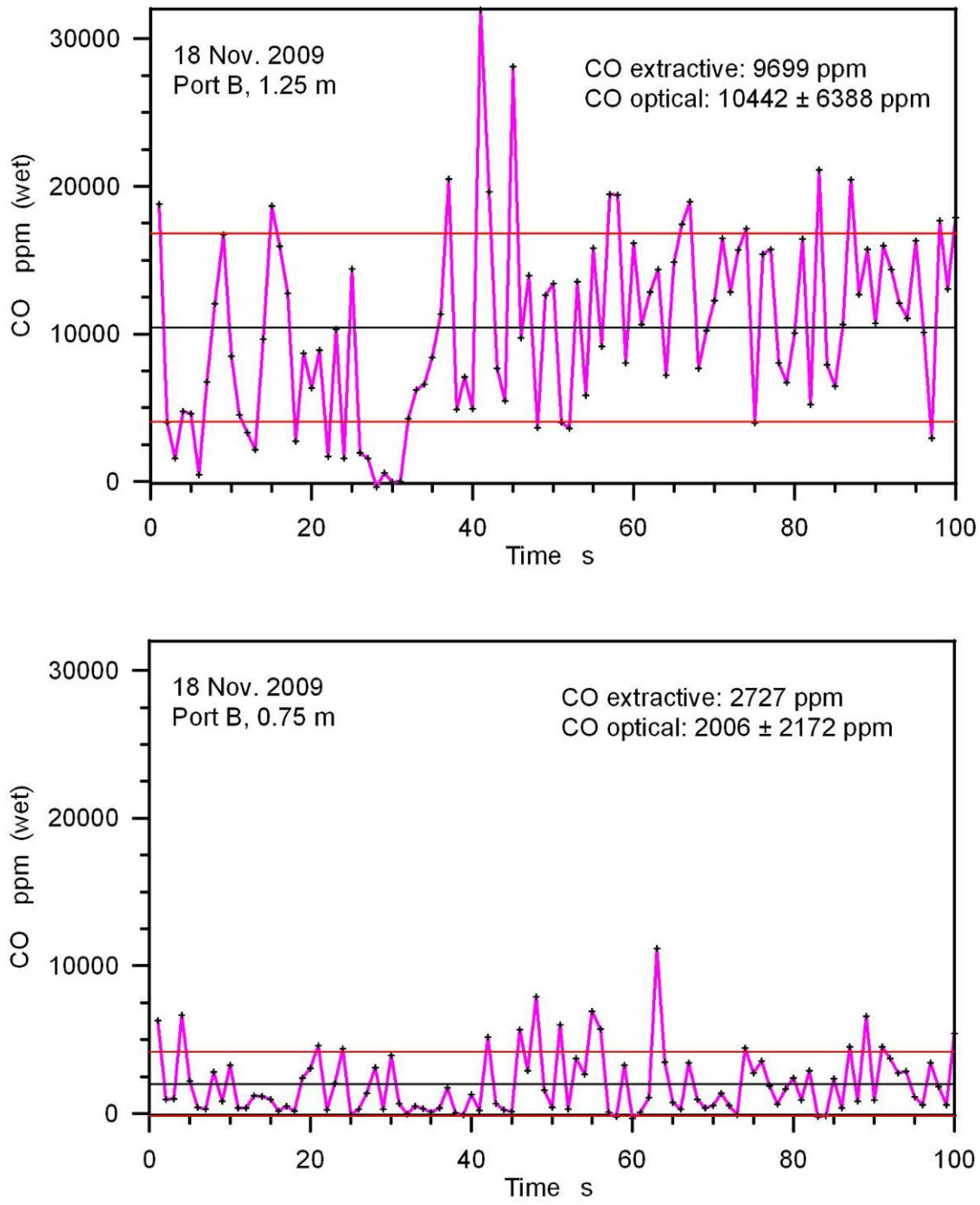

Figure 66 Comparison of measured CO concentration by optical method (FTIR fibre-optic probe) and extractive gas sampling at 2 positions. Black and red lines are average and standard deviation on optical measurements. Coal-wood flame Studstrup Unit 4.

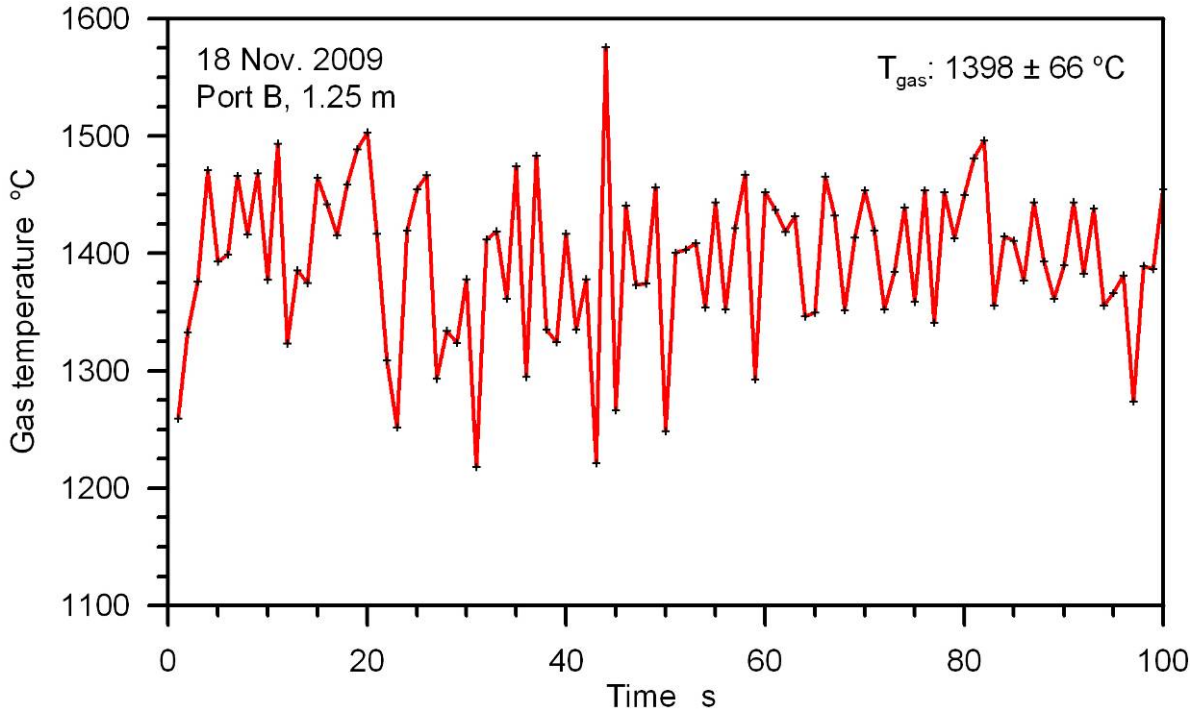

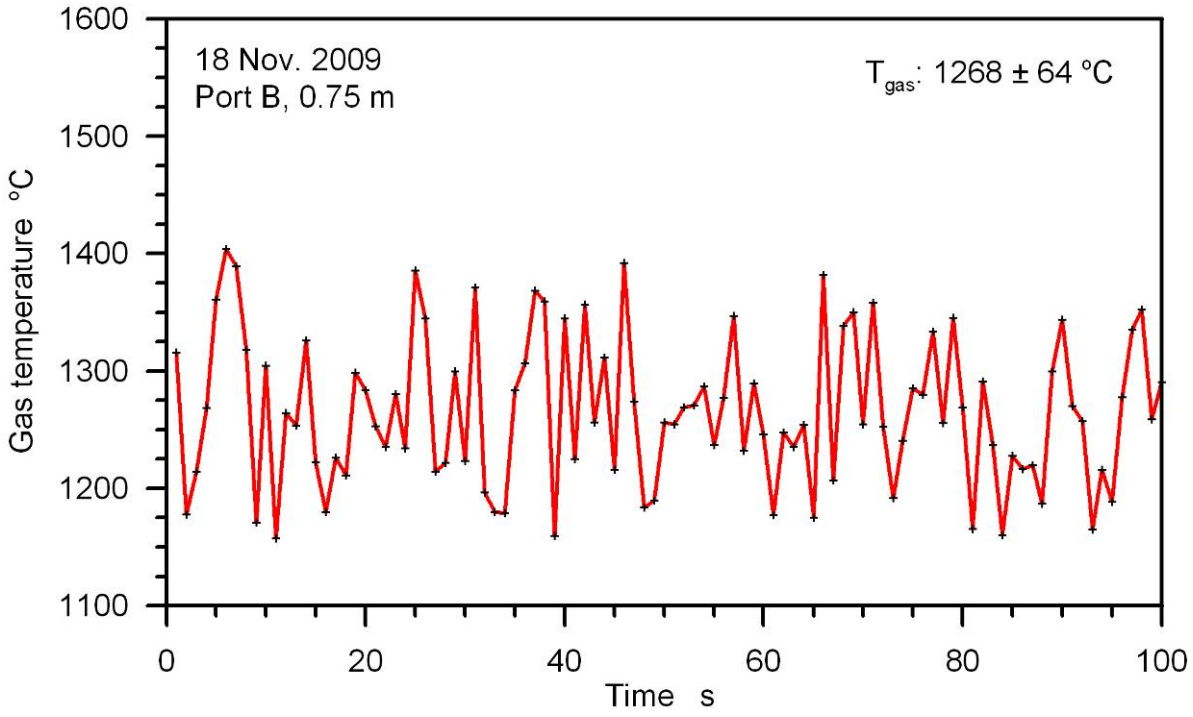

Figure 67 Gas temperature by optical method (FTIR fibre-optic probe) using radiation intensity of CO_2 band at 4.3 μm. Coal-wood flame Studstrup Unit 4.

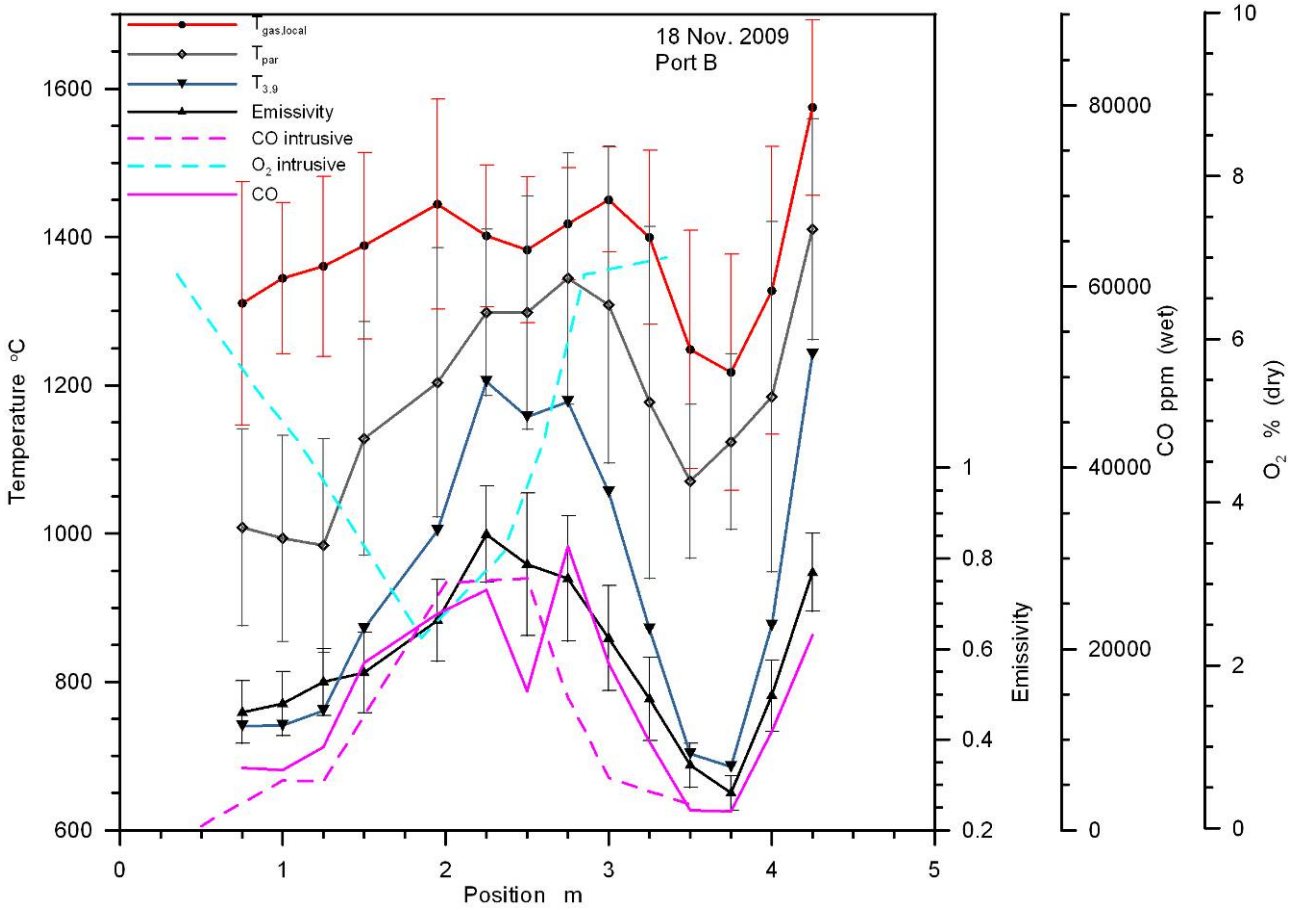

Figure 68 Comparison of FTIR probe measurements with extractive CO and O_2 measurements at port B for coal-wood flame. Error bars show 1 standard deviation on average value based on 100 single-shot optical measurements. Similar CO level is measured optically and extractive.

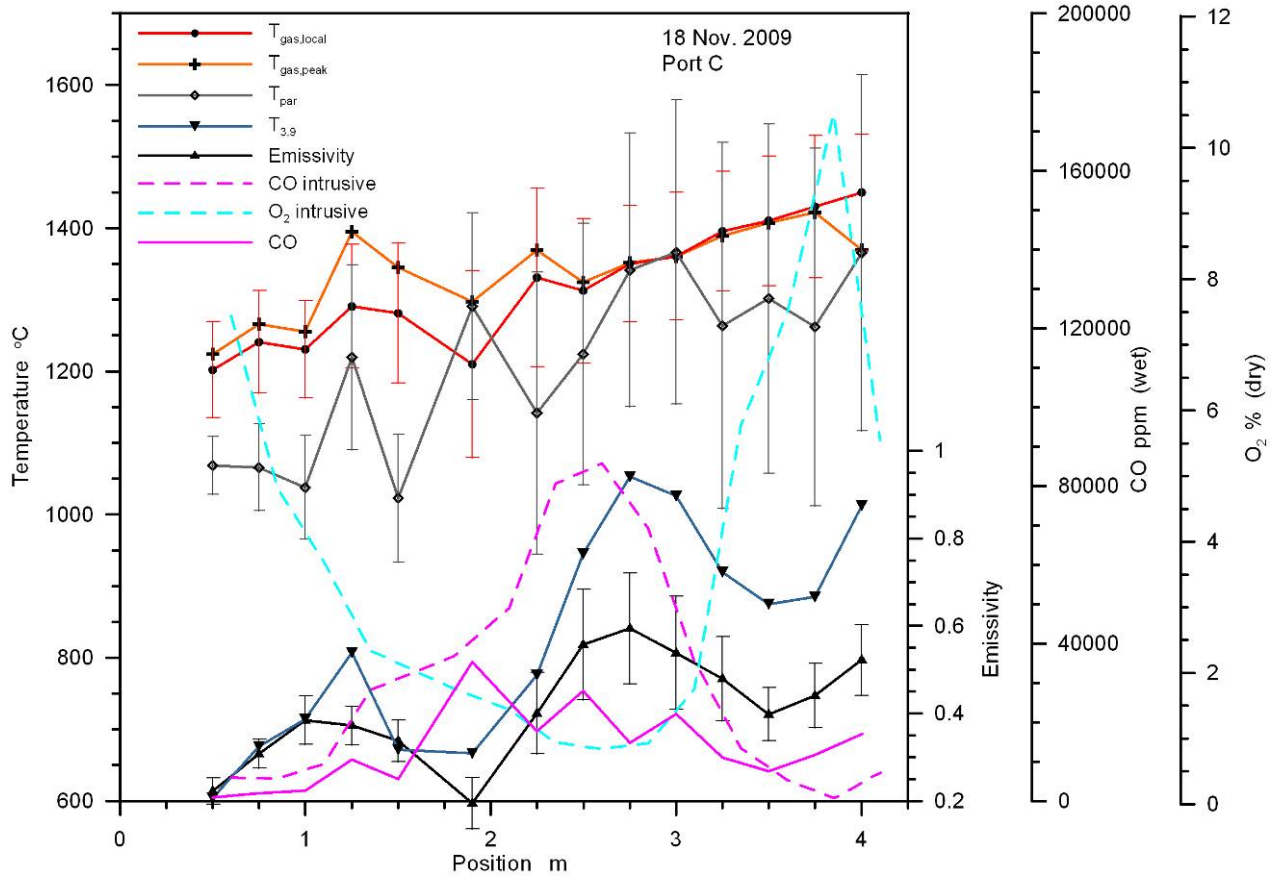

Figure 69 Comparison of FTIR probe measurements with extractive CO and O_2 measurements at port C for coal-wood flame. Error bars show 1 standard deviation on optical measurement.

7.2.5 FTIR results coal-straw flame

CO concentration level is clearly linked to the particle concentration in coal-straw flame as seen in figure below. This behaviour is not seen as clearly for other flames, which might be caused by a larger size of straw structures.

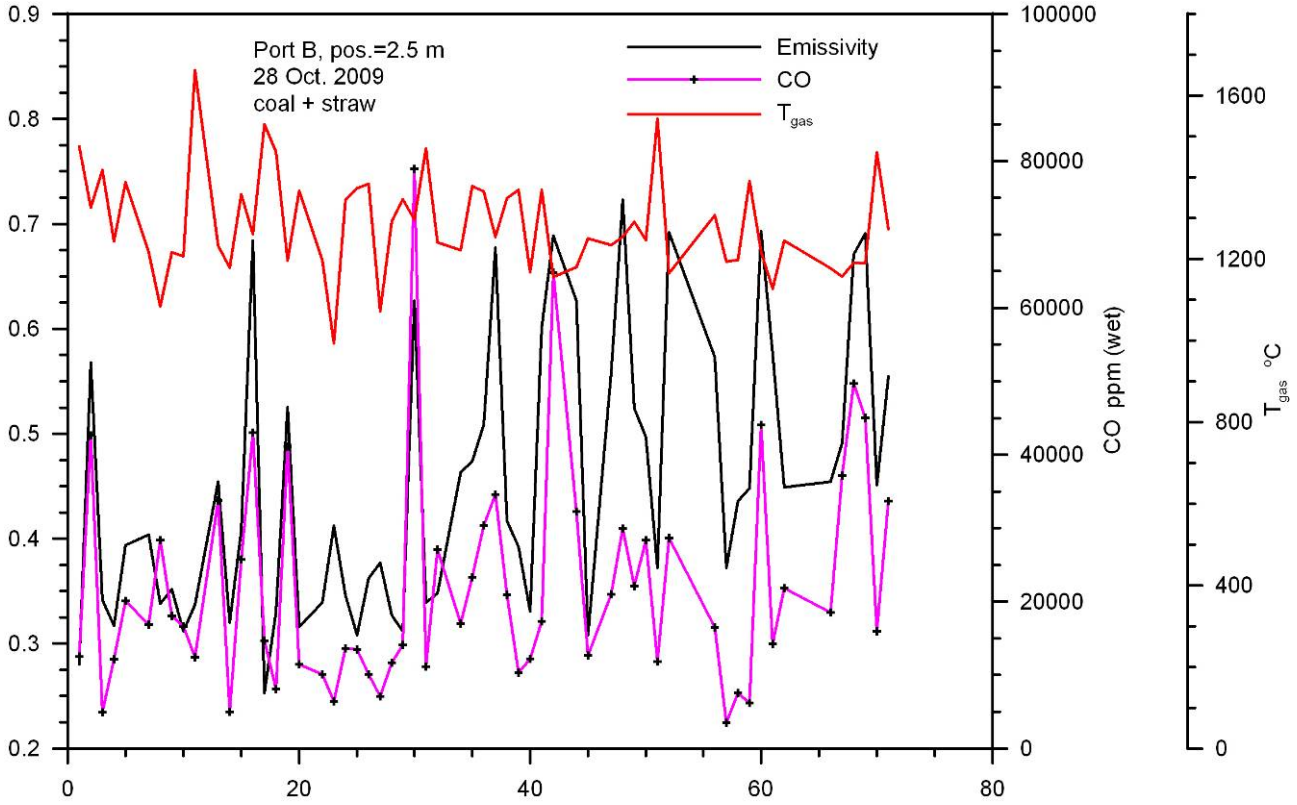

Figure 70 Comparison of measured emissivity (fuel particle concentration), CO concentration of gas temperature using FTIR fibre-optic probe in center region of coal-straw flame 2.62 m from burner wall and 2.5 m from side wall. x-axis time in seconds and y-axis left emissivity.

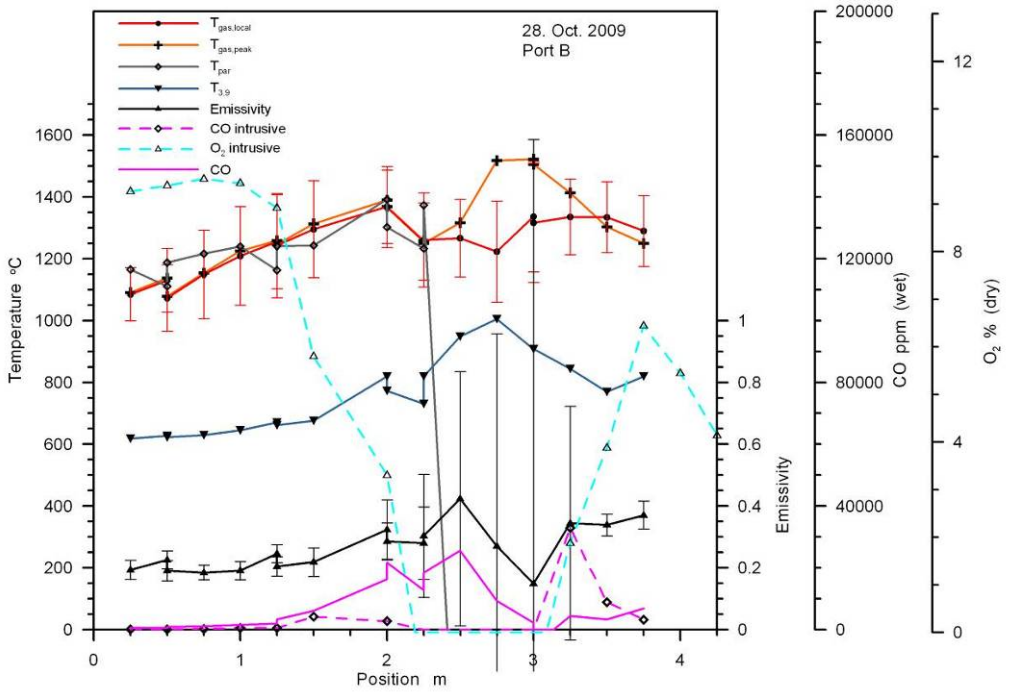

Figure 71 Gas temperature and comparison of FTIR probe measurements with extractive gas measurements at port B for coal-straw flame. Note, magnitude of error bars on emissivity large in region with straw, i.e. fluctuations in particle density. Extractive gas sampling not possible at 2.25 – 3.0 m (set to zero).

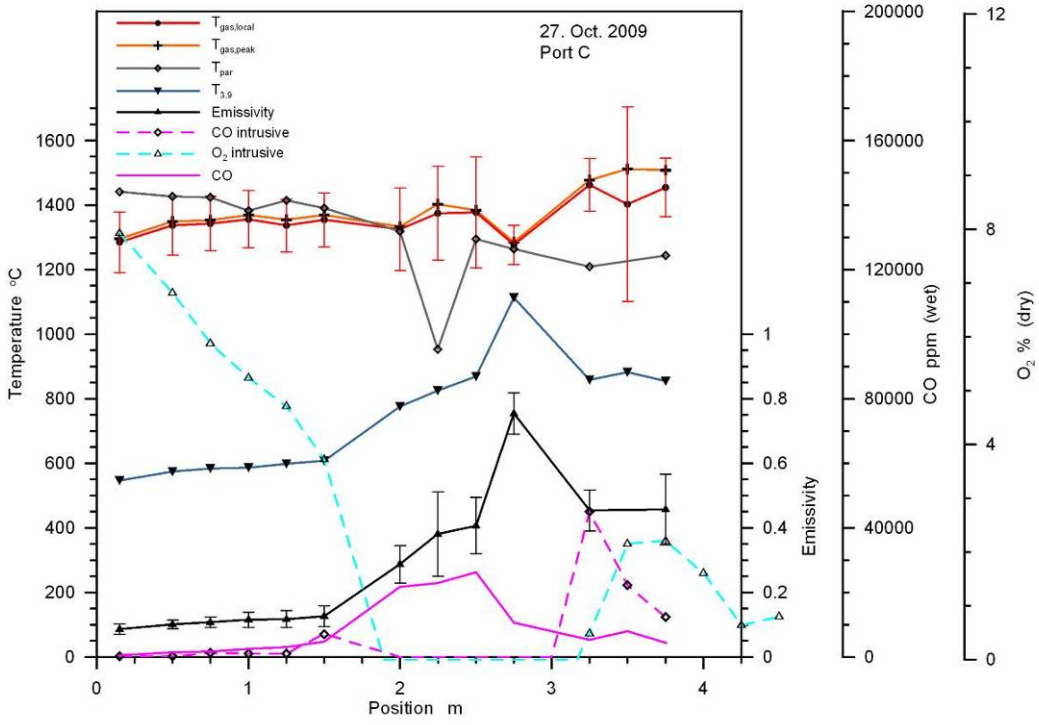

Figure 72 Gas temperature and comparison of FTIR probe measurements with extractive gas measurements at port C for coal-straw flame. Extractive gas sampling not possible at 2.25 – 2.75 m (set to zero).

7.2.6 FTIR results coal flame

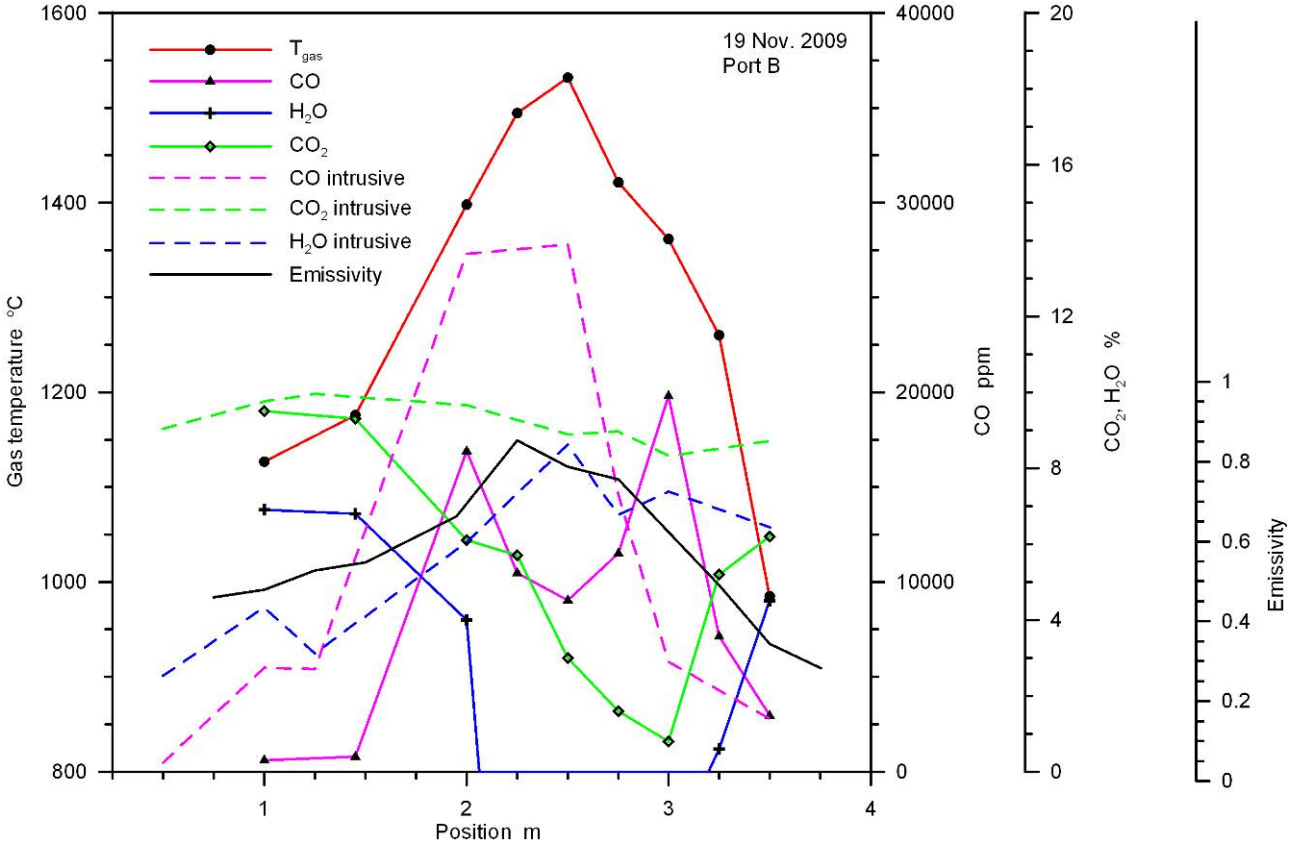

Figure 73 Comparison of FTIR probe measurements with extractive gas measurements at port B for coal flame. Low values of CO_2 measured in centre of flame by FTIR optical probe are caused by complex conditions (non-uniform slab of gas over 25 cm) that lead to too low values. Similar, FTIR optical probe fail for H_2O in centre region of flame. The effect for CO is less pronounced, but might lead to errors of 50% in centre of flame.

Limitations of the FTIR probe technique in near burner zone with strong mixing of cold and hot gas/fuel is visible in Figure 73. Too low values of CO_2 and H_2O are measured in centre of flame. Similar results were found for a laboratory pulverised flame in PSO-project 010016, "Advanced Diagnostics in Oxy-Fuel Combustion Processes", ref. 18. The efficacy of the FTIR technique for estimation of gas phase concentrations of H_2O, CO_2 and CO in 30kW pulverised flame showed that the method is reliable though it can not be stated as accurate. The length of the optical path length also affects the accuracy of the technique in flame measurements. The optical path should ideally be of same scale of smallest structures of the gas temperature field to obtain highly accurate results.

UV/FTIR optical results and standard extractive gas analysis by Horiba Mexa 7100 instrument in exhaust pip after turbo charger has been compared in EU-project Hercules Beta in 2010. Results from the test after turbo charger on MAN Diesels ship test engine show that the difference of CO_2 and NO concentration is within 5-6 % using same principles as in this project.

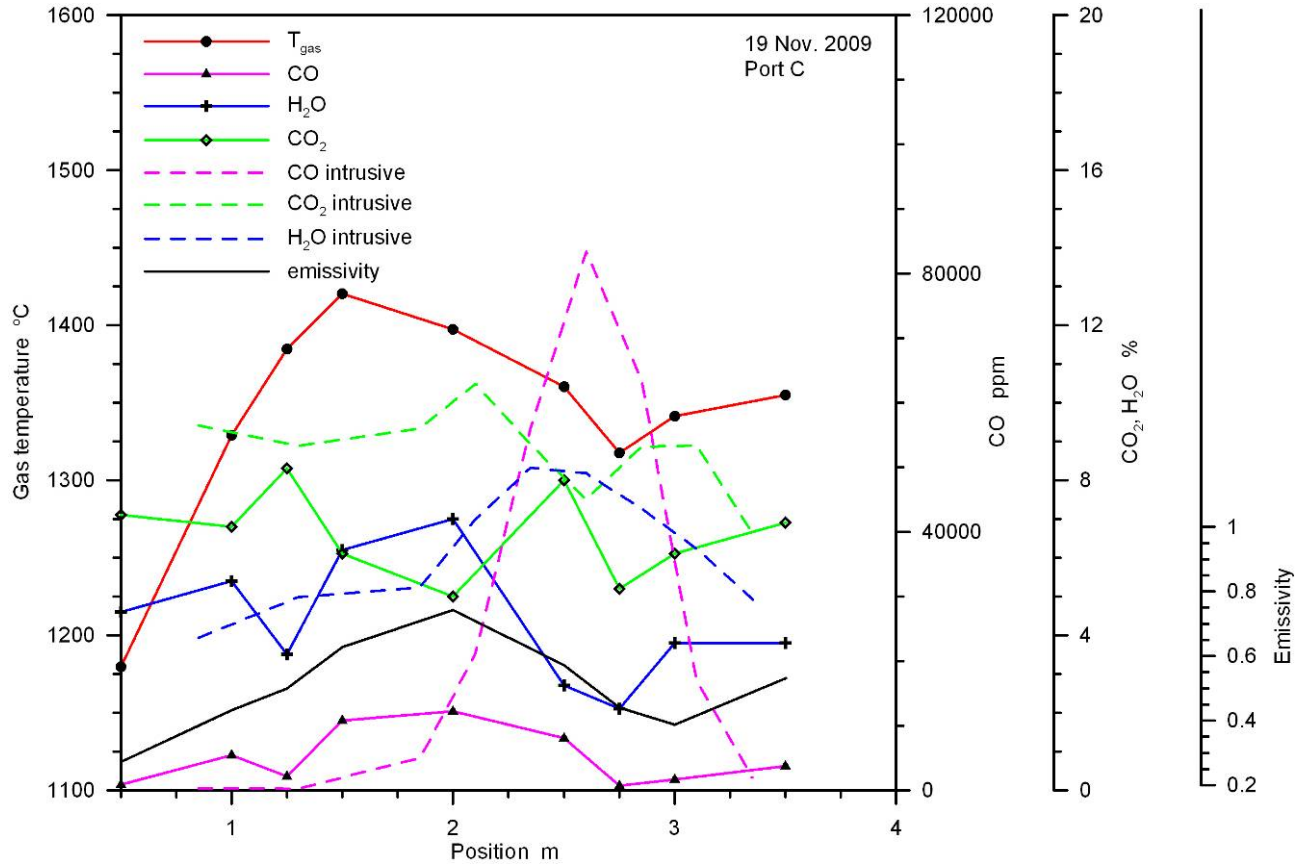

Figure 74 Gas temperature and comparison of FTIR probe measurements with extractive gas measurements at port C for coal flame. Very large deviations are observed for extractive and optical measured gas concentrations.

Very large deviations are observed for extractive and optical measured gas concentrations, Figure 74, that is hard to explain. Risø DTU has used the FTIR optical probe for mapping of large coal flames since and never seen deviations between optical and extractive measurements of this scale.

8 Measurements of gas composition with UV-probe

An optically based technique is beneficial because it is non-intrusive, accurate, fast and can be performed in situ for various extremely hard conditions. Fast Fourier Transform Infrared (FTIR) spectroscopy for in situ optical diagnostics of hot gases has extensively been developed for many years in our group and FTIR fibre-optic probes have successfully been used in practice on various industrial sites in Denmark and Europe [1] for temperature measurements. In humid and hot gas flows ultraviolet (UV) technique is more sensitive than FTIR for fast gas concentration measurements of NO and SO_2 and gives a great opportunity for simultaneous measurements of O_2 concentration. Analysis of the fine structure of the UV absorption bands of, for example, NO, SO_2 or O_2 allows also to determine a value of the gas temperature.

A measurement of OH and gas temperature by UV spectroscopy has been raised several times. Therefore, a note on UV measurements in a methane/air lab-burner at Risø DTU is included in report, see appendix C. It is shown from experiment at lab burner at Risø DTU that OH concentration and gas temperature can be quantified fairly well.

UV-probe, data analysis of UV-spectra and measurement results for coal, coal-wood and coal-straw flame is described in this chapter. It is the first time that the UV-probe is used for large scale flame measurements.

8.1 UV-probe and principles

The experimental layout used in UV *in situ* measurements includes a 5-m long water-cooled probe with removable optical head suitable both for UV and IR absorption measurements and the optical set-up described below.

8.1.1 Multi-function water-cooled probe

The water-cooled probe was designed for intrusive as well as non-contact combustion measurements in large scale flames, boilers and systems with particle loaded hot flue gas stream based on our previous experience, e.g. [2]. The diameter of the probe, 60 mm, was chosen based on calculations of the heat transfer, mechanical stiffness, cooling water requirements, weight and safe operation demands for the probe operated with insertions up to 8 m into a hot gas flow and temperatures over 1600^{o}C.

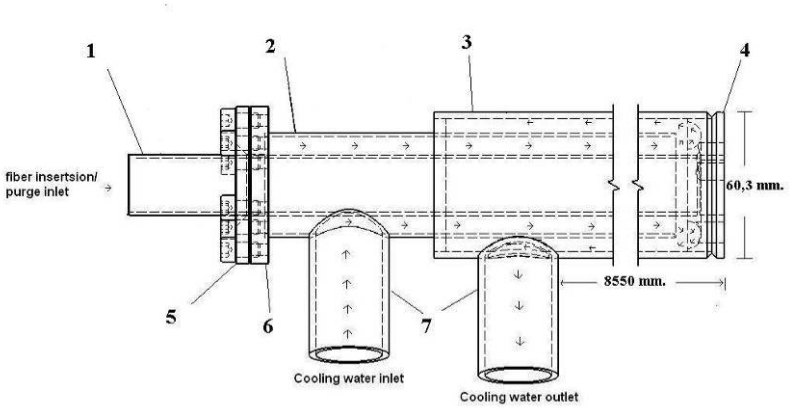

Figure 75 Design of multi-function water-cooled probe used for optical measurements (UV, LDA) and extractive particle sampling.

The probe consists of three stainless steel tubes 1-3, Figure 75. The outer tube 3 is made from commercially available the SAF2205 duplex stainless steel having a good strength at high temperature and deep insertions. All other components of the probe are made from the AISI 304 stainless steel. Cooling water is guided between tubes 1 and 2 to the probe front from where it returns back between tubes 2 and 3, Figure 75. Between tubes 1-2 and 2-3 there are spirals twisted around the corresponding inner tube to keep the tubes centred and create vortices in cooling water flow. The flange 4 is welded together with tube 1. An o-ring seals between tubes 1 and 2 at the back end.

This design makes it possible to insert the probe safely into a high temperature zone of a flame or flue gas flow without creating any stress on the tubes due to different thermal expansion of the components.

In the flange 4 there is a ¾ inch thread for mounting of the optical head (or other accessories) and three holes with M10 mm thread allowing cooling water to reach the optical head. The holes can be plugged when the optical head is not being in use. An optical fibre is drawn out through the inner part of the tube 1 that is also used as flow channel for the purge gas.

8.1.2 Design of a removable optical head

A removable optical head was mounted on the 5-m long probe for *in situ* measurement of UV gas absorption measurements. The optical head was made from AISI 304 stainless steel. In the Figure 76 a transparent view of the optical head without exterior cover is shown. A UV light source is inserted from the front end and kept in the correct position by a spring fixed with the front cap. A fibre adapter/lens module is inserted and fixed from the back side in a ¾ inch thread which is also used for mounting of the optical head onto the 5-m probe through a matching plug. Electrical wires and the purge gas for the UV light source are guided through two channels on the each side of the optical head.

Cooling water to the optical head is provided from the 5-m probe through a groove in the optical head end that is sealed by two o-rings. Water after passing through the groove is re-directed to the gap between the optical head main body and exterior cover through ten 5 mm holes. Return water leaves the UV head through 16x1 mm stainless steel tube fixed outside on the 5-m probe.

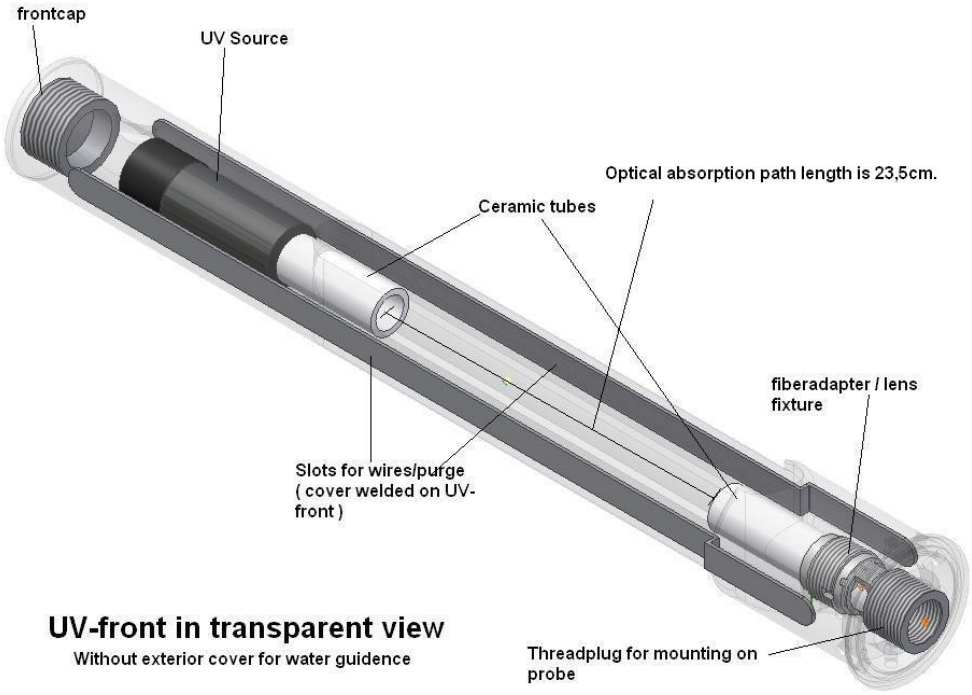

Figure 76 UV head to be mounted on water-cooled probe.

For protection of the optical components, i.e. the UV light source and lens/fibre module, from the heat radiation and contamination by soot and dust particles two ceramic tubes variable length enclosed in the optical head body are used. The tubes are kept in the place by a small spring loaded balls. Small nitrogen purge flow flowing around the source and fibre adapter/lens and next through the ceramic tubes is utilized to keep optics clean. The maximum optical absorption path length (or shortest acceptable ceramic tubes length) between both ends of the ceramic tubes is 23.5 cm, but optical path length was decreased to 18.0 – 18.5 cm to avoid deposit of particles on optics.

8.1.3 Optical set-up

A stable 20 W deuterium lamp (Cathodeon, model F05) with a plano-convex fused silica lens (LOT) was placed in the optical head and utilized as a parallel-beam light source in the range 190-400 nm. The UV light beam, after passing through a gas column was focused by a plano-convex fused silica lens (ISP optics) placed in fiber adapter/lens module into the entrance of 10-m long premium-grade solarization-resistant quartz fiber with 0.6 mm core diameter (Ocean Optics). The fiber was coupled to a high-resolution spectrometer.

High-resolution UV-absorption measurements were performed with a spectrometer (SpectraPro 2500i, Acton Research) equipped a CCD-camera (PIXIS-100B, Princeton Instruments). The dispersion of the grating (Holographic, 1800 mm^{-1}) was sufficient to cover a spectral range of 28 nm on the CCD. A spectral resolution was $\Delta\lambda$=0.046 nm with an entrance slit width of 40 μm.

8.2 Analysis of UV spectra

UV absorption spectra of hot gases and flames are rather complex. At elevated temperatures gases like O_2, NO, CO_2 and H_2O begin to absorb strongly UV light in the range 200-250 nm. It gives an opportunity to measure their concentrations. If Lambert-Beer law is applicable concentration of specie X can be calculated from relation:

$$\ln\left[\frac{I_0(\lambda)}{I(\lambda)}\right] = \sigma_x(\lambda,T)\cdot L\cdot[X], \qquad (1)$$

where:

I_0 - is measured light intensity without absorbing specie X;
I - is measured light intensity with absorbing specie X;
σ – is (temperature dependent) absorption cross section of specie X;
L – absorption pathlength, 18..18.5 cm;
$[X]$ – concentration of specie X.

In case of multi-component gas mixture Eq. 1 becomes:

$$\ln\left[\frac{I_0(\lambda)}{I(\lambda)}\right] = \sum_x \sigma_x(\lambda,T)\cdot L\cdot[X] = \sum_x c_x I_x^{ref}(\lambda), \qquad (2)$$

where,

X = NO, O_2, CO_2, H_2O etc;
$I_x^{ref}(\lambda,T)$ - reference absorption spectrum of specie X at temperature T, concentration $[X]$ and L;
c_x - scaling coefficient.

Assuming that temperature and temperature-dependent absorption cross sections are known, Eq. 2 can be solved for concentrations by advanced numerical methods (e.g. least squares with singular value decomposition, SVD).

For some species of interest (e.g. O_2, OH or NO) absorption cross sections $\sigma(\lambda,T)$ can be calculated with use of, for example, band oscillator strengths calculated from the first principles or experimentally measured.

An evolution of true oxygen absorption cross sections with temperature is shown in Figure 77. The major contribution into the absorption gives Schumann-Runge (S-R) system that is placed at low temperatures below 195 nm, Figure 77 (blue). Rise of the temperature causes population of low rovibronic states of X-state and, as consequence a lot of additional transitions from low-lying v'', J''-levels appear in the absorption, Figure 77 (red). Herzberg continuum, Figure 77 (olive) plays a negligible role in absorption even at high temperatures. O_2 Schumann-Runge continuum is only needed to be considered at wavelengths shorter than 195 nm.

An example of high-resolution O_2(4.37%) absorption spectrum at T=1300°C and 1.015 bar measured in Risø DTU hot flow gas cell (HGC) is shown in Figure 78 (blue). The spectrum was calculated based on

Eq. 1. Calculated S-R O_2 absorption spectrum for the same optical path-length, temperature and oxygen concentration is also shown by the red line (red). As one can see there is a good agreement between experiment and calculations.

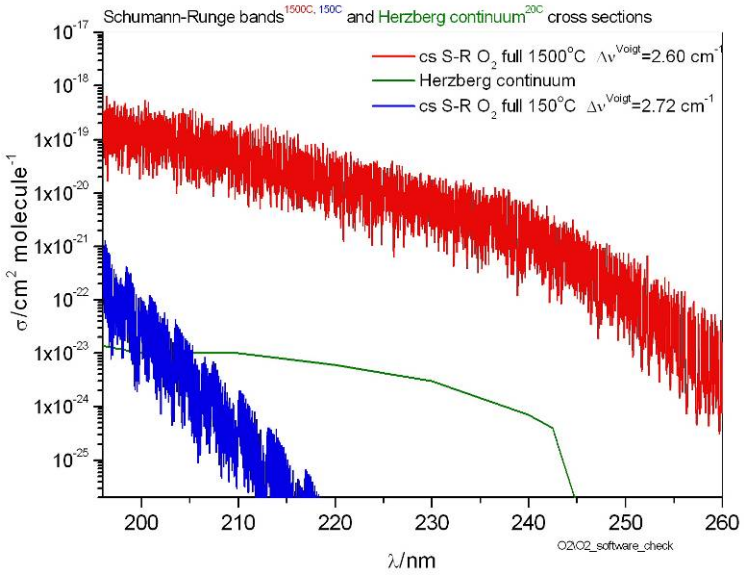

Figure 77 Calculated S-R O_2 absorption cross sections at T=150°C (blue), 1500°C (red) and Herzberg continuum at 23°C (olive).

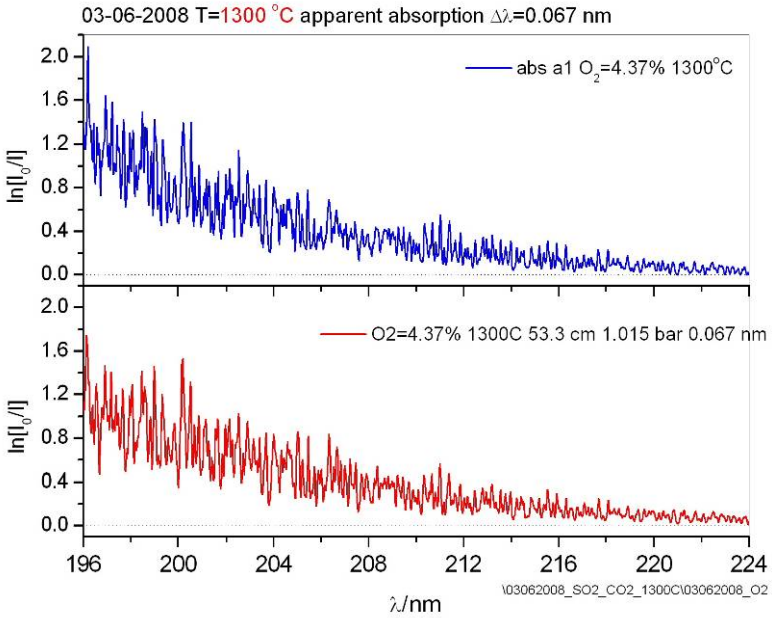

Figure 78 O_2(4.37%) absorption at T=1300°C and 1 bar in HGC (blue) and calculated S-R O_2 absorption bands at O_2=4.37%, T=1300°C, L=53.3 cm and $\Delta\lambda$=0.067 nm (red).

In case of OH radical or NO molecule rise of the temperature causes significant population of rotational levels with high J''-numbers within one X(v'')-state. As a consequence in a v'-v'' absorption band a "hot tail" is observed. Spectral extension of the tail depends on the gas temperature in question and fine structure of the v'-v'' absorption band can be used for calculation of the gas temperature (not brightness one). In Figure 79 OH absorption spectrum measured at Port B (2 m, 0^o) during test measurement campaign in May 2009 is shown (blue). The spectrum is on the top of SO_2 spectrum. The calculated OH absorption spectrum at OH=140 ppm and T=1300°C is shown in the same figure in red. One can see very well agreement between experiment and calculations.

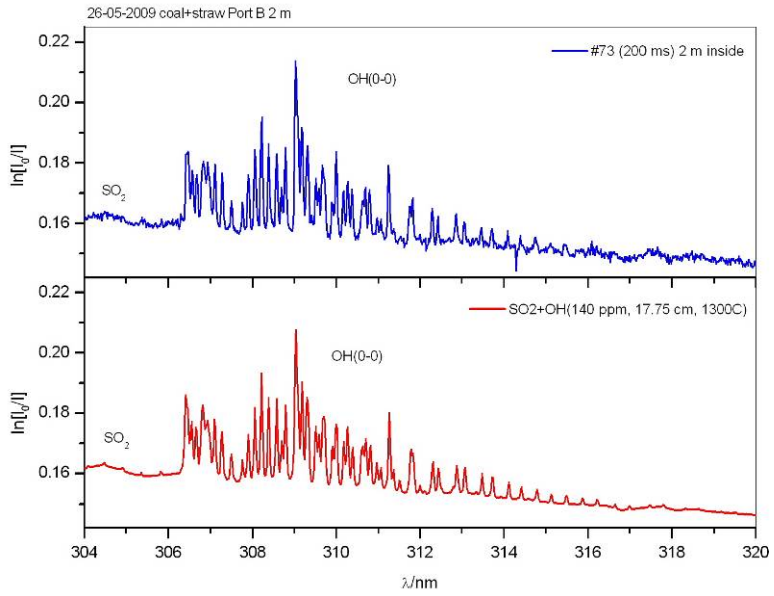

Figure 79 In-flame OH high-resolution UV absorption spectrum (Δλ=0.046 nm) measured at Port B (2 m, 0^o, blue) and calculated one at OH=140 ppm, 1300°C, L=17.75 cm (red).

High temperature UV absorption spectra of NO measured in HGC, their calculations and applicability of Lambert-Beer law for NO absorption were discussed in the ref. 4.

In case polyatomic molecules like H_2O, CO_2 and SO_2 calculations normally are impossible because band oscillator strengths are unknown. Therefore absorption cross sections should be experimentally measured.

UV absorption spectra of polyatomic molecules are complicated and consist of various absorption bands overlapping with each other. The spectral resolution of a spectrometer in UV is normally not enough to resolve a fine structure in the absorption spectra. UV high temperatures absorption spectra of H_2O and CO_2 show continuum-like structure without any characteristic features. An example of measured UV absorption cross sections of CO_2 in HGC at temperatures 1000°C and 1500°C is shown in Figure 80.

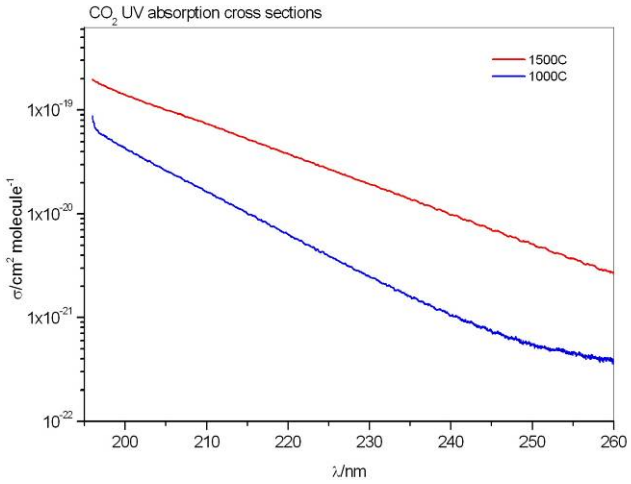

Figure 80 CO_2 absorption cross sections measured in HGC at T=1000°C (blue) and 1500°C (red).

CO_2 and H_2O absorption cross sections can be described in form

$$\ln\sigma(\lambda,T) = a(T)+b(T)\lambda, \qquad (3)$$

where coefficients *a(T)* and *b(T)* are functions of *T*. Several measurements performed at temperatures 800-1500°C in HGC have been used in order to determine *a(T)* and *b(T)* functions. Because low-resolution UV absorption spectra measured in flame shown continuum-like behavior (below), Eq. 3 has also been used to fit calculated oxygen absorption cross sections at various temperatures (e.g. in Figure 77).

In opposite, an UV absorption spectrum of SO_2 shows two broad maxima (200-230 nm and 260-320 nm) with some temperature-pressure dependent "saw"-like structure, Figure 81.

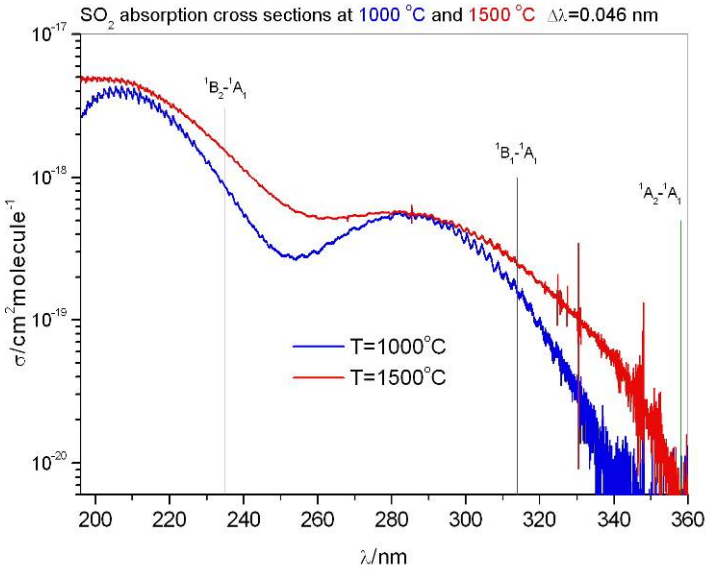

Figure 81 Absorption cross sections of SO_2 measured in HGC at T=1000°C (blue) and 1500°C (red). Vertical lines show positions of the origins for three SO_2 absorption bands.

SO_2 absorption cross-sections measured between 800-1500^{o}C with temperature step of 100^{o}C in HGC were tabulated and used in calculations (Eq. 2).

In order to calculate species concentrations gas temperature has to be calculated first. It was done by using CO_2 absorption in 216-223 nm spectral range where CO_2 absorption dominates over O_2, H_2O and SO_2 ones at concentrations typical for coal (and straw) combustion. A part of an experimental spectrum (after subtraction of scattered light offset, absorption by soot and "KCl"-like absorption structure in 230-270 nm) in $\ln(\ln\left[\frac{I_0(\lambda)}{I(\lambda)}\right]), \lambda$ coordinates can be fitted by a straight line, like Eq. 3. Then the slope of the line ($b(\lambda)$ coefficient in Eq. 3) will give a gas temperature. It should be noted that this method uses CO_2 UV absorption which is strong enough at temperatures more than 800^{o}C. Therefore if, for example, gas in the measurement volume is inhomogeneous like a mixture of hot, > 800^{o}C and cold < 800^{o}C parts calculated species concentrations will be underestimated.

Once gas temperature is calculated reference absorption spectra of O_2(2%), CO_2(12%) and H_2O(8%) were calculated. Because at low-resolution ($\Delta\lambda$=0.19 nm) NO absorption bands measured in a coal or coal/straw flames can well be described by some effective absorption spectrum at T=1000^{o}C and NO=120 ppm that spectrum has been used as a NO reference spectrum. Tabulated SO_2 absorption cross sections were used to calculate a reference SO_2 (200 ppm) spectrum. Finally by solving of Eq. 2 with least squares SVD method (ref. 5) scaling coefficients c_x were calculated and species concentrations were determined.

8.3 Results of UV probe measurements

UV absorption measurements were performed with high ($\Delta\lambda$=0.046 nm) and low ($\Delta\lambda$=0.19 nm) spectral resolutions. Two different gratings (1800 mm^{-1} and 300 mm^{-1}) have been used. High resolution allows one to see fine structures in the spectra but reduces useful spectral range. Low resolution gives an opportunity to cover a broad spectral range but hide fine details. An example of high resolution absorption spectra is shown in Figure 82.

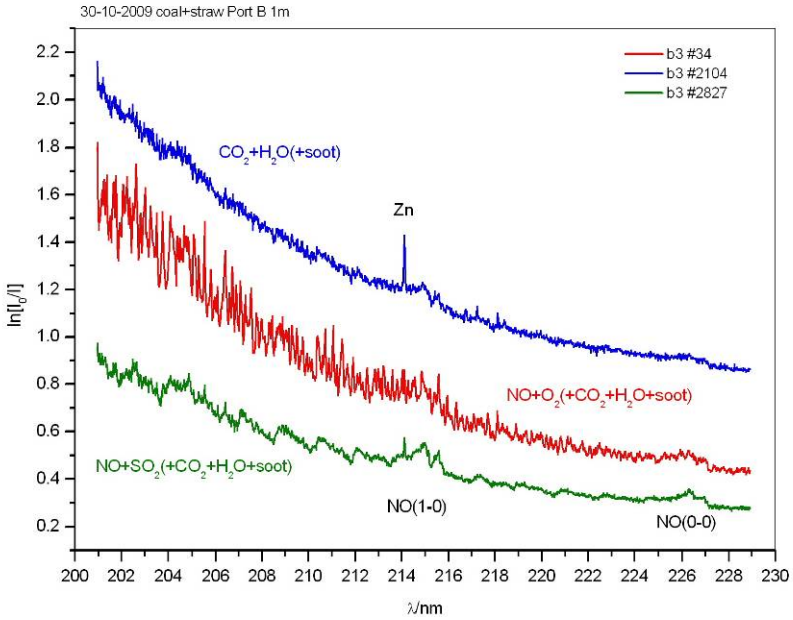

Figure 82 An example of raw UV high resolution spectra (1 ms, $\Delta\lambda$=0.046 nm) measured at Port B (1 m, 0^o) in coal/straw flame.

In Figure 82 three typical absorption spectra are shown. The first (olive) has clear SO_2 fingerprints, the second (red): O_2 (see also Fig. 8-2-2) and the third (blue): CO_2+H_2O continuum. Well localized NO absorption bands and an atomic absorption line (Zn) are clearly seen. Offsets in the spectra are due to scattered light and soot absorption. Soot has weak wavelength dependence in the range 190-250 nm (ref. 6) and can be assumed to give a fairly constant offset in the absorption base line. Gas temperature can be calculated from an analysis of fine structure of NO absorption bands (olive), O_2 absorption features (red) or CO_2 spectra in 216-223 nm (olive). Following analysis may be done by solving of Eq. 2. Some recognition algorithms should also be used in the spectra analysis. A method for the analysis spectra in Figure 82 is under development.

An example of low resolution spectra ($\Delta\lambda$=0.19 nm) is shown in Figure 83. The spectra in 195-360 nm have been measured without any grating movement. Three spectra in Figure 83 show typical absorptions features observed in the measurements. In the range 195-230 nm absorption is due to CO_2/H_2O/O_2. In the range 230-320 nm there is absorption by OH radical and "KCl-like" structure (230-270 nm). At 320 nm < λ absorption is mainly due to soot. Scattered light gives also some constant offset.

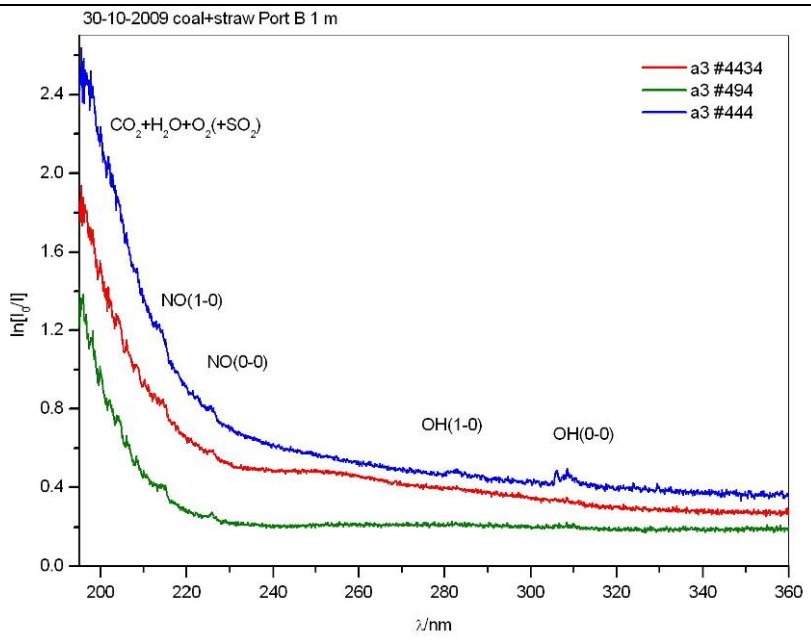

Figure 83 An example of raw UV low resolution spectra (1 ms, $\Delta\lambda$=0.19 nm) measured at Port B (1 m, 0°) in coal/straw flame.

An example of results of low resolution spectra analysis is shown in Figure 83 and Figure 84 at Port B (3.25 m, 0°). "0"-values in concentrations or temperatures correspond to "bad frames" where the absorption was too strong (> 2.99) or gas temperature calculated was too low (< 200°C) or too high (2000°C <). A lot of bad frames are observed in particle dense zones of the flame.

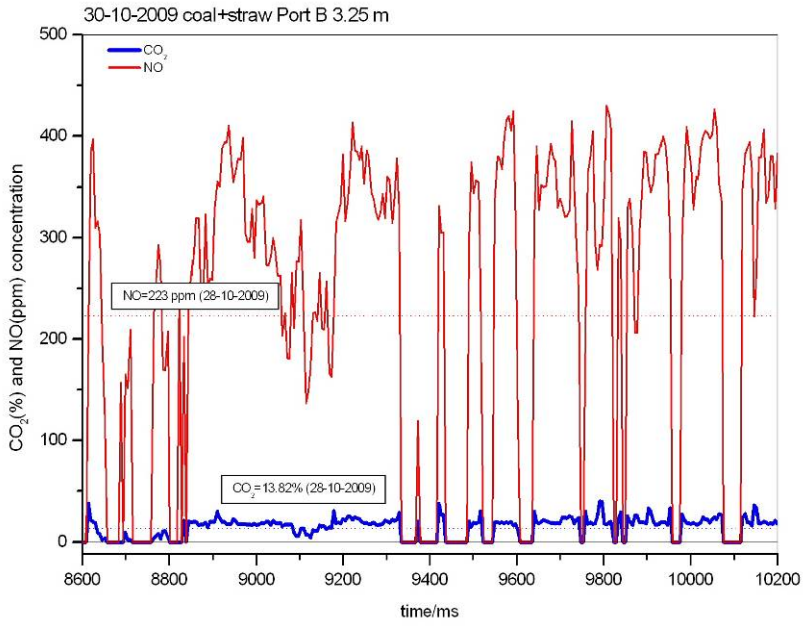

Figure 84 CO2 (blue) and NO (red) concentrations versus time at Port B (3.25 m, 0°) calculated from low-resolution UV absorption spectra measured in coal-straw flame. CO_2/NO concentrations calculated from gas sampling measurements on 28-10-2009 are shown by horizontal dot lines.

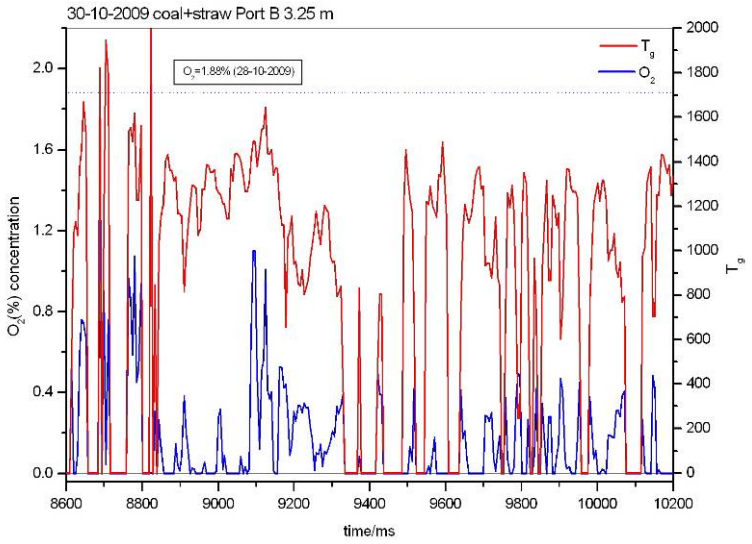

Figure 85 Gas temperature (red) and O_2 concentration (blue) versus time at Port B (3.25 m, 0^o) calculated from low-resolution UV absorption spectra measured in coal-straw flame. O_2 concentration calculated from gas sampling measurements on 28-10-2009 is shown by horizontal dot line.

As one can see from Figure 84 in average there is well agreement between fast UV measurements and gas sampling measurements performed at the same location (but in another day) for NO and CO_2 concentrations (extractive results in Figure 41). The gas temperature is highly fluctuating between 800°C and 1600°C that is also in agreement with IR *in situ* measurements of gas temperature. However there is significant difference between fast UV and gas sampling measurements of oxygen. In general, fast UV measurements give significantly less oxygen concentration as measured by gas sampling. One explanation may be due to inhomogeneous gas mixture in the absorption volume as discussed before because oxygen absorption is very temperature dependent. Other one is due to solution of Eq. 2 in the spectral range 200-360 nm. Oxygen absorption in fact is very weak compared to CO_2 and narrow localized (200-220 nm). Finding of a solution in Eq. 2 over 200-360 nm spectral range with noisy experimental data may give reduced oxygen concentration. However it is unlikely that the reduction will be as significant as one can see in the Figure 85.

NO formation in flames has been one of the issues in combustion for many years. Three possible mechanisms of NO formation are well discussed. In the flame core where the temperature is high thermal NO formation (Zeldovich) mechanism is very likely. In Figure 86 a part of time behaviour of NO concentration together with temperature variations at Port B (2 m, 0^o) is shown. One can see correlation between NO concentration variation and temperature fluctuations supporting Zeldovich mechanism of NO formation. Temperature variation on full time scale is shown in Figure 88. On average gas temperature is ca. 1200°C which is just in the middle of temperature variations in the Figure 86.

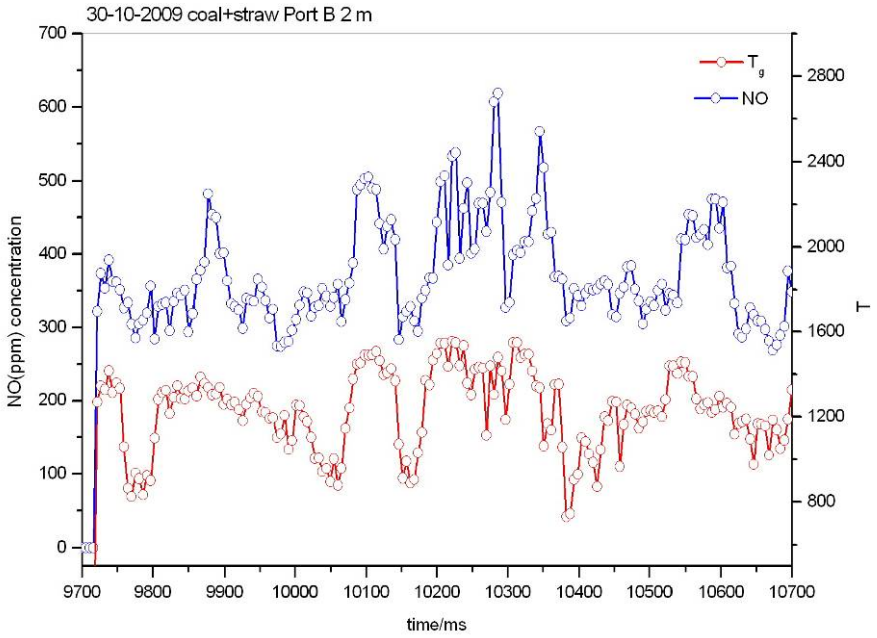

Figure 86 Time variations in gas temperature (red) and NO concentration (blue) at Port B (2 m, 0^o) calculated from low-resolution UV absorption spectra measured in coal/straw flame.

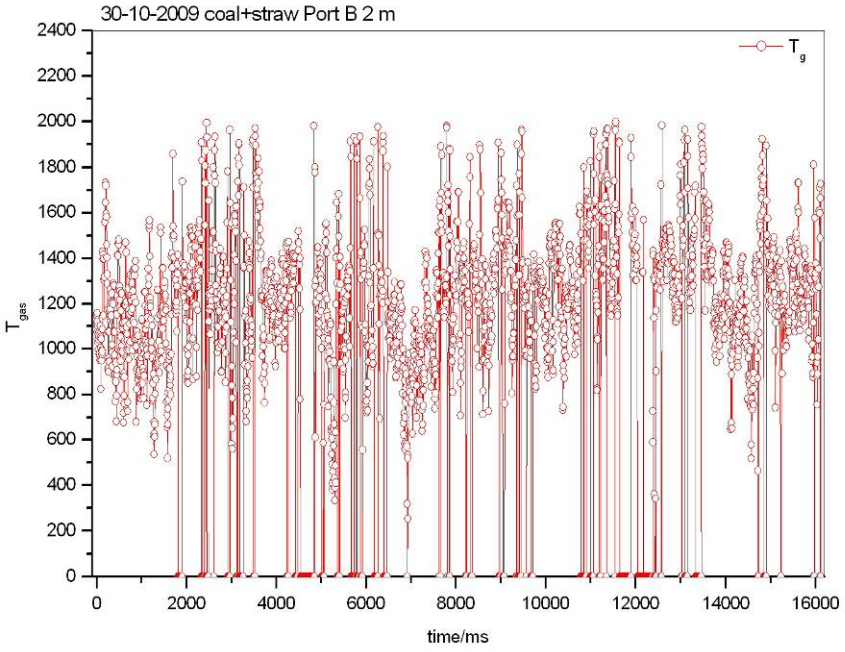

Figure 87 Time variation in gas temperature at Port B (2 m, 0^o) calculated from low-resolution UV absorption spectra measured in coal/straw flame.

In pure coal flame measurements at the same location show significant amount "bad frames" compare to coal/straw ones, Figure 88. Mean gas temperature is somewhere between 800°C and 1100°C. Such large variations in gas temperature can be understood by significantly higher turbulence compared to the coal/straw case.

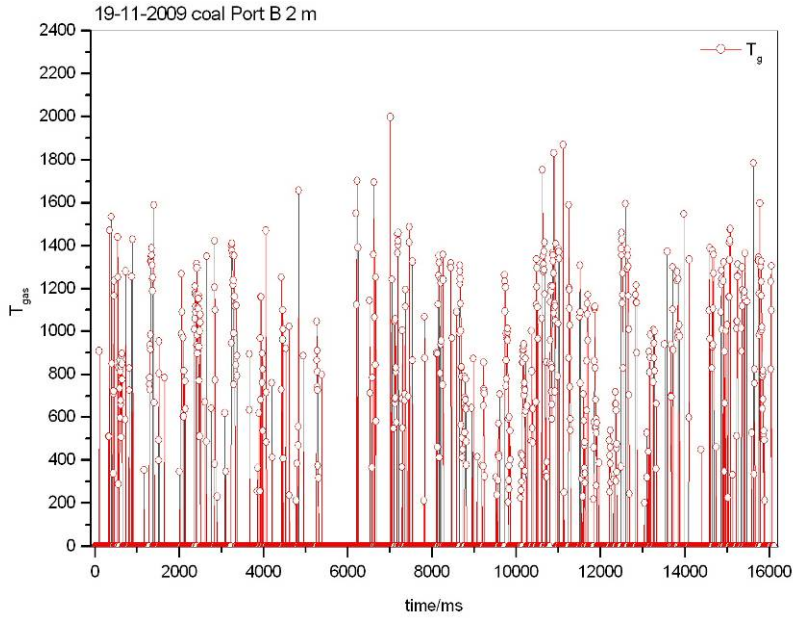

Figure 88 Time variation in gas temperature at Port B (2 m, 0°) calculated from low resolution UV absorption spectra measured in coal flame.

A part of the temperature variation taken from Figure 88 is shown in Figure 89. In the same figure NO concentration variation is also shown.

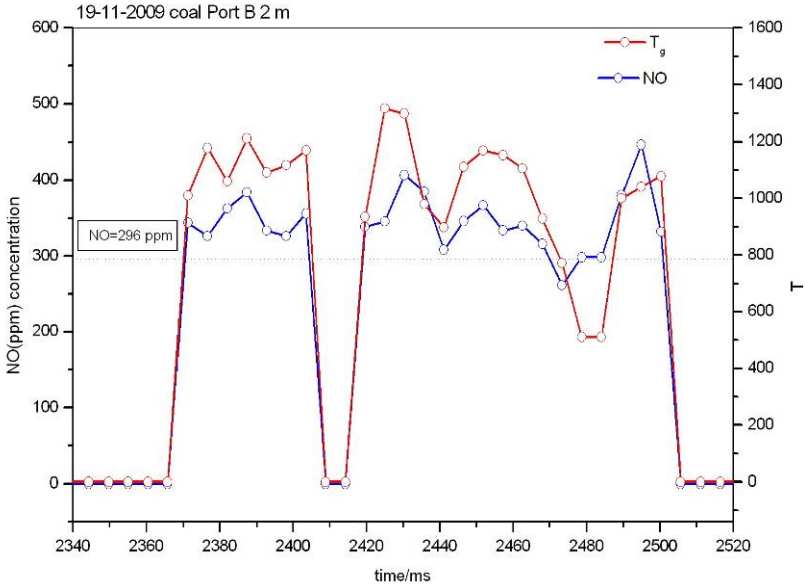

Figure 89 Time variations in gas temperature (red) and NO concentration (blue) at Port B (2 m, 0°) calculated from low-resolution UV absorption spectra measured in coal flame. NO concentration from gas sampling measurements is 296 ppm.

Several observations can be made from the Figure 89: 1) averaged NO concentration calculated from fast UV measurements fits with the value from gas extraction measurements; 2) average temperature is approx. 1100°C and 3) NO concentration follows temperature variation.

Several conclusions about fast UV measurements performed during near burner measurements at Studstrup (SSV unit 4) can be made.

- fast UV absorption technique has been successfully used for in flame measurements;
- UV technique can be used for O_2, NO and OH (precursor of NO formation) *in situ* concentration measurements;
- gas temperature can be calculated from NO or OH high-resolution absorption spectra;
- SO_2, CO_2 and H_2O concentrations can also be measured;
- it is necessary to use high-resolution absorption measurements for accurate calculations of O_2 and SO_2;
- method for the analysis of high resolution UV spectra for gas temperature, NO and O_2 is under development.

Discussion of results, comparisons

Results were discussed in earlier chapters, but some additional plots and comments are given in the following.

Oxygen and gas temperature profiles at port B and C for all three flames are compared in Figure 90. Gas temperature profiles differ at port B (2.6 m from burner wall), but approach same temperature level at port C (4.0 m). A dip of approx. 150°C is seen in temperature of the coal-straw flame in region with high density of straw particles and gas temperature level lower than for other flames at port B.

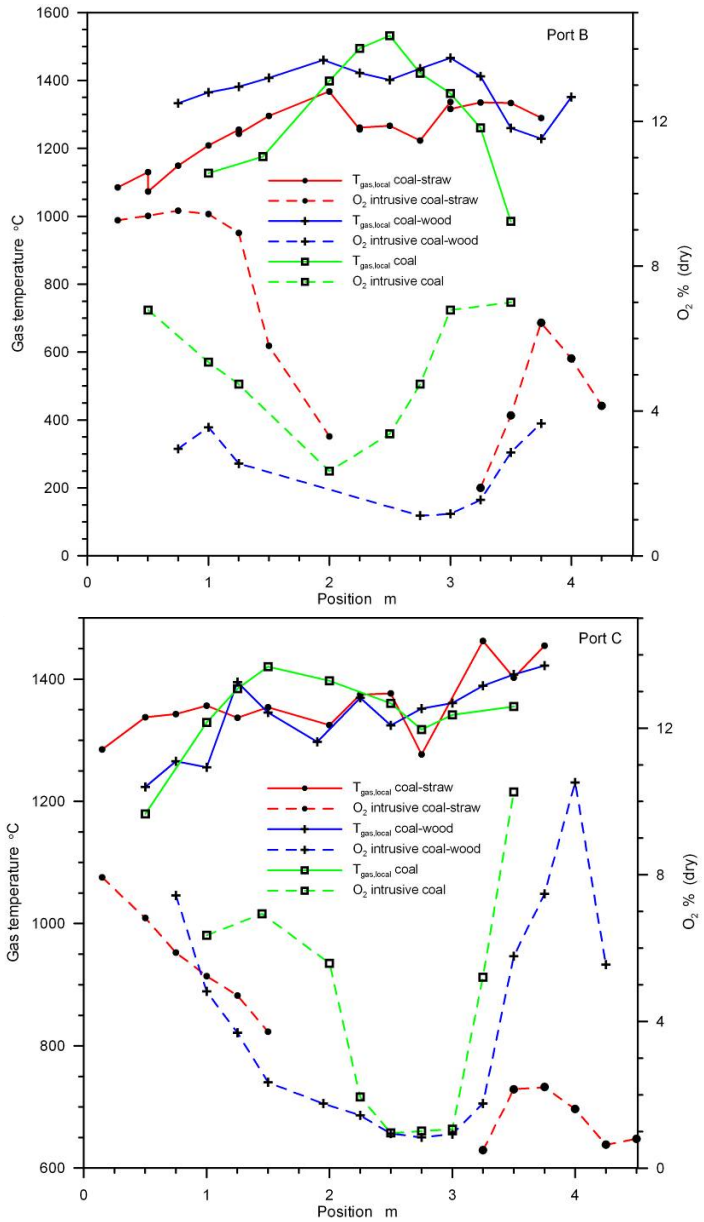

Figure 90 Gas temperature and oxygen (dry) profiles at port B (upper plot) and port C (lower plot) for coal-straw (red curves), coal-wood (blue curves) and coal flame (green curves).

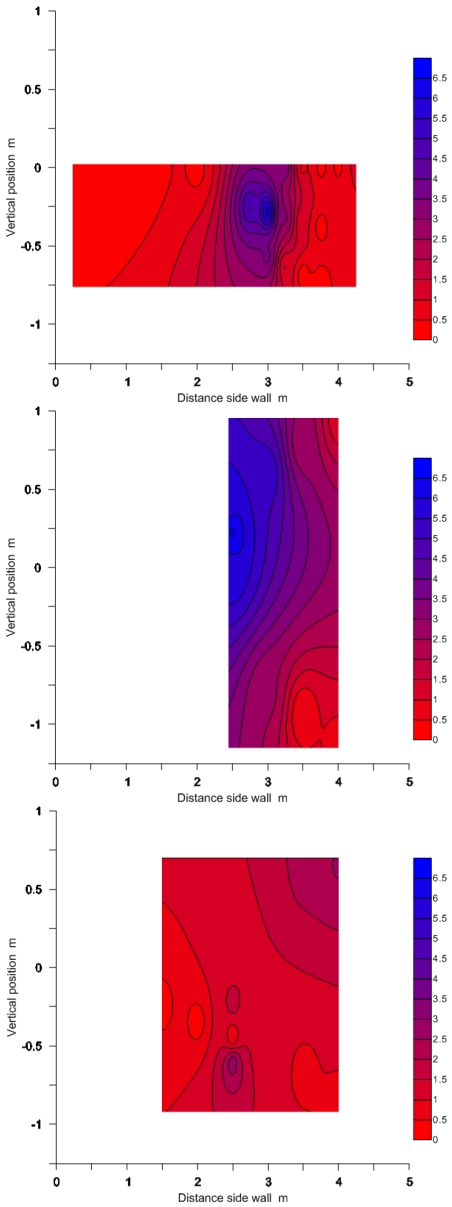

Figure 91 3D surface plot of CO concentration (wet) at port B (plot top), C (plot middle) and D (2.6 m, 4.0 m and 6.7 m from burner wall) for coal-straw flame based on extractive measurement.

Location of flame is sometimes hard to see from gas temperature and flow measurements at a certain distance from burner, but it can be seen from plot of CO concentration, Figure 91. The coal-straw flame is at port B and C centred on the geometric burner axis and very little effect of flame lift is observed. Centre of coal-straw flame moves away from side wall and upwards (with more than 1 m) at port D, which probably is due to flame lift due to gravity and flow from burners below. CO level of 6% is seen at port B and C, and CO level is still high (ca. 2.5%) at port D. The high CO level at port D is expected as large and cold straw particles are still present at this location.

9 Conclusion

Full-scale validation data have been obtained at the Studstrup power plant. Measurement campaign on 3 different large scale pulverized flames was carried out on burner 46 at Studstrup unit 4 boiler in October – November 2009. 4 measurement ports were established in the project to obtain access to flame, and the burner was rebuilt to enable a switch of co-fire fuel from straw to wood dust from a separate fuel line. A combination of intrusive and non-intrusive measurement techniques were used in order to obtain a data set with information on gas and particle flow field, fast temporal fluctuations/turbulence, temperature, gas composition and particle burn-out. Many of the measurement techniques were used for the first time on a large scale burner and special 5 m long multi-function water-cooled probes have been developed for the purpose. LDA velocity measurements have been carried out earlier at Risø on a 1.3 MW coal flame through a quartz window, but long water-cooled fibre-optic probes must be used for large scale measurements due to size of flame and high particle density. Experimental time is usually limited for large scale experiments due to operation costs. All new instrumentation was tested before the measurement campaign to avoid and minimise technical problems and collect data as scheduled in a fast manner.

A new generation of multi-function water-cooled probes were developed to protect sensitive measurement equipment from heat and deposits of particles on windows. Two identical 5 m long water-cooled probes was used for LDA velocity measurements, particle sampling and UV-spectroscopy. The same probe can be used for extractive gas sampling and FTIR spectroscopy, but a special probe was used in this case to obtain extractive and FTIR optical measurements simultaneously with the same probe. Optical measurements with a special combined IR and UV optical head was originally planed, using results from ForskEL project no. 7319 “New IR-UV gas sensor to energy and transport sector”, but it was decided to minimise risks and perform separate UV-spectroscopy measurements as it was the first time this method was to be used for large scale flame measurements.

Risø DTU’s older LDA system was upgraded in the project. It was a nice experience to the team that 2D LDA velocity measurements can be performed in all regions of the flames without any problems or delays. Temperature in tip of probe was only raised by 7°C when probe was fully inserted (4 m) into a 1400-1600°C hot flame. It is concluded that it is in principle possible to map flow fields in boilers with up to 9 m long ø60 mm water-cooled probes. A 5 m long probe was used in the project that is easier to handle and long enough to map a wall burner. Axial and tangential velocities were measured at 235 points in coal-straw flame at 4 distances from burner. These may be the first data of this type describing co-fired flames and possibly any near-burner flame from a utility-scale boiler. Variation among replicates is small compared to the trends in the data and the measured velocity fluctuation at that point. Characteristics of the well known swirl burner flow are seen in first part of flame.

Mapping of the flame was mainly performed from port B and C with all measurement techniques. Major changes in the flame happens between port B and C (2.6 – 4.0 m from burner wall), i.e. jet like behaviour of flame at port B and impact from swirl/recirculation zone is clearly seen at port C. A simple picture of the flame vanishes at port D due to asymmetry and influence from other burners. The probes were swept approx. ±12° up and down to map a vertical plane to follow lift of flame and flow of biomass particle in bottom of flame. Coal-straw flame appears for measured CO concentrations in grid to be close to geometrical burner axis at port C (4.0 m). Movement and mixing of the larger biomass particles can be seen in thermal images from exit of burner to port D approx. 6 m from boiler back wall. Structures of straw and wood particles can still be seen at port C

and D, i.e. very large particle density fluctuations are seen locally. The poor mixing of biomass particles with gas is seen in IR pictures and movement of larger particle structures can be observed with 10 ms time step. The poor mixing is clearly seen in the fast optical measurements of temperature and gas composition, e.g. CO large concentration fluctuations.
Fluctuations of intensities from fuel particles in infrared pictures have an approximately 1/f noise power spectrum that in this system can be seen as a long-term effect, where something suddenly happens like straw moves from one side of burner to another, suddenly no straw flow, etc.

Fast UV absorption technique has been successfully used in low and high resolution measurements for the first time. The UV technique can be used for O_2, NO and OH (precursor of NO formation) in situ concentration measurements.
Gas temperatures can be calculated from NO or OH high-resolution absorption spectra. Risø DTU was in 2011 involved in UV measurements on premixed natural gas flame at ultra-wet conditions using UV method and principles establish in this project. It was concluded that a reactor network is capable of predicting NO_x and CO emissions with good agreement to the experimental results, and the calculated OH concentration in the gas flame agree well with the measurements (ref. 17). However, conditions are far more complex and dynamic in this project as seen in chapter 8.3.

SO_2, CO_2 and H_2O concentrations can also in principle be measured based on low resolution UV-spectra, but the methodology is sensitive to soot absorption and might fail for some conditions. It is necessary to use high-resolution absorption measurements for accurate calculations of O_2 and SO_2 concentrations. A method for the analysis of high resolution UV spectra for gas temperature, NO and O_2 is under development. Selected measurement points in flames was analysed manually and results appears to be consistent with other measurements.

Gas concentration measurements by FTIR fibre-optic probe and extractive gas sampling were performed in all three flames. The combination of fast optical measurements and extractive measurements gives a more complete picture of conditions in flame, including gas temperature measurements. Problems arise in most particle dense zones beginning of flames with blocking of the gas sampling line and noisy FTIR signals, and some measurement points were skipped to save experimental time. A major problem seems to be very large particles (straw and wood particles several mm) entering the point of measurement in a highly unstable way. Another problem that can affect performance of FTIR optical method, especially for measurement of CO_2, is that gas temperature is assumed to be constant over the 25 cm optical path. The FTIR method has been used in other large scale flames in 2010 (air and oxy-fuel coal flames) with good results for gas temperature, CO and H_2O, but deviations were observed for CO_2 in particle dense near burner region.

Some improvements in instrumental setup should be considered in future measurement campaigns, e.g. electrical heating of gas sampling line inside the water-cooled probe that will probably reduce problems with blocking and extend list of components (PAH, HCl, …). The optical path could be reduced for use of the FTIR fibre-optic probe in flames to obtain more uniform gas temperature conditions along the optical path and more accurate results; however, this would require a more complex optical setup. Combination of extractive gas composition measurements and IR based gas temperature measurements appears to be the simplest and fastest tool for basic flame diagnostics.

Parts of work have been presented at conferences, ref. 14-16. Methods and experience gained from project will be useful in future work and projects. The report and methods established is expected to play a role in the start up process of experimental large scale campaigns in DSF project “GREEN”.

10 References

[1] S. Clausen, Meas. Sci. Technol. 7 (1996) 888-896

[2] J. Bak, S. Clausen, Meas. Sci. Technol. 13 (2002) 150-156

[3] Jensen, P.A.; Ereaut, P.R.; Clausen, S.; Rathmann, O., Local measurements of velocity, temperature and gas composition in a pulverised-coal flame. J. Inst. Energy (1994) 67 , 37-46

[4] A Fateev and S Clausen, Int. J. Thermophys, 2008, DOI 10.1007/s10765-008-0438-5

[5] CL Lawson and RJ Hanson, Solving least squares problems, SIAM, Prentice-Hall Inc., New Jersey, 1995

[6] G. Basile, A. Rolando, A. D'Alessio, A. D'Anna, P.Minutolo, Proc. Combust. Inst. 29 (2002) 2391-2397

[7] Nazeer, W. A.; Pickett, L. M.; TREE, D. R., In-Situ Species, Temperature and Velocity Measurements in a Pulverized Coal Flame. Combustion Science and Technology 1999, 143 (1), 63 - 77.

[8] Weber, R.; Dugué, J.; Sayre, A.; Visser, B. M., Quarl zone flow field and chemistry of swirling pulverized coal flames: Measurements and computation. Symposium (International) on Combustion 1992, 24 (1), 1373-1380.

[9] Truelove, J. S.; Holcombe, D., Measurement and modelling of coal flame stability in a pilot-scale combustor. Symposium (International) on Combustion 1991, 23 (1), 963-971.

[10] Godoy, S. G.; Ismail, M.; Lockwood, F. C., Measurements in a Cylindrical Pulverized Coal Furnace. Influence of Swirl Number on Combustion Performance. Combustion Science and Technology 1989, 67 (1), 59 - 72.

[11] Costa, M.; Costen, P.; Lockwood, F. C.; Mahmud, T., Detailed measurements in and modelling of an industry-type pulverised-coal flame. Symposium (International) on Combustion 1991, 23 (1), 973-980.

[12] Smart, J. P.; Woycenco, D. M.; Morgan, D. J.; vandeKamp, W. L., Studies on scale-up of swirl-stabilised pulverised-coal burners in the thermal input range 2.5-12 MW. Journal of the Institute of Energy 1996, 69 (480), 131-143.

[13] Clausen S; Astrup P., Oblique laser-sheet visualization. Applied Optics, Vol. 34, Issue 19, pp. 3800-3805 (1995)

[14] Evseev, V.; Clausen, S., On Developing a Spectroscopic System for Fast Gas Temperature Measurements in Combustion Environments. Presented at: 1st Joint Meeting of the Scandinavian-Nordic and French Sections of the Combustion Institute. Copenhagen (DK), 9-10 Nov., 2009

[15] Beutler, J. B.; Baxter, L.; Clausen, S.; Fateev, A.; Hvid, S. L., Biomass co-firing for CO_2 management: Full-scale field test. Presented at: 2010 AIChE Annual Meeting. Salt Lake City (US), 7-12 Nov, 2010. Conference paper published in book/proceeding.

[16] Jacob B.; Clausen S.; Fateev; Hvid S.; Kær S.;Baxter L., Cofiring Field Test in a Full-Scale 350 MWe Power Production Plant: Near-Burner Measurements, 2010 Clearwater Clean Coal Conference.

[17] Göke S.; Schimek S., Fateev A., Clausen S.; Kuhnz P; Terhaar S.; Paschereit C. O., Investigation of NOx and CO Formation in a Premixed Swirl-Stabilized Flame at Ultra Wet Conditions, paper submitted 2011 to the AIAA Joint Propulsion Conference

[18] Jacob Brix J.; Toftegaard M.B.; Clausen S.; Jensen A.D., Advanced Diagnostics in Oxy-Fuel Combustion Processes, The Use of IR- and FT-IR in Pilot- and Laboratory Scale Reactors. Final Report, project no.: PSO-010069, 2011.

Appendix A Plant Operating Conditions

ID-tag description:

SSV0-EPC20DF901BXQ02	Total straw consumption, [Tons/hr]
SSV4-HAH00FU600XQ01	Boiler heat delivery to steam, [MWth]
SSV4-HHA10DU002XQ02	Coal feed rate to mill #10 (corrected value), [kg/s]
SSV4-HHA20DU002XQ02	Coal feed rate to mill #20 (corrected value), [kg/s]
SSV4-HHA30DU002XQ02	Coal feed rate to mill #30 (corrected value), [kg/s]
SSV4-HHA40DU002XQ02	Coal feed rate to mill #40 (corrected value), [kg/s]
SSV0-EPC20DF901BXQ01	Straw feed rate as coal equivalent, [kg/s]
SSV4-HFE71CF001XQ01	Primary Air flow to mill #10, [Nm^3/s]
SSV4-HFE72CF001XQ01	Primary Air flow to mill #20, [Nm^3/s]
SSV4-HFE73CF001XQ01	Primary Air flow to mill #30, [Nm^3/s]
SSV4-HFE74CF001XQ01	Primary Air flow to mill #40, [Nm^3/s]
SSV4-HHL11FF301XQ01	Secondary Air flow to burner gallery #10, [Nm^3/s]
SSV4-HHL21FF301XQ01	Secondary Air flow to burner gallery #20, [Nm^3/s]
SSV4-HHL31FF301XQ01	Secondary Air flow to burner gallery #30, [Nm^3/s]
SSV4-HHL41FF301XQ01	Secondary Air flow to burner gallery #40, [Nm^3/s]
SSV0-EPC21DF901BXQ01	Secondary Air supplement for dual-fuel burner #42, [Nm^3/s]
SSV0-EPC22DF901BXQ01	Secondary Air supplement for dual-fuel burner #43, [Nm^3/s]
SSV0-EPC23DF901BXQ01	Secondary Air supplement for dual-fuel burner #44, [Nm^3/s]
SSV0-EPC24DF901BXQ01	Secondary Air supplement for dual-fuel burner #45, [Nm^3/s]

Note: The secondary air supplement per dual-fuel burner is calculated as follows: If the straw conveying air fan is active, the secondary air supplied for that burner is reduced by approximately 1.1 Nm^3/s (which equals to the amount of conveying air which is kept at a constant rate). If the straw feeding line is active, supplemental secondary air is now added according to the straw feeding rate of that individual line (lines may operate at different feed rates). The aim is to compensate the coal burner for the introduction of straw, including the presence of conveying air. In the event, as may be seen on the graphs for November 18, during the feeding of wood dust the secondary air supply to burner #45 (which was allocated to burner #46 during the period where the straw line for burner #45 was shifted to burner #46) was considerably lower than what it would normally have been during straw feeding. This is due to the fact that the straw feeding line was inactive, thereby not activating the signal to supplement secondary air. At the same time, since the straw conveying air fan was in operation (carrying wood dust to the burner) this resulted in a reduction of 1.1 Nm^3/s of secondary air to that burner. The significance of this is that burner #46 has been operating in a “fuel rich” mode. It is believed that this has no large effect on the flame core (where secondary air has not yet mixed with the fuel) but may have had some impact on conversion in the outer regions of the flame.

SSV4-HHL45FU401XQ01	Secondary Air delivered to burner #45, [Nm^3/s]
SSV4-HHL46FU401XQ01	Secondary Air delivered to burner #46, [Nm^3/s]

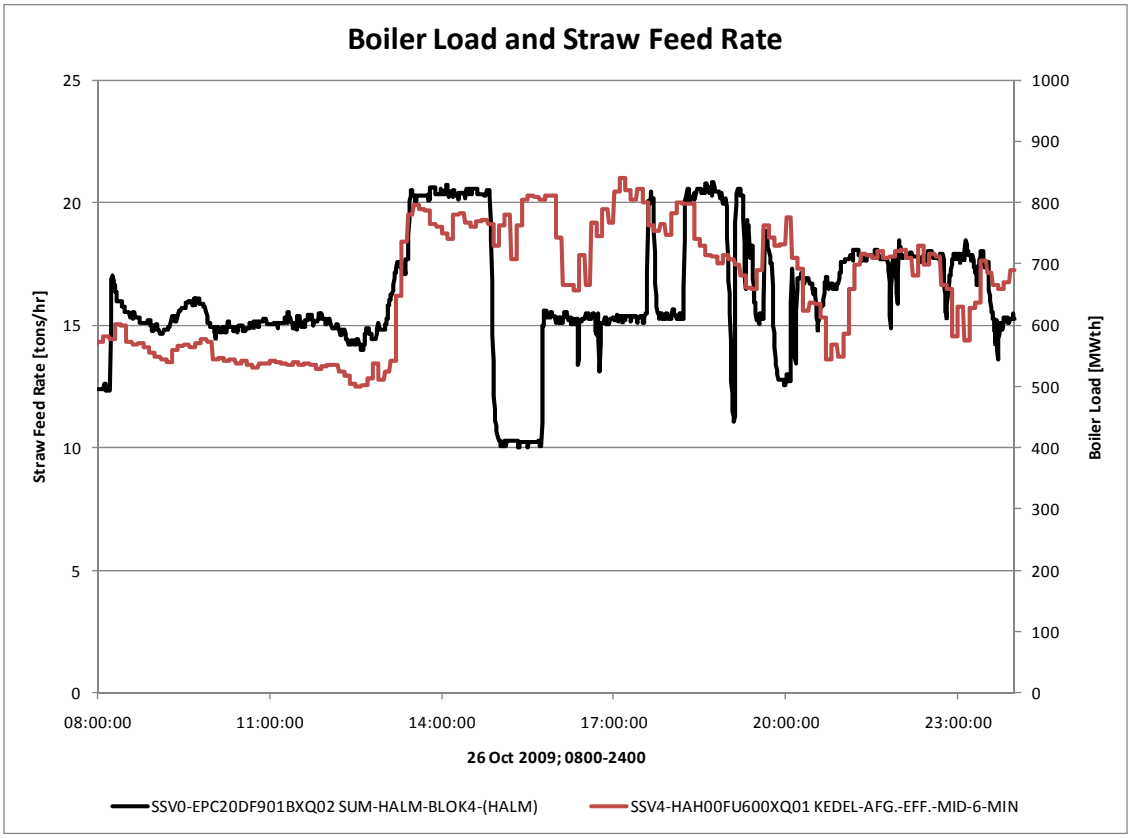
Boiler Load and Straw Feed Rate
Straw Feed Rate [tons/hr]
Boiler Load [MWth]
25
20
15
10
5
0
1000
900
800
700
600
500
400
300
200
100
0
08:00:00
11:00:00
14:00:00
17:00:00
20:00:00
23:00:00
26 Oct 2009; 0800-2400
SSV0-EPC20DF901BXQ02 SUM-HALM-BLOK4-(HALM)
SSV4-HAH00FU600XQ01 KEDEL-AFG.-EFF.-MID-6-MIN

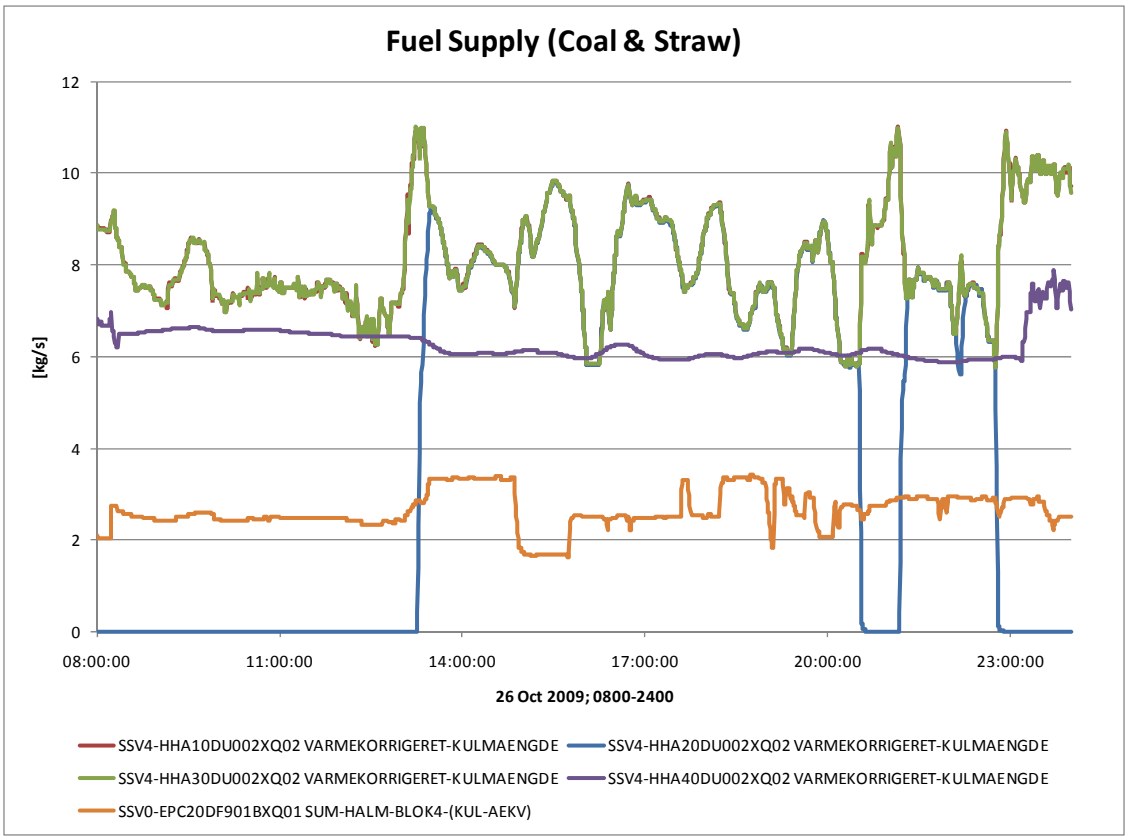
Fuel Supply (Coal & Straw)
[kg/s]
12
10
8
6
4
2
0
08:00:00
11:00:00
14:00:00
17:00:00
20:00:00
23:00:00
26 Oct 2009; 0800-2400
SSV4-HHA10DU002XQ02 VARMEKORRIGERET-KULMAENGDE
SSV4-HHA20DU002XQ02 VARMEKORRIGERET-KULMAENGDE
SSV4-HHA30DU002XQ02 VARMEKORRIGERET-KULMAENGDE
SSV4-HHA40DU002XQ02 VARMEKORRIGERET-KULMAENGDE
SSV0-EPC20DF901BXQ01 SUM-HALM-BLOK4-(KUL-AEKV)

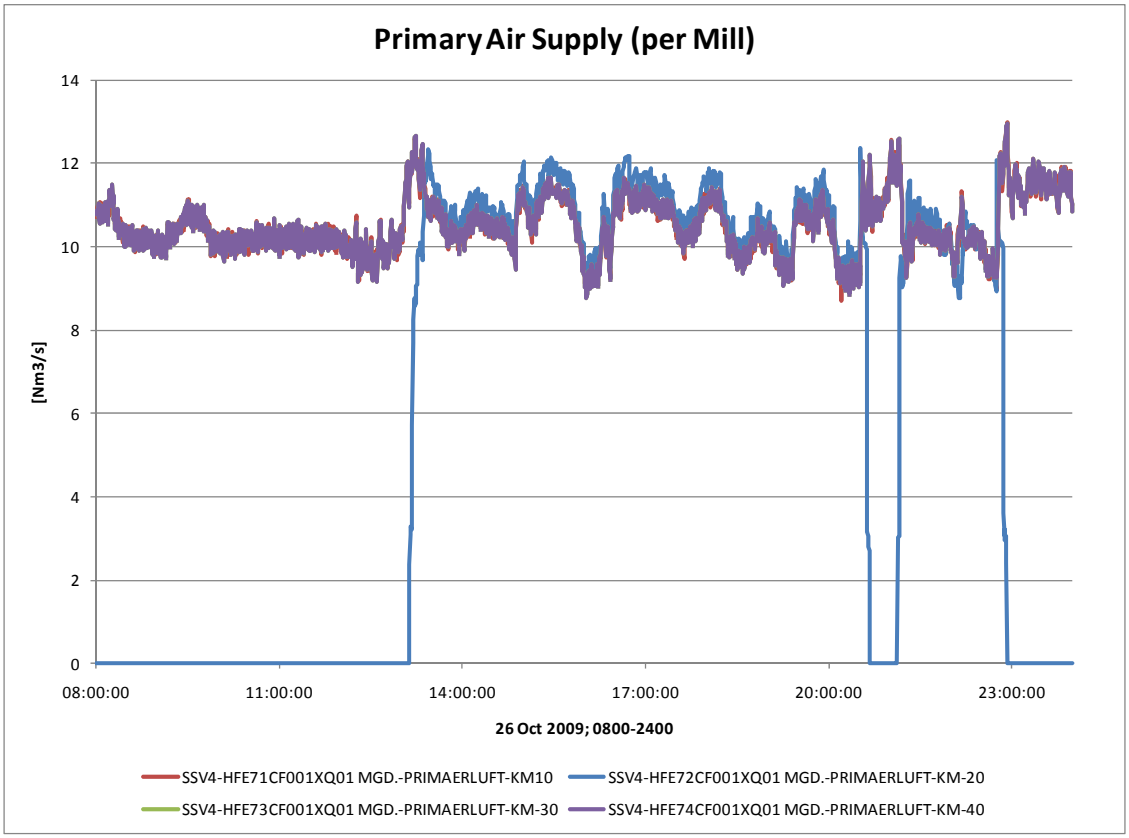
Primary Air Supply (per Mill)
[Nm3/s]
14
12
10
8
6
4
2
0
08:00:00
11:00:00
14:00:00
17:00:00
20:00:00
23:00:00
26 Oct 2009; 0800-2400
SSV4-HFE71CF001XQ01 MGD.-PRIMAERLUFT-KM10
SSV4-HFE72CF001XQ01 MGD.-PRIMAERLUFT-KM-20
SSV4-HFE73CF001XQ01 MGD.-PRIMAERLUFT-KM-30
SSV4-HFE74CF001XQ01 MGD.-PRIMAERLUFT-KM-40

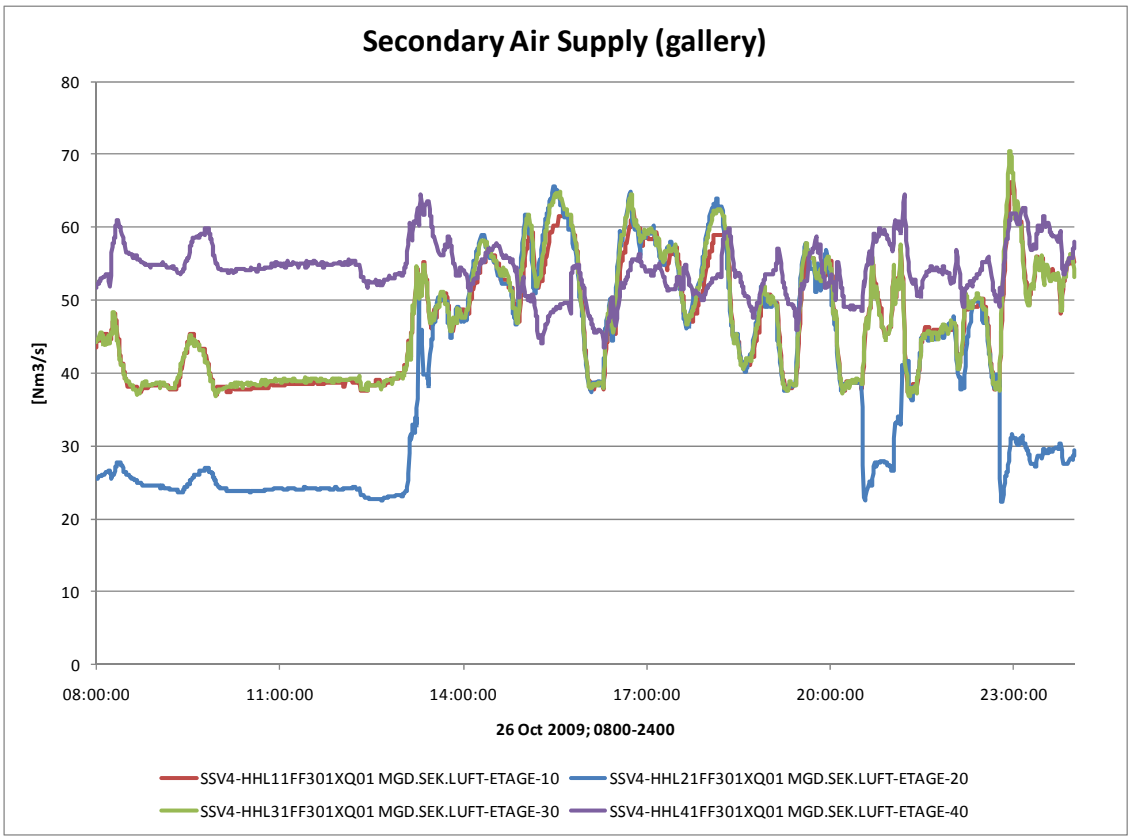
Secondary Air Supply (gallery)
[Nm3/s]
80
70
60
50
40
30
20
10
0
08:00:00
11:00:00
14:00:00
17:00:00
20:00:00
23:00:00
26 Oct 2009; 0800-2400
SSV4-HHL11FF301XQ01 MGD.SEK.LUFT-ETAGE-10
SSV4-HHL21FF301XQ01 MGD.SEK.LUFT-ETAGE-20
SSV4-HHL31FF301XQ01 MGD.SEK.LUFT-ETAGE-30
SSV4-HHL41FF301XQ01 MGD.SEK.LUFT-ETAGE-40

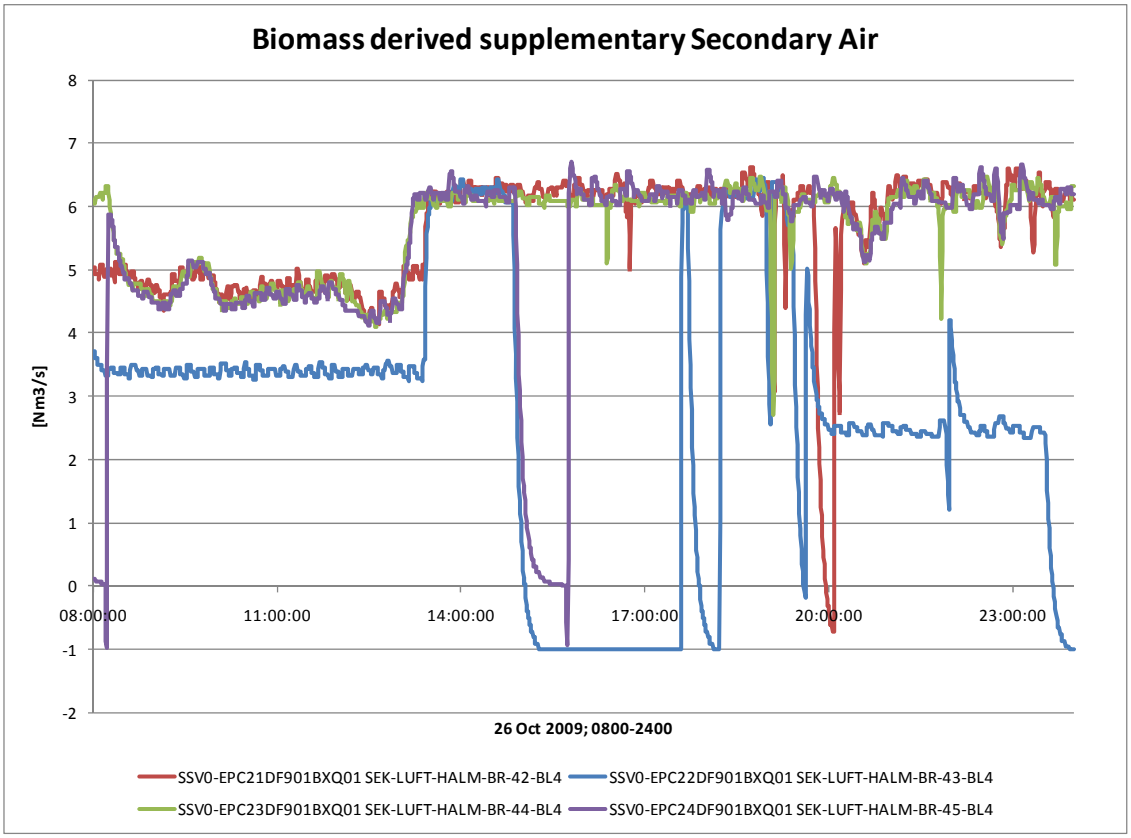
Biomass derived supplementary Secondary Air
[Nm3/s]
8
7
6
5
4
3
2
1
0
-1
-2
08:00:00
11:00:00
14:00:00
17:00:00
20:00:00
23:00:00
26 Oct 2009; 0800-2400
SSV0-EPC21DF901BXQ01 SEK-LUFT-HALM-BR-42-BL4
SSV0-EPC22DF901BXQ01 SEK-LUFT-HALM-BR-43-BL4
SSV0-EPC23DF901BXQ01 SEK-LUFT-HALM-BR-44-BL4
SSV0-EPC24DF901BXQ01 SEK-LUFT-HALM-BR-45-BL4

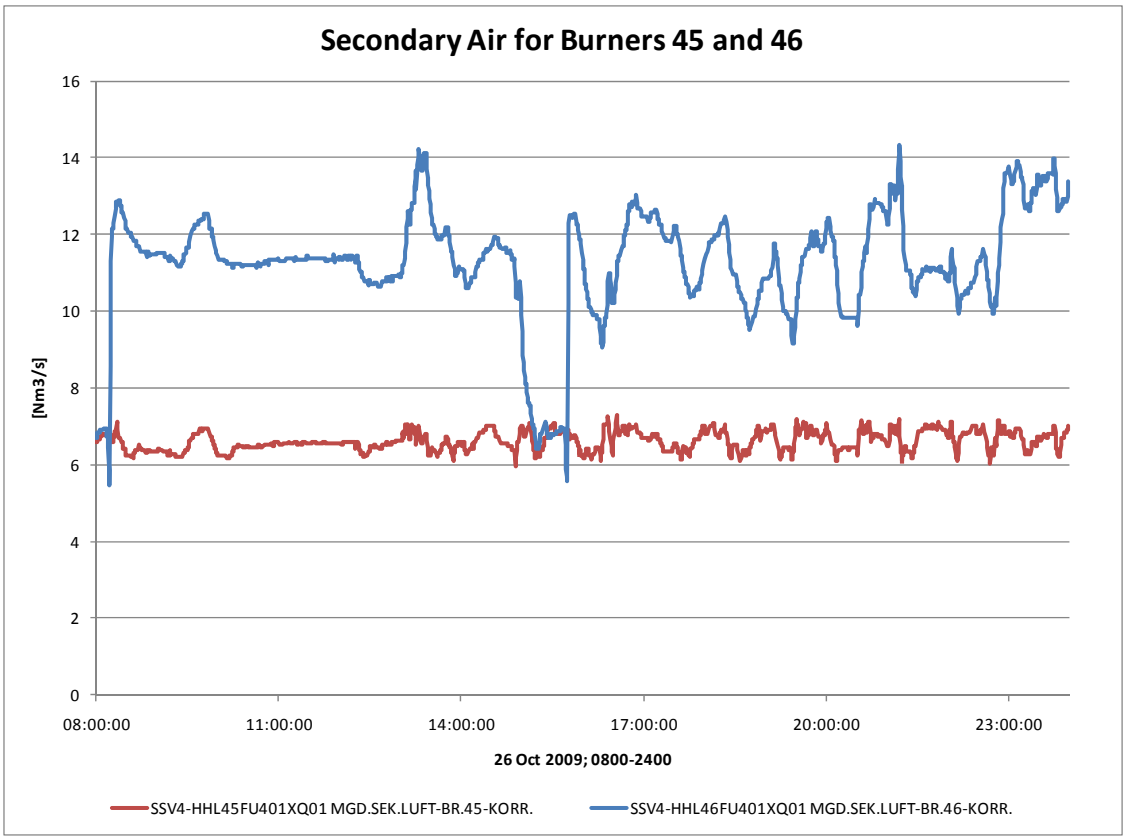
Secondary Air for Burners 45 and 46
[Nm3/s]
16
14
12
10
8
6
4
2
0
08:00:00
11:00:00
14:00:00
17:00:00
20:00:00
23:00:00
26 Oct 2009; 0800-2400
SSV4-HHL45FU401XQ01 MGD.SEK.LUFT-BR.45-KORR.
SSV4-HHL46FU401XQ01 MGD.SEK.LUFT-BR.46-KORR.

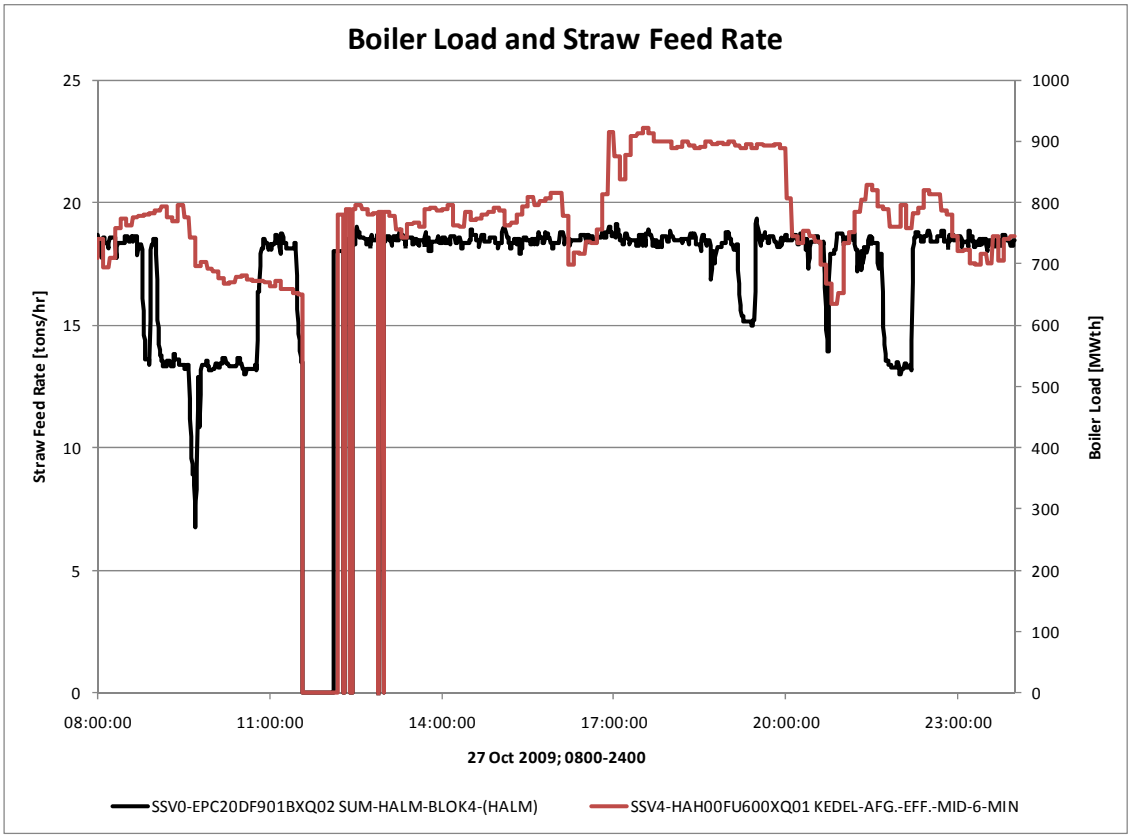
Boiler Load and Straw Feed Rate
Straw Feed Rate [tons/hr]
Boiler Load [MWth]
25
20
15
10
5
0
1000
900
800
700
600
500
400
300
200
100
0
08:00:00
11:00:00
14:00:00
17:00:00
20:00:00
23:00:00
27 Oct 2009; 0800-2400
SSV0-EPC20DF901BXQ02 SUM-HALM-BLOK4-(HALM)
SSV4-HAH00FU600XQ01 KEDEL-AFG.-EFF.-MID-6-MIN

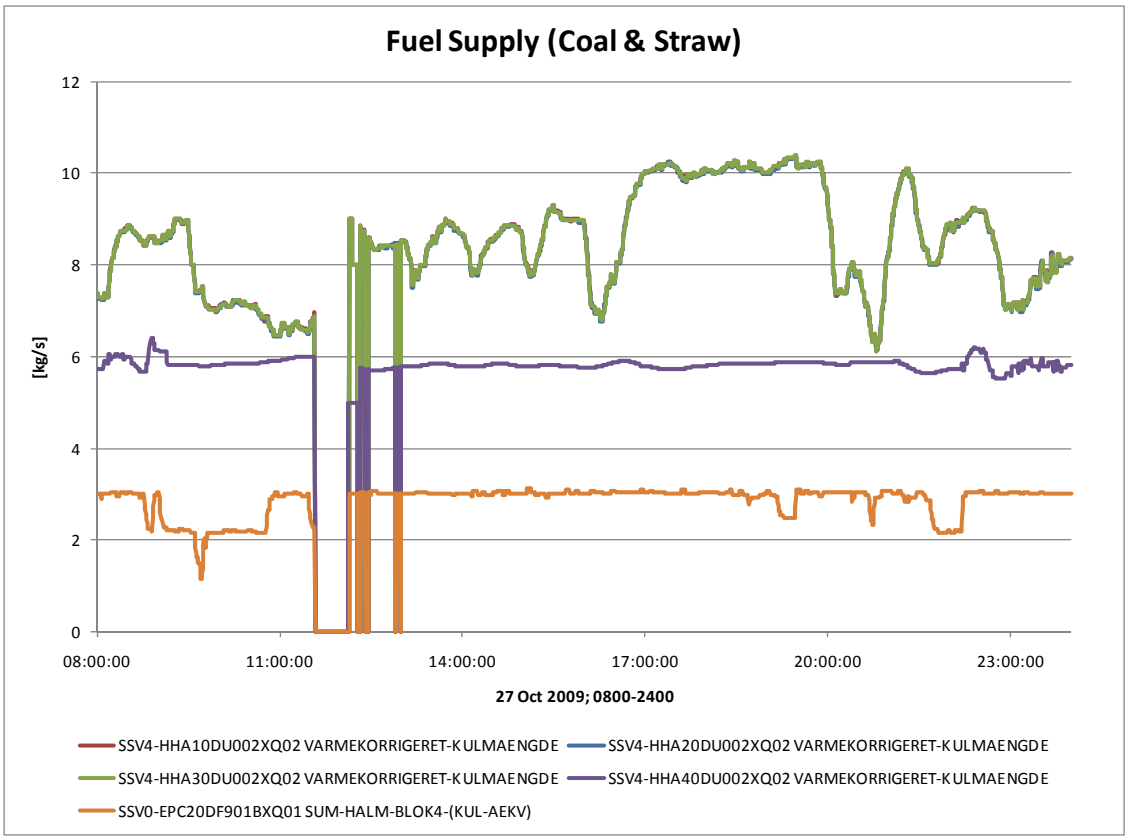
Fuel Supply (Coal & Straw)
[kg/s]
12
10
8
6
4
2
0
08:00:00
11:00:00
14:00:00
17:00:00
20:00:00
23:00:00
27 Oct 2009; 0800-2400
SSV4-HHA10DU002XQ02 VARMEKORRIGERET-KULMAENGDE
SSV4-HHA20DU002XQ02 VARMEKORRIGERET-KULMAENGDE
SSV4-HHA30DU002XQ02 VARMEKORRIGERET-KULMAENGDE
SSV4-HHA40DU002XQ02 VARMEKORRIGERET-KULMAENGDE
SSV0-EPC20DF901BXQ01 SUM-HALM-BLOK4-(KUL-AEKV)

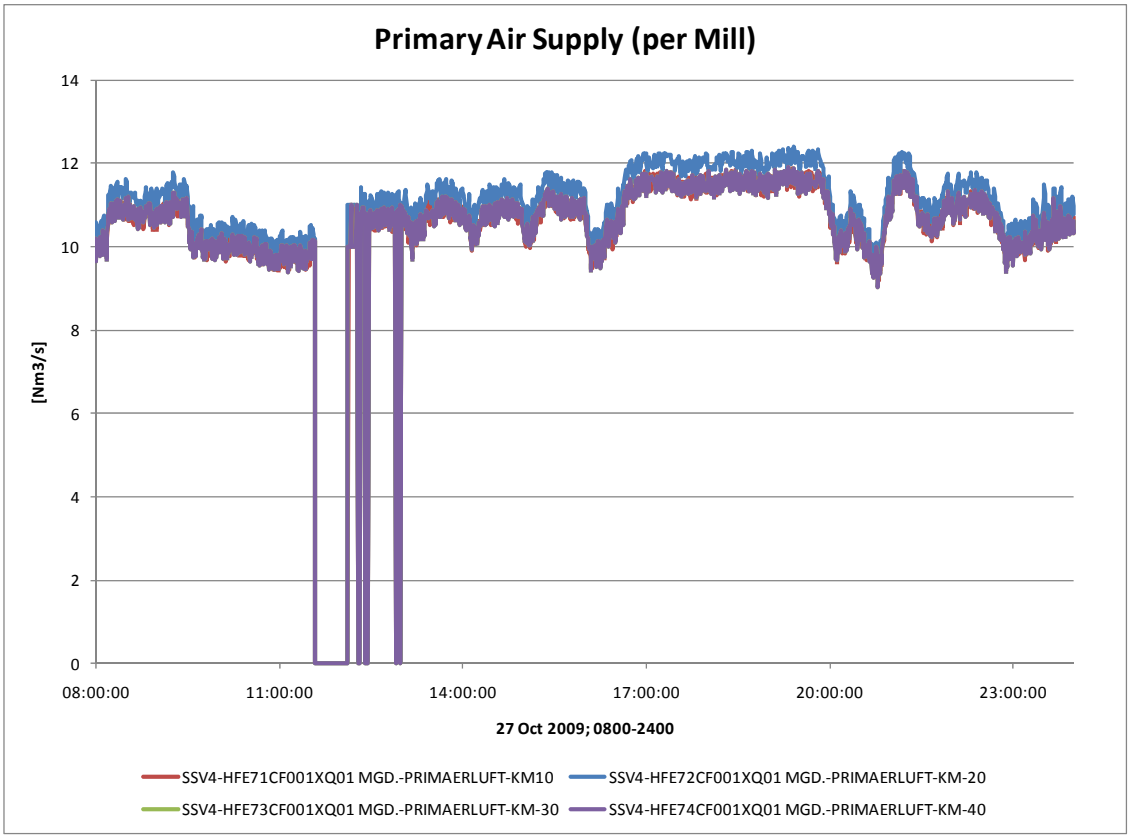
Primary Air Supply (per Mill)
[Nm3/s]
14
12
10
8
6
4
2
0
08:00:00
11:00:00
14:00:00
17:00:00
20:00:00
23:00:00
27 Oct 2009; 0800-2400
SSV4-HFE71CF001XQ01 MGD.-PRIMAERLUFT-KM10
SSV4-HFE72CF001XQ01 MGD.-PRIMAERLUFT-KM-20
SSV4-HFE73CF001XQ01 MGD.-PRIMAERLUFT-KM-30
SSV4-HFE74CF001XQ01 MGD.-PRIMAERLUFT-KM-40

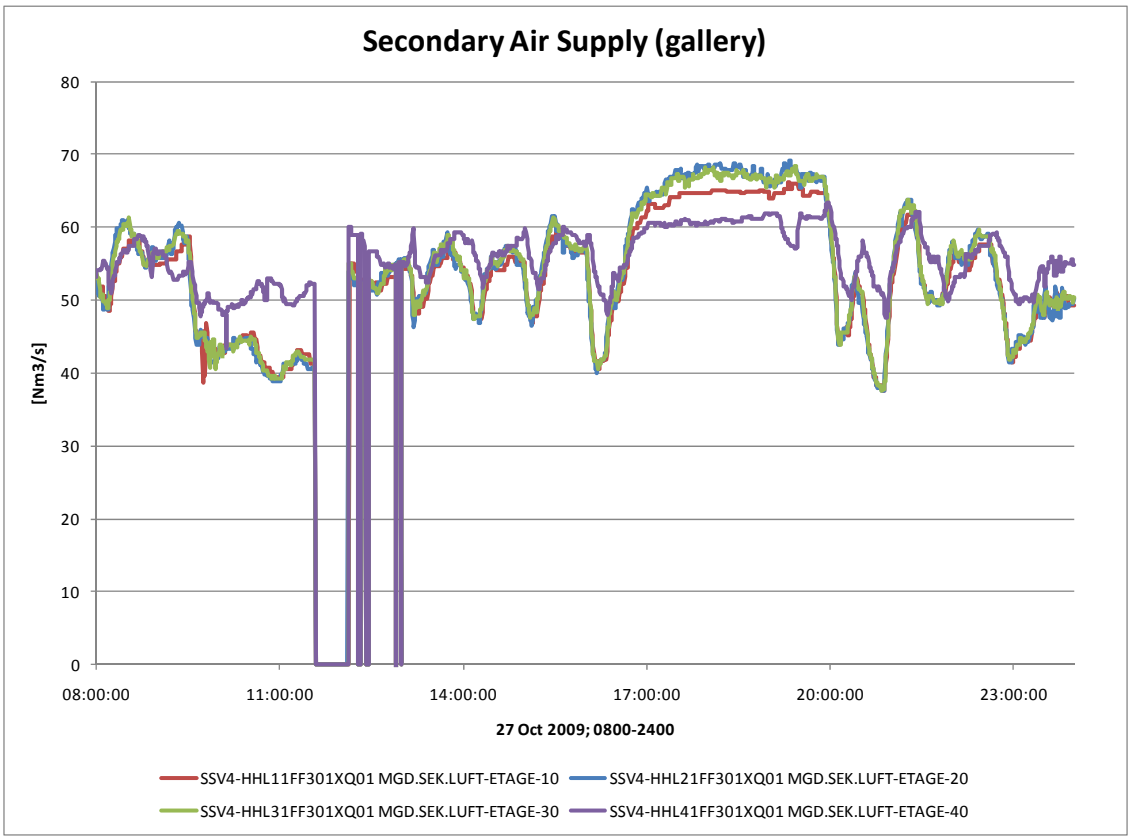
Secondary Air Supply (gallery)
[Nm3/s]
80
70
60
50
40
30
20
10
0
08:00:00
11:00:00
14:00:00
17:00:00
20:00:00
23:00:00
27 Oct 2009; 0800-2400
SSV4-HHL11FF301XQ01 MGD.SEK.LUFT-ETAGE-10
SSV4-HHL21FF301XQ01 MGD.SEK.LUFT-ETAGE-20
SSV4-HHL31FF301XQ01 MGD.SEK.LUFT-ETAGE-30
SSV4-HHL41FF301XQ01 MGD.SEK.LUFT-ETAGE-40

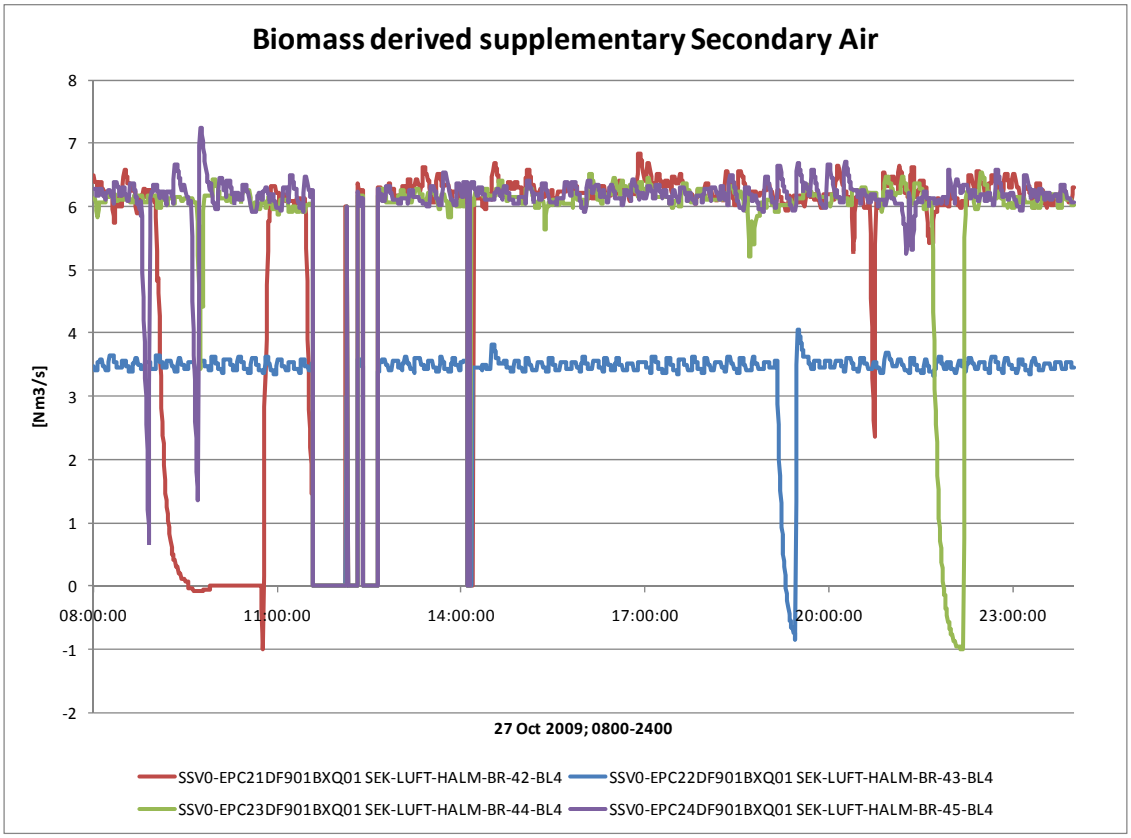
Biomass derived supplementary Secondary Air
[Nm3/s]
8
7
6
5
4
3
2
1
0
-1
-2
08:00:00
11:00:00
14:00:00
17:00:00
20:00:00
23:00:00
27 Oct 2009; 0800-2400
SSV0-EPC21DF901BXQ01 SEK-LUFT-HALM-BR-42-BL4
SSV0-EPC22DF901BXQ01 SEK-LUFT-HALM-BR-43-BL4
SSV0-EPC23DF901BXQ01 SEK-LUFT-HALM-BR-44-BL4
SSV0-EPC24DF901BXQ01 SEK-LUFT-HALM-BR-45-BL4

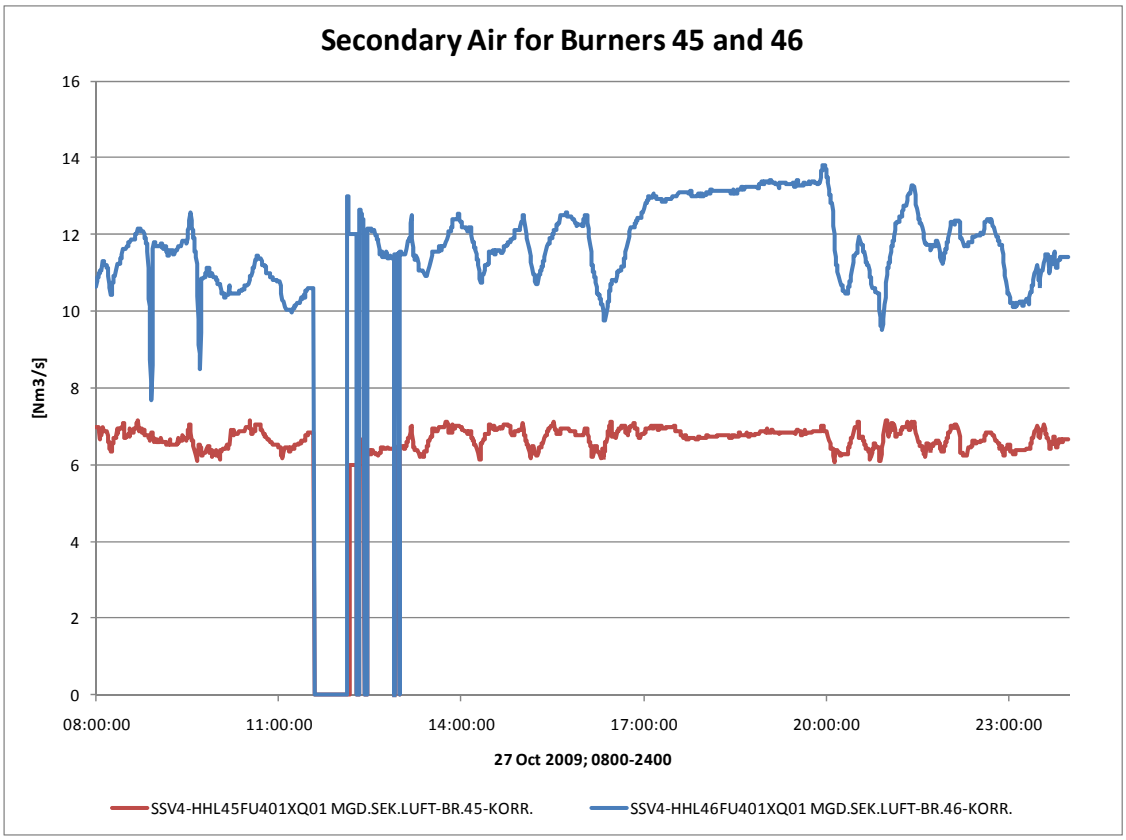
Secondary Air for Burners 45 and 46
[Nm3/s]
16
14
12
10
8
6
4
2
0
08:00:00
11:00:00
14:00:00
17:00:00
20:00:00
23:00:00
27 Oct 2009; 0800-2400
SSV4-HHL45FU401XQ01 MGD.SEK.LUFT-BR.45-KORR.
SSV4-HHL46FU401XQ01 MGD.SEK.LUFT-BR.46-KORR.

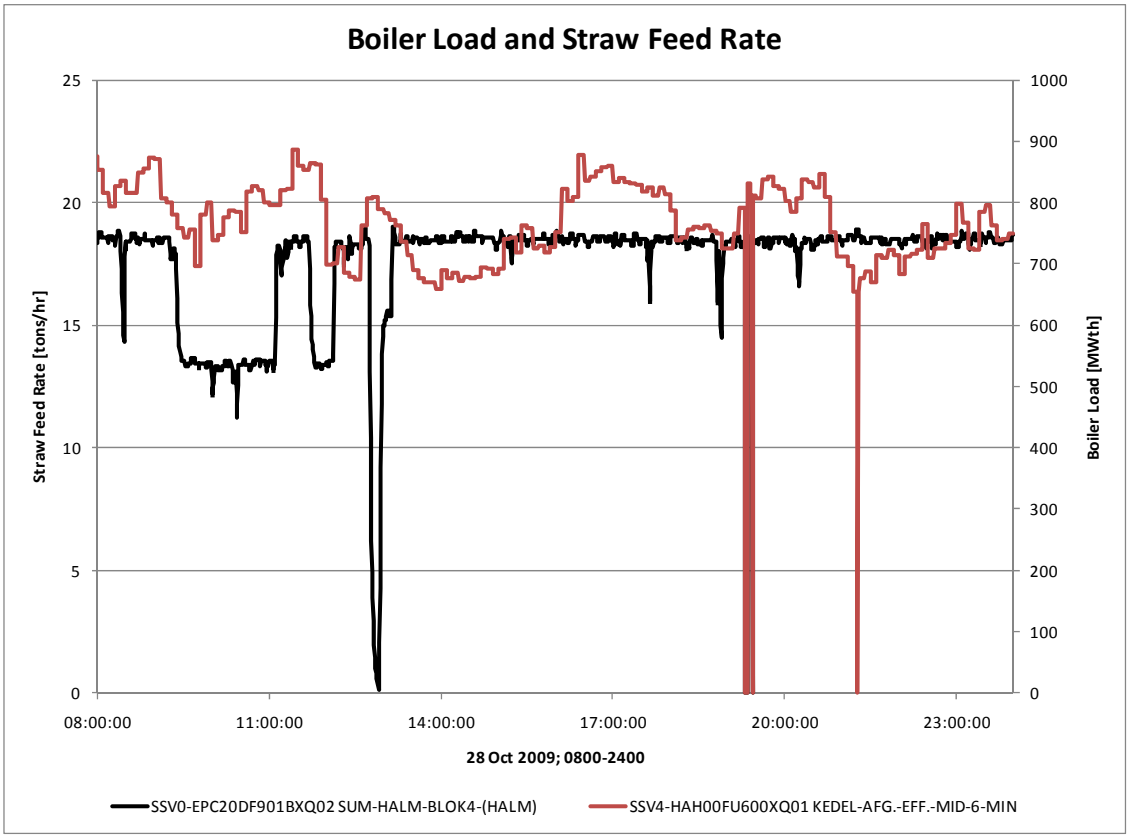
Boiler Load and Straw Feed Rate
Straw Feed Rate [tons/hr]
Boiler Load [MWth]
25
20
15
10
5
0
1000
900
800
700
600
500
400
300
200
100
0
08:00:00
11:00:00
14:00:00
17:00:00
20:00:00
23:00:00
28 Oct 2009; 0800-2400
SSV0-EPC20DF901BXQ02 SUM-HALM-BLOK4-(HALM)
SSV4-HAH00FU600XQ01 KEDEL-AFG.-EFF.-MID-6-MIN

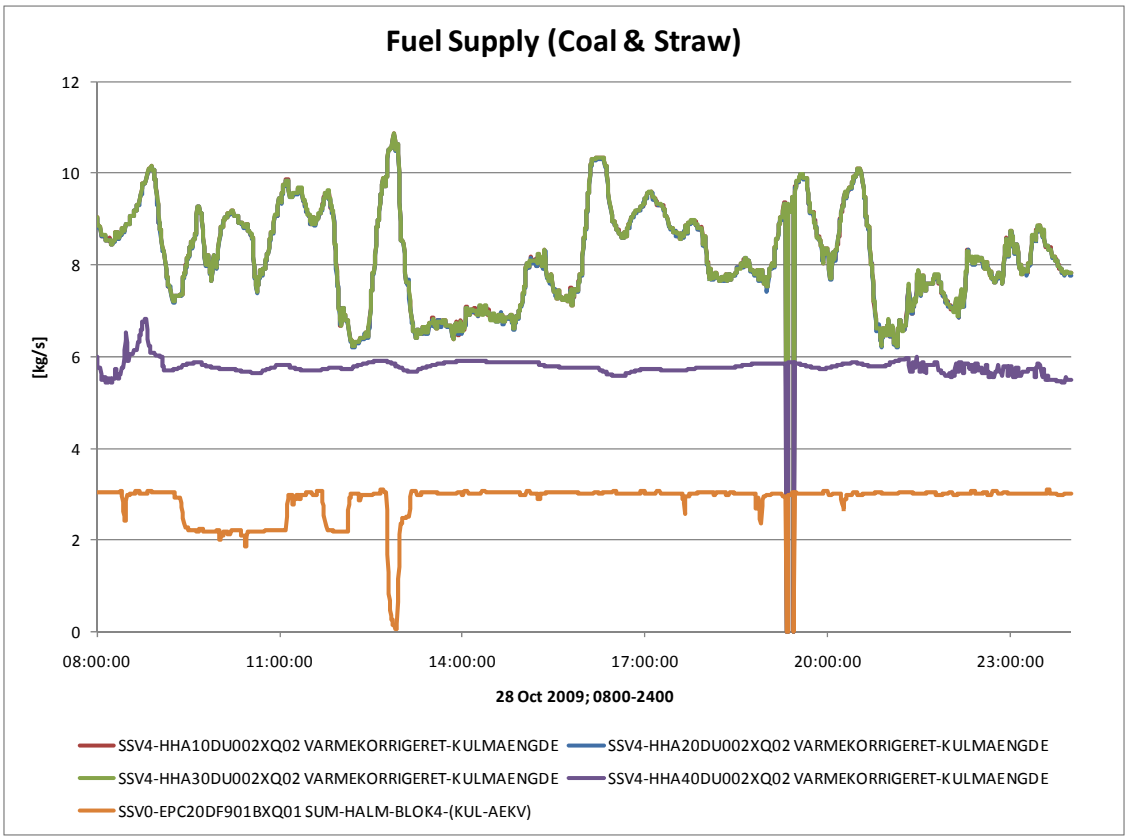
Fuel Supply (Coal & Straw)
[kg/s]
12
10
8
6
4
2
0
08:00:00
11:00:00
14:00:00
17:00:00
20:00:00
23:00:00
28 Oct 2009; 0800-2400
SSV4-HHA10DU002XQ02 VARMEKORRIGERET-KULMAENGDE
SSV4-HHA20DU002XQ02 VARMEKORRIGERET-KULMAENGDE
SSV4-HHA30DU002XQ02 VARMEKORRIGERET-KULMAENGDE
SSV4-HHA40DU002XQ02 VARMEKORRIGERET-KULMAENGDE
SSV0-EPC20DF901BXQ01 SUM-HALM-BLOK4-(KUL-AEKV)

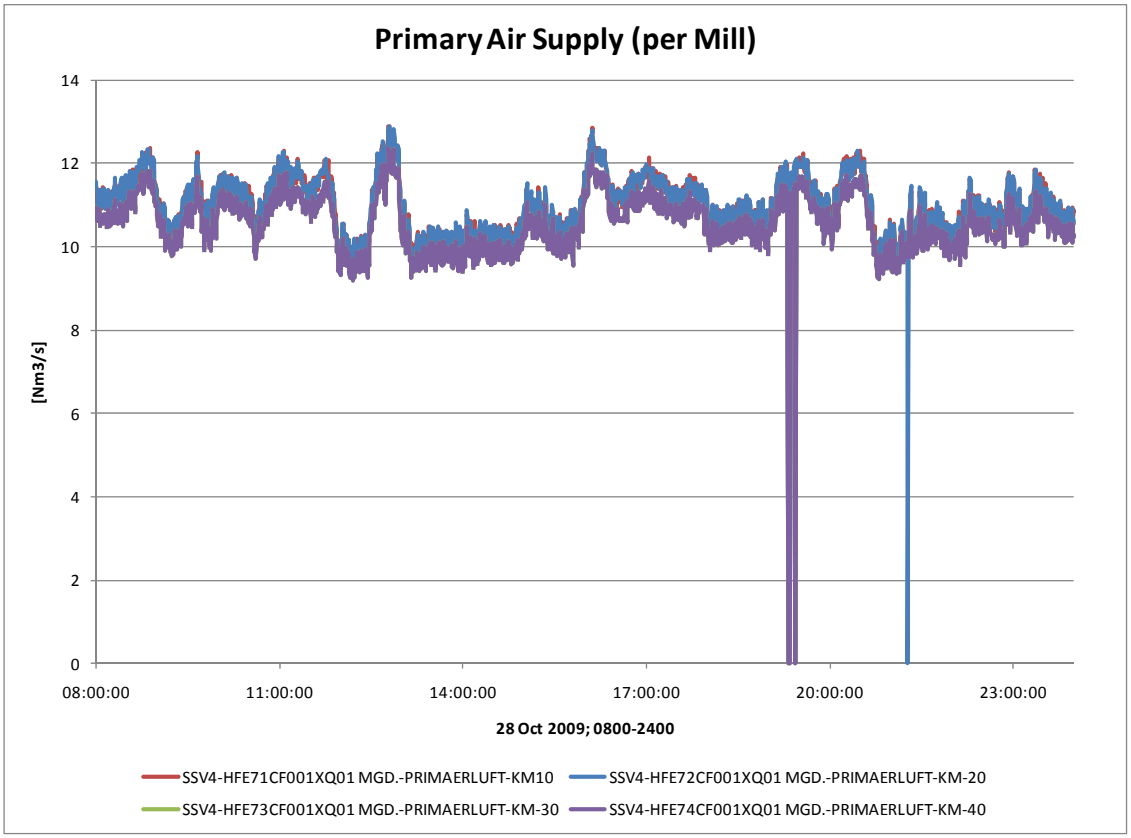
Primary Air Supply (per Mill)
[Nm3/s]
14
12
10
8
6
4
2
0
08:00:00
11:00:00
14:00:00
17:00:00
20:00:00
23:00:00
28 Oct 2009; 0800-2400
SSV4-HFE71CF001XQ01 MGD.-PRIMAERLUFT-KM10
SSV4-HFE72CF001XQ01 MGD.-PRIMAERLUFT-KM-20
SSV4-HFE73CF001XQ01 MGD.-PRIMAERLUFT-KM-30
SSV4-HFE74CF001XQ01 MGD.-PRIMAERLUFT-KM-40

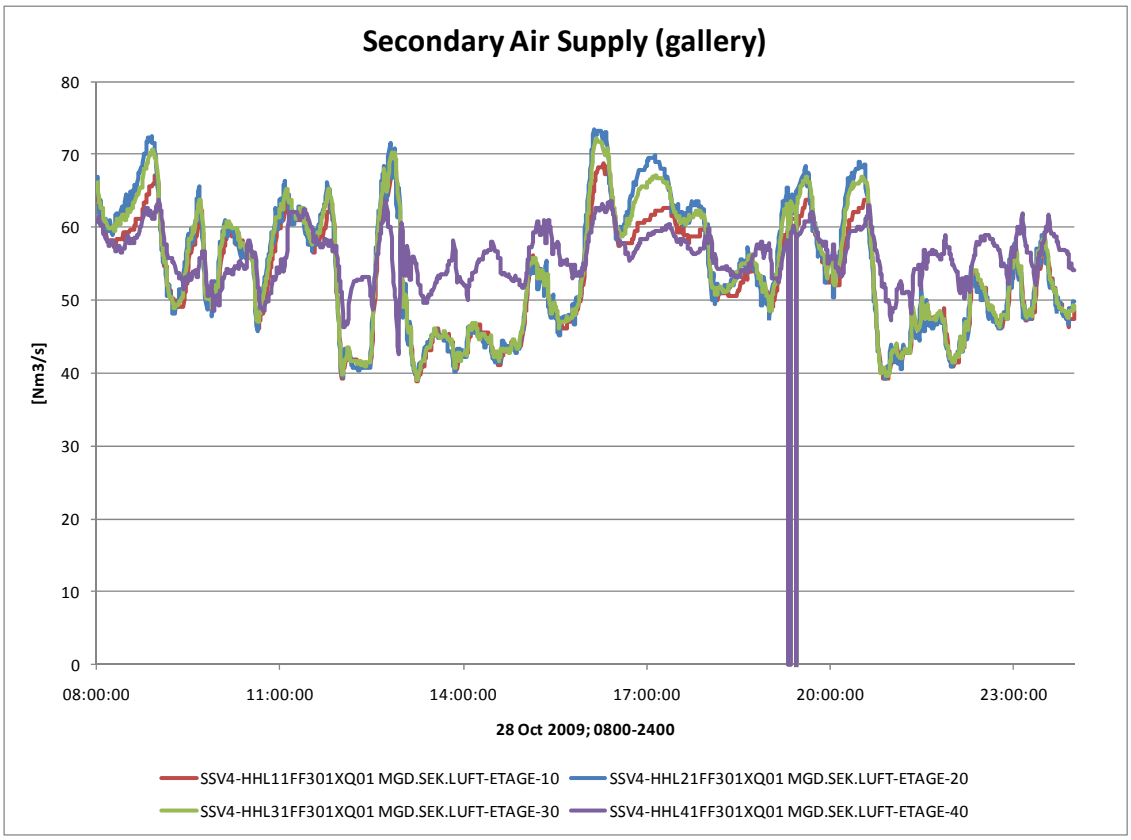
Secondary Air Supply (gallery)
[Nm3/s]
80
70
60
50
40
30
20
10
0
08:00:00
11:00:00
14:00:00
17:00:00
20:00:00
23:00:00
28 Oct 2009; 0800-2400
SSV4-HHL11FF301XQ01 MGD.SEK.LUFT-ETAGE-10
SSV4-HHL21FF301XQ01 MGD.SEK.LUFT-ETAGE-20
SSV4-HHL31FF301XQ01 MGD.SEK.LUFT-ETAGE-30
SSV4-HHL41FF301XQ01 MGD.SEK.LUFT-ETAGE-40

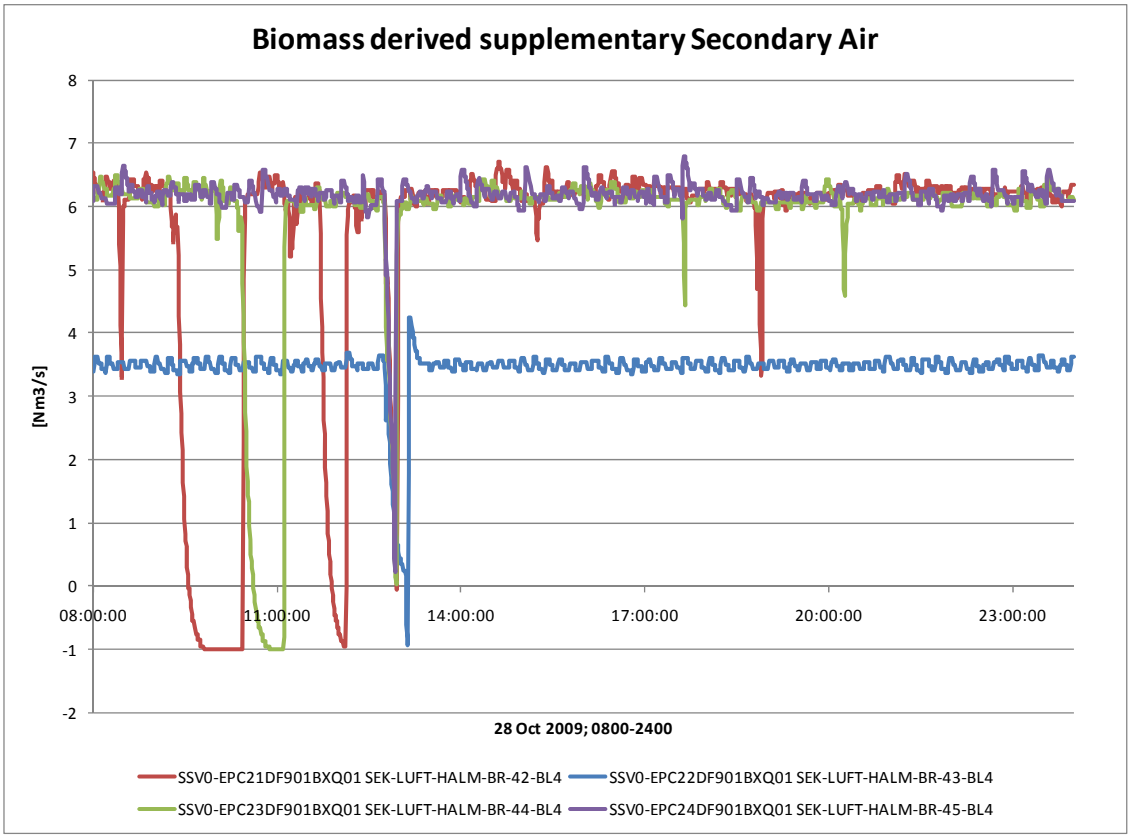
Biomass derived supplementary Secondary Air
[Nm3/s]
8
7
6
5
4
3
2
1
0
-1
-2
08:00:00
11:00:00
14:00:00
17:00:00
20:00:00
23:00:00
28 Oct 2009; 0800-2400
SSV0-EPC21DF901BXQ01 SEK-LUFT-HALM-BR-42-BL4
SSV0-EPC22DF901BXQ01 SEK-LUFT-HALM-BR-43-BL4
SSV0-EPC23DF901BXQ01 SEK-LUFT-HALM-BR-44-BL4
SSV0-EPC24DF901BXQ01 SEK-LUFT-HALM-BR-45-BL4

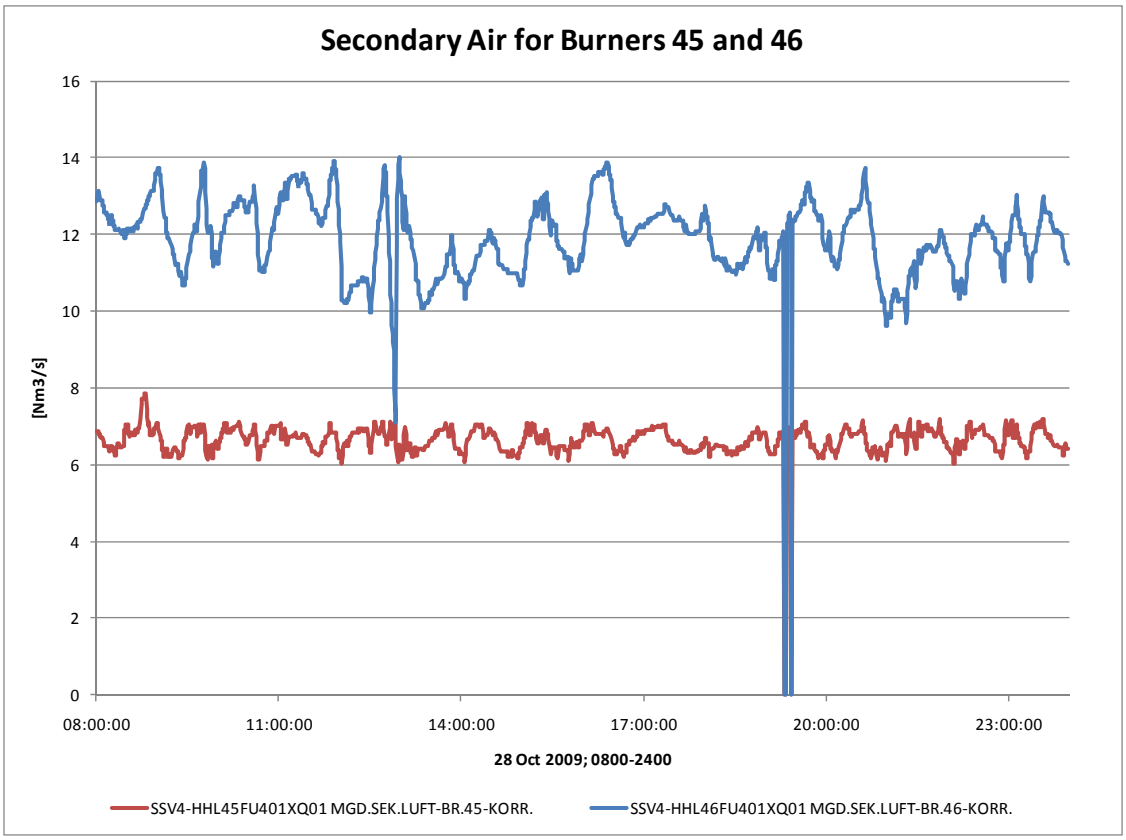
Secondary Air for Burners 45 and 46
[Nm3/s]
16
14
12
10
8
6
4
2
0
08:00:00
11:00:00
14:00:00
17:00:00
20:00:00
23:00:00
28 Oct 2009; 0800-2400
SSV4-HHL45FU401XQ01 MGD.SEK.LUFT-BR.45-KORR.
SSV4-HHL46FU401XQ01 MGD.SEK.LUFT-BR.46-KORR.

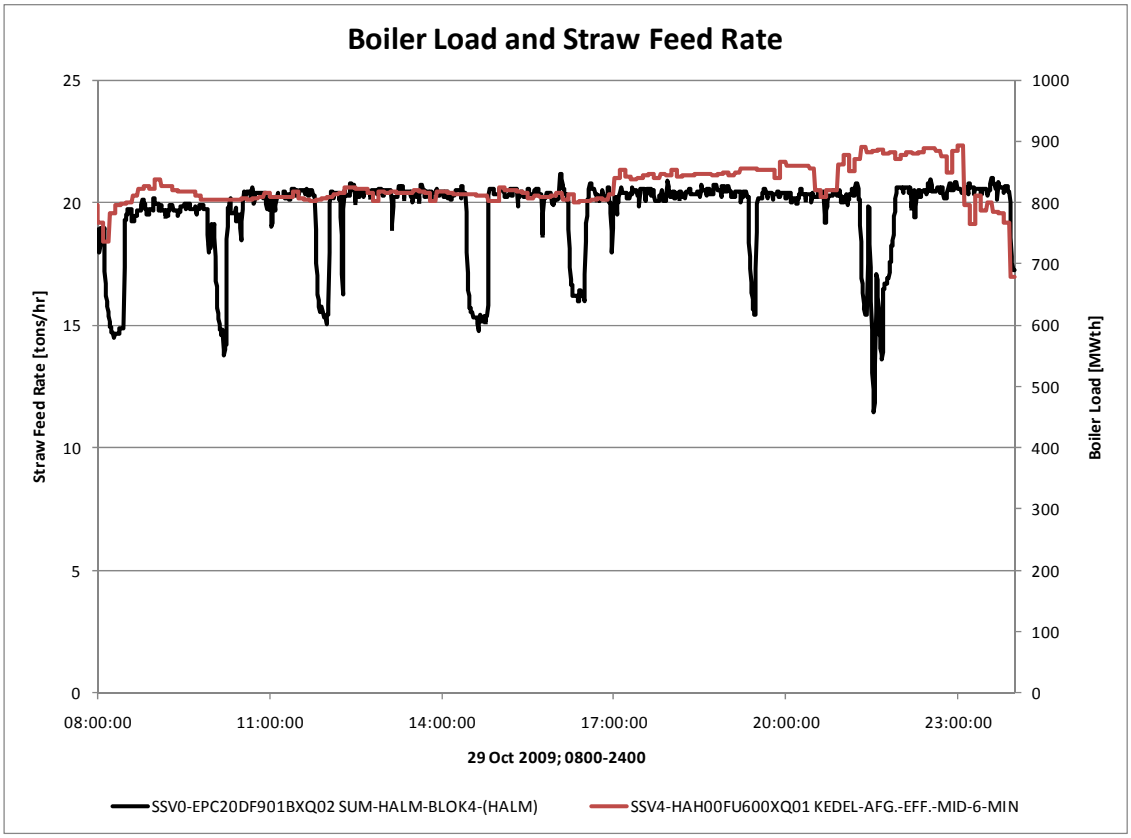
Boiler Load and Straw Feed Rate
Straw Feed Rate [tons/hr]
Boiler Load [MWth]
25
20
15
10
5
0
1000
900
800
700
600
500
400
300
200
100
0
08:00:00
11:00:00
14:00:00
17:00:00
20:00:00
23:00:00
29 Oct 2009; 0800-2400
SSV0-EPC20DF901BXQ02 SUM-HALM-BLOK4-(HALM)
SSV4-HAH00FU600XQ01 KEDEL-AFG.-EFF.-MID-6-MIN

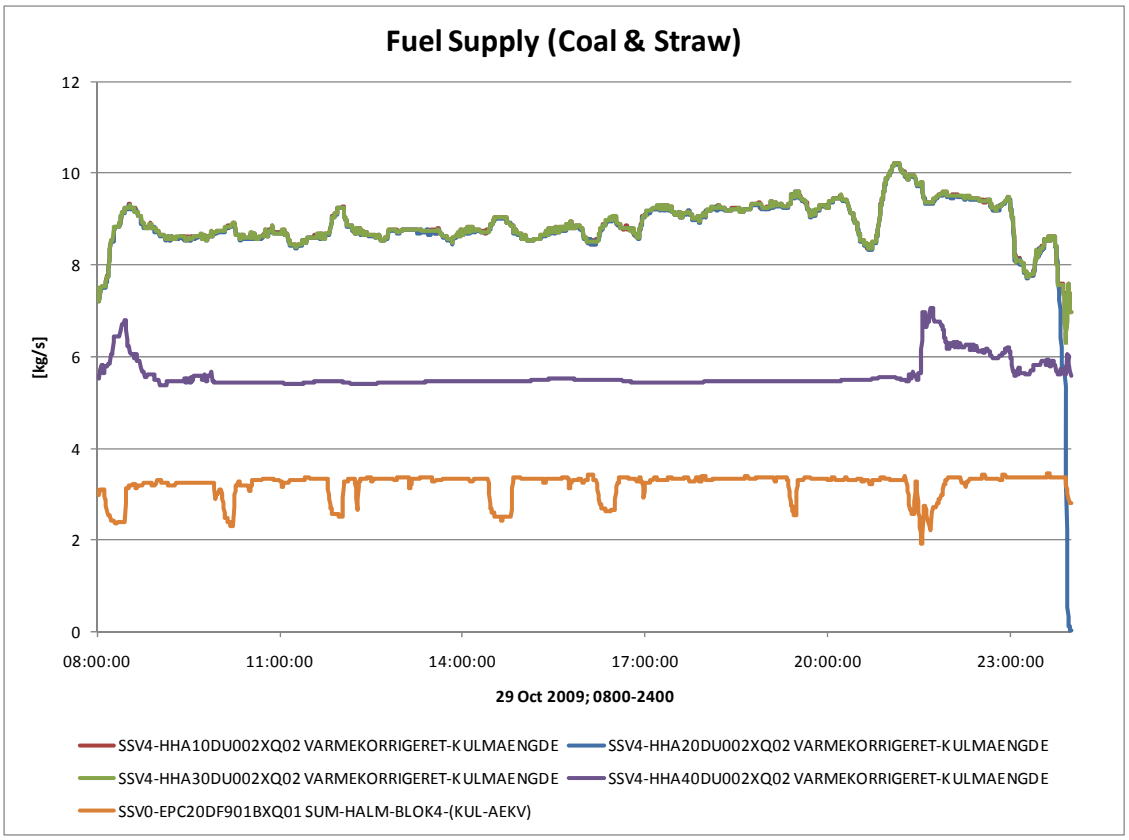
Fuel Supply (Coal & Straw)
[kg/s]
12
10
8
6
4
2
0
08:00:00
11:00:00
14:00:00
17:00:00
20:00:00
23:00:00
29 Oct 2009; 0800-2400
SSV4-HHA10DU002XQ02 VARMEKORRIGERET-KULMAENGDE
SSV4-HHA20DU002XQ02 VARMEKORRIGERET-KULMAENGDE
SSV4-HHA30DU002XQ02 VARMEKORRIGERET-KULMAENGDE
SSV4-HHA40DU002XQ02 VARMEKORRIGERET-KULMAENGDE
SSV0-EPC20DF901BXQ01 SUM-HALM-BLOK4-(KUL-AEKV)

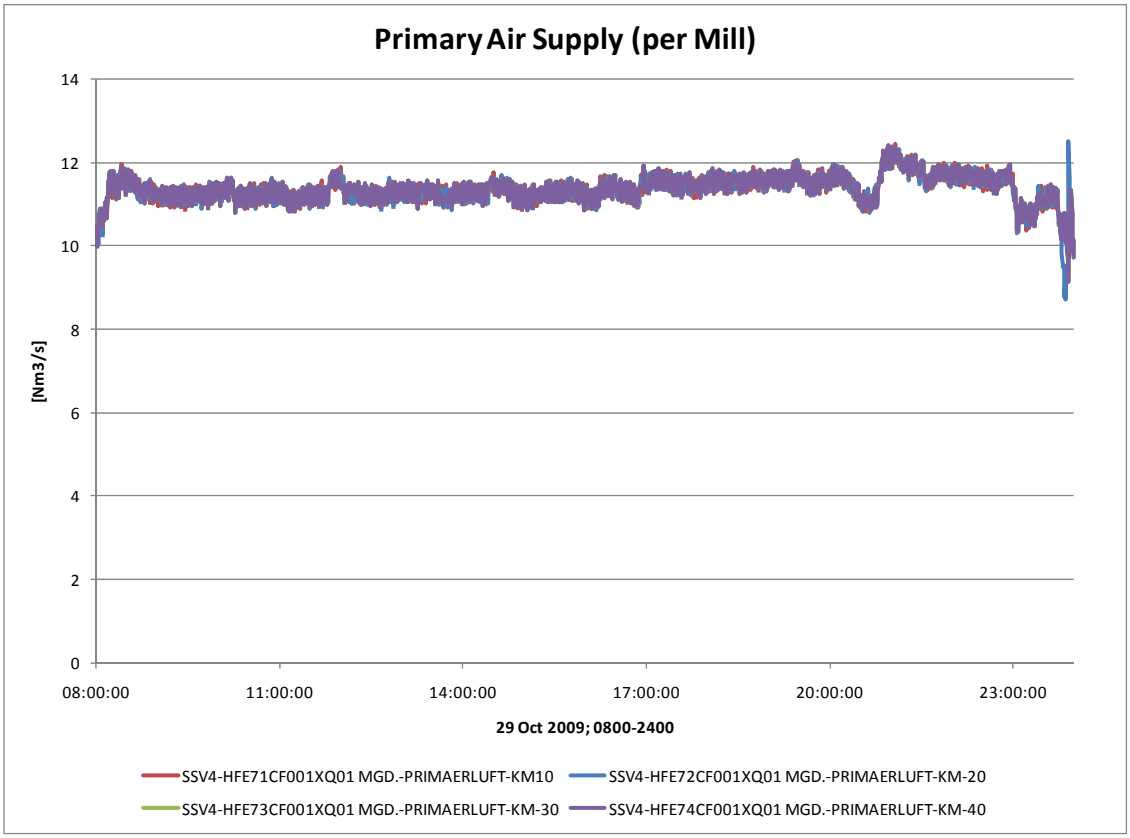
Primary Air Supply (per Mill)
[Nm3/s]
14
12
10
8
6
4
2
0
08:00:00
11:00:00
14:00:00
17:00:00
20:00:00
23:00:00
29 Oct 2009; 0800-2400
SSV4-HFE71CF001XQ01 MGD.-PRIMAERLUFT-KM10
SSV4-HFE72CF001XQ01 MGD.-PRIMAERLUFT-KM-20
SSV4-HFE73CF001XQ01 MGD.-PRIMAERLUFT-KM-30
SSV4-HFE74CF001XQ01 MGD.-PRIMAERLUFT-KM-40

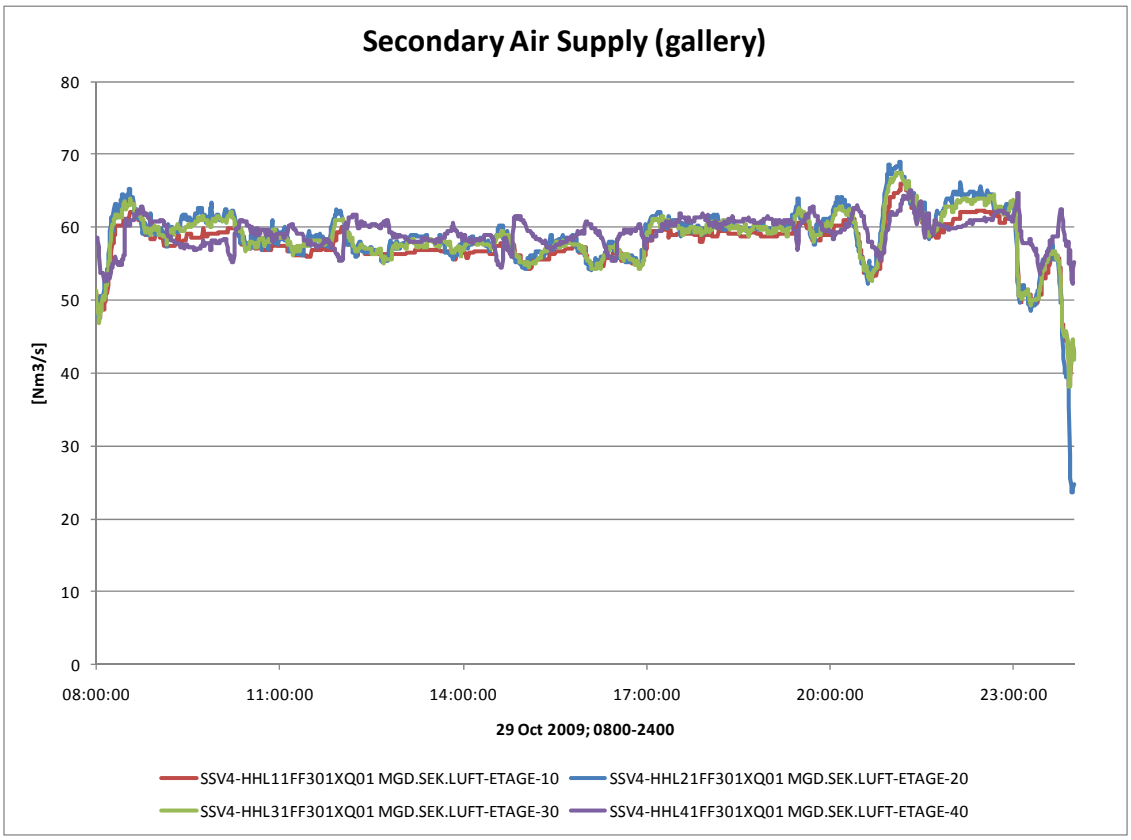
Secondary Air Supply (gallery)
[Nm3/s]
80
70
60
50
40
30
20
10
0
08:00:00
11:00:00
14:00:00
17:00:00
20:00:00
23:00:00
29 Oct 2009; 0800-2400
SSV4-HHL11FF301XQ01 MGD.SEK.LUFT-ETAGE-10
SSV4-HHL21FF301XQ01 MGD.SEK.LUFT-ETAGE-20
SSV4-HHL31FF301XQ01 MGD.SEK.LUFT-ETAGE-30
SSV4-HHL41FF301XQ01 MGD.SEK.LUFT-ETAGE-40

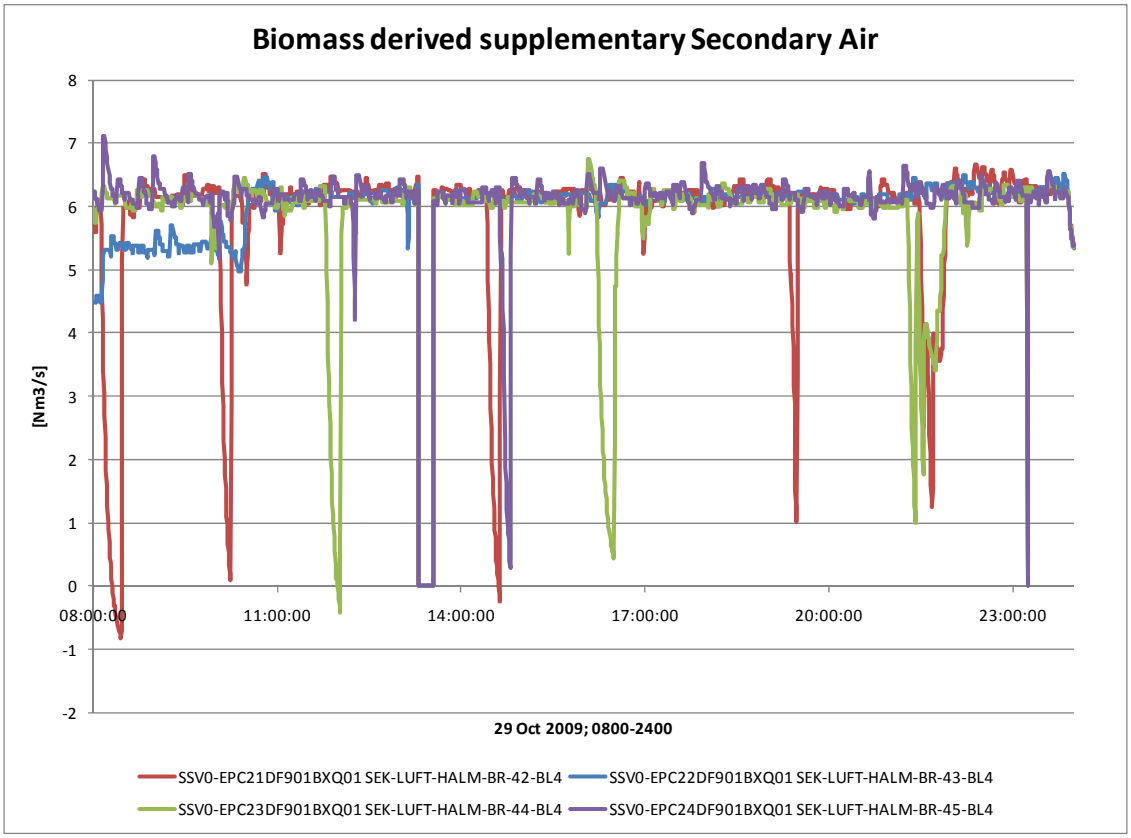
Biomass derived supplementary Secondary Air
[Nm3/s]
8
7
6
5
4
3
2
1
0
-1
-2
08:00:00
11:00:00
14:00:00
17:00:00
20:00:00
23:00:00
29 Oct 2009; 0800-2400
SSV0-EPC21DF901BXQ01 SEK-LUFT-HALM-BR-42-BL4
SSV0-EPC22DF901BXQ01 SEK-LUFT-HALM-BR-43-BL4
SSV0-EPC23DF901BXQ01 SEK-LUFT-HALM-BR-44-BL4
SSV0-EPC24DF901BXQ01 SEK-LUFT-HALM-BR-45-BL4

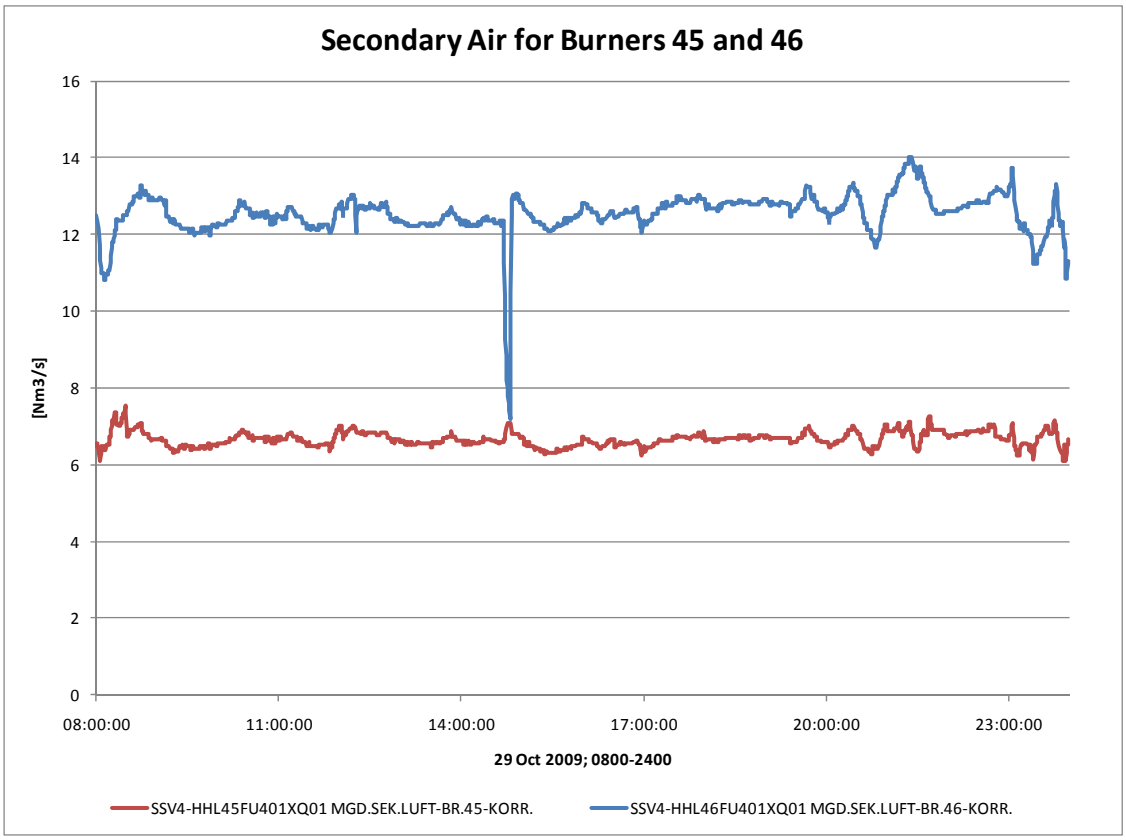
Secondary Air for Burners 45 and 46
[Nm3/s]
16
14
12
10
8
6
4
2
0
08:00:00
11:00:00
14:00:00
17:00:00
20:00:00
23:00:00
29 Oct 2009; 0800-2400
SSV4-HHL45FU401XQ01 MGD.SEK.LUFT-BR.45-KORR.
SSV4-HHL46FU401XQ01 MGD.SEK.LUFT-BR.46-KORR.

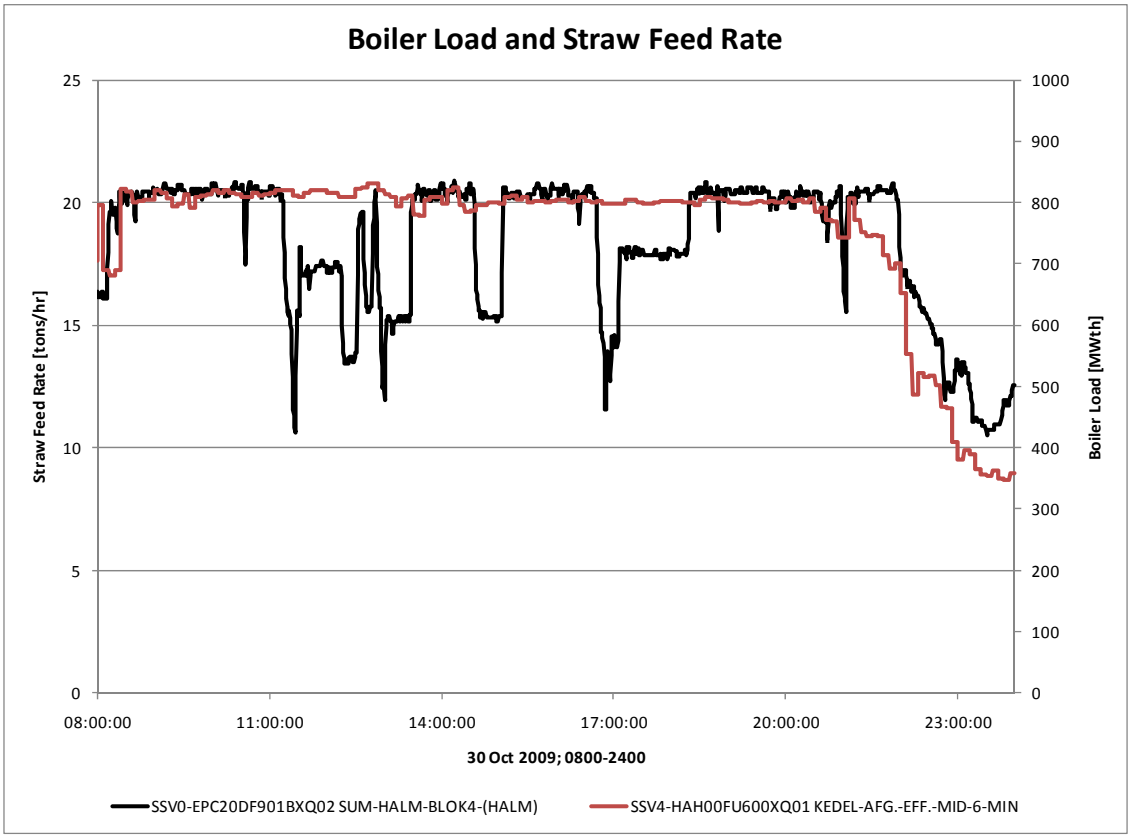
Boiler Load and Straw Feed Rate
Straw Feed Rate [tons/hr]
Boiler Load [MWth]
25
20
15
10
5
0
1000
900
800
700
600
500
400
300
200
100
0
08:00:00
11:00:00
14:00:00
17:00:00
20:00:00
23:00:00
30 Oct 2009; 0800-2400
SSV0-EPC20DF901BXQ02 SUM-HALM-BLOK4-(HALM)
SSV4-HAH00FU600XQ01 KEDEL-AFG.-EFF.-MID-6-MIN

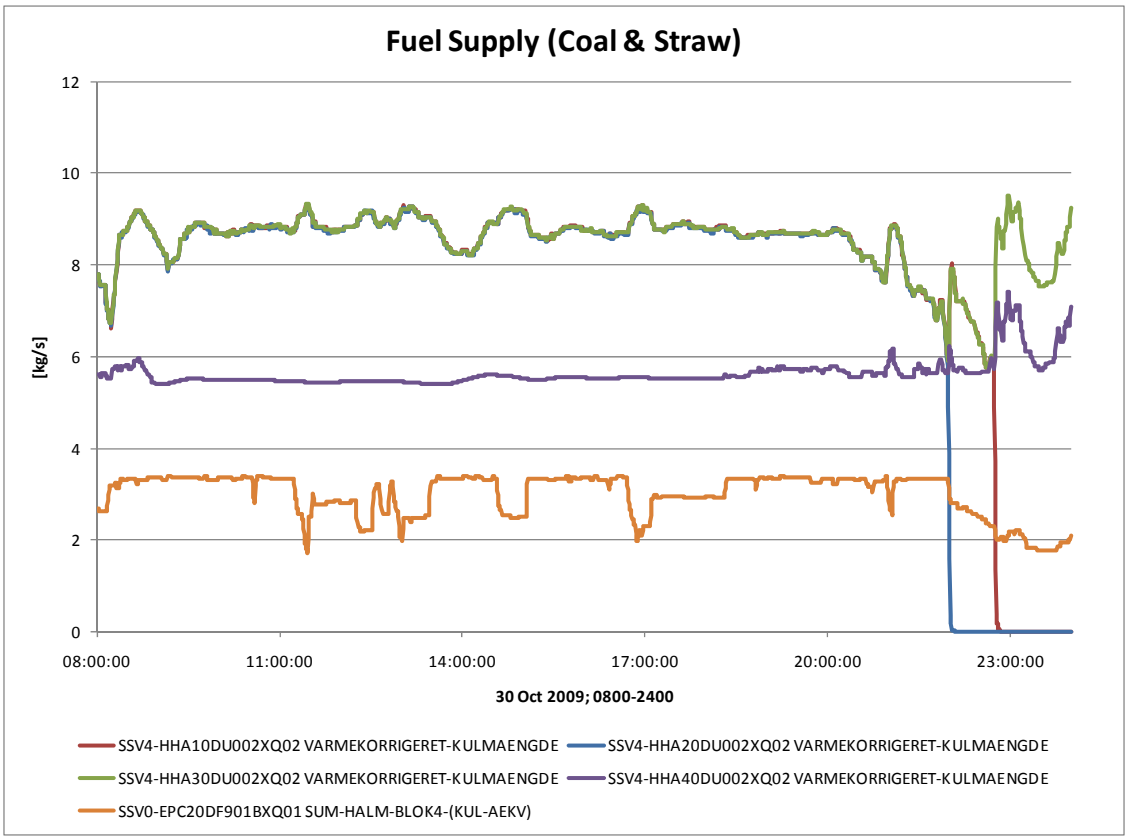
Fuel Supply (Coal & Straw)
[kg/s]
12
10
8
6
4
2
0
08:00:00
11:00:00
14:00:00
17:00:00
20:00:00
23:00:00
30 Oct 2009; 0800-2400
SSV4-HHA10DU002XQ02 VARMEKORRIGERET-KULMAENGDE
SSV4-HHA20DU002XQ02 VARMEKORRIGERET-KULMAENGDE
SSV4-HHA30DU002XQ02 VARMEKORRIGERET-KULMAENGDE
SSV4-HHA40DU002XQ02 VARMEKORRIGERET-KULMAENGDE
SSV0-EPC20DF901BXQ01 SUM-HALM-BLOK4-(KUL-AEKV)

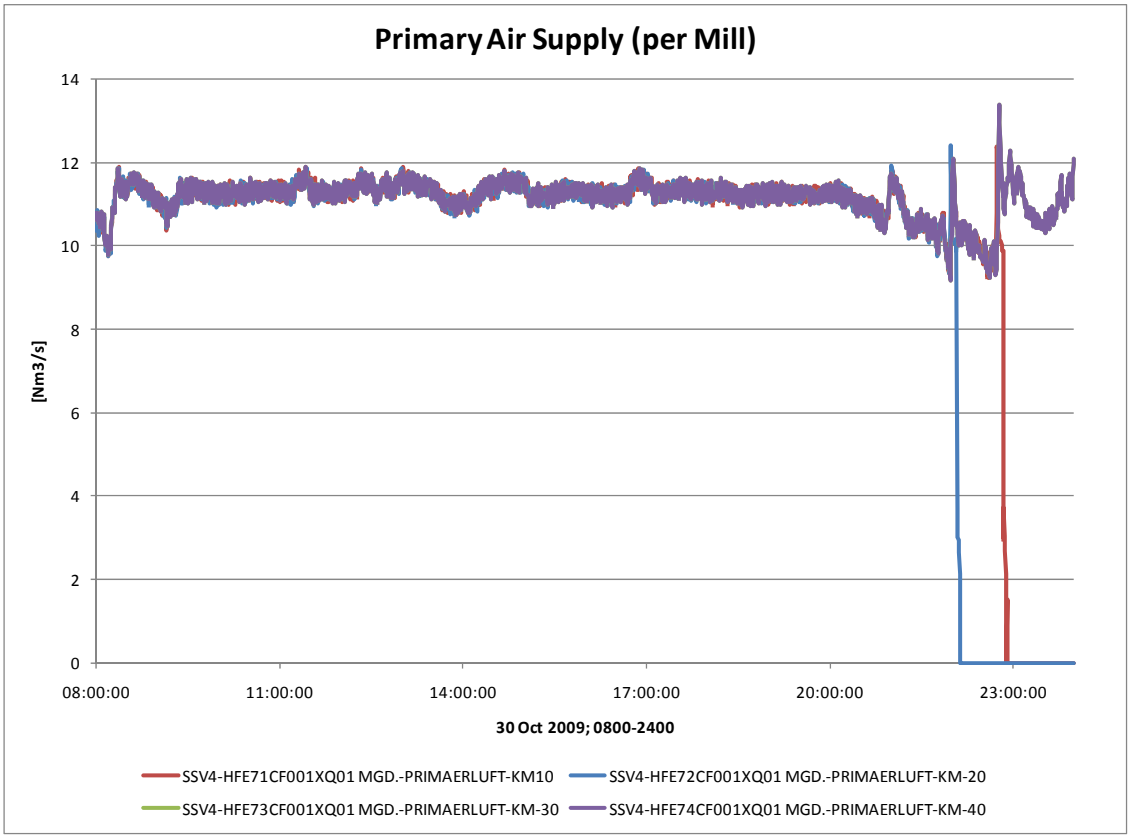
Primary Air Supply (per Mill)
[Nm3/s]
14
12
10
8
6
4
2
0
08:00:00
11:00:00
14:00:00
17:00:00
20:00:00
23:00:00
30 Oct 2009; 0800-2400
SSV4-HFE71CF001XQ01 MGD.-PRIMAERLUFT-KM10
SSV4-HFE72CF001XQ01 MGD.-PRIMAERLUFT-KM-20
SSV4-HFE73CF001XQ01 MGD.-PRIMAERLUFT-KM-30
SSV4-HFE74CF001XQ01 MGD.-PRIMAERLUFT-KM-40

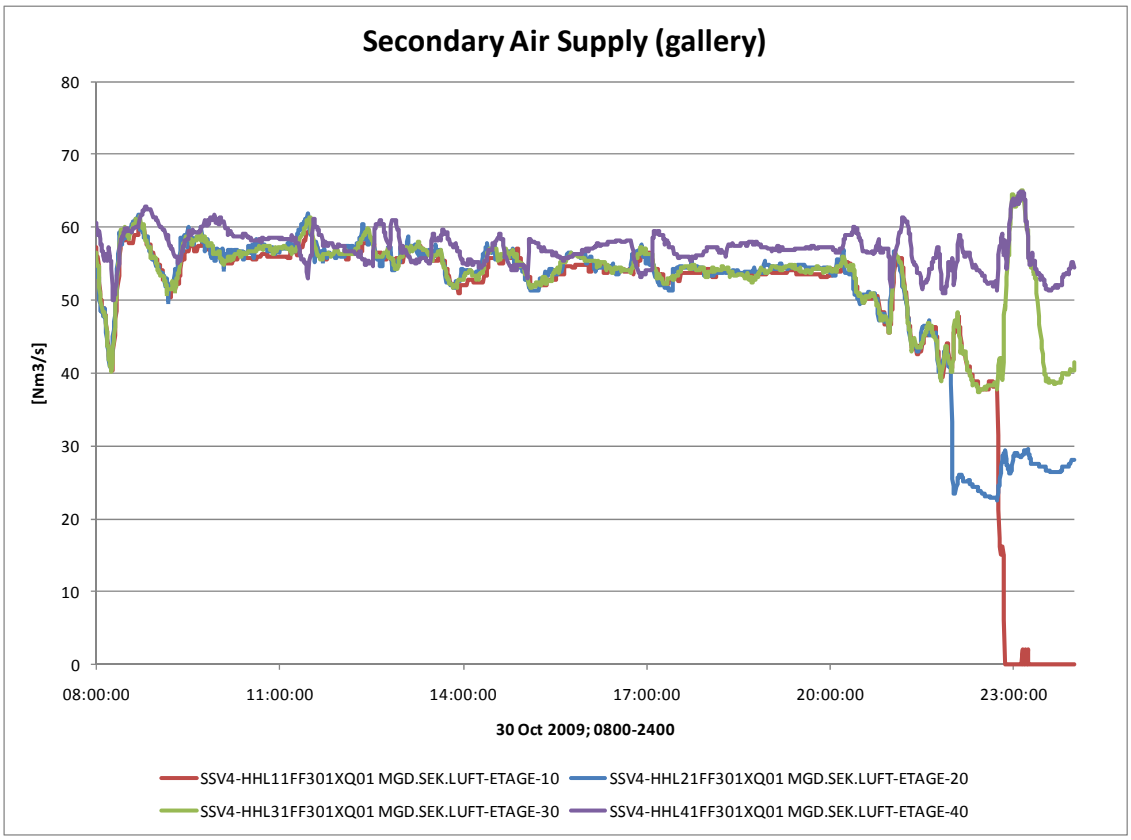
Secondary Air Supply (gallery)
[Nm3/s]
80
70
60
50
40
30
20
10
0
08:00:00
11:00:00
14:00:00
17:00:00
20:00:00
23:00:00
30 Oct 2009; 0800-2400
SSV4-HHL11FF301XQ01 MGD.SEK.LUFT-ETAGE-10
SSV4-HHL21FF301XQ01 MGD.SEK.LUFT-ETAGE-20
SSV4-HHL31FF301XQ01 MGD.SEK.LUFT-ETAGE-30
SSV4-HHL41FF301XQ01 MGD.SEK.LUFT-ETAGE-40

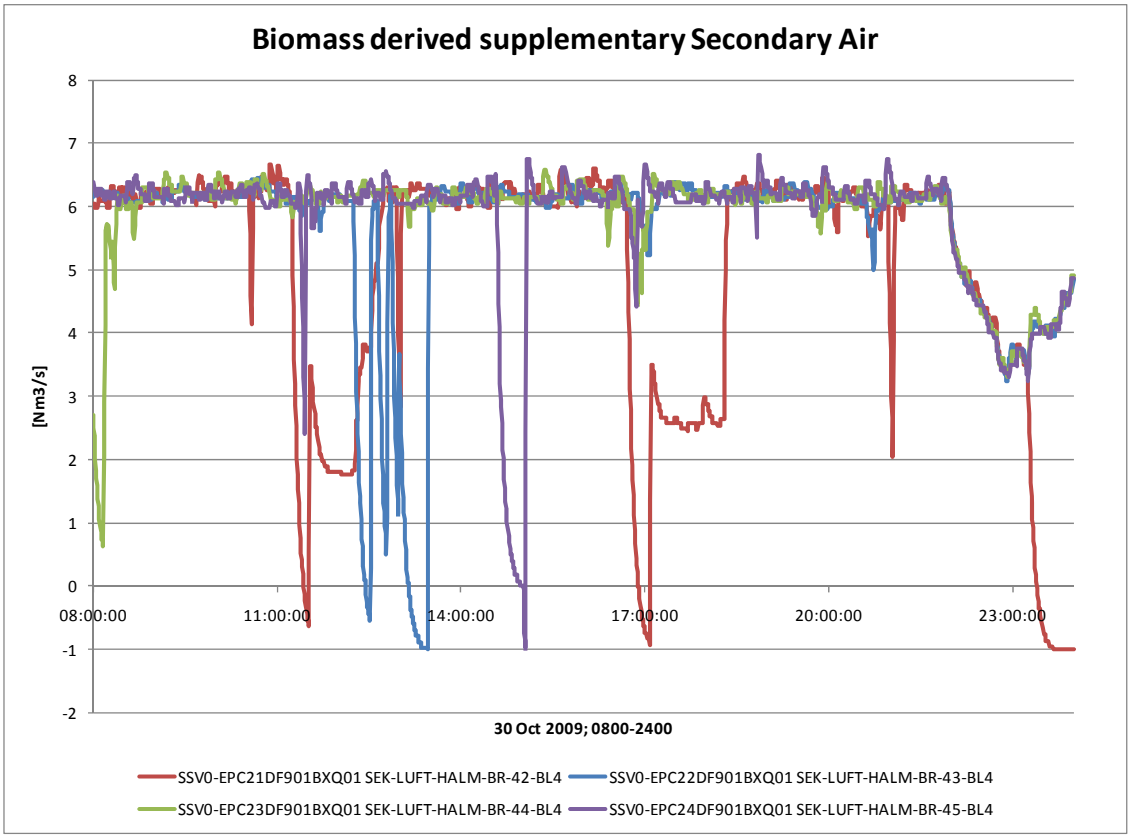
Biomass derived supplementary Secondary Air
[Nm3/s]
8
7
6
5
4
3
2
1
0
-1
-2
08:00:00
11:00:00
14:00:00
17:00:00
20:00:00
23:00:00
30 Oct 2009; 0800-2400
SSV0-EPC21DF901BXQ01 SEK-LUFT-HALM-BR-42-BL4
SSV0-EPC22DF901BXQ01 SEK-LUFT-HALM-BR-43-BL4
SSV0-EPC23DF901BXQ01 SEK-LUFT-HALM-BR-44-BL4
SSV0-EPC24DF901BXQ01 SEK-LUFT-HALM-BR-45-BL4

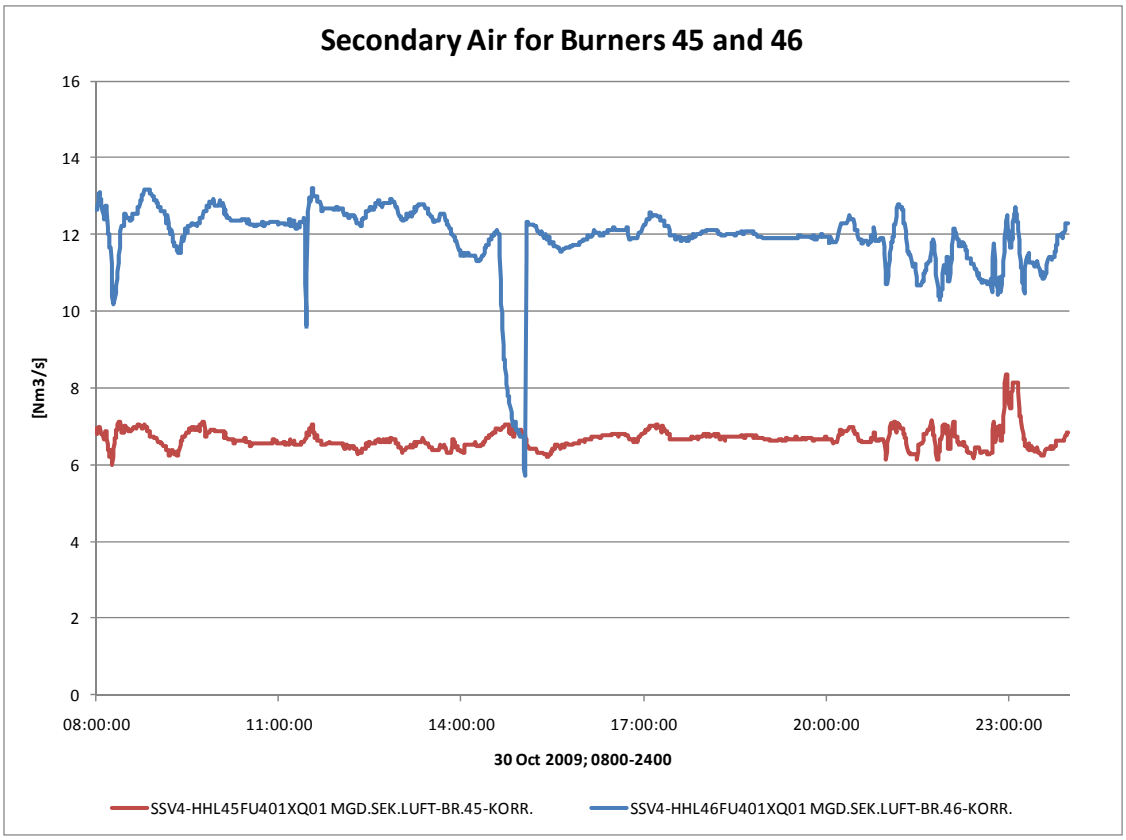
Secondary Air for Burners 45 and 46
[Nm3/s]
16
14
12
10
8
6
4
2
0
08:00:00
11:00:00
14:00:00
17:00:00
20:00:00
23:00:00
30 Oct 2009; 0800-2400
SSV4-HHL45FU401XQ01 MGD.SEK.LUFT-BR.45-KORR.
SSV4-HHL46FU401XQ01 MGD.SEK.LUFT-BR.46-KORR.

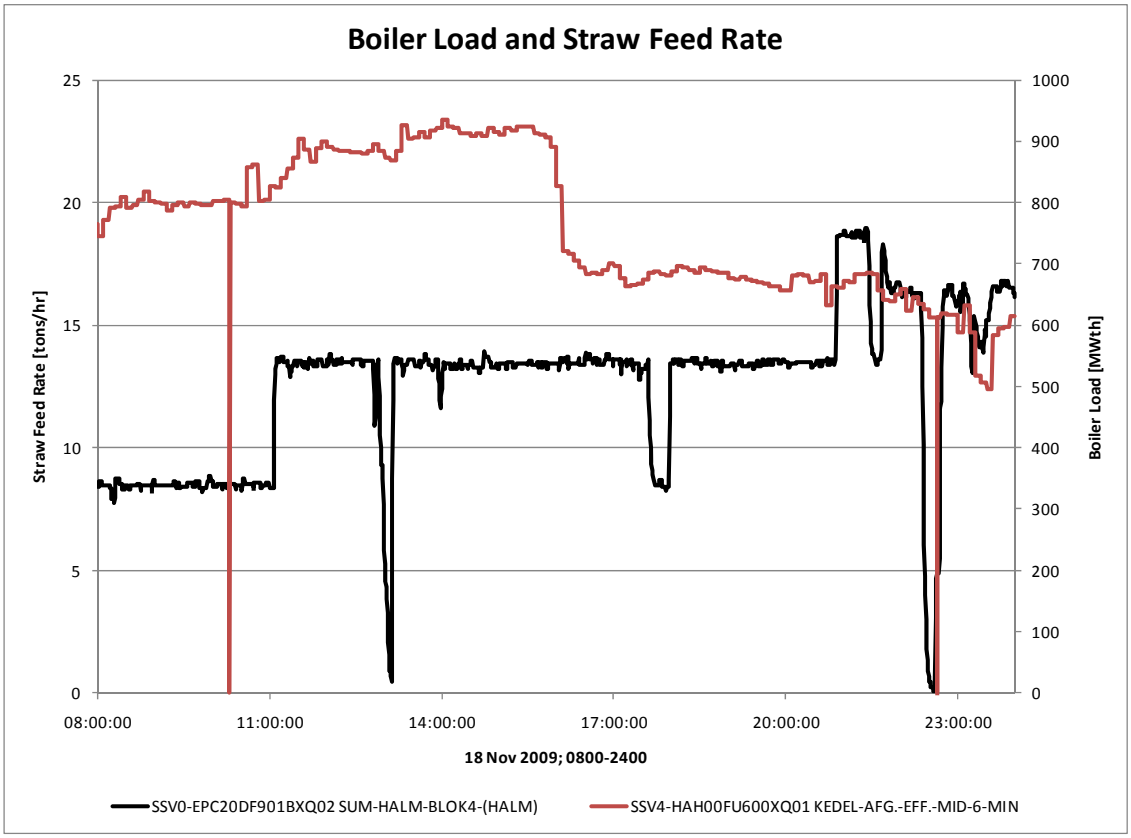
Boiler Load and Straw Feed Rate
Straw Feed Rate [tons/hr]
Boiler Load [MWth]
25
20
15
10
5
0
1000
900
800
700
600
500
400
300
200
100
0
08:00:00
11:00:00
14:00:00
17:00:00
20:00:00
23:00:00
18 Nov 2009; 0800-2400
SSV0-EPC20DF901BXQ02 SUM-HALM-BLOK4-(HALM)
SSV4-HAH00FU600XQ01 KEDEL-AFG.-EFF.-MID-6-MIN

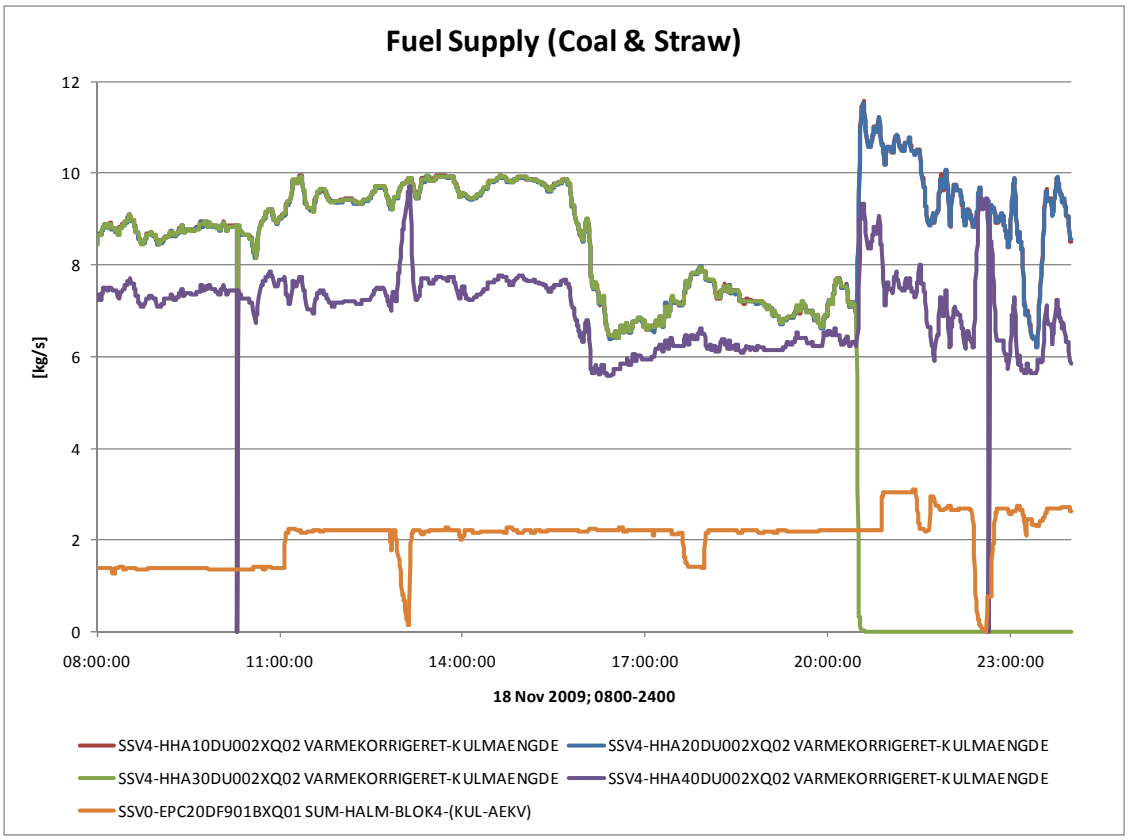
Fuel Supply (Coal & Straw)
[kg/s]
12
10
8
6
4
2
0
08:00:00
11:00:00
14:00:00
17:00:00
20:00:00
23:00:00
18 Nov 2009; 0800-2400
SSV4-HHA10DU002XQ02 VARMEKORRIGERET-KULMAENGDE
SSV4-HHA20DU002XQ02 VARMEKORRIGERET-KULMAENGDE
SSV4-HHA30DU002XQ02 VARMEKORRIGERET-KULMAENGDE
SSV4-HHA40DU002XQ02 VARMEKORRIGERET-KULMAENGDE
SSV0-EPC20DF901BXQ01 SUM-HALM-BLOK4-(KUL-AEKV)

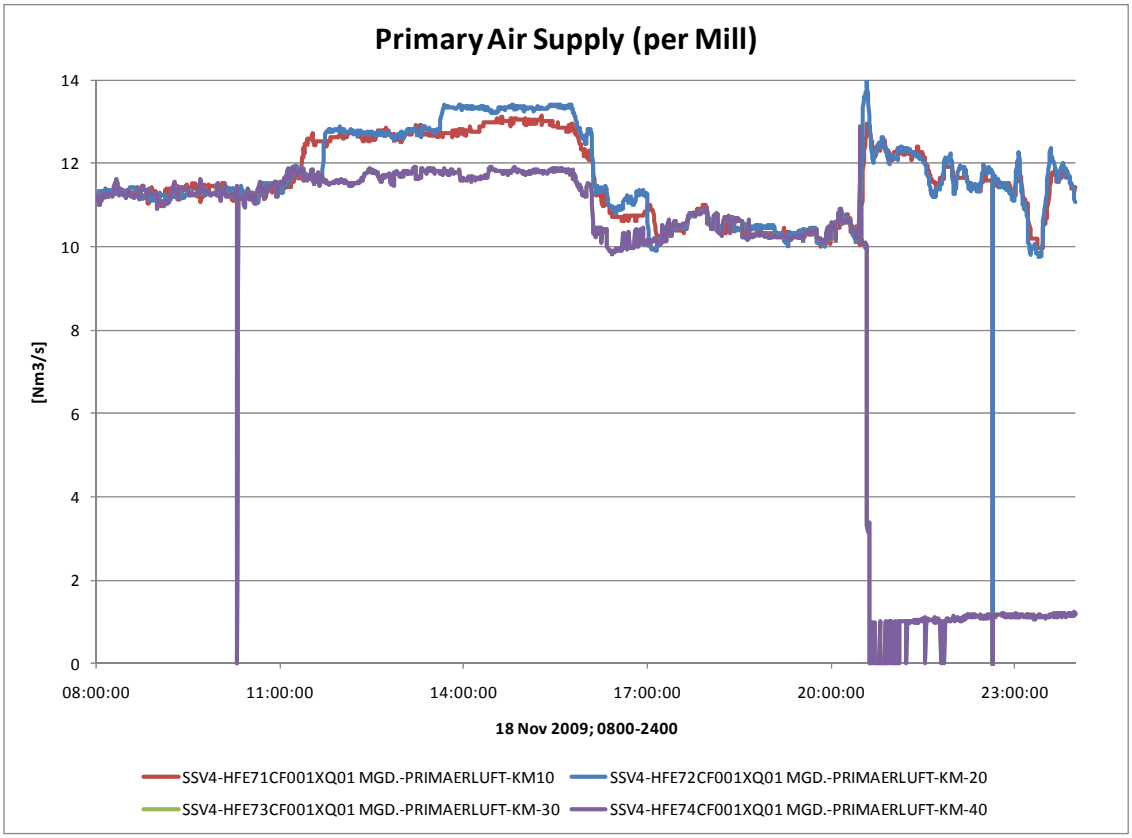
Primary Air Supply (per Mill)
[Nm3/s]
0
2
4
6
8
10
12
14
08:00:00
11:00:00
14:00:00
17:00:00
20:00:00
23:00:00
18 Nov 2009; 0800-2400
SSV4-HFE71CF001XQ01 MGD.-PRIMAERLUFT-KM10
SSV4-HFE72CF001XQ01 MGD.-PRIMAERLUFT-KM-20
SSV4-HFE73CF001XQ01 MGD.-PRIMAERLUFT-KM-30
SSV4-HFE74CF001XQ01 MGD.-PRIMAERLUFT-KM-40

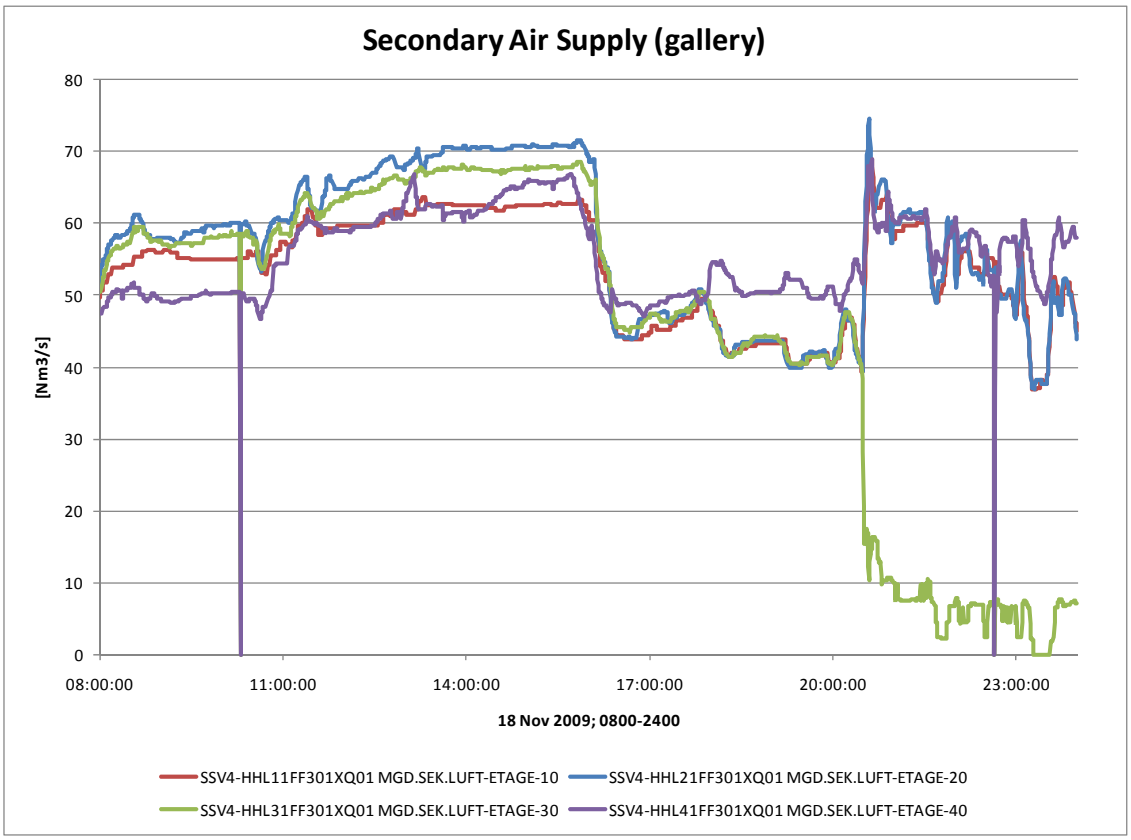
Secondary Air Supply (gallery)
[Nm3/s]
0
10
20
30
40
50
60
70
80
08:00:00
11:00:00
14:00:00
17:00:00
20:00:00
23:00:00
18 Nov 2009; 0800-2400
SSV4-HHL11FF301XQ01 MGD.SEK.LUFT-ETAGE-10
SSV4-HHL21FF301XQ01 MGD.SEK.LUFT-ETAGE-20
SSV4-HHL31FF301XQ01 MGD.SEK.LUFT-ETAGE-30
SSV4-HHL41FF301XQ01 MGD.SEK.LUFT-ETAGE-40

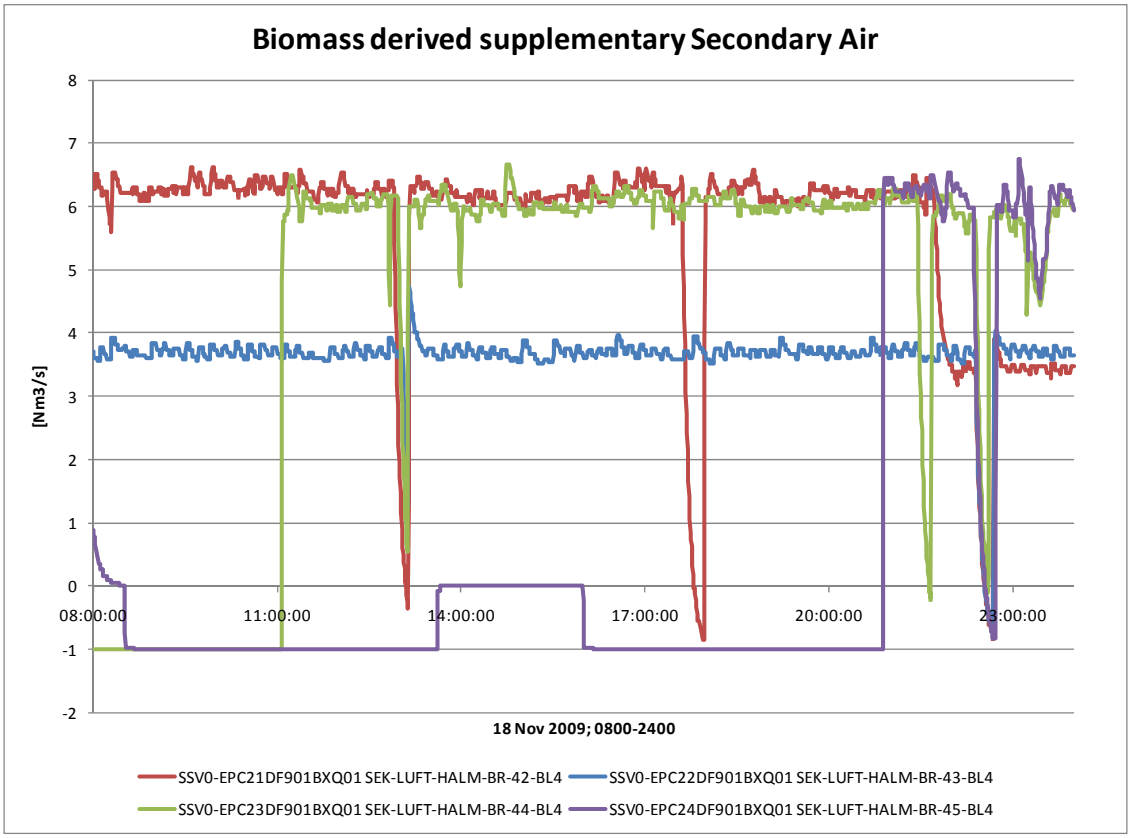
Biomass derived supplementary Secondary Air
[Nm3/s]
8
7
6
5
4
3
2
1
0
-1
-2
08:00:00
11:00:00
14:00:00
17:00:00
20:00:00
23:00:00
18 Nov 2009; 0800-2400
SSV0-EPC21DF901BXQ01 SEK-LUFT-HALM-BR-42-BL4
SSV0-EPC22DF901BXQ01 SEK-LUFT-HALM-BR-43-BL4
SSV0-EPC23DF901BXQ01 SEK-LUFT-HALM-BR-44-BL4
SSV0-EPC24DF901BXQ01 SEK-LUFT-HALM-BR-45-BL4

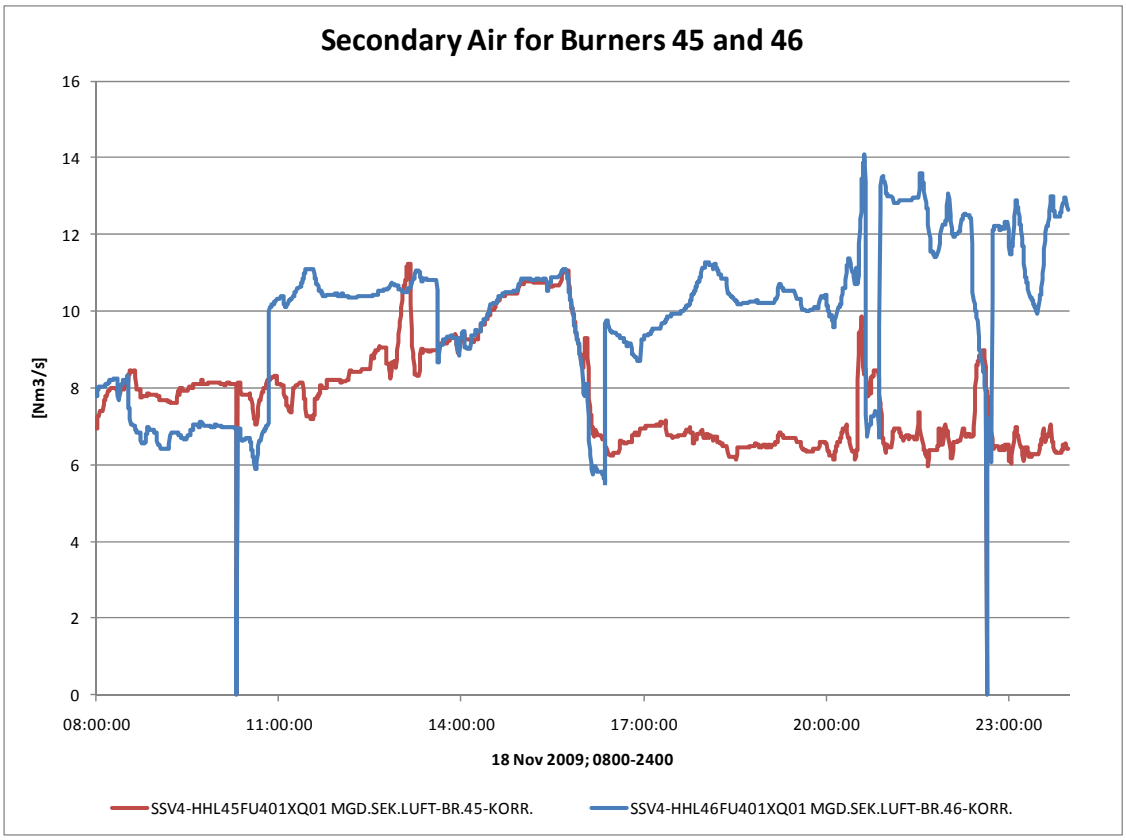
Secondary Air for Burners 45 and 46
[Nm3/s]
16
14
12
10
8
6
4
2
0
08:00:00
11:00:00
14:00:00
17:00:00
20:00:00
23:00:00
18 Nov 2009; 0800-2400
SSV4-HHL45FU401XQ01 MGD.SEK.LUFT-BR.45-KORR.
SSV4-HHL46FU401XQ01 MGD.SEK.LUFT-BR.46-KORR.

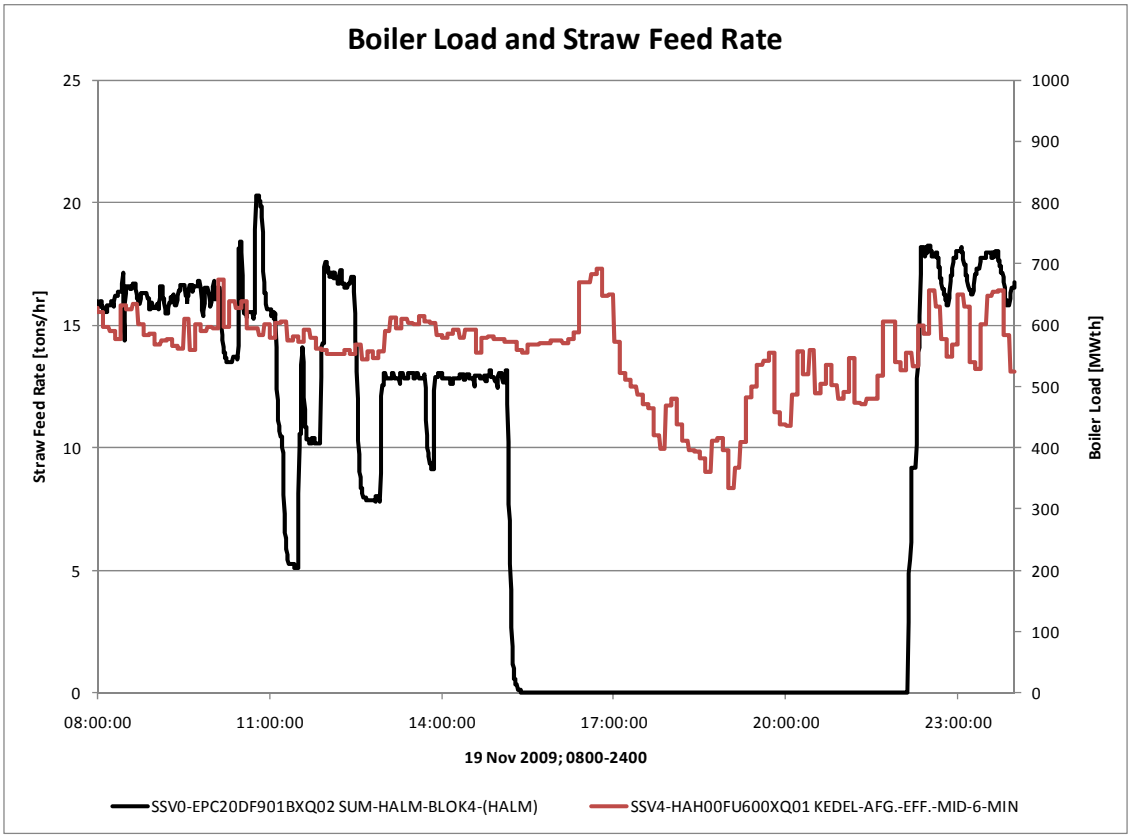
Boiler Load and Straw Feed Rate
Straw Feed Rate [tons/hr]
Boiler Load [MWth]
25
20
15
10
5
0
1000
900
800
700
600
500
400
300
200
100
0
08:00:00
11:00:00
14:00:00
17:00:00
20:00:00
23:00:00
19 Nov 2009; 0800-2400
SSV0-EPC20DF901BXQ02 SUM-HALM-BLOK4-(HALM)
SSV4-HAH00FU600XQ01 KEDEL-AFG.-EFF.-MID-6-MIN

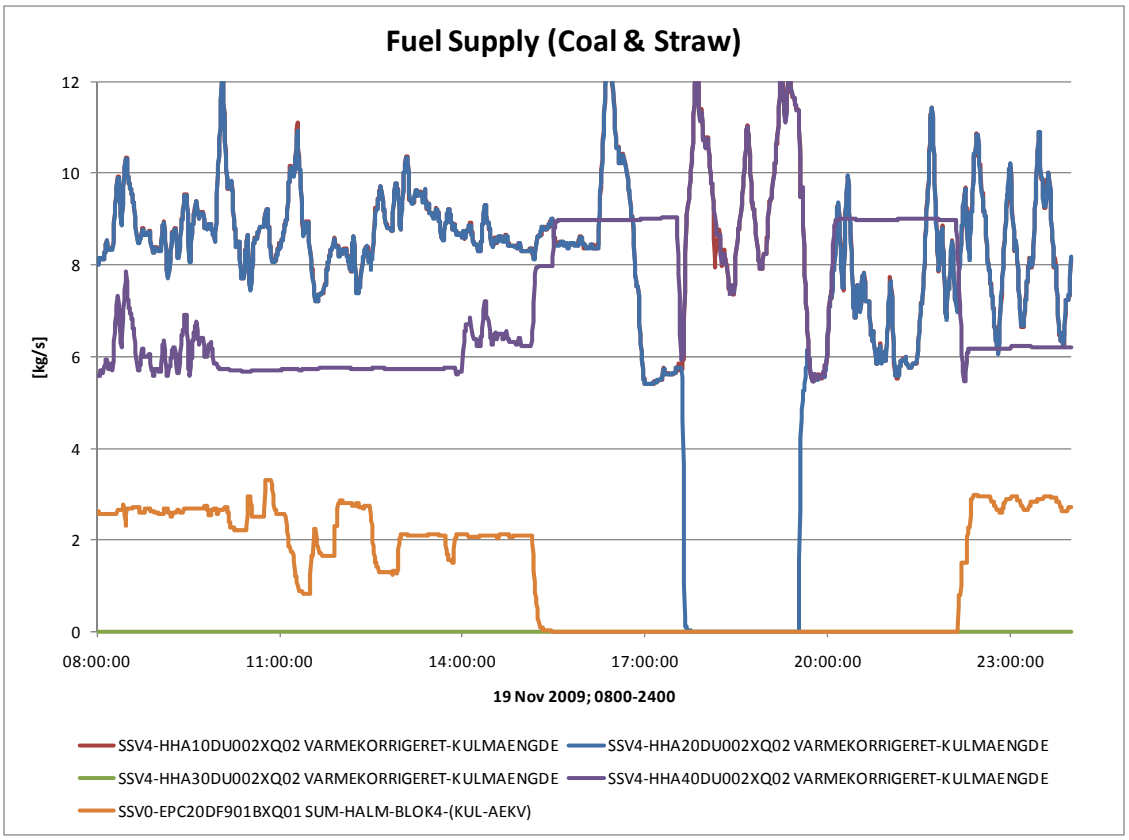
Fuel Supply (Coal & Straw)
[kg/s]
12
10
8
6
4
2
0
08:00:00
11:00:00
14:00:00
17:00:00
20:00:00
23:00:00
19 Nov 2009; 0800-2400
SSV4-HHA10DU002XQ02 VARMEKORRIGERET-KULMAENGDE
SSV4-HHA20DU002XQ02 VARMEKORRIGERET-KULMAENGDE
SSV4-HHA30DU002XQ02 VARMEKORRIGERET-KULMAENGDE
SSV4-HHA40DU002XQ02 VARMEKORRIGERET-KULMAENGDE
SSV0-EPC20DF901BXQ01 SUM-HALM-BLOK4-(KUL-AEKV)

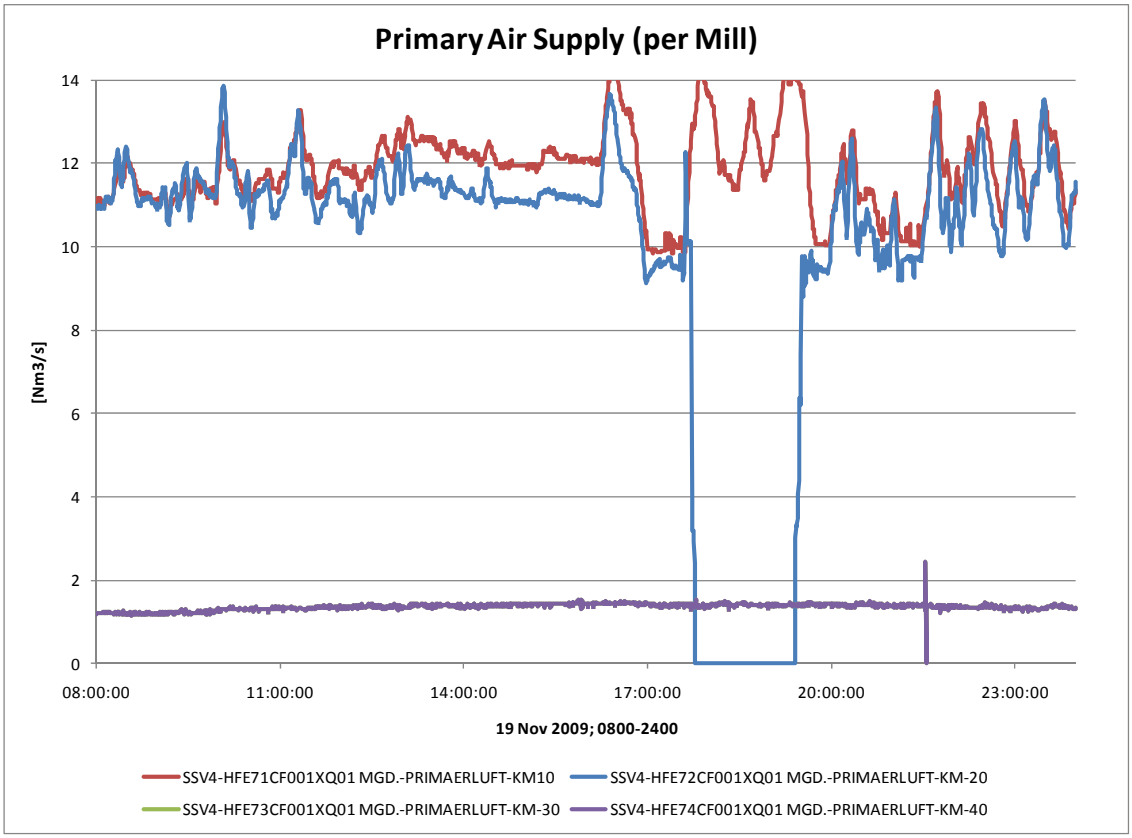
Primary Air Supply (per Mill)
[Nm3/s]
14
12
10
8
6
4
2
0
08:00:00
11:00:00
14:00:00
17:00:00
20:00:00
23:00:00
19 Nov 2009; 0800-2400
SSV4-HFE71CF001XQ01 MGD.-PRIMAERLUFT-KM10
SSV4-HFE72CF001XQ01 MGD.-PRIMAERLUFT-KM-20
SSV4-HFE73CF001XQ01 MGD.-PRIMAERLUFT-KM-30
SSV4-HFE74CF001XQ01 MGD.-PRIMAERLUFT-KM-40

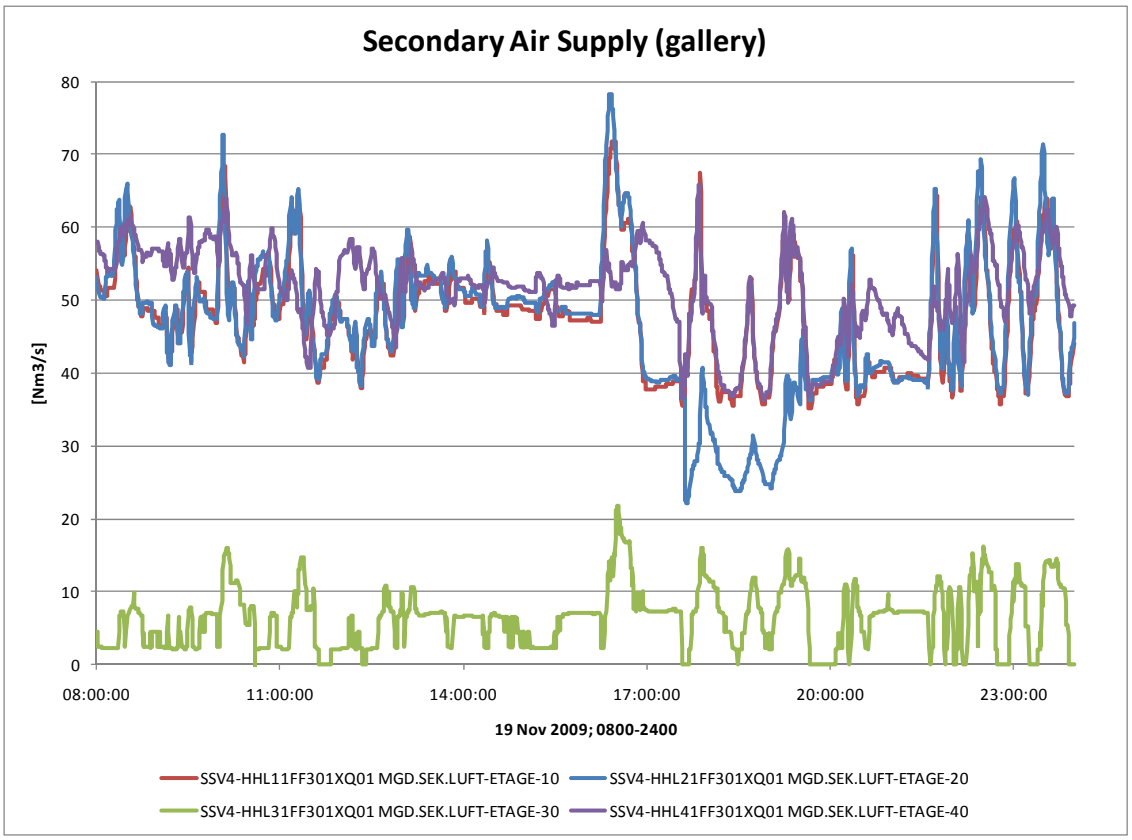
Secondary Air Supply (gallery)
[Nm3/s]
80
70
60
50
40
30
20
10
0
08:00:00
11:00:00
14:00:00
17:00:00
20:00:00
23:00:00
19 Nov 2009; 0800-2400
SSV4-HHL11FF301XQ01 MGD.SEK.LUFT-ETAGE-10
SSV4-HHL21FF301XQ01 MGD.SEK.LUFT-ETAGE-20
SSV4-HHL31FF301XQ01 MGD.SEK.LUFT-ETAGE-30
SSV4-HHL41FF301XQ01 MGD.SEK.LUFT-ETAGE-40

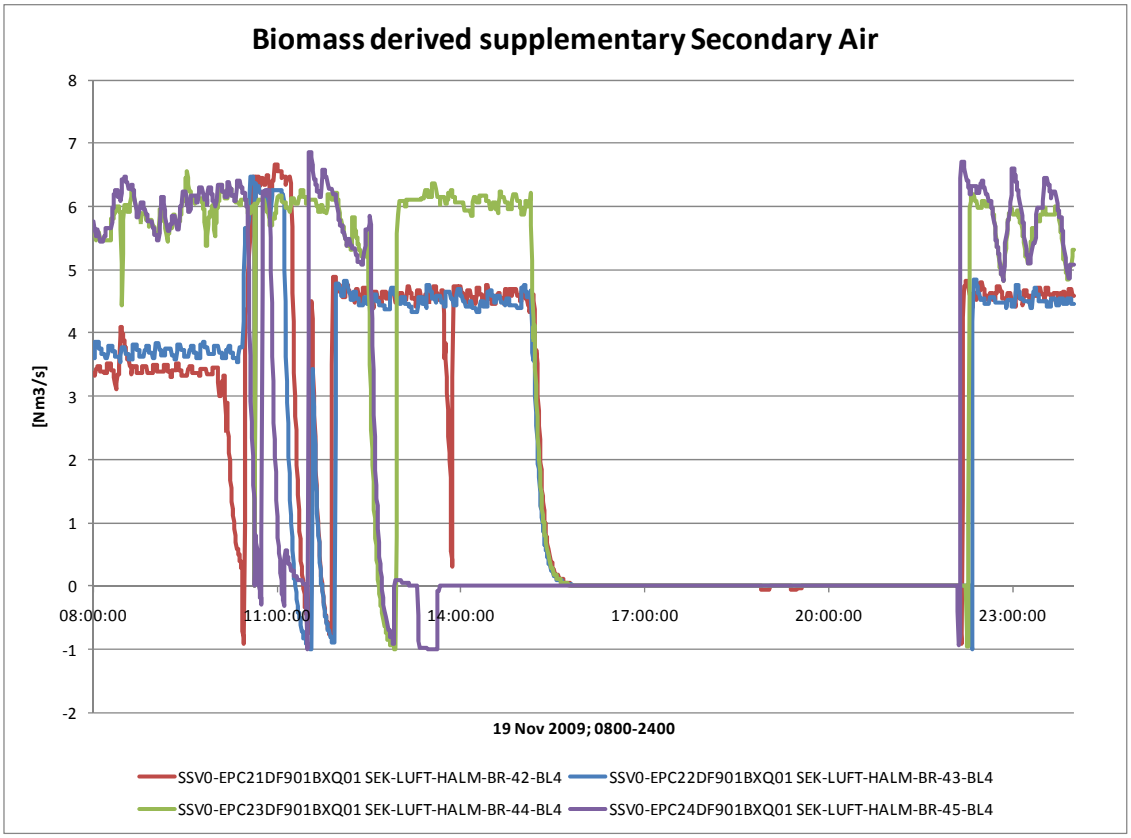
Biomass derived supplementary Secondary Air
[Nm3/s]
8
7
6
5
4
3
2
1
0
-1
-2
08:00:00
11:00:00
14:00:00
17:00:00
20:00:00
23:00:00
19 Nov 2009; 0800-2400
SSV0-EPC21DF901BXQ01 SEK-LUFT-HALM-BR-42-BL4
SSV0-EPC22DF901BXQ01 SEK-LUFT-HALM-BR-43-BL4
SSV0-EPC23DF901BXQ01 SEK-LUFT-HALM-BR-44-BL4
SSV0-EPC24DF901BXQ01 SEK-LUFT-HALM-BR-45-BL4

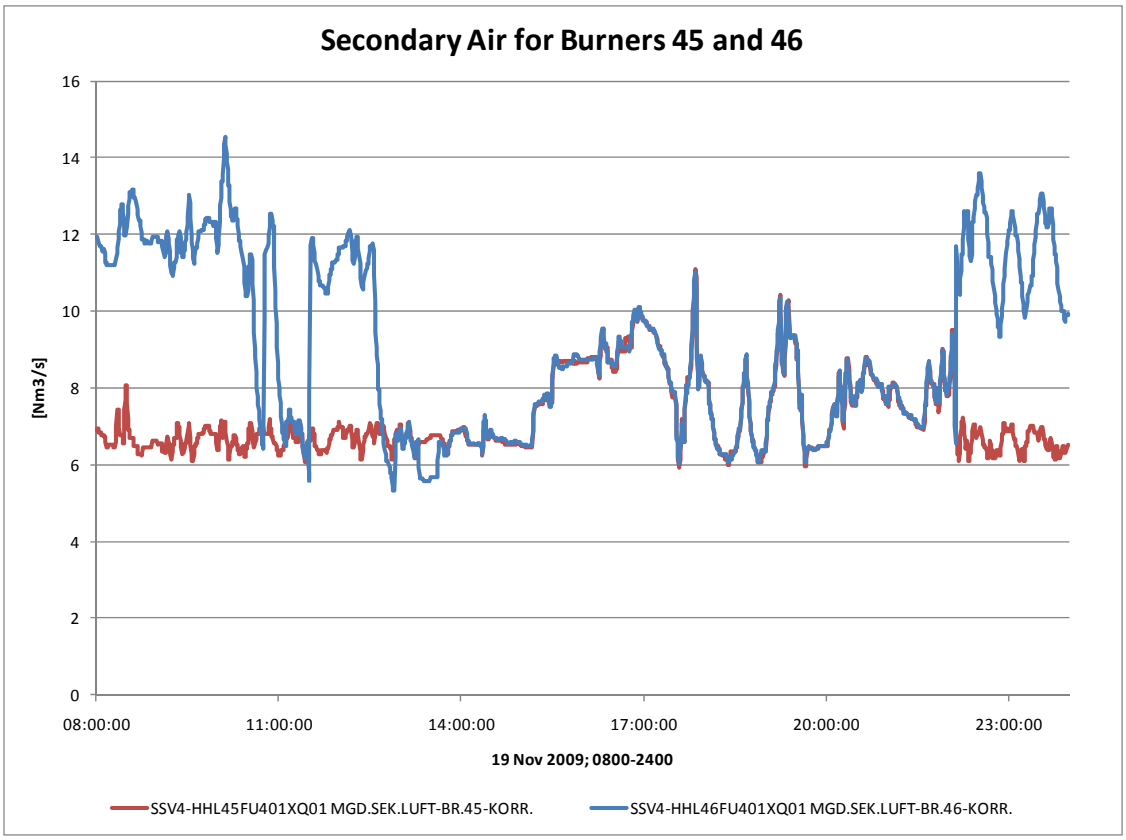
Secondary Air for Burners 45 and 46
[Nm3/s]
16
14
12
10
8
6
4
2
0
08:00:00
11:00:00
14:00:00
17:00:00
20:00:00
23:00:00
19 Nov 2009; 0800-2400
SSV4-HHL45FU401XQ01 MGD.SEK.LUFT-BR.45-KORR.
SSV4-HHL46FU401XQ01 MGD.SEK.LUFT-BR.46-KORR.

Appendix B Particle images coal-straw flame

Images taken of the extracted particles give an indication of the combustion rates of different types of particles. Figures 18-28 are a series of images of particles sampled mainly in the highly concentrated straw portion of the flame as you move axially into the boiler. The very thin leaf portions and thin needle like portions of the straw burn out earliest and are almost completely burned out in the first 260 cm. However a large portion of the smashed stalk and straw ~~needs~~ knees are still very yellow as far as 350 cm into the boiler indicating these portions are still in the devolatilization stage of combustion. The majority of the stalk appears to be completely oxidized by the center of the boiler leaving only straw ~~needs~~ knees and ash. The straw knees are still intact at this point and some still may be devolatilizing. The continued devolatilization of straw knees after all other particles appear to be burned out could cause secondary flame structures completely detached from the primary flame structure. Further investigation of gas compositions is needed to see if a large secondary flame structure exists.

Figure B1. From the straw feed line

Figure B2 75 cm from Front Wall

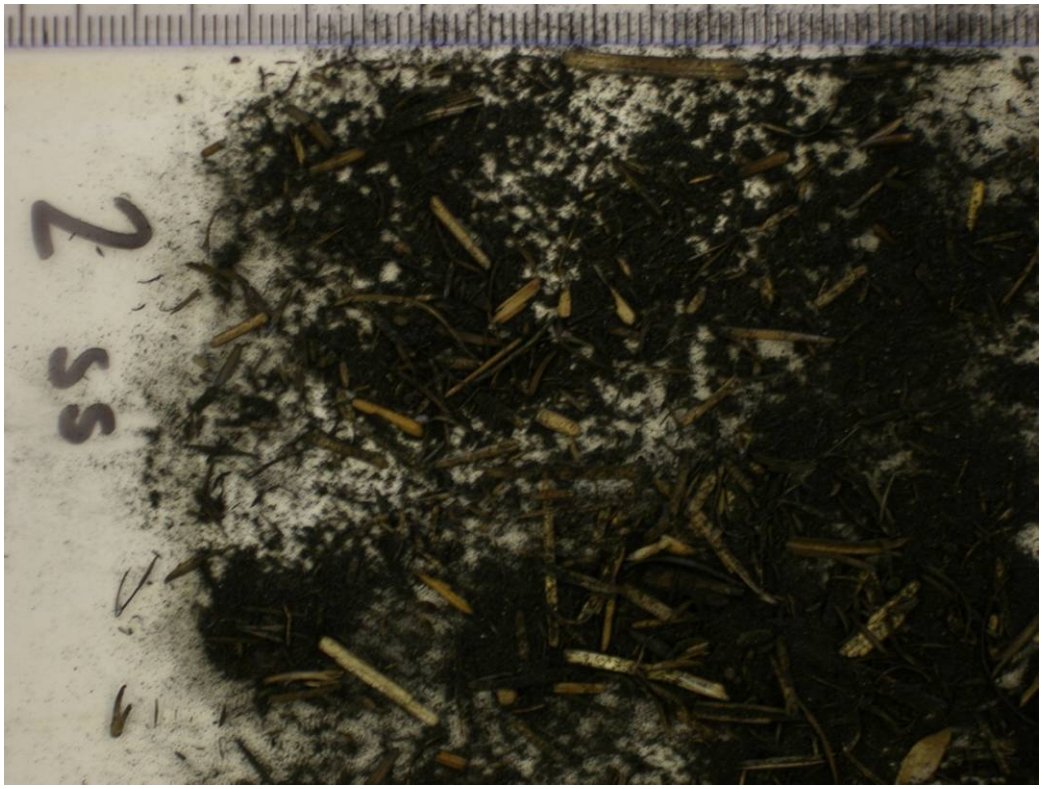

Figure B3 210 cm from Front Wall

Figure B4 260 cm from Front Wall

Figure B5 295 cm from Front Wall

Figure B6 350 cm from Front Wall

Figure B7 400 cm from Front Wall

Figure B8 450 cm from Front Wall

Figure B9 500 cm from Front Wall

Figure B10 620 cm from Front Wall

Figure B11 670 cm from Front Wall (center of boiler)

Appendix C UV emission/absorption measurements in lab-scale burner

1 Experimental set-up

Experimental set-up used in UV absorption/emission measurements consists from a methane/air flat burner [C1], D_2-lamp, two optical fibres with appropriate optics and a high-resolution UV/VIS spectrometer with an UV-enhanced CCD camera. A part of the system is shown in Fig. C1 and typical visible picture of the methane/air flame at $\varphi = 1$ stoichiometry is shown in Fig. C2.

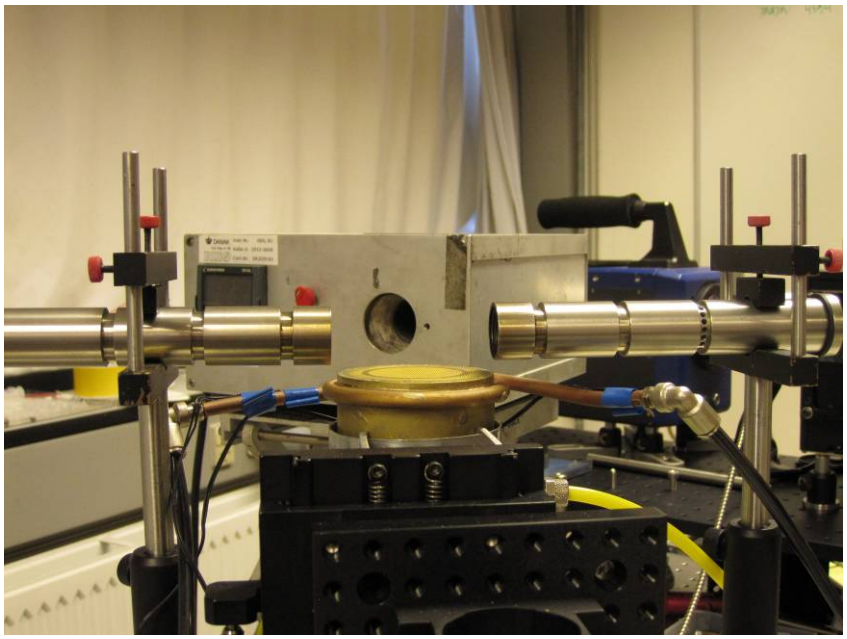

Figure C1: Experimental layout for UV emission/absorption measurements. Lens adapters (from left and right sides) are aligned to the burner plate edges and placed at 16 mm height above the burner.

Figure C2: Visible picture of the methane/air flame at φ = 1. Lens adapters are also seen.

2 Experimental results

UV absorption/emission measurements have been performed at 16 cm height above the burner (HAB). In the paper [C1] several temperature profiles measured by CARS technique are reported. The results were compared with calculations and Na-line reversal measurements and a good agreement has been found. In Fig. C3 the temperature profile at HAB=17 is shown for φ = 1 [C1].

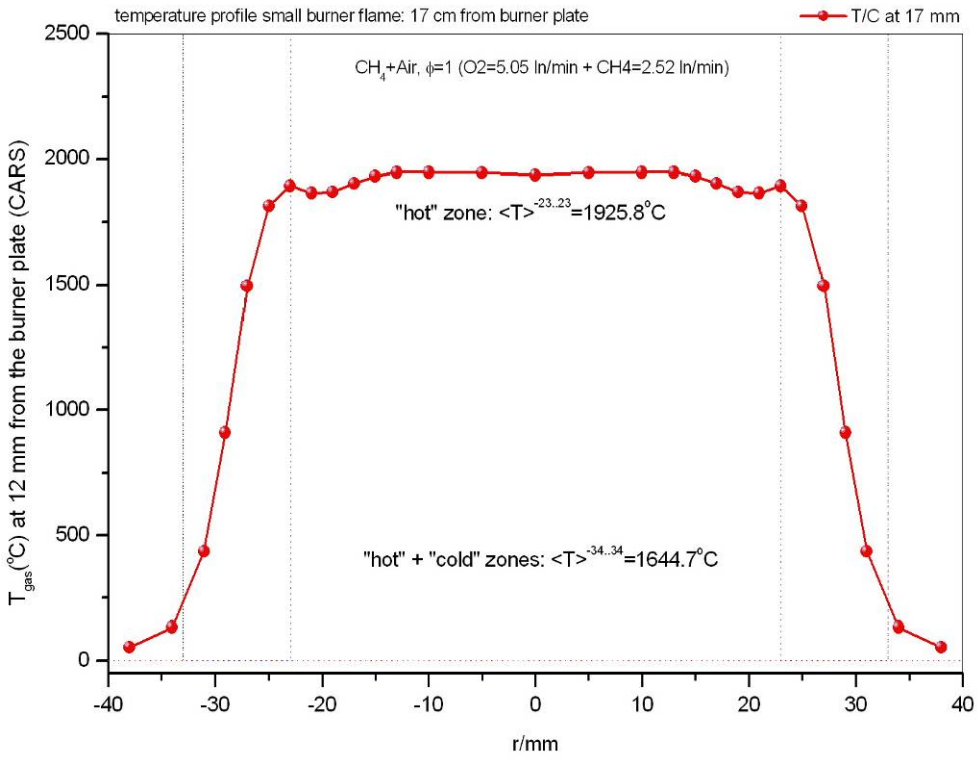

Figure C3: Gas temperature profile at HAB=17 mm measured by CARS technique as a function of the burner radius [C1]. Averaged temperatures in -23..23 mm and -34..34 mm are 1925.8°C and 1644.7°C, respectively. Areas for averaging are shown by vertical dot lines.

Averaged temperature in the "hot" zone (or flame region) is 1925.8°C whereas in more extended "hot" and "cold" zones the averaged temperature is less, 1644.7°C. Vertical dot lines at -34 and 34 mm show positions of the lens adapters.

A part of UV absorption spectrum measured at φ = 1 in methane/air flame is shown in Fig. C4 (upper panel). Experimental OH absorption bands (0-0 and 1-1) can be modeled and detailed analysis of the fine structure in 0-0 and 1-1 bands gives flame temperature of (1910.2 ± 118. 7)°C that is in excellent agreement with averaged gas (flame) temperature in the "hot" zone in Fig. C3 (1925.8°C).

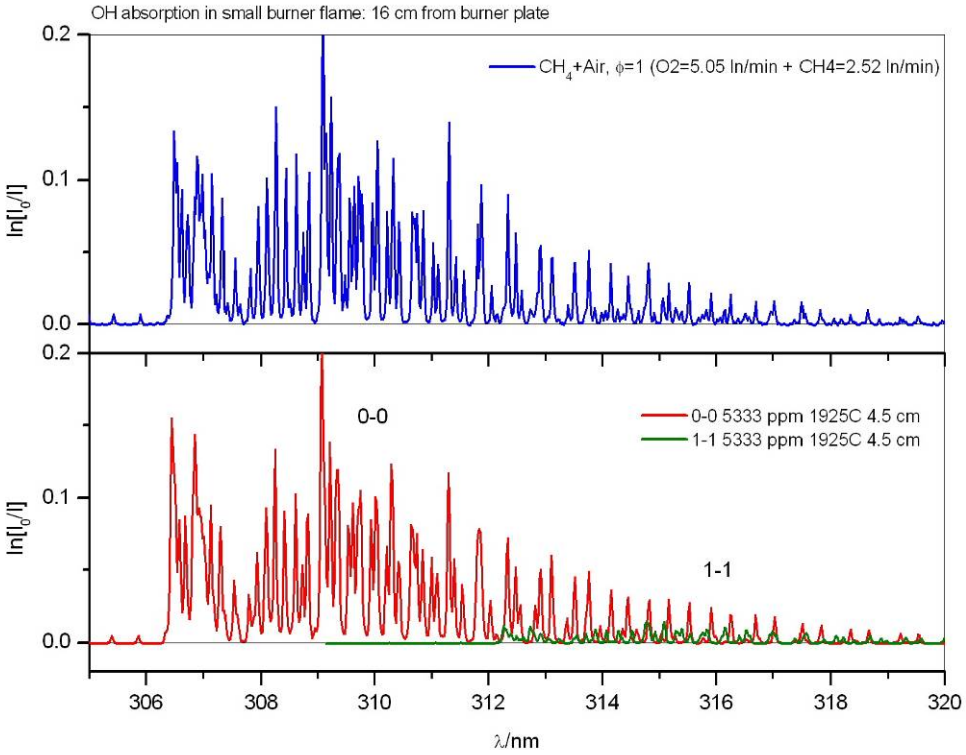

Figure C4: Experimental OH absorption spectrum (upper panel) measured at HAB=16 cm and modeled ones (lower panel). Fine structure of the 0-0/1-1bands and their ratio give flame temperature of (1910.2 ± 118. 7)^{o}C.

Full UV absorption spectrum measured at φ = 1 in methane/air flame is shown in Fig. C5 (upper panel). The spectrum consists from well localized OH bands (2-0, 1-0, 0-0) and CO_2+H_2O broad band absorption features (197-280 nm).

Detailed analysis of the CO_2 absorption spectrum gives temperature of 1621.2^{o}C that is, indeed, averaged gas temperature across "hot" + "cold" zones marked in the Fig. C3. This value is also in excellent agreement with the averaged gas temperature pointed in the Fig C3: 1644.7^{o}C.

Knowing of averaged gas temperature and that CO_2=12 vol % at φ = 1 in methane/air combustion UV absorption pathlength (45 mm) has been calculated. The last value is also in agreement with visual flame structure seen in the Fig. C2.

Finally water concentration (24 vol %) was calculated from experimental spectrum in the Fig. C5 taking into account CO_2 content (12%), averaged gas temperature (1621.2^{o}C) and optical absorption pathlentgh (45 mm). The H_2O=24% is also in excellent agreement with the theoretical value at φ = 1 in methane/air combustion.

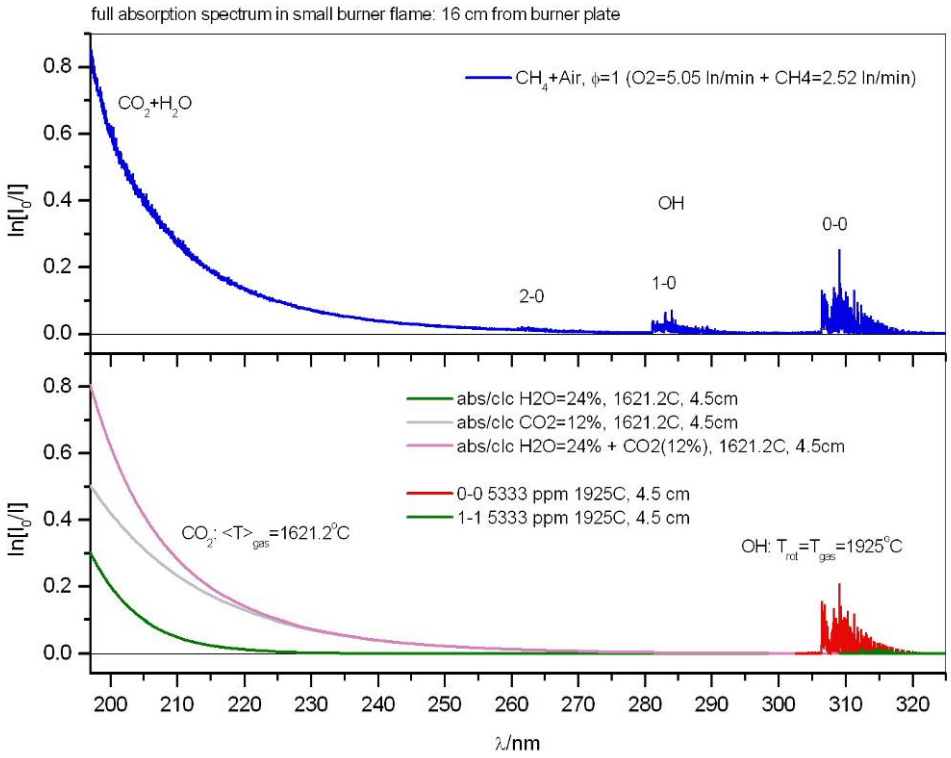

Figure C5: Experimental UV absorption spectrum (upper panel) measured at HAB=16 cm and modeled ones (lower panel). CO_2 absorption gives averaged temperature in "hot" and "cold" zones of 1621.2 ^{o}C. See the Fig. C3 for comparison.

Reference:

[C1] G Hartung, J Hult and CF Kaminskii *Meas. Sci. Technol.* **17** (2006) 2485-2493

Risø DTU is the National Laboratory for Sustainable Energy. Our research focuses on development of energy technologies and systems with minimal effect on climate, and contributes to innovation, education and policy. Risø has large experimental facilities and interdisciplinary research environments, and includes the national centre for nuclear technologies.

Risø DTU
National Laboratory for Sustainable Energy
Technical University of Denmark

Frederiksborgvej 399
PO Box 49
DK-4000 Roskilde
Denmark
Phone +45 4677 4677
Fax +45 4677 5688

www.risoe.dtu.dk